Caspase-Specific DARPins: From Binding Characterization, Inhibition and Modulation of Apoptosis towards Biomedical Applications

---

Dissertation

zur

Erlangung der naturwissenschaftlichen Doktorwürde
(Dr. sc. nat.)

vorgelegt der

Mathematisch-naturwissenschaftlichen Fakultät

der

Universität Zürich

von

Andreas Flütsch

von

Schiers GR

Promotionskomitee:

Prof. Dr. Markus G. Grütter (Vorsitz)

Prof. Dr. Ben Schuler

Prof. Dr. Klaudia Brix

Zürich, 2013

Abstract

The controlled induction of cellular demise is an essential mechanism in multicellular animals to ensure their correct development, to remove malignant cells and to maintain tissue homeostasis. Since cell deletion in a well-organized manner is so important, several different pathways have been evolved to ensure the organisms' adaptation to various death stimuli and environmental influences. Among the different cell death cascades, one of the best-characterized mechanism, known as apoptosis, leads to a non-inflammatory removal of cells and occurs for example in embryos during morphogenesis of fingers and toes. Apparently, the apoptotic non-inflammatory cell deletion is beneficial for an organism by preventing a severe immune response and thereby protecting its physical condition. However, misregulation of apoptosis has been related to severe diseases such as cancer or Alzheimer.

The key players during apoptosis have been determined as proteolytic enzymes of the caspase-family, which are able to either induce (caspase-2, -8, -9 and -10) or execute (caspase-3, -6 and -7) the apoptotic signaling. Besides that, other family members (caspase-1, -4, -5 and -12) are classified as inflammatory related peptidases. Since all the family members share a high sequence homology, the specific targeting of a particular caspase is limited with the contemporary available small molecules, which lack specificity due to their targeting of the highly conserved active site. To overcome the evident problem of caspase-specificity, we have followed the approach of using bigger molecules that provide larger binding interfaces. These interfaces may involve non-conserved residues resulting in increased target specificity. For our studies, we have used artificial binding proteins known as designed ankyrin repeat proteins (DARPins) as the molecule of choice for specific caspase targeting.

Using ribosome display, we performed DARPin selections against caspase-1 to -9, which resulted in a variety of specific caspase binders. With the exception of caspase-4, we were able to identify highly specific DARPins for each family member with binding affinities in the low nanomolar range. Our high-resolution crystal structures of DARPins in complex with caspases revealed two particular different epitopes located either at the active site forming loops or laterally at the large subunit.

Our studies on caspase-3 selected DARPins identified D3.4S76R as a very specific binder with high affinity (K_d = 6.0 nM), which inhibits the enzyme (K_i = 3.5 nM) in a pure competitive manner. Furthermore, we could demonstrate with a complex structure of caspase-3/D3.4S76R that inhibition is achieved by a similar mechanism as the one of the natural caspase inhibitor XIAP.

The characterization of caspase-7 selected DARPins was primarily focused on two particular binders D7.18 and D7.43. Both DARPins share a similar epitope with high specificity for caspase-7 but exhibited no inhibitory effect on the active enzyme. Strikingly, these molecules can also bind to the zymogenic form and thereby interfere with its activation. Our crystal structure of caspase-7/D7.18 unraveled a binding epitope sideways at the large subunit explaining the high specificity of these binders. In addition, the lateral binding of the DARPin presumably leads to steric hindrance during inter-domain linker cleavage, which is a prerequisite for successful zymogen activation.

With these two new and highly specific inhibitors of the main executioner caspase-3 and -7, we were able to further study the effect of these enzymes inside HeLa cells. Interestingly, co-transfected cells expressing D3.4S76R and D7.43 displayed significantly reduced caspase activity compared to single- or non-transfected cells indicating a successful intracellular caspase inhibition. In fact, double transfected HeLa cells were less susceptible for TRAIL induced apoptosis and survived longer in TRAIL complemented medium, which we have directly monitored using live cell imaging.

Our knowledge in the selection of caspase specific DARPins was also applied for the characterization of a second generation DARPin library with reduced hydrophobicity. We have used caspase-3 and -7 as targets during selection and thoroughly analyzed the selected DARPins using surface plasmon resonance and equilibrium unfolding. Although the new DARPins exhibited a slightly reduced thermodynamic stability, their affinity for caspase-3 and -7 were comparable to our previously selected DARPins derived from the original library. The high-resolution crystal structure of a new DARPin C7_16 in complex with caspase-7 not only verified an unchanged scaffold but also demonstrated that the intended surface entropy reduction of certain residues helped to provide crystal contacts.

Overall, this thesis will provide insights into the selection of caspase-specific DARPins and their binding characterization. The two identified highly specific caspase inhibitors were structurally investigated to elucidate their mode of action while application in cellular assays could demonstrate their potential to target these enzymes during apoptosis.

Zusammenfassung

Der kontrollierte Zelltod ist ein essentieller Mechanismus in mehrzelligen Lebewesen. Damit wird die korrekte Entwicklung gewährleistet, bösartige Zellen entfernt und die Homöostase im Gewebe aufrechterhalten. Das koordinierte Entfernen von Zellen ist für einen Organismus sehr wichtig, weshalb sich im Laufe der Evolution zahlreiche unterschiedliche Prozesse entwickelt haben. Unter den verschiedenen Todes Kaskaden ist Apoptose der wohl am besten untersuchte Prozess. Apoptose entfernt Zellen ohne eine Entzündungsreaktion auszulösen und findet zum Beispiel während der embryonalen Entwicklung von Fingern und Zehen statt. Auf der einen Seite ist klar, dass das Entfernen von Zellen ohne Entzündungsreaktion eine Immunreaktion im Körper verhindert und so zur allgemeinen Gesundheit des Lebewesens beiträgt. Auf der anderen Seite kann eine falsche Regulierung von Apoptose auch zu schweren Krankheiten wie Krebs oder Alzheimer führen.

Während der Apoptose spielen proteolytische Enzyme der Caspase Familie eine wichtige Schlüsselrolle, da sie die apoptotische Signalkaskade entweder induzieren (Caspase-2, -8, -9 und -10) oder ausführen (Caspase-3, -6 und -7). Des Weiteren wurden andere Peptidasen dieser Familie (Caspase-1, -4, -5 und -12) zu unterschiedlichen Entzündungsreaktionen zugeordnet. Die spezifische Untersuchung einer einzelnen Caspase ist mit heutigen Mitteln limitiert: Einerseits weisen die verschiedenen Caspasen eine hohe Sequenzhomologie auf. Andererseits zielen kommerziell erhältliche Stoffe auf das enzymatisch aktive und stark konservierte Zentrum. Um dieses Problem der Caspase-Spezifität umgehen zu können, dürften grössere Moleküle mit ausgedehnten Bindungsoberflächen eine entscheidende Hilfestellung bieten. Die vergrösserten Bindungsstellen können unter anderem auch nicht-konservierte Aminosäuren in die Bindung miteinbeziehen und somit eine höhere Spezifität für das gewünschte Protein liefern. Aus diesem Grund haben wir uns für die spezifische Untersuchung von Caspasen für ein künstlich hergestelltes Bindungsprotein entschieden. Diese Proteine sind bekannt unter dem Namen Designed Ankyrin Repeat Protein oder kurz DARPin.

Mit Hilfe der Technik Ribosome Display haben wir eine Vielzahl an DARPins gegen Caspase-1 bis -9 selektioniert. Mit Ausnahme von Caspase-4 haben wir für alle Caspase Familienmitglieder sehr spezifische DARPins identifizieren können. Diese DARPins bin-

den die jeweilige Caspase mit einer hohen Affinität im tiefen nanomolaren Bereich. In unseren Bindungs-Analysen haben wir unter Anderem mit hochauflösenden Proteinkristallstrukturen zwei verschiedene, favorisierte Bindungsstellen auf den Caspasen lokalisieren können: Während ein Epitop in der Nähe oder am enzymatisch aktiven Zentrum liegt, gibt es ein weiteres bevorzugtes Epitop lateral an der grossen Untereinheit des Enzyms.

Durch unsere Studien an Caspase-3 selektionierten DARPins haben wir einen sehr spezifischen Binder (D3.4S76R) mit hoher Affinität ($K_{\mathrm{d}} = 6.0$ nM) entdeckt. Dieser inhibiert das Enzym ($K_{\mathrm{i}} = 3.5$ nM) mittels eines kompetitiven Mechanismus. Nähere Untersuchungen an der Kristallstruktur eines Caspase-3/D3.4S76R Proteinkomplexes zeigte, dass dieser Inhibitionsmechanismus ähnlich dem eines natürlich vorkommenden Caspase-Inhibitors (XIAP) ist.

Unsere Forschung an Caspase-7 selektionierten DARPins war hauptsächlich auf zwei Binder (D7.18 und D7.43) fokussiert. Beide DARPins haben ein ähnliches Epitop auf Caspase-7 und binden mit hoher Spezifität wobei die Aktivität der Peptidase nicht beeinflusst wird. Interessanterweise können beide Moleküle auch an die Procaspase-7 binden und verhindern dadurch deren erfolgreiche Aktivierung. Die Röntgenstrukturanalyse von Caspase-7 im Komplex mit D7.18 zeigte eine Bindungsstelle lateral an der grossen Untereinheit und erklärt, wie die hohe Spezifität für Caspase-7 zustande kommt. Zusätzlich liefert sie Hinweise, warum die Bindung an die Procaspasen mit deren Aktivierung interferiert: Die Peptidkette zwischen der grossen und kleinen Untereinheit von Caspasen muss für deren Aktivierung proteolytisch gespalten werden. Dies wird durch einen lateral gebunden DARPin sterisch verhindert.

Die Inhibition der zwei wichtigsten Caspasen (-3 und -7) für die Ausführung von Apoptose haben wir mit Hilfe dieser zwei DARPins in HeLa Zellen studiert. Cotransfektierte Zellen (D3.4S76R und D7.43) zeigten weniger Caspase-Aktivität nach der Induktion von Apoptose als einzeln-transfektierte Zellen. Zusätzlich konnten wir mit Lebendzell-Mikroskopie zeigen, dass doppel-transfektierte HeLa Zellen weniger empfänglich für TRAIL-induzierte Apoptose sind, da diese im Vergleich zu einzeln- oder nichttransfektierten Zellen in Medium mit TRAIL länger überleben können.

Unsere Erkenntnisse in der Selektion und Charakterisierung von caspase-spezifischen DARPins haben wir für die Validierung einer neuen Generation von DARPins eingesetzt. Dazu haben wir Caspase-3 und -7 als Testproteine verwendet und die selektionierten Binder genau analysiert. Auch wenn die thermodynamische Stabilität der neuen DARPins etwas abgenommen hat, besitzen die selektionierten Binder der neuen Generation eine vergleichbare Affinität für Caspase-3 und -7. Eine hochaufgelöste Röntgenstruktur eines

DARPins (C7_16) im Komplex mit Caspase-7 demonstrierte, dass sich die allgemeine Struktur der DARPins nicht geändert hat, und dass die beabsichtigte Reduktion der Oberflächen-Entropie geholfen hat, Kristallkontakte zu begünstigen.

Zusammenfassend liefert diese Doktorarbeit Einblicke in die Selektion und Charakterisierung von caspase-spezifischen DARPins. Die dadurch entdeckten, sehr spezifischen Inhibitoren wurden strukturell untersucht, um den Inhibitions-Mechanismus aufzuklären. Zusätzlich konnten intrazelluläre Experimente aufzeigen, dass diese Bindungsproteine hohes Potential haben, um die Funktion der Caspasen während der Apoptose weiter aufzuklären.

Acknowledgment

At the first place, I have to express my deepest gratitude to my *doctorial father* Prof. Dr. Markus G. Grütter who accepted me as the very last PhD student of his group. He was always available for supportive inputs and scientific discussions but also gave me the freedom to work and manage my project(s) independently. In addition, he was a major contributor to my current scientific network by sending me to numerous conferences. Especially the International Proteolysis Meeting in San Diego in 2011 was a highlight, not only scientifically but also personally. Over there, I have met Prof. Dr. Klaudia Brix from the Jacobs University in Bremen who joined my PhD thesis committee and invited me to work for a few weeks in her lab as a guest scientist. Klaudias' support in my imaging project was of great help and her guided tour through ice-cold Bremen was unforgettable. Klaudia and her husband Klaus offered an amazing hospitality that I have to recommend at this point. I am also very grateful to my third PhD thesis committee member, Prof. Dr. Ben Schuler, who provided good ideas for my FRET based project during spontaneously organized meetings.

My thesis was based on the previous work performed by Dr. Thilo Schroeder, a former PhD student in our lab who became a very good friend of mine. Without his caspase-specific DARPins, my projects would not have been possible and I do appreciate it very much. It was an honor that he introduced me into the caspase field and that I was able to work with his selective binders. Besides Thilo, my master student and co-worker Rafael Ackermann was of outstanding help for my projects. Rafael had to work hard (and sometimes long) under my supervision and produced all the fluorescent DARPin constructs, which I could use for the final experiments. Without his pull-down experiments, the procaspase-7 activation inhibitor would not have been identified.

A good working atmosphere with interesting discussions is of course very important to the success of my thesis. Therefore, I would like to thank all my colleagues, collaborators and internship students, namely: Maria Lukarska, Jon Graf, Jürg Laederach, Nicole Schüle, Jonas Barandun, Dominic Zahn, Maren Rehders, Dr. Sofia Tedelind, Dr. Stephanie Dauth, Jonas Weber, Christopher Weinert, Damien Morger, Peter Gutte, Heidi Roschitzki-Voser, Michael Hohl, Georg Hausammann, Magdalena Bukowska, Reto

Zbinden, Aleksandra Djekic, Lea Hürlimann, Manuel Simon, Nikolas Stefan, Martin Bühlmann, Céline Stutz-Ducommun, Beat Blattmann, Brian Brissoni, Sara Züger, Christophe Briand, Chaithanya Madhurantakam, Florence Bourquin, Anshumali Mittal, Frank Kroner, Thomas Heitkamp and Tobias Merz. Furthermore, I appreciate the equipment at the imaging centers at the University of Zurich (ZMB) as well as at the ETH (LMC) and I would like to acknowledge especially Dr. Urs Ziegler, Caroline Aemisegger, Dr. Justine Kusch and Dr. Gábor Csúcs for their technical support.

I am also very thankful to all my friends and the members of the accordion orchestra ZHJO. They offered me a non-scientific environment to relax and to forget the biochemical problems I have approached (and sometimes solved..) during my thesis. All of them were always very appreciative of my workaholic lifestyle and they have never forgotten to invite me to awesome parties and holiday trips. I also thank my mother and my stepfather for the great support personally as well as financially during my studies.

Last but not least, I thank my spouse Susi for her support and patience during the last four years, when I had long working days or when I spent nights in front of the microscope. She has for sure more contributed to my scientific success than she believes and I am looking forward to new adventures with her around the globe.

Table of Contents

1 Introduction

1.1 Book Chapter: Proteases in Death Pathways

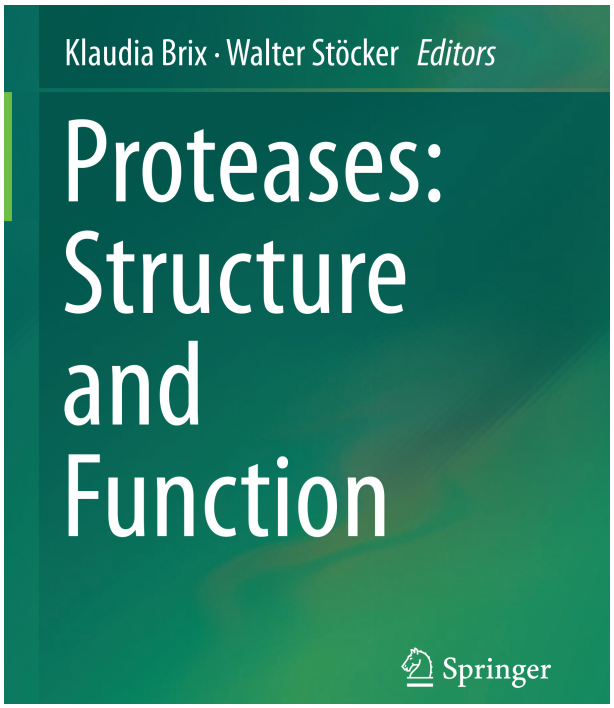

"Chapter 8: Proteases in Death Pathways"
Andreas Flütsch and Markus G. Grütter

DOI: 10.1007/978-3-7091-0885-7_8,

Chapter 8
Proteases in Death Pathways

Andreas Flütsch and Markus G. Grütter

Abbreviations

Aβ	Amyloid-β
AIF	Apoptosis-inducing factor
Apaf-1	Apoptotic protease activating factor 1
APP	Amyloid precursor protein
BH	Bcl-2 homology
Bid	BB3-interacting domain
BIR	Baculoviral IAP repeat
C. elegans	Caenorhabditis elegans
CAD	Caspase-activated DNAse
CARD	Caspase activation and recruitment domain
DAMP	danger associated molecular pattern
DARPin	Designed ankyrin repeat protein
DD	Death domain
DED	Death effector domain
DFF40	DNA fragmentation factor 40 also termed CAD
DIABLO	Direct IAP binding protein with low pI, also termed Smac
DISC	Death-inducing signaling complex
ENDOG	Endonuclease g
FADD	Fas-associated death domain
FLICE	FADD-like interleukin-1 beta-converting enzyme, today known as caspase-8
FLIP	FLICE-inhibitory protein
HTRA2	High temperature requirement protein 2
htt	Huntingtin

A. Flütsch • M.G. Grütter (✉)
Department of Biochemistry, University of Zurich, Winterthurerstrasse 190, 8057 Zürich, Switzerland
e-mail: gruetter@bioc.uzh.ch

DOI: 10.1007/978-3-7091-0885-7_8,

IAP	Inhibitor of apoptosis protein
ICAD	Inhibitor of CAD, also known as DFF45
ICE	Interleukin-1β-converting enzyme
IMS	Inter-membrane space
LRR	Leucine-rich repeat
MOMP	Mitochondrial outer membrane permeabilization
NC-IUBMB	Nomenclature Committee of the International Union of Biochemistry and Molecular Biology
NCCD	Nomenclature Committee on Cell Death
NFT	Neurofibrillary tangle
NLR	NOD-like receptor
NOD	Nucleotide binding and oligomerization domain
PARP	Poly(ADP-ribose) polymerase
PIDD	p53-induced protein with a death domain
PS	Phosphatidylserine
RIP	Receptor-interacting protein
ROCK	Rho-associated kinase
Smac	Second mitochondria-derived activator of caspase, also termed DIABLO
tBid	Truncated Bid
TNF	Tumor necrosis factor
TRAIL	TNF-related apoptosis-inducing ligand
UBA	Ubiquitin associated
XIAP	X-linked inhibitor of apoptosis protein

8.1 Introduction

The theory of the cell as the basic unit of life was developed by the German scientists Schleiden and Schwann in 1839. Shortly afterwards, cellular demise was observed by researches in different tissues and cell types. A landmark was in 1885, when Walther Flemming morphologically described the process of dying ovarian follicles containing "chromatin chunks", which he termed chromatolysis (Flemming 1885). In fact, the condensation of chromatin is nowadays well known as a morphological feature of apoptosis.

In 1972, Kerr et al. (1972) described the morphology of cell deletion in tissues with a reproducible and different mechanism compared to the known process of necrosis. Disappearing cells showed aggregation of nuclear chromatin similar to Flemmings observations. The mechanism could be dissected into two stages: A step of nuclear and cytoplasmic condensation into membrane-bound cellular fragments and a degradation step performed by other cells after phagocytosis. Kerr proposed the term apoptosis for this programmed cell death derived from the Greek word for "falling off".

Studies on embryonic development of *Caenorhabditis elegans* (*C. elegans*) by Ellis and Horvitz (1986) yielded in the discovery of the cell death controlling genes

ced-3 and ced-4. A fundamental starting point in death pathway research was in 1993, when this *C. elegans* gene ced-3 was recognized to encode a protein similar to the mammalian interleukin-1β-converting enzyme (ICE) (Yuan et al. 1993). Several homologues of ICE were identified in mammals forming a proteolytic network as the molecular basis for apoptosis. The increasing amount of identified cysteine-aspartic-dependent proteases with inconsistent and multiple names were unified for simplicity with the name caspase in 1996 (Alnemri et al. 1996).

Caspases were further investigated and revealed a complex network of regulation and activation during apoptosis. They are known as the key-players in apoptosis and besides of this crucial role, caspases are involved in inflammatory pathways and immunity and can regulate proliferation and differentiation.

Besides the caspase-mediated apoptosis, other death pathways like necroptosis, autophagy and pyroptosis were discovered and expanded the research field of death pathways with caspase-dependent and -independent mechanisms.

The numerous different ways of cell removal and destruction underlines the significance of cell deletion. It is crucial for multicellular organisms to maintain the correct numbers of cells in tissues and to shape the architecture of organs. In addition, unspecific cell proliferation and tumor development is related to down-regulation of apoptosis whereas its up-regulation is associated to degenerative diseases like Parkinson and Alzheimer.

8.2 Death Pathways

8.2.1 Nomenclature

Various distinctive death pathways have been discovered till date and were historically classified by cellular morphology. Since 2012, the Nomenclature Committee on Cell Death (NCCD) suggests a classification based not only on morphological observations but also on biochemical data analysis (Galluzzi et al. 2012). It has been revealed that similar morphological features in cell death show biochemical, functional and immunological heterogeneity. This renders the nomenclature based on morphology as not sufficient and the exact identification of a specific pathway as a rather challenging task. The suggested classification on quantitative biochemical analysis is less prone to misinterpretations, since morphological observations require an experienced operator. Thus, the following pathway definitions will consider the NCCD recommendations.

DOI: 10.1007/978-3-7091-0885-7_8,

8.2.2 Extrinsic Apoptosis

The extrinsic apoptotic pathway is a caspase-dependent mechanism, which is initiated by extracellular stress signals. Extracellular death ligands bind to death receptors like FAS, tumor necrosis factor (TNF) receptor 1 or TNF-related apoptosis inducing ligand (TRAIL) receptor 1 and 2 leading to receptor trimerization. The activated receptor conformation triggers the assembly of an intracellular death inducing signaling complex (DISC) involving the adaptor protein Fas-associated death domain (FADD) and the initiator pro-caspases-8 or -10.

The DISC recruitment of pro-caspases leads to activation by dimerization and subsequent autocatalytic processing. Then, initiator caspases catalyze the maturation of executioner caspases to start the apoptotic removal of the cell. In particular cells like hepatocytes (type II cells), caspase-8 cleaves the death agonist BB3-interacting domain (Bid) to a truncated form (tBid) instead of activating executioner caspases (Yin et al. 1999). Bid-cleavage leads to mitochondrial outer membrane permeabilization (MOMP) that activates apoptosis in a similar manner as the intrinsic apoptosis driven by caspase-9. Bid-cleavage can thus substitute a direct caspase-8 mediated activation of executioner caspases and can provide an amplification loop of extrinsic apoptosis through the intrinsic apoptotic pathway in selected cells (Yin et al. 1999).

8.2.3 Intrinsic Apoptosis

Intrinsic apoptosis is triggered by intracellular stress signals such as DNA damage, oxidative stress and accumulation of unfolded protein. The NCCD suggests a classification into two different mechanisms due to highly heterogeneous signaling cascades with the mitochondrion as the main control mechanism. Predominance of pro-apoptotic proteins like Bak or Bax can lead to MOMP due to their pore forming activity. Consequently, inter-membrane space (IMS) residential proteins are released into the cytosol where they mediate two apoptotic pathways:

- ***Caspase-dependent***
  The release of cytochrome c upon MOMP triggers the caspase-dependent mechanism of intrinsic apoptosis. Cytochrome c assembles together with the apoptotic protease activating factor 1 (Apaf-1) to the recruitment platform for pro-caspase-9, known as the apoptosome. After the activation by dimerization, caspase-9 facilitates downstream cleavage of executioner caspases leading to cellular demise.
- ***Caspase-independent***
  The release of IMS proteins, such as apoptosis-inducing factor (AIF) and endonuclease g (ENDOG), leads to caspase-independent fragmentation of DNA after relocation into the nucleus. The IMS serine protease high temperature requirement protein A2 (HTRA2) cleaves numerous cytoplasmic substrates

including cytoskeleton proteins and contributes to the caspase-independent mechanism of intrinsic apoptosis.

8.2.4 Pyroptosis

Pyroptosis is a regulated death pathway highly connected to caspase-1 activation and inflammatory responses. Brennan and Cookson (2000) described the death of macrophages that were infected by *Salmonella typhimurium* and named this reproducible mechanism pyroptosis (Cookson and Brennan 2001). Indeed, several other bacteria are able to induce pyroptosis like *Shigella flexneri*, *Bacillus anthracis toxin* and *Pseudomona aeruginosa*.

It became clear that activation of caspase-1 is a crucial step, which is promoted by a multi-protein complex known as the inflammasome. In contrast to the apoptotic pathways, executioner caspases are not involved during pyroptosis.

The caspase-1-activating inflammasome is a large protein complex, which is formed upon infection with bacteria, viruses or parasites, as well as by host-derived danger associated molecular patterns (DAMP). NOD-like receptor (NLR) proteins recognize danger signals and bind via the adaptor protein ASC and its caspase activation and recruitment domain (CARD) to pro-caspase-1. Proximity-induced oligomerization and activation of caspase-1 leads to the maturation of pro-interleukins. The activated cytokines interleukin-1 and -18 are secreted to recruit and activate immune cells for an inflammatory response. The activation of caspase-1 results in cleavage of several other substrates, however the complex mechanism of inflammasome activation and pyroptotic cell death is still not completely understood but has recently been well reviewed by Rathinam et al. (2012).

8.2.5 Regulated Necrosis

Necrosis is commonly known as an accidental cell death with a morphotype of disrupted membranes and release of intracellular content. Hitomi et al. (2008) recently pointed out that there is as well a regulated form of necrosis, which can be triggered under specific energy dependent circumstances. Key mediators of the regulated necrotic pathway are ATP-dependent enzymes like poly(ADP-ribose) polymerase 1 (PARP-1) or receptor-interacting protein kinase 1 (RIP1). Alkylated DNA damage can act as an inducing signal leading to PARP-1 hyperactivation and cytosolic ATP reduction. The depletion of the cellular energy storage results in activation of RIP1 or its homolog RIP3, which triggers the execution of necrosis.

DOI: 10.1007/978-3-7091-0885-7_8,

8.2.6 *Autophagy*

Morphological features like massive cytoplasmic vacuolization were first described in the 1950s. In most cases, autophagy is activated upon cell stress and as a cytoprotective response of dying cells. It is a conserved, kinase-dependent cell degradation pathway in eukaryotes with autophagy related proteins and Beclin-1 as the key players of autophagosome biogenesis. A clear elucidation of autophagosome formation and its regulation is beyond the scope of this chapter but reviewed by Yang and Klionsky (2009) and Rubinsztein et al. (2012). Like apoptosis, the autophagic cell degradation is non-inflammatory due to vacuolization of cytoplasmic content.

8.2.7 *Other Modalities*

Numerous additional death pathways exist that are in some cases overlapping or bypassing other mechanisms. Thus, a variety of cell death pathways can be observed in cultures induced by the same stimulus. This makes a clear identification of the exact molecular mechanism even more important. In addition to apoptosis as the most important non-inflammatory pathway and pyroptosis as the inflammatory pathway, the following mechanisms are known:

- **Mitotic catastrophe** is initiated in an arrested M-phase in the cell cycle due to mitotic machinery aberrations. It finally leads to cell death or senescence.
- **Anoikis** is an apoptotic response due to loss of cell-to-matrix interactions
- **Entosis** or "cell-cannibalism" describes the complete engulfment of a cell into another cell, which is never released and finally degraded.
- **Parthanatos** is initiated by PARP-1 hyperactivation and its resulting ATP-depletion. It is a particular form of regulated necrosis.
- **Netosis** is a cell death mechanism restricted to granulocytic cells, sharing biochemical features with autophagy and regulated necrosis.
- **Cornification** is important for epidermis formation and restricted to keratinocytes.

8.3 Caspases: The Essential Proteases in Death Pathways

The caspase family members are well known as the key players in apoptosis. They play important roles in initiation and execution of the extrinsic and caspase-dependent intrinsic apoptotic pathways as well as in pyroptotic cell deletion. The first hint of these pro-apoptotic proteins was found in *C. elegans* in 1986, when Ellis and Horvitz (1986) identified that the genes ced-3 and ced-4 are required for the initiation of apoptosis. Deletion of these two genes leads to the survival of cells,

which otherwise usually died during embryonic development. Using the simple model organism *C. elegans*, more apoptosis-related genes and proteins like ced-9 (Hengartner et al. 1992) and EGL-1 (Conradt and Horvitz 1998) were unraveled decomposing the complex molecular system of apoptosis into its relevant proteins. CED-4 dimeric proteins are blocked in an inactive form by CED-9 in living cells. Apoptotic stimuli induce the production of EGL-1, which binds to CED-9 and thus liberates the CED-4 dimers. The released dimers build the apoptosome by tetramerization of the asymmetric dimers and recruitment of proCED-3, where CED-3 is activated by proteolysis or conformational changes and then released to trigger apoptosis.

Apoptotic research on mammalian cells and human proteins was boosted after the discovery of ICE as a unique cysteine protease (Thornberry et al. 1992) and its homology to the nematodic CED-3 (Yuan et al. 1993). The unified name caspase was finally introduced after the identification of several ICE homologues and their confusing nomenclature (Alnemri et al. 1996). In fact, the mammalian genomes encode numerous ced-like genes that may have arisen by gene duplication during evolution. Compared to nematodes, this emphasizes a much more complex apoptotic system with more redundancy and regulatory effectors.

In 1994, the first high-resolution crystal structure of human ICE was reported at a resolution of 2.6 Å and gave first insights into the catalytic mechanism and its regulation (Wilson et al. 1994). The tetrameric enzyme consists of two identical heterodimers made by a small (p10) and a large (p20) subunit. Two substrate-binding pockets are shaped between the p10 and p20 of the individual heterodimer. The active sites are formed by a catalytic diad (Cys-285 and His-237) and cleave substrates specifically after aspartate residues. Both, the conserved catalytic diad residues Cys-285 and His-237 as well as the requirement of a substrate with an aspartic acid at P_1 are common for all caspase family members.

Based on the structure and selective mutagenesis, an allosteric regulation of ICE activity was proposed (Wilson et al. 1994). Mutations in the dimer interface of the heterodimeric subunits, far away from the active site cleft, resulted in an inactive ICE suggesting the tetrameric enzyme as a prerequisite for activity.

During the last two decades, 12 different human caspases have been identified and biochemically characterized. Seven of them could be crystallized or studied by NMR spectroscopy till date. Even though this progress led to one of the best-characterized protease families among proteolytic enzymes, open questions are still remaining.

8.3.1 Classification, Nomenclature and Family Members

The Nomenclature Committee of the International Union of Biochemistry and Molecular Biology (NC-IUBMB) classifies the family of caspases as cysteine endopeptidases with the enzyme category (EC) number 3.4.22 where today caspase-1 to caspase-11 are listed in the IUBMB database with individual EC

DOI: 10.1007/978-3-7091-0885-7_8,

numbers. The MEROPS database assigned these enzymes to the clan CD with the family C14 [http://merops.sanger.ac.uk/ (Rawlings et al. 2012)].

The term caspase was introduced in 1996 with "c" abbreviating the catalytic residue cysteine and "aspase" referring to the required aspartic acid at position P_1 of the peptidase (Alnemri et al. 1996). Other similar terminologies for caspase can be found in the literature like "cysteine-dependent aspartate-directed proteases" (Eckhart et al. 2008).

The number of each family member is assigned to the date of publication and reflects the history of caspase research. Caspases are expressed as zymogens, indicated by the prefix "pro" (e.g. pro-caspase-1). The polypeptide chain consists of either a N-terminal pro-domain or a short pro-peptide and a catalytic domain that can be proteolytically separated from the former.

The architecture of the catalytic domain is made by a large and a small subunit, connected by a short linker. The individual subunits are particularly named by their exact molecular weight (e.g. caspase-1-p10 for the small subunit of caspase-1). Complete caspase activation is achieved by proteolytic removal of the N-terminal pro-domain or short pro-peptide as well as the inter-subunit linker. In addition, two catalytic domains dimerize and form a heterotetrameric structure also known as the caspase-fold.

A total of 16 different mammalian caspases could be identified by comparative genomics and evolutionary analysis (Eckhart et al. 2008). The individual family members can be classified according to their function, their length and structure of the N-terminal pro-domain, their optimal cleavage motives or their phylogenetic analysis of the amino acid sequence. The existing human homologues are generally grouped according to sequence identity and functionality.

8.3.1.1 Human Caspases

Homology based analysis of the human caspases divides the family into three subgroups that can be assigned as well to their function (Fig. 8.1).

Caspase-1, -4, -5 and -12 are inflammatory caspases according to their roles in cytokine activation. For instance, caspase-1 gets activated by the inflammasome formation and triggers pyroptosis, an inflammatory death pathway (Rathinam et al. 2012). The role of caspase-5, a close homologue to caspase-1, could be assigned to cytokine maturation and inflammasome formation (reviewed by Martinon and Tschopp 2004) whereas caspase-4 was recently shown to be involved in inflammasome activation (Sollberger et al. 2012). A special case is the full-length caspase-12, known for increased susceptibility to severe sepsis. It is expressed only in a small population of African descent, while the human majority expresses a truncated, pro-domain-only form due to a single nucleotide polymorphism (Saleh et al. 2004).

Caspase-2, -8, -9 and -10 are known as apoptotic-inducing peptidases, which are activated in response to either extra- or intracellular apoptotic stimuli. The characteristic N-terminal CARD or two death effector domains (DED) are a prerequisite

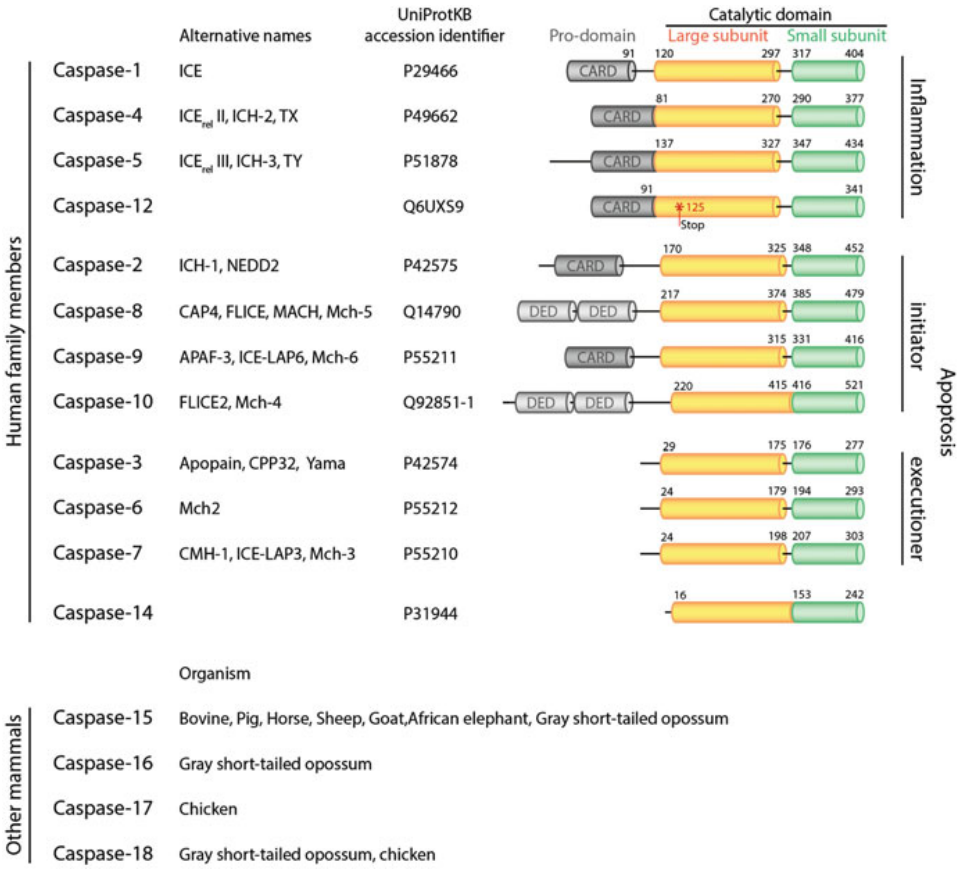

Fig. 8.1 The caspase family. The human caspase family members are ordered by their function into inflammatory and apoptotic initiator and executioner caspases. Caspase-14 is mainly expressed in keratinocytes and assigned to cornification processes. A human majority expresses a truncated form of caspase-12 due to a single nucleotide polymorphism, which leads to a stop codon at position 125 (indicated by *asterisk*). Numbers indicate terminal residues of domains. UniProtKB accession numbers and alternative names are listed for the human members. More mammalian caspase family members have been identified in other species. Caspase-11 and caspase-13 are orthologues of human caspase-4 and thus not listed

for initiator caspase activation. These domains control the oligomerization at activation platforms like the apoptosome and provoke autocatalytic activation by induced-proximity (Salvesen and Dixit 1999). In this manner, a pro-apoptotic signal can be translated into a proteolytic response.

Activated initiator caspases are responsible for the proteolytic maturation of the executioner caspases-3, -6 and -7. Executioner caspases are lacking the structured N-terminal domains and contain only a short N-terminal peptide sequence, which is thought to be a regulatory signal (Meergans et al. 2000; Denault and Salvesen 2003). In cells, these enzymes exist as heterotetrameric pro-forms and are activated by proteolysis of the N-terminal peptide and the inter-subunit linker. Once

DOI: 10.1007/978-3-7091-0885-7_8,

activated, they provoke the majority of proteolytic events leading to the known morphology of apoptotic cells.

Caspase-14 is a special member and mainly expressed in keratinocytes (reviewed by Denecker et al. 2008). Its function is assigned to cornification processes and mice experiments recently showed a relationship between caspase-14-deficiency and UVB-induced photodamage (Hoste et al. 2013).

8.3.1.2 Caspases in Mammals

Besides the well-characterized human members, numerous other homologues have been discovered in different mammalian species increasing the family members from caspase-1 to caspase-18 (Eckhart et al. 2008). Notably, murine caspase-11 and bovine caspase-13 are orthologues of human caspase-4 (Koenig et al. 2001; Eckhart et al. 2008) and thus named inconsistently with respect to the nomenclature guidelines of Alnemri et al. (1996).

A remarkable finding was published in 2011, when Kayagaki et al. (2011) discovered that the generally used caspase-1 knockout mouse (strain 129) is particularly a double knockout of caspase-1 and -11. A new caspase-1-only-deficient mouse strain depicts a crucial role of caspase-11 in the non-canonical activation of inflammation. Translated to humans, this suggests a similar role for caspase-4 and -5 and thus a specific function in incidents such as sepsis. The findings suggest a careful interpretation of the role of caspase-1 versus -11, which so far only has been determined experimentally using the mouse strain 129.

The evolutionary relationship of mammalian caspases has recently been studied. This revealed that the caspase family has gone through extensive changes with numerous gene deletions and duplications (Eckhart et al. 2008) (Fig. 8.1).

8.3.1.3 Non-mammalian Caspases and Metacaspases

Identification of the cell death related gene ced-3 in *C. elegans* was a landmark in the discovery of caspases (Ellis and Horvitz 1986; Yuan et al. 1993). CED-3 gets activated upon binding to the nematodic apoptosome formed by a CED-4 octamer and then executes the apoptotic pathway in C. elegans. A crystal structure of the formed complex between CED-3 and CED-4 revealed a funnel shaped octamer formed by CED-4, on which CED-3 is supposed to become activated, although no electron density could be observed for CED-3 in the structure (Qi et al. 2010).

Caspase homologues exist as well in insects. The initiator caspase Dronc is a caspase-9 ortholog in *Drosophila* and involved in apoptosis and cell proliferation (Steller 2008). Additional initiator (Dredd, Strica) and executioner (Drice, Dcp-1, Decay, Damm) caspases have been discovered in *Drosophila* (reviewed by Kumar and Doumanis 2000; Steller 2008). Recently, another Dredd homologue was characterized from an insect vector of human disease: *Aedis* Dredd (AeDredd) from the yellow fever mosquito *Aedis aegypti* (Cooper et al. 2007). This finding

could be a first step to unravel the role of apoptosis in innate immune response of insects and in the particular case of mosquitoes to understand their exceptional vectorial capacity.

While caspases can be found in metazoan, distant homologues could be identified as well in protozoa, fungi and plants. These distantly related cysteine-dependent peptidases cleave after arginine or lysine and are called metacaspases (Tsiatsiani et al. 2011).

8.3.2 The Caspase Fold

The tetrameric caspase structure can be described as a globular fold made by two equivalent and symmetry-related catalytic domains with a α/β topology.

Each subdomain derives from a single polypeptide chain, encoding a N-terminal pro-domain or -peptide, and a large (17–20 kDa) and a small subunit (10–12 kDa). The N-terminal domains are separated from the caspase structure by an inter-domain linker, which can be cleaved during activation processes. Due to this flexible linker, the crystallization of a full-length caspase with its pro-domain was not successful and thus their hypothetical interactions remain unclear. However, several pro-domain homologues have been separately crystallized or investigated by NMR spectroscopy. These dead domains revealed a globular fold of six antiparallel α-helices with α1–α5 forming a conserved Greek key motive (Vaughn et al. 1999; reviewed by Kersse et al. 2011).

A tightly packed caspase catalytic domain roughly forms a cuboid with the approximate dimension of 25 Å × 35 Å × 42 Å. It is composed of a β-sheet, which is sandwiched between two layers of overall five α-helices. The twisted β-sheet involves five parallel strands (β1–β5) and one antiparallel strand (β6). The latter aligns with the β6 strand of the second catalytic domain in antiparallel manner. This results in a continuous β-sheet with 12 strands and together with ten α-helices in a twofold symmetry related structure (Fig. 8.2a).

8.3.3 The Active Site, Substrate Recognition and Cleavage Mechanism

The numbering of a specific amino acid in different caspase family members can diverge due to residue insertions or deletions. In general, a facilitated numbering based on caspase-1 sequence is used as proposed by Fuentes-Prior and Salvesen (2004).

DOI: 10.1007/978-3-7091-0885-7_8,

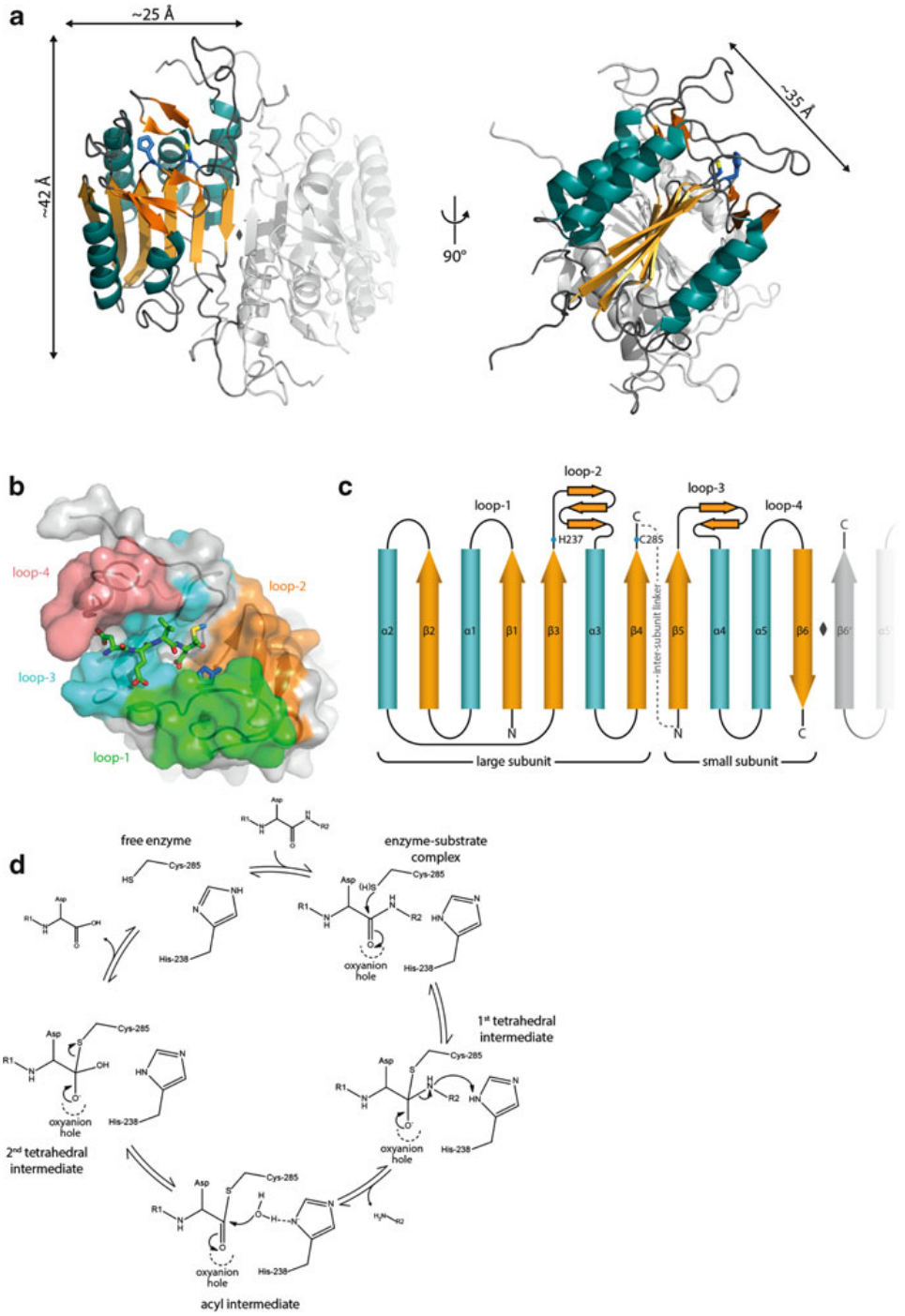

Fig. 8.2 The caspase fold. (**a**) Cartoon representation of caspase-3 crystal structure (2DKO) representing a dimer of two catalytic subunits (colored in *green*/*orange* and *gray*). Twelve central β-strands are sandwiched between ten α-helices. Active site residues His-237 and Cys-285 are colored in *blue* and located after strand β3 and β4, respectively. The five parallel β-strands of a catalytic domain points towards the substrate-binding cleft. A 90° rotation reveals a square-like arrangement of the α-helices. (**b**) Substrate-binding groove of caspase-3 (2DKO) covalently bound

8.3.3.1 Active Site Architecture and Substrate Recognition

The active site and binding groove of the catalytic domain is constructed by loops of its large and small subunits (Fig. 8.2b). The catalytic Cys-285 resides at the end of the central β-strand 4 whereas His-237 is located at the end of β-strand 3 (Fig. 8.2c). In a cartoon representation, the five parallel β-strands point towards the substrate-binding groove, with the tip of β-strand 3 and 4 indicating the position of the active site residues.

A strictly conserved Arg-179 positioned in front of helix α1 in loop-1 is crucial for the P_1 specificity. It shapes the aspartate specific binding pocket S_1 together with the conserved residues Gln-283 and Arg-341. In addition, loop-3 residue Arg-341 is involved in the formation of the binding subsite S_3 mediating main-chain-main-chain hydrogen bonds and interacting with the carboxylate group of a preferred glutamate at P_3 (Fuentes-Prior and Salvesen 2004).

The S_2 and S_4 pocket residues are less conserved. This leads to more substrate variability at P_2 and P_4 that can be observed directly by comparing small, peptide-based substrates (Roschitzki-Voser et al. 2012).

In inflammatory and initiator caspases, Val-338 of loop-3 shapes a large hydrophobic S_2 pocket that tolerates bulky side chains like His or Thr as P_2 residue. In contrast, in executioner caspases Val-338 is substituted by Tyr leading to a preference for small aliphatic substrate residues such as Val or Ala. A similar effect is observed at the S_4 subsite, where a bulky Trp-348 in apoptotic caspases shapes a small S_4 pocket with an increased affinity for branched aliphatic residues or aspartate at position P_4 (Fuentes-Prior and Salvesen 2004). A substitution in caspase-1 (Trp-348 by Val) or caspase-4 and -5 (Trp-348 by Ile) reshapes the S_4 subsite that favors large and hydrophobic residues.

A S_5 pocket could only be characterized in caspase-2 with its preferential accommodation of a small hydrophobic substrate residue (Fuentes-Prior and Salvesen 2004). Furthermore, residues after the scissile bond do not require special properties to be accommodated in the less restrictive primed subsite. An exception is the S_1' pocket that mildly discriminates for charged or bulky residues (Timmer and Salvesen 2007).

In summary, a consensus caspase substrate sequence can be defined as (D or W)-E-X-D ↓ ϕ with P_4-P_3-P_2-P_1 ↓ P_1' where Asp at position P4 is preferred by caspases of the apoptotic subfamily, X can be substituted by any amino acid and ϕ stands for a small uncharged residue (Timmer and Salvesen 2007). Today, a large number of caspase substrates are commercially available with a proposed high specificity for a single caspase family member. When looking at the consensus substrate sequence,

Fig. 8.2 (continued) to substrate-analogue inhibitor DEVD-chloromethylketone. Binding cleft forming loops are colored in *green* (loop-1), *orange* (loop-2), *blue* (loop-3) and *red* (loop-4). (**c**) Topology map of caspases colored according to crystal structure shown in (**a**). Active site residues His-237 and Cys-285 are indicated. Loop-2 is also known as 240-loop. (**d**) Catalytic mechanism according to Fuentes-Prior and Salvesen (2004)

DOI: 10.1007/978-3-7091-0885-7_8,

it is evident that such specificity is difficult to achieve and in fact could not be observed experimentally (McStay et al. 2008). This effect is not only observed for specific caspase substrates but also for peptide inhibitors, which are designed based on the consensus sequence and thus are not feasible for a highly specific caspase inhibition.

8.3.3.2 Catalytic Mechanism

Fuentes-Prior and Salvesen (2004) proposed a first catalytic mechanism in 2004. The authors suggested a mechanism with close similarity to the proteolytic reaction of serine peptidases (Fig. 8.2d). Their mechanism is based on crystal structures with active site covalently bound inhibitors mimicking a tetrahedral intermediate.

In a hypothetical enzyme-substrate complex, the P_1 carbonyl oxygen is oriented by hydrogen bonds towards the oxyanion hole, which is formed by backbone amine groups of the conserved residues Gly-238 and Cys-285. A nucleophilic attack of the Cys-285 sulfur atom on the carbonyl carbon forms a tetrahedral intermediate with covalently bound substrate. This state is stabilized by the imidaloze moiety of His-237, which protonates the α-amino group of the P_1' residue and thus triggers the release of the C-terminal peptide product from the S_1' subsite. The formed acyl intermediate is subsequently hydrolytically processed. The deprotonated π-nitrogen of His-237 abstracts a proton from a water molecule, which itself attacks the thioester carbonyl. This forms a second tetrahedral intermediate followed by a cleavage of the covalent bond formed between the carbonyl carbon and the sulfur of Cys-285. The non-covalently bound N-terminal peptide product is released and the regenerated enzyme starts a new catalytic cycle.

8.3.4 Activation in Death Pathways

Caspases are expressed as zymogens that undergo proteolytic activation in a highly regulated manner. Monomeric initiator and inflammatory caspases are activated at macromolecular platforms formed by adapter proteins. According to the induced-proximity model, the recruitment to these platforms results in a dimerization of two catalytic subunits followed by activation and autocatalytic processing (Salvesen and Dixit 1999). In contrast, the executioner caspases exist as intracellular dimers of two catalytic subunits and are activated upon cleavage by inducer or as well active executioner caspases without the requirement of additional adapter proteins.

8.3.4.1 Caspase-Dependent Intrinsic Apoptosis: The Apoptosome

Formation of the macromolecular complex known as the apoptosome is the pivotal point of caspase activation in intrinsic apoptosis (Fig. 8.3a). MOMP-mediated release

of cytochrome c from the mitochondrial IMS into the cytosol triggers the assembly of Apaf-1 into a wheel-like heptamer (Yuan et al. 2010).

The adapter protein Apaf-1 consists of a N-terminal CARD, a nucleotide binding and oligomerization domain (NOD) and a C-terminal regulatory region with two domains (WD1 and WD2). Its fundamental role in apoptosome formation relies on the Apaf-1 oligomerization with a molecular mechanism proposed based on the crystal structure of a full-length murine Apaf-1 protein (Reubold et al. 2011). Binding of cytochrome c to the regulatory region of monomeric Apaf-1 releases the attached NOD, which rotates upon binding of ATP to expose its oligomerization areas and thereby relocates the now accessible CARD. This conformational change leads to the assembly into a circular structure of seven Apaf-1 subunits with central NOD and propeller-like regulatory regions (Reubold et al. 2011). The N-terminal CARDs form a recruitment disk on top of the protomer, accessible for the targeted pro-caspase-9.

Recruitment of pro-caspase-9 to the apoptosome via homotypic interactions between the Apaf-1 and the pro-caspase-9 CARDs results in dimerization of two catalytic domains and activation of the enzyme by cleavage (Pop et al. 2006). Notably, inter-subunit linker cleavage is not necessary for activity (Stennicke et al. 1999) but may provide stability to the active dimer (Fuentes-Prior and Salvesen 2004). Thus, the Apaf-1 based apoptosome can be defined as a cofactor of caspase-9 (Pop et al. 2006). As a last step, limited proteolysis of downstream executioner caspases by caspase-9 promotes the execution of apoptosis.

8.3.4.2 Extrinsic Apoptosis: Death Inducing Signaling Complex (DISC)

Numerous extracellular death stimuli provoke the intracellular formation of a macromolecular recruitment platform for caspase-8 or -10, known as the death inducing signaling complex (DISC) (Kischkel et al. 1995). Initially, a death ligand binds to its receptor and induces oligomerization (Fig. 8.3b). A prominent and well-studied example is the receptor Fas (also known as APO-1 or CD95), which binds to Fas ligand and thereby forms a trimeric complex (Kischkel et al. 1995). TRAIL receptors (death receptor 4 and 5) are other examples that form a homotrimer upon binding to their ligand (Chaudhary et al. 1997; Pan et al. 1997; Walczak et al. 1997). Both receptor types are members of the death receptor family with its superfamily of TNF receptors and trigger the intracellular DISC formation.

Death receptor oligomerization results in a conformational change that exposes the intracellular death domains (DD) of the receptor as structurally shown for Fas (Scott et al. 2009). Then, homotypic interactions of the accessible DDs with the DDs of the adaptor protein FADD build the recruitment platform for the apical caspases.

FADD is a cytosolic protein with a N-terminal DED and a C-terminal DD (Chinnaiyan et al. 1995). The crystal structure of the protein-complex between DDs from Fas and FADD revealed a circular assembly of 5–7 Fas-DDs and 5 FADD-DDs, which optimally orients the FADD-DEDs for caspase recruitment

DOI: 10.1007/978-3-7091-0885-7_8,

(Wang et al. 2010). Additionally, both recent structural studies on DISC formation described the observation of higher oligomeric clusters and denote at least two trimeric Fas receptors as a prerequisite for signal transduction (Scott et al. 2009; Wang et al. 2010).

The complete DISC is formed upon the recruitment of pro-caspase-8 or -10 via homotypic interactions of their N-terminal DED to FADD-DEDs. This leads to an increased local pro-caspase concentration, a dimerization of two catalytic domains by induced proximity and enzymatic activity of the caspase dimer (Salvesen and Dixit 1999; Pop et al. 2007).

Caspase-8 is autocatalytically processed in the inter-subunit linker to stabilize the active dimeric conformation (Pop et al. 2007) and cleavage of the pro-domain linker allows the release of the peptidase into the cytosole (Martin et al. 1998).

Structural investigations on the unprocessed catalytic domain of caspase-8 by NMR spectroscopy visualized a highly flexible inter-subunit linker and an activation induced rearrangement of loop-1 and -3 in comparison to the X-ray structure of an active dimer (Keller et al. 2009). Included mutational studies stressed the combination of proteolytic cleavage and dimerization as a prerequisite for full activity.

Further studies on caspase-8 using a reconstituted DISC revealed a substrate specificity switch between pro- and active caspase-8 (Hughes et al. 2009). Initial dimerization of pro-caspase-8 induces activity for a limited substrate range, including autoproteolysis of pro-caspase-8 or cleavage of c-FLIP, a caspase-related regulatory protein involved in death survival signaling (Scaffidi et al. 1999; Micheau et al. 2002). Autocatalytic processing then forms the fully active enzyme with the complete substrate repertoire, including the executioner caspases and Bid that are responsible for the downstream signaling in apoptosis.

The activation mechanism for caspase-10 is similar to caspase-8 initiation (Wachmann et al. 2010). Induced proximity results in the formation of an active dimer and the further autocatalytic processing accelerates the cleavage of downstream proteins. However, the authors could show that Bid cleavage does not require processed caspase-10 in contrast to tBid production by caspase-8. This finding suggested a pro-apoptotic role of this enzyme in the uncleaved form and further research will be needed to clarify this function.

8.3.4.3 Pyroptosis: The Inflammasome

The activation of inflammatory caspases remained elusive until 2002 with the discovery of a molecular activation platform termed the inflammasome (Martinon et al. 2002). This intracellular protein complex triggers the activation of caspase-1 and -5 and is formed by NLRP1 and an adapter protein ASC (Fig. 8.3c). Subsequently, researchers identified more NLR family members that are involved in inflammasome formation, like NLRP3 (Agostini et al. 2004), NLRC4 (Mariathasan et al. 2004) and others (reviewed by Rathinam et al. 2012).

NLR proteins act as the danger-sensing molecule in the inflammasome and contain three important domains: A leucine-reach repeat (LRR) with an assumed function of danger signal recognition similar to Toll like receptors (Martinon et al. 2002), a nucleotide-binding and oligomerization domain NACHT and a death mediating domain, which is either a PYD in NLRP1 and NLRP3 or a CARD in NLRC4. Although the initiation of inflammasomes remains unclear, Martinon and Tschopp (2005) proposed a possible mechanism: Binding of a danger-associated ligand to LRR induces a conformational change that exposes the NACHT domain and thereby triggers oligomerization and recruitment of adapter proteins and inflammatory caspases.

The activation of pro-caspase-1 by NLRP1- or NLRP3-inflammasomes involves the adapter protein ASC, which contains a N-terminal CARD and a C-terminal PYD. The solution structure of full-length ASC visualized the two isolated domains connected via a flexible linker in a back-to-back orientation (de Alba 2009). This may prevent steric hindrance between the two domains and raises the capture radius for pro-caspases and NRL molecules. In addition, NLRP1 contains a C-terminal CARD that is able to directly recruit pro-caspase-1 although the presence of ASC increases caspase-1 activation (Faustin et al. 2007). A similar observation has been reported for the NLRC4 inflammasome, which can directly recruit pro-caspase-1 via its N-terminal CARD (Miao et al. 2010) but showed an ASC-dependent increase of activation (Mariathasan et al. 2004; Miao et al. 2010).

Insights into the activation mechanism of inflammatory caspases have been obtained with the crystal structure of pro-caspase-1 (Elliott et al. 2009). The inter-subunit linker of one chain occupies the central cavity of the zymogen dimer and locates its residue Asp-297 in close proximity to the active site of the other chain. After a possible interdimeric cleavage at Asp-297, the peptide chain is released and the central cavity can then harbor the other inter-subunit linker to trigger a second interdimeric processing. Additional autoproteolysis at a second cleavage site (Asp-316) then stabilizes the active dimer by conversion of an α-helix from one chain into an intradimer β-sheet (Elliott et al. 2009). These findings support the induced proximity model (Salvesen and Dixit 1999) for inflammatory caspases and emphasizes the crucial role of macromolecular oligomerization platforms for dimerization.

8.3.4.4 Caspase-2 Activation: The PIDDosome

The activation platform for caspase-2 was termed PIDDosome after the identification of the involved proteins by Tinel and Tschopp (2004). This large protein complex is formed by oligomerization of PIDD (p53-induced protein with a death domain) and the adapter protein RAIDD (Fig. 8.3d).

PIDD consists of a N-terminal LRR domain, two central ZU-5 domains and a C-terminal DD. Autoproteolysis between or after the two ZU-5 domains has been observed as a switch for pro-survival or pro-death signaling (Tinel et al. 2007). The adapter protein RAIDD, a N-terminal CARD and a C-terminal DD, is responsible

DOI: 10.1007/978-3-7091-0885-7_8,

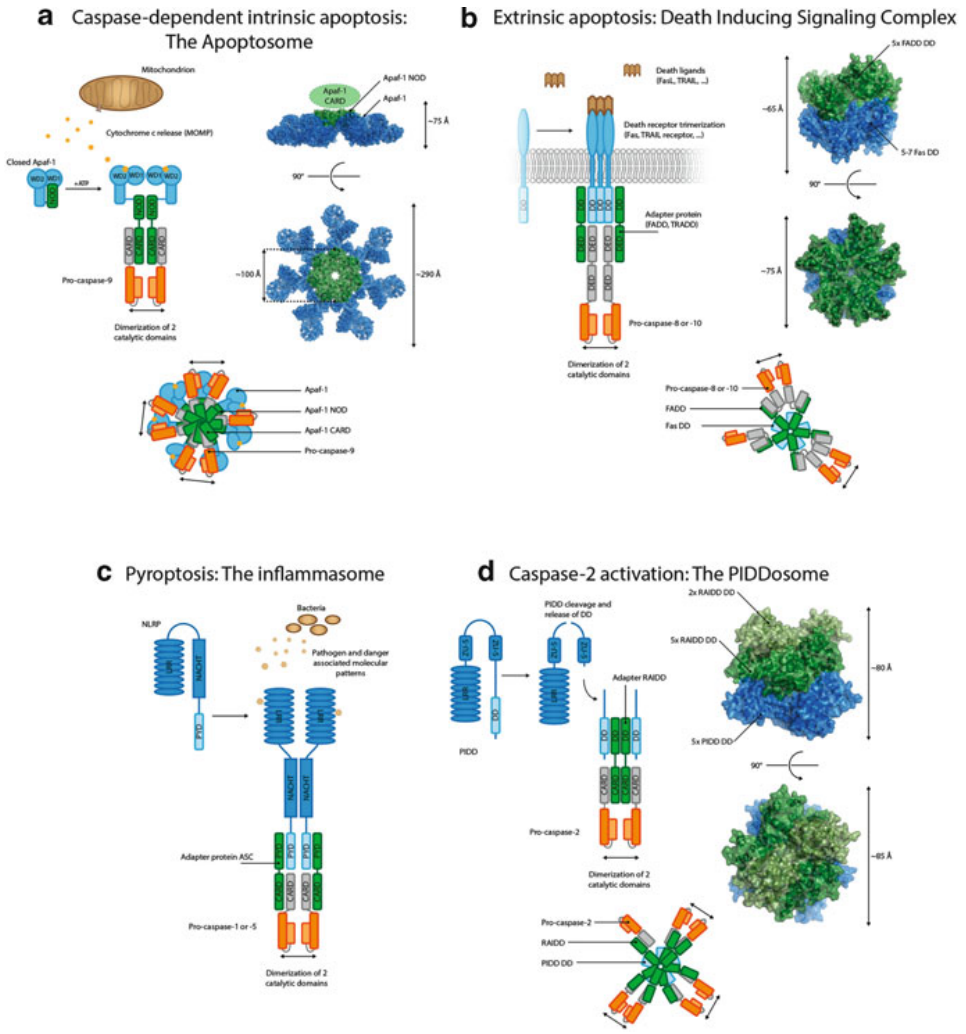

Fig. 8.3 Caspase activation platforms. Inflammatory and apoptotic initator caspases are activated at macromolecular complexes, which induces dimerization and autoproteolytic cleavage. (**a**) Apoptosome formation: released cytochrome c from the mitochondrion binds to Apaf-1 and induces a conformational change that reorients its NOD and CARD. Seven Apaf-1 molecules then form a wheel-like heptamer, which have been analyzed by electron microscopy (3IZA). The structure revealed a CARD-CARD interaction between the Apaf-1 and caspase-9 that form a disc above the central hub. (**b**) Death inducing signaling complex: activation of caspase-8 or -10 occurs at the DISC, which is initiated by trimerization of death receptors. Trimeric receptors recruit pro-caspase-8 or -10 via adapter proteins (FADD, TRADD). The assembly of FAS/FADD DDs have been structurally characterized (3OQ9) and showed a pentameric arrangement of 5–7 Fas DD and 5 FADD DDs. First, this structure shows a ring-like arrangement of the DDs similar to the Apaf-1 arrangement. Second, it indicates a requirement of more than one trimeric Fas receptor to initiate the DISC formation. (**c**) Proposed mechanism of inflammasome formation: NLRP as well as NLRC proteins exist in a conformation, where its NACHT domain is blocked. Pathogen and danger associated molecular patterns can be recognized by the LRR, which triggers a conformational change leading to a freed NACHT domain and subsequent oligomerization. Adapter proteins like ASC are then recruiting caspase-1 or -5 for activation. (**d**) PIDDosome formation: sequential cleavage of PIDD releases its DD, which recruits pro-caspase-2 via the adapter protein RAIDD. The crystal structure of PIDD-RAIDD DD assembly (2OF5) revealed a ring like structure

for caspase-2 recruitment via CARD-CARD interactions. Besides its involvement in the PIDDosome, RAIDD has been observed in specific binding of RIP1, a serine/threonine protein kinase involved in death pathway (Duan and Dixit 1997).

The crystal structure of a complex of the DDs that are involved in PIDDosome formation discovered a stoichiometry of seven RAIDD DDs and five PIDD DD molecules (Park et al. 2007). Five RAIDD DDs are stacked in a ring-like structure on top of an asymmetric, pentameric ring of PIDD DDs. Two additional RAIDD DD molecules are located in a third level on top of the RAIDD DD ring-like structure. In principal, this complete assembly is able to recruit seven pro-caspase-2 molecules for activation although only three active enzymes can be formed.

8.3.4.5 Activation of Executioner Caspases

Executioner caspases exist as stable dimers in solution in contrast to the zymogens of the inflammatory and initiator related family members. Activation occurs upon partial proteolysis by initiator or executioner caspases and results in a rearrangement of the inter-subunit linker (Riedl et al. 2001a).

The pro-caspase-7 crystal structures revealed an asymmetric blocking of the central cavity by the inter-subunit linker (Chai et al. 2001b; Riedl et al. 2001a). Linker cleavage at Asp-297 promotes its release from the central cavity. It then stabilizes the active conformation via bundle formation, which is promoted between the new C-terminus of the large subunit of one catalytic domain and the newly formed N-terminus of the small subunit of the other adjacent catalytic domain. This bundle is further interacting with loop-4 and enables the formation of the active site as shown in peptide-bound caspase-7 structures (Riedl et al. 2001a; Fuentes-Prior and Salvesen 2004).

The important role of the central cavity in caspase activation is not only depicted by the zymogen structures of caspase-1 and -7 (Chai et al. 2001b; Riedl et al. 2001a; Elliott et al. 2009) but also by the identification of allosteric inhibitors of caspase-3 and -7 (Hardy et al. 2004). These inhibitors bind in the central cavity and trap the protease in a zymogen-like conformation.

Fig. 8.3 (continued) with five RAIDD DD (*dark green*) stacked on top of five PIDD DD (*blue*). Two additional RAIDD DD (*light green*) are located on a third level. (**a**–**d**) The available complex structures of these oligomeric activation platforms point out a stoichiometric asymmetry: in principal, one of the pro-caspase monomers will not dimerize due to the odd-numbered adapter proteins

DOI: 10.1007/978-3-7091-0885-7_8,

8.3.5 Caspase Substrates

The commercially available short peptide substrates have been derived from a combinatorial approach by scanning of large peptide libraries (Thornberry et al. 1997) unraveling the caspase substrate consensus. These small molecule substrates are coupled to a fluorophore reporter and have generally been used for caspase characterization *in-vitro* (Roschitzki-Voser et al. 2012).

Diverse methods to identify *in-vivo* cleavage sites have been developed in the field of degradomics, like scanning of the transcriptome using bioinformatics (Boyd et al. 2005) as well as cell-based degradation methods, recently reviewed by Agard and Wells (2009). A growing list of identified *in-vivo* caspase substrates is available in the MEROPS database [http://merops.sanger.ac.uk/ (Rawlings et al. 2012)] with almost 900 physiological relevant entries. Undoubtedly, some of these entries are cleaved only in specific cell types or not explicitly in cell death pathways while others are well known for being processed during apoptosis. Proteolysis of those proteins typically leads to a loss-of-function or a gain-of-function. While the executioner caspases are prominent examples for the latter, several other important substrates have been described.

8.3.5.1 Rho-Associated Kinase I (ROCK I)

The family of Rho GTPases is known as an actin cytoskeleton regulator with the Rho-associated kinases (ROCK) as their effectors (Hall 1998). These serine/threonine kinase isoforms are activated upon interaction with GTP-bound Rho proteins.

During apoptosis, caspases cleave ROCK 1 at a DETD ↓ G motive near the C-terminus and thereby remove a putative autophosphorylation/auto-inhibitory domain (Coleman et al. 2001). The result is an intrinsically more active kinase, which promotes membrane blebbing in apoptotic cells by phosphorylation of downstream targets. It was further shown that a truncated ROCK 1 is independent of Rho GTPases and triggers membrane blebbing without activated caspases.

8.3.5.2 Caspase-Activated DNAse (CAD)

A morphological feature of apoptosis is the degradation of chromosomal DNA observable as a characteristic DNA ladder. A crucial nuclease for this process has been identified as the caspase-activated DNAse (CAD, also known as DNA fragmentation factor DFF40) (Nagata et al. 2003). In cells, this enzyme forms an inactive dimeric complex with the inhibitor of CAD (ICAD, also known as DFF45).

The cleavage sites DETD ↓ S and DAVD ↓ T are located in two flexible interdomain linkers of CAD and get cleaved by caspase-3. This triggers the release from ICAD and a formation of active CAD dimers. Notably, CAD is not only responsible for apoptotic degradation of nucleosomal DNA, it also promotes cell differentiation

induced by DNA strand breaks (Larsen et al. 2010). Thus, CAD is an excellent example for the caspase-3 functional dualism in cell death execution and cell proliferation.

8.3.5.3 Poly(ADP-Ribose) Polymerase (PARP)

First notices of cleavage of poly(ADP-ribose) polymerase (PARP) have been described in chicken cells in 1994 (Lazebnik et al. 1994). PARP is involved in repair mechanisms of single and double strand DNA breaks. It forms branched poly(ADP-ribose) molecules, attaches them to acceptor proteins, including itself, leading to the recruitment of repair proteins to the DNA breakage site (Javle and Curtin 2011).

The executioner caspase-3 and -7 cleave the 116 kDa PARP after a canonical sequence DEVD ↓ G into an 85 kDa fragment having no enzymatic activity. This loss-of-function prevents the repair of DNA fragments induced by CAD. Remarkably, hyperactivation of PARP can lead to a low ATP level inside cells that is a known trigger of regulated necrosis. In this prospect, the loss-of-function supports not only the apoptotic pathway but also prevents the activation of necrotic cell death and inflammatory responses.

Furthermore, PARP cleavage is a good example for exosite interactions between a protease and its target protein. It could be shown that PARP, which has been modified with long branched poly(ADP-ribose) molecules, is cleaved with higher efficiency by caspase-7 than by caspase-3 (Germain et al. 1999) although the latter cleaves short peptide substrates more efficiently. The enhanced affinity to caspase-7 was assigned to exosite interactions between the caspase-7-p20 and the branched poly(ADP-ribose) molecule.

8.3.5.4 Human Telomerase Reverse Transcriptase (hTERT)

The human telomerase hTERT maintains the length of DNA telomeres by its reverse transcriptase activity and ensures chromosomal stability. The reverse transcriptase as the catalytic domain of the protein was recently identified as a unique caspase-6 and -7 substrate that is cleaved during apoptosis (Soares et al. 2011). Four cleavage sites have been identified with TVTD ↓ A and VNMD ↓ Y cleaved by caspase-6 and TSLE ↓ G and PKPD ↓ G cleaved by caspase-7. These cleavage sites are conserved in old world monkeys and apes although the function of the persistent fragments during apoptosis remains unclear. hTERT is a recent example for a non-canonical substrate recognition of caspases.

8.3.5.5 Pro-interleukins and Interleukins

The starting point of caspase research was the identification of the ICE, today known as caspase-1 (Thornberry et al. 1992). Indeed, interleukin precursors and

DOI: 10.1007/978-3-7091-0885-7_8,

their active forms are caspase substrates that either provoke inflammatory responses or prevent inflammation during apoptosis.

For example, bacterial infections of cells can lead to caspase-mediated processing of pro-interleukin-1β (YVHD ↓ A) and -18 (LESD ↓ Y) with followed secretion of these activated cytokines. Caspases-1 and -4 are able to process the pro-forms (Thornberry et al. 1992; Kamens et al. 1995; Akita et al. 1997; Gu et al. 1997) and have been reported to be involved in the inflammasome-mediated response (Sahoo et al. 2011; Sollberger et al. 2012).

Remarkably, pro-interleukins are not only activated by inflammatory caspases but also by apoptotic members as reported for pro-interleukin-16 activation (PKPD ↓ G) by caspase-3 (Zhang et al. 1998). Pro-interleukin-16 is expressed in more than 90 % of all T cells (Chupp et al. 1998), is located in the cytoplasm and the nucleus, while a nuclear presence inhibits progression (Center et al. 2004). Thus, proteolytic modification of such a cell cycle regulator by caspase-3 illustrates the important role of these proteases in other molecular mechanisms.

In contrast to other cytokines, interleukin-33 is expressed in its active form and is not secreted after inflammatory stimuli (Lüthi et al. 2009). It is more likely to be released after membrane disruption during necrosis, while apoptotic cell death leads to interleukin-33 deactivation mediated by caspase-3 and -7 after cleavage at DGVD ↓ G (Lüthi et al. 2009). In principal, the proteolysis of interleukin-33 by apoptotic executioner caspases acts as an intracellular proinflammatory extinguisher in a tissue protective manner.

The enormous variety of caspase substrates illustrates the important roles of these enzymes in cell death, proliferation and inflammatory pathways. Although, a consensus sequence has been defined (Timmer and Salvesen 2007), natural substrates can as well be cleaved at non-canonical sites as demonstrated in rare cases (Krippner-Heidenreich et al. 2001; Soares et al. 2011).

8.3.6 Morphological Changes upon Activation

Activation of cellular death pathways results in major morphological changes that can be observed under the light microscope. Biochemical techniques have been used to characterize death pathways (Galluzzi et al. 2012). Particular morphological features (reviewed by Ziegler and Groscurth 2004) are well characterized and especially the apoptotic morphological hallmarks can be explained by caspase-mediated activation of effector proteins.

Nuclear condensation and DNA fragmentation during apoptosis relies on executioner caspases. On one hand, the cleavage of nuclear lamins by caspase-3 and -6 induces a loss of structural integrity and a nuclear shrinkage, which promotes a collapse into smaller nuclear particles in a late apoptotic state (Rao et al. 1996) (Fig. 8.4). On the other hand, CAD is activated by caspase-3 and produces DNA fragments of 180- to 200-bp length, visible by gel electrophoresis (Nagata et al. 2003; Larsen et al. 2010). In addition, cleavage of the DNA repair enzyme

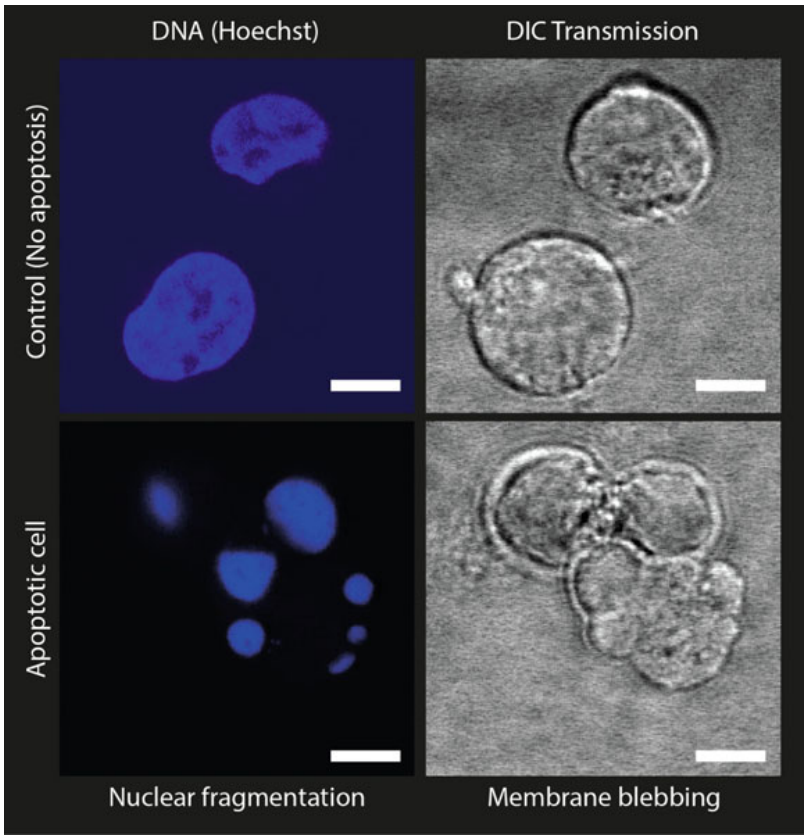

Fig. 8.4 Morphology of apoptosis. Jurkat cells were growing in media containing etoposide (100 µM, *lower panels*) or without etoposide (*upper panels*). Paraformaldehyde fixation was performed after 6 h. Etoposide treated cells show condensed and fragmented nuclei while untreated cells possess round shaped nuclei (*left panels*, DNA staining with Hoechst33342). Transmission images show round shaped healthy cells, whereas etoposide treatment leads to apoptotic cells displaying membrane blebbing (*right panels*)

PARP by caspase-3 and -7 (Germain et al. 1999) prevents the repair response thus further provoking apoptosis.

ROCK 1 cleavage by executioner caspases leads to an intrinsically more active kinase that phosphorylates downstream targets in the actin-myosin system (Coleman et al. 2001). Actin-myosin related cell contractility initiates the formation of membrane protrusions commonly known as membrane blebs (Fig. 8.4). Further progression of cell shrinkage separates these blebs into apoptotic bodies, packed with organelles and nuclear fragments, which are subsequently engulfed by surrounding cells via phagocytosis (Ziegler and Groscurth 2004).

Other phosphorylation targets in the Rho-ROCK signaling pathway are flippases, which maintain the membrane asymmetry of phosphatidylserine (PS) that is located within the inner membrane leaflet of a normal cell (Krijnen et al. 2010). In an early stage of apoptosis, PS is presented at the outer membrane as

DOI: 10.1007/978-3-7091-0885-7_8,

an "eat-me" signal for phagocytes (Grimsley and Ravichandran 2003). First studies on oxidatively stressed erythrocytes indicated caspase-related PS externalization (Mandal et al. 2002) while research on cardiomyocytes identified a Rho-ROCK signaling to be crucial for PS exposure (Krijnen et al. 2010).

8.3.7 Regulation and Specific Inhibition

A tight regulation of caspase activation is essential to avoid accidental induction of cellular demise. Thus, a complex network involving numerous proteins has been evolved, which in particular cases guarantees the survival or decease of a cell (Fig. 8.5). Most of those proteins belong to the Bcl-2 family or to the inhibitor of apoptosis protein (IAP) family. In addition, released mitochondrial proteins upon MOMP can interact with members of these two families and facilitate the progression of apoptosis.

Members of the Bcl-2 family are known to have cell regulatory functions and often possess either pro- or anti-apoptotic activity, depending on the environmental conditions (reviewed by Hardwick et al. 2012). Bcl-2 proteins (e.g. Bcl-2, Bcl-B, Bax, Bak,. . .) consist of 3–4 Bcl-2 homology (BH) domains enumerated from BH1 to BH4. Members of this family (e.g. Bim, Bid, Puma,. . .) contain only one BH3 domain, are thus called BH3-only proteins and known as promoters of apoptosis. Certain family members contain an additional C-terminal transmembrane domain (e.g. Bcl-2, Bax, Bim,. . .) that localizes them at membranes. Bcl-2 proteins exist in the cytosol, at outer mitochondrial membranes and supposedly inside mitochondria, however this submitochondrial localization remains controversial (Hardwick et al. 2012).

The IAP family members are multi domain proteins that directly suppress apoptosis by caspase inhibition (Deveraux et al. 1997) or indirectly via interaction with pro-apoptotic signaling complexes (Fulda and Vucic 2012). In addition, several members contain a C-terminal RING domain that functions as an E3 ubiquitin ligase with increasing significance in cell survival (Vaux and Silke 2005; Vucic et al. 2011).

Intracellular apoptotic stimuli can activate BH3-only proteins, which promotes Bax and Bak oligomerization and pore formation at the outer mitochondrial membrane (Kuwana et al. 2002). This leads to the release of cytochrome c and other mitochondrial proteins that function in a pro-apoptotic manner. The second mitochondria-derived activator of caspases (Smac, also termed DIABLO) is known to bind and inhibit IAP (Verhagen et al. 2000) but can itself be antagonized by IAPs (Vucic et al. 2005). Another released protein is HtrA2 (also known as Omi), a serine protease that is involved in apoptosis and suppression of IAP (Verhagen et al. 2002). In addition, caspase-8 can cleave the BH3-only protein Bid, forming a truncated form tBid and thus integrates the extracellular apoptotic stimulus by inducing MOMP.

Furthermore, phosphorylation of caspases and upstream adapter proteins has been reported as regulatory mechanisms in cell death pathways (Kitazumi and

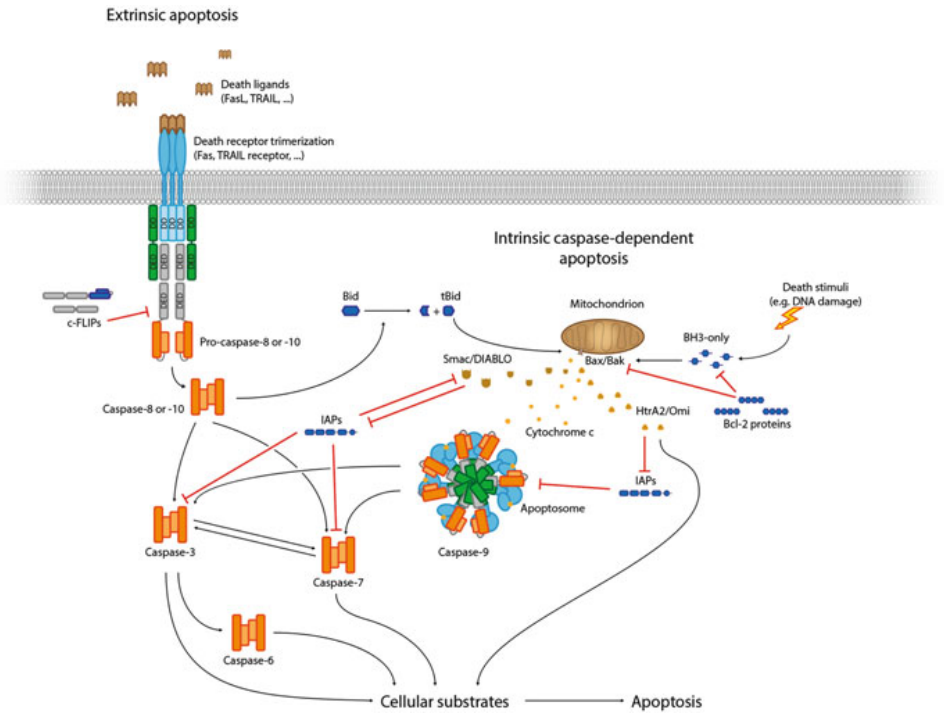

Fig. 8.5 Regulatory network. Activation of caspase-8 or -10 at the DISC can be repressed by cFLIPs. Once activated, these caspases cleave downstream executioner caspases that trigger the apoptotic pathway. In addition, caspase-8 or -10 can produce tBid that stimulates the intrinsic caspase-dependent apoptotic pathway. This pathway is also triggered by intracellular death stimuli like DNA damage and activates pro-apoptotic Bcl-2 proteins, known as the subfamily BH3-only proteins. These proteins are regulated by anti-apoptotic Bcl-2 family members that provide a first threshold for death stimuli. The BH3-only proteins Bax and Bak possess a pore forming activity to induce MOMP. Released mitochondrial proteins then trigger the progression of the intrinsic apoptotic pathway: cytochrome c binds to Apaf-1 and induces apoptosome formation and caspase-9 activation. Released Smac/DIABLO is binding and inhibiting IAPs and HtrA2/Omi not only antagonizes IAPs but also cleave cellular substrates. Additional important regulators of apoptosis are the IAPs: they specifically inhibit caspases and are able to counteract with Smac/DIABLO in anti-apoptotic manner

Tsukahara 2011). For instance, caspase-9 can be phosphorylated at the catalytic domain residue Ser-196 and in the CARD at Thr-125, which both prevents caspase-9 activation (Cardone et al. 1998; Allan et al. 2003). Phosphorylation of caspase-8 at Ser-364 and caspase-3 at Ser-150 has been reported as survival signals during neutrophil apoptosis (Alvarado-Kristensson et al. 2004). Other phosphorylation sites on caspase-8 have been discovered (Tyr-310, Tyr-397, Tyr-465) and revealed a dynamic post-translational regulation of apoptosis in neutrophils (Jia et al. 2008). These findings strongly emphasize the important control functions of kinases and phosphatases in death pathways.

DOI: 10.1007/978-3-7091-0885-7_8,

8.3.7.1 X-Linked Inhibitor of Apoptosis Protein (XIAP)

A well-studied IAP family member is the X-linked IAP (XIAP) that is able to directly inhibit caspases-3, -7 and -9 (Deveraux et al. 1997, 1998). It is characterized by three baculoviral IAP repeat (BIR1–3) modules, an ubiquitin associated (UBA) domain and a C-terminal RING domain. Structural investigations on XIAP binding to caspase-3, -7 and -9 unraveled two different binding and inhibition mechanisms, which are mainly related to binding of linker regions near the BIR2 and BIR3 domains, respectively (Chai et al. 2001a; Riedl et al. 2001b; Shiozaki et al. 2003). In addition, XIAP can simultaneously bind and inhibit both, initiator caspase-9 and executioner caspase-3 (Bratton et al. 2002) at a tightly packed "holo-apoptosome" that not only recruits pro-caspase-9 but also binds active caspase-3 (Yuan et al. 2011).

Crystal structures of caspase-3 and -7 have been reported with a truncated XIAP containing a short N-terminal linker peptide and the BIR2 domain (Fig. 8.6a). Remarkably, both homologue caspases showed the same principle of inhibition: The XIAP residues involved in binding interactions are located in the peptide linker, which lies inside the substrate-binding cleft of the enzyme in opposite direction when compared to the observed natural binding of substrate (Riedl et al. 2001b). Furthermore, the S_4 pocket is occupied by Asp-148 of XIAP whereas upstream residues sterically block the access to the S1 and S1′ subsites and thus competitively inhibit the enzyme.

The complex of caspase-9 with the XIAP-BIR3 domain revealed a completely different inhibition mechanism: The BIR3 domain binds at the caspase-9 dimer interface of the catalytic domain and consequently traps caspase-9 in an inactive, monomeric form thus preventing active site formation (Shiozaki et al. 2003) (Fig. 8.6b). This interaction is further provoked by the N-terminal peptide of the small subunit of caspase-9, which interacts with BIR3 at the so-called Smac pocket (Shiozaki et al. 2003).

As other IAPs, XIAP can regulate the apoptotic pathway via its C-terminal RING domain. Ubiquitination of caspase-3 mediates proteosomal degradation (Suzuki et al. 2001) while RING domain truncations of XIAP lead to elevated caspase-3 activity (Schile et al. 2008). In contrast, ubiquitination of AIF is nondegradative but also attenuates its death-inducing activity (Lewis et al. 2011).

8.3.7.2 c-FLIP: A Structural Homologue of Caspase-8

The family of FLICE-inhibitory proteins (FLIPs) has been discovered in viral genomes (termed vFLIPs) and supports viral infections by down regulation of cellular death responses (Thome et al. 1997). In humans, numerous splice variants of cellular FLIPs (c-FLIPs) have been reported whereas three isoforms are expressed (Krueger et al. 2001; Golks et al. 2005; Safa 2012). The two known short forms, c-$FLIP_S$ and c-$FLIP_R$, consist of two DEDs that can be recruited to the

DISC where they block binding of caspase-8 and thus prevent a death-receptor mediated apoptosis (Krueger et al. 2001; Golks et al. 2005).

A longer isoform c-FLIP$_L$ is structurally similar to caspase-8 and comprises two DED and a C-terminal caspase-like domain lacking enzymatic activity (Yu et al. 2009). Its regulation of the extrinsic-apoptotic pathway is more adaptive and concentration dependent compared to its short isoforms. On one hand, FLIP$_L$ is recruited to the DISC where it can form heterodimers with catalytic domains of caspase-8 at physiological conditions and thus mediates its activation (Chang et al. 2002). In contrast, a high expression level of FLIP$_L$ induces partial autocatalytic processing of caspase-8 (Krueger et al. 2001), which then remains at the DISC-platform, cleaves local substrates like RIP1 and prevents apoptosis (Micheau et al. 2002; Kavuri et al. 2011). Furthermore, c-FLIP$_L$ is also known as a limiting factor of kinase-dependent necrosis (reviewed by Green et al. 2011; Oberst et al. 2011).

The highly variable signal transduction from death receptors to caspase-8 and c-FLIP$_L$ strongly emphasizes the critical interplay of these proteins in regulation of pro- or anti-apoptotic responses.

8.3.7.3 Non-natural Inhibition: Designed Ankyrin Repeat Proteins (DARPins)

Gene knockouts or artificial inhibition of a specific protein are general methods used in cell biology to target its distinct role in diverse cellular processes. These methods have also been applied to unravel the known functions of the caspase family members, which have been broadly studied in cells derived from gene knockout mice. However, the production of a knockout mouse is a time-consuming process, not always successful or occasionally inaccurate, as shown for the caspase-1 deficient strain 129 that also harbors a deficient caspase-11 (Kayagaki et al. 2011).

A protein knock-out by specific inhibition is a second approach to study the role of a specific protein in cellular processes. In the case of caspases this is rather difficult to achieve due to the high structural homology of these enzymes. The commercially available substrate-based inhibitors target the conserved active site and are thus not very specific (McStay et al. 2008). In contrast, selected binding proteins like anti- and nanobodies or designed ankyrin repeat proteins (DARPins) bind via an increased protein-protein interaction surface that may enhance the specificity. Furthermore, the binding may induce functional modification of the target protein, as shown in several examples like a Fas receptor agonistic antibody (Chodorge et al. 2012) or an ABC transporter modulating DARPin (Seeger et al. 2012).

Highly specific inhibition of caspase-2 and -3 has been achieved with two different DARPins (Schweizer et al. 2007; Schroeder et al. 2013). These binding proteins were designed based on the ankyrin protein scaffold and usually contain two or three internal repeats that are sandwiched between a N- and C-terminal capping repeat (Binz et al. 2004). Each internal repeat obtains six randomized positions that are potentially involved in interactions, forming a diverse library with at least 10^{10} different molecules that can be selected by phage- or ribosome

DOI: 10.1007/978-3-7091-0885-7_8,

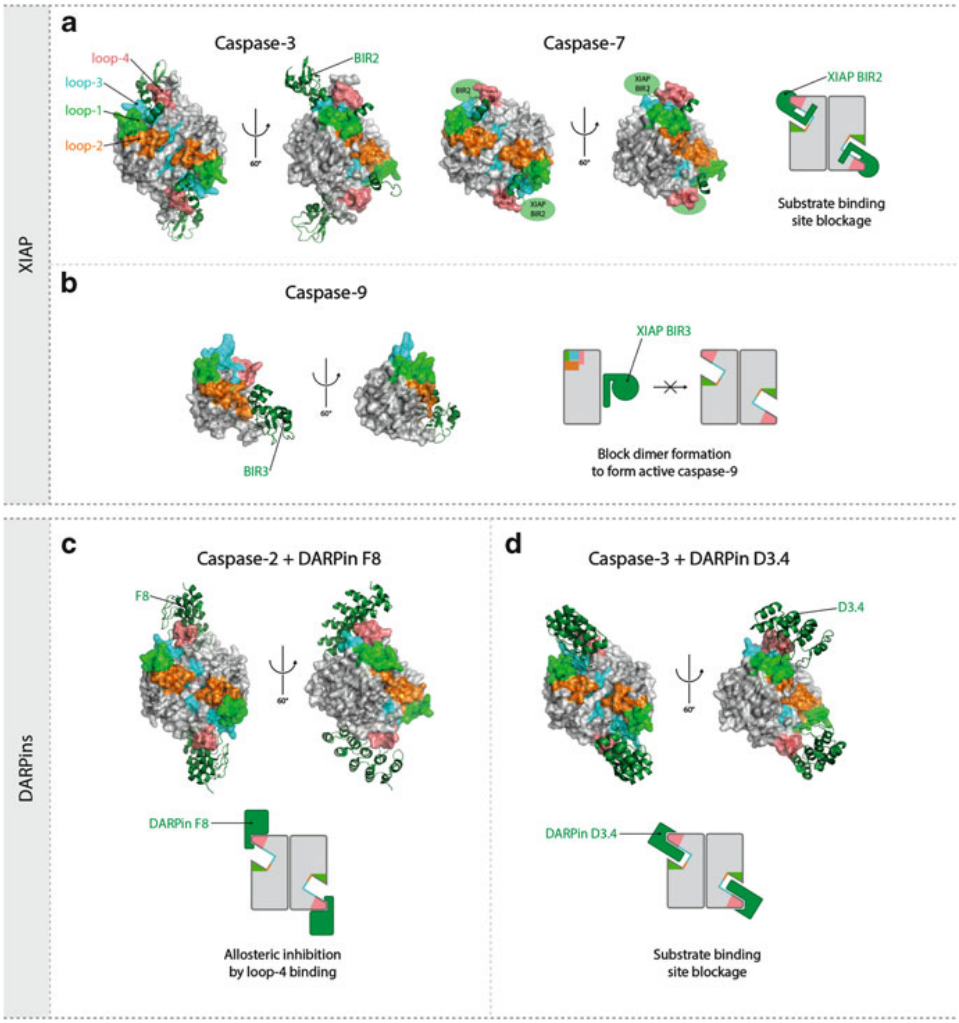

Fig. 8.6 Specific inhibition. (**a**) XIAP inhibition of caspase-3 and -7. Crystal structures of XIAP-BIR2 domain in complex with either caspase-3 (1I3O) or caspase-7 (1I51) revealed a competitive inhibition mechanism by direct binding into the substrate-binding groove. The BIR2 domain was crystallized in both complexes, although no electron density for the domain could be observed in the complex with caspase-7. (**b**) The crystal structure of XIAP-BIR3 domain in complex with caspase-9 (1NW9) unraveled a different inhibition mechanism: BIR3 interacts with residues in the dimer interface and thus prevents a dimerization of caspase-9. (**c**) Complex structure of caspase-2 with DARPin F8 (2P2C) showed a binding of the DARPin to loop-4. This binding stabilizes the loop in a distinct conformation compared to substrate bound caspase-2 and thus inhibits the enzyme allosteric. (**d**) DARPin D3.4 binds to caspase-3 (2XZD) at the substrate-binding cleft and inhibits the enzyme in a linear competitive mechanism

display (Hanes and Plückthun 1997; Steiner et al. 2008). Selected DARPins combine the advantages of high affinity and stability with high purity and expression yields in a cysteine less framework.

The caspase-2 specific DARPin (AR_F8) binds and inhibits the enzyme with a tight binding mixed-type inhibition mechanism (Schweizer et al. 2007). AR_F8 binding to caspase-2 occurs primarily at the binding groove forming loop-4 and stabilizes a distinct conformation of this loop compared to substrate analogue bound caspase-2 (Fig. 8.6c). Additional structural rearrangements have been observed N-terminal at the small subunit of the adjacent catalytic domain that finally results in a displacement of the catalytic residue Cys-285. Altogether, the structural and kinetic analysis of this DARPin clearly revealed an allosteric inhibition of caspase-2 with high specificity.

Another selected DARPin (D3.4) has been reported to specifically target caspase-3 (Schroeder et al. 2013). This binder inhibits the protease in a tight binding and purely competitive mechanism (Fig. 8.6d). Structural data uncovered a complex formation of D3.4 and caspase-3 at the active site cleft leading to obstructed binding pockets. D3.4 positions its residue Asp-45 inside the S_4 pocket mimicking a natural peptide binding. Further interactions of the second internal repeat lock the caspase-3 residue Tyr-204 in a closed state that occupies the subsite S_2 as seen in the XIAP caspase-3 complex structure (Riedl et al. 2001b). Although the structural mechanism of inhibition displays similarities to XIAP, the active site occupying peptide is not in a reversal orientation. Furthermore, this binder is a decent example for active site directed inhibition that is combined with an enlarged target-inhibitor interaction surface to achieve high specificity.

8.4 Caspase-Related Diseases

The important roles that caspases mediate in cell death and differentiation pathways are highly regulated and often include redundant mechanisms. However, their importance in cellular processes also increases the susceptibility for severe diseases in case of misregulation. For instance, alteration of the apoptotic pathway is related to cancer, neurological and cardiovascular disorders as well as autoimmune diseases (reviewed by Favaloro et al. 2012).

Cancer development and progression is highly connected to overexpression of regulatory Bcl-2 proteins, down-regulation of apoptosome forming Apaf-1 and modulation of death receptor pathways by reduced or increased expression of death receptors or death ligands, respectively (Favaloro et al. 2012). Direct mutations of the caspase genes can lead to a reduction or loss of enzymatic activity, while other studies reported dominant negative caspase variants that prevent activation of the wild type form (reviewed by Olsson and Zhivotovsky 2011). This results in a decrease of apoptotic capacity that may favor cancer manifestation. However, there is little evidence for tumorigenesis induced by an individual caspase-mutant that indeed emphasizes a redundant network with tumor suppressor functionalities (Olsson and Zhivotovsky 2011).

Caspases have been reported as major conductors in the development of Alzheimer's disease (reviewed by Rohn 2010). Two of the major pathological

DOI: 10.1007/978-3-7091-0885-7_8,

markers in Alzheimer's disease are the formation of neurofibrillary tangles (NFTs), consisting of hyperphosphorylated microtubule-associated protein tau and the extracellular deposition of amyloid-β (Aβ) in plaques. Aβ is created after sequential proteolysis of the amyloid precursor protein (APP) by β- and γ-secretases. However, caspase involvement of APP cleavage has also been observed (Zhang et al. 2011).

In addition, it has been proposed that the presence of Aβ stimulates caspase activation that leads to tau cleavage, predominantly mediated by caspase-3 and -6, and a following tau hyperphosphorylation (Rohn 2010). Moreover, this hypothesis of Aβ-linked tau cleavage has been verified using a transgenic mouse model that overexpresses the antiapoptotic protein Bcl-2 (Rohn et al. 2008). Thus, the role of caspases in Alzheimer's disease lays assumably not only terminal in the execution of neuronal cell death but also proximal in the initiation of the disease mechanism.

Caspase involvement has also been shown in Huntington's disease, a neuronal disorder that is caused by mutation of the huntingtin (htt) protein (reviewed by Ehrnhoefer et al. 2011). Disease related htt mutations lead to an abnormal elongation of a polyglutamine stretch in the N-terminal region, which is supposed to prevent aggregation in wildtype proteins by turnover regulation (Ehrnhoefer et al. 2011). Both, either wildtype or mutant proteins can be processed by proteases, including the caspase family.

N-terminal cleavage fragments of the htt mutant have been reported to increase the apoptotic susceptibility in dependence of fragment and polyglutamine extension length (Hackam et al. 1998). Removal of the five predicted caspase cleavage site in htt could reduce its toxicity and furthermore unraveled a specific caspase-6 cleavage site that is crucial in the development of Huntington's disease symptoms (Graham et al. 2006). Active caspase-6 has been proposed as an early disease marker due to its activation before the manifestation of the first motor abnormalities (Graham et al. 2010).

Activation of caspase-6 and downstream cleavage of this enzyme has been shown to be a fundamental step in the development of neurodegenerative diseases and highlights its potential as a novel therapeutic target (reviewed by Graham et al. 2011).

Alterations in the inflammasome formation mechanisms can lead to hyperactivation of caspase-1 and extensive production of IL-1β and IL-18, which can be related to autoimmune diseases (reviewed by Lamkanfi et al. 2011). For instance, enhanced expression of caspase-1 and IL-18 has been found in patients suffering from multiple sclerosis (Huang et al. 2004).

8.5 Concluding Remarks

Death pathways are fundamental mechanisms of multicellular organisms to ensure the correct development, tissue maintenance and homeostasis. The diverse processes are tightly regulated to prevent accidental cellular demise but also to facilitate a fast removal of cells upon cell death activation. Its redundant system of overlapping, distinctive pathways secures the multicellular integrity upon various cytotoxic stimuli in an exceptional manner.

The particular death pathways of apoptosis and pyroptosis are primarily driven by caspases. These enzymes are classified according to their activity related to inflammation and apoptosis. Active caspases cleave specific substrates, which results in either activation of demise effectors or deactivation of survival proteins that both accelerate cell destruction. Thus, a precise regulation is indispensable and occurs at numerous steps. Although this highly specific and minimal error-prone regulatory system has been evolved with redundancy, imbalances result in severe diseases including cancer and neurodegenerative disorders.

In conclusion, modern research unraveled a broad contribution of caspases not only in cell death mechanism but also in inflammatory responses and tissue protection by anti-inflammatory activity during apoptosis. Thus, researchers began to reconsider the general classification of inflammatory and apoptotic caspases. Martin et al. (2012) recently suggested a new classification of positive and negative regulators of inflammation: Besides the pro-inflammatory caspases-1, -4 and -5, the nowadays known apoptotic caspases are categorized as anti-inflammatory proteases. Overall, it further underlines the remarkable role of this protease family in numerous distinctive cellular processes besides death pathways.

Acknowledgement This work was supported by the Swiss National Science Foundation grant 310030-122342 to Markus G. Grütter.

References

Agard NJ, Wells JA (2009) Methods for the proteomic identification of protease substrates. Curr Opin Chem Biol 13(5–6):503–509

Agostini L, Martinon F, Burns K, McDermott MF, Hawkins PN, Tschopp J (2004) NALP3 forms an IL-1beta-processing inflammasome with increased activity in Muckle-Wells autoinflammatory disorder. Immunity 20(3):319–325

Akita K, Ohtsuki T, Nukada Y, Tanimoto T, Namba M, Okura T, Takakura-Yamamoto R, Torigoe K, Gu Y, Su MS, Fujii M, Satoh-Itoh M, Yamamoto K, Kohno K, Ikeda M, Kurimoto M (1997) Involvement of caspase-1 and caspase-3 in the production and processing of mature human interleukin 18 in monocytic THP.1 cells. J Biol Chem 272(42):26595–26603

Allan LA, Morrice N, Brady S, Magee G, Pathak S, Clarke PR (2003) Inhibition of caspase-9 through phosphorylation at Thr 125 by ERK MAPK. Nat Cell Biol 5(7):647–654

Alnemri ES, Livingston DJ, Nicholson DW, Salvesen G, Thornberry NA, Wong WW, Yuan J (1996) Human ICE/CED-3 protease nomenclature. Cell 87(2):171

Alvarado-Kristensson M, Melander F, Leandersson K, Rönnstrand L, Wernstedt C, Andersson T (2004) p38-MAPK signals survival by phosphorylation of caspase-8 and caspase-3 in human neutrophils. J Exp Med 199(4):449–458

Binz HK, Amstutz P, Kohl A, Stumpp MT, Briand C, Forrer P, Grütter MG, Plückthun A (2004) High-affinity binders selected from designed ankyrin repeat protein libraries. Nat Biotechnol 22(5):575–582

Boyd SE, Pike RN, Rudy GB, Whisstock JC, Garcia de la Banda M (2005) PoPS: a computational tool for modeling and predicting protease specificity. J Bioinform Comput Biol 3(3):551–585

Bratton SB, Lewis J, Butterworth M, Duckett CS, Cohen GM (2002) XIAP inhibition of caspase-3 preserves its association with the Apaf-1 apoptosome and prevents CD95- and Bax-induced apoptosis. Cell Death Differ 9(9):881–892

DOI: 10.1007/978-3-7091-0885-7_8,

Brennan MA, Cookson BT (2000) Salmonella induces macrophage death by caspase-1-dependent necrosis. Mol Microbiol 38(1):31–40

Cardone MH, Roy N, Stennicke HR, Salvesen GS, Franke TF, Stanbridge E, Frisch S, Reed JC (1998) Regulation of cell death protease caspase-9 by phosphorylation. Science 282(5392): 1318–1321

Center DM, Cruikshank WW, Zhang Y (2004) Nuclear pro-IL-16 regulation of T cell proliferation: p27(KIP1)-dependent G0/G1 arrest mediated by inhibition of Skp2 transcription. J Immunol 172(3):1654–1660

Chai J, Shiozaki E, Srinivasula SM, Wu Q, Datta P, Alnemri ES, Shi Y, Dataa P (2001a) Structural basis of caspase-7 inhibition by XIAP. Cell 104(5):769–780

Chai J, Wu Q, Shiozaki E, Srinivasula SM, Alnemri ES, Shi Y (2001b) Crystal structure of a procaspase-7 zymogen: mechanisms of activation and substrate binding. Cell 107(3):399–407

Chang DW, Xing Z, Pan Y, Algeciras-Schimnich A, Barnhart BC, Yaish-Ohad S, Peter ME, Yang X (2002) c-FLIP(L) is a dual function regulator for caspase-8 activation and CD95-mediated apoptosis. EMBO J 21(14):3704–3714

Chaudhary PM, Eby M, Jasmin A, Bookwalter A, Murray J, Hood L (1997) Death receptor 5, a new member of the TNFR family, and DR4 induce FADD-dependent apoptosis and activate the NF-kappaB pathway. Immunity 7(6):821–830

Chinnaiyan AM, O'Rourke K, Tewari M, Dixit VM (1995) FADD, a novel death domain-containing protein, interacts with the death domain of Fas and initiates apoptosis. Cell 81 (4):505–512

Chodorge M, Züger S, Stirnimann C, Briand C, Jermutus L, Grütter MG, Minter RR (2012) A series of Fas receptor agonist antibodies that demonstrate an inverse correlation between affinity and potency. Cell Death Differ 19(7):1187–1195

Chupp GL, Wright EA, Wu D, Vallen-Mashikian M, Cruikshank WW, Center DM, Kornfeld H, Berman JS (1998) Tissue and T cell distribution of precursor and mature IL-16. J Immunol 161 (6):3114–3119

Coleman ML, Sahai EA, Yeo M, Bosch M, Dewar A, Olson MF (2001) Membrane blebbing during apoptosis results from caspase-mediated activation of ROCK I. Nat Cell Biol 3(4): 339–345

Conradt B, Horvitz HR (1998) The C. elegans protein EGL-1 is required for programmed cell death and interacts with the Bcl-2-like protein CED-9. Cell 93(4):519–529

Cookson BT, Brennan MA (2001) Pro-inflammatory programmed cell death. Trends Microbiol 9 (3):113–114

Cooper DM, Pio F, Thi EP, Theilmann D, Lowenberger C (2007) Characterization of Aedes Dredd: a novel initiator caspase from the yellow fever mosquito, Aedes aegypti. Insect Biochem Mol Biol 37(6):559–569

de Alba E (2009) Structure and interdomain dynamics of apoptosis-associated speck-like protein containing a CARD (ASC). J Biol Chem 284(47):32932–32941

Denault J-B, Salvesen GS (2003) Human caspase-7 activity and regulation by its N-terminal peptide. J Biol Chem 278(36):34042–34050

Denecker G, Ovaere P, Vandenabeele P, Declercq W (2008) Caspase-14 reveals its secrets. J Cell Biol 180(3):451–458

Deveraux QL, Takahashi R, Salvesen GS, Reed JC (1997) X-linked IAP is a direct inhibitor of cell-death proteases. Nature 388(6639):300–304

Deveraux QL, Roy N, Stennicke HR, Van Arsdale T, Zhou Q, Srinivasula SM, Alnemri ES, Salvesen GS, Reed JC (1998) IAPs block apoptotic events induced by caspase-8 and cytochrome c by direct inhibition of distinct caspases. EMBO J 17(8):2215–2223

Duan H, Dixit VM (1997) RAIDD is a new 'death' adaptor molecule. Nature 385(6611):86–89

Eckhart L, Ballaun C, Hermann M, VandeBerg JL, Sipos W, Uthman A, Fischer H, Tschachler E (2008) Identification of novel mammalian caspases reveals an important role of gene loss in shaping the human caspase repertoire. Mol Biol Evol 25(5):831–841

Ehrnhoefer DE, Sutton L, Hayden MR (2011) Small changes, big impact: posttranslational modifications and function of huntingtin in Huntington disease. Neuroscientist 17(5):475–492

Elliott JM, Rouge L, Wiesmann C, Scheer JM (2009) Crystal structure of procaspase-1 zymogen domain reveals insight into inflammatory caspase autoactivation. J Biol Chem 284(10): 6546–6553

Ellis HM, Horvitz HR (1986) Genetic control of programmed cell death in the nematode C. elegans. Cell 44(6):817–829

Faustin B, Lartigue L, Bruey J-M, Luciano F, Sergienko E, Bailly-Maitre B, Volkmann N, Hanein D, Rouiller I, Reed JC (2007) Reconstituted NALP1 inflammasome reveals two-step mechanism of caspase-1 activation. Mol Cell 25(5):713–724

Favaloro B, Allocati N, Graziano V, Di Ilio C, De Laurenzi V (2012) Role of apoptosis in disease. Aging 4(5):330–349

Flemming W (1885) Ueber die Bildung von Richtungsfiguren in Säugethiereiern beim Untergang Graaf'scher Follikel. Arch Anat Entw Gesch (Veit & Comp). 221–244

Fuentes-Prior P, Salvesen GS (2004) The protein structures that shape caspase activity, specificity, activation and inhibition. Biochem J 384(Pt 2):201–232

Fulda S, Vucic D (2012) Targeting IAP proteins for therapeutic intervention in cancer. Nat Rev Drug Discov 11(2):109–124

Galluzzi L, Vitale I, Abrams JM, Alnemri ES, Baehrecke EH, Blagosklonny MV, Dawson TM, Dawson VL, El-Deiry WS, Fulda S, Gottlieb E, Green DR, Hengartner MO, Kepp O, Knight RA, Kumar S, Lipton SA, Lu X, Madeo F, Malorni W, Mehlen P, Nuñez G, Peter ME, Piacentini M, Rubinsztein DC, Shi Y, Simon H-U, Vandenabeele P, White E, Yuan J, Zhivotovsky B, Melino G, Kroemer G (2012) Molecular definitions of cell death subroutines: recommendations of the Nomenclature Committee on Cell Death 2012. Cell Death Differ 19(1):107–120

Germain M, Affar EB, D'Amours D, Dixit VM, Salvesen GS, Poirier GG (1999) Cleavage of automodified poly(ADP-ribose) polymerase during apoptosis. Evidence for involvement of caspase-7. J Biol Chem 274(40):28379–28384

Golks A, Brenner D, Fritsch C, Krammer PH, Lavrik IN (2005) c-FLIPR, a new regulator of death receptor-induced apoptosis. J Biol Chem 280(15):14507–14513

Graham RK, Deng Y, Slow EJ, Haigh B, Bissada N, Lu G, Pearson J, Shehadeh J, Bertram L, Murphy Z, Warby SC, Doty CN, Roy S, Wellington CL, Leavitt BR, Raymond LA, Nicholson DW, Hayden MR (2006) Cleavage at the caspase-6 site is required for neuronal dysfunction and degeneration due to mutant huntingtin. Cell 125(6):1179–1191

Graham RK, Deng Y, Carroll J, Vaid K, Cowan C, Pouladi MA, Metzler M, Bissada N, Wang L, Faull RLM, Gray M, Yang XW, Raymond LA, Hayden MR (2010) Cleavage at the 586 amino acid caspase-6 site in mutant huntingtin influences caspase-6 activation in vivo. J Neurosci 30 (45):15019–15029

Graham RK, Ehrnhoefer DE, Hayden MR (2011) Caspase-6 and neurodegeneration. Trends Neurosci 34(12):646–656

Green DR, Oberst A, Dillon CP, Weinlich R, Salvesen GS (2011) RIPK-dependent necrosis and its regulation by caspases: a mystery in five acts. Mol Cell 44(1):9–16

Grimsley C, Ravichandran KS (2003) Cues for apoptotic cell engulfment: eat-me, don't eat-me and come-get-me signals. Trends Cell Biol 13(12):648–656

Gu Y, Kuida K, Tsutsui H, Ku G, Hsiao K, Fleming MA, Hayashi N, Higashino K, Okamura H, Nakanishi K, Kurimoto M, Tanimoto T, Flavell RA, Sato V, Harding MW, Livingston DJ, Su MS (1997) Activation of interferon-gamma inducing factor mediated by interleukin-1beta converting enzyme. Science 275(5297):206–209

Hackam AS, Singaraja R, Wellington CL, Metzler M, McCutcheon K, Zhang T, Kalchman M, Hayden MR (1998) The influence of huntingtin protein size on nuclear localization and cellular toxicity. J Cell Biol 141(5):1097–1105

Hall A (1998) Rho GTPases and the actin cytoskeleton. Science 279(5350):509–514

Hanes J, Plückthun A (1997) In vitro selection and evolution of functional proteins by using ribosome display. Proc Natl Acad Sci U S A 94(10):4937–4942

DOI: 10.1007/978-3-7091-0885-7_8,

Hardwick JM, Chen Y-b, Jonas EA (2012) Multipolar functions of BCL-2 proteins link energetics to apoptosis. Trends Cell Biol 22(6):318–328

Hardy JA, Lam J, Nguyen JT, O'Brien T, Wells JA (2004) Discovery of an allosteric site in the caspases. Proc Natl Acad Sci U S A 101(34):12461–12466

Hengartner MO, Ellis RE, Horvitz HR (1992) Caenorhabditis elegans gene ced-9 protects cells from programmed cell death. Nature 356(6369):494–499

Hitomi J, Christofferson DE, Ng A, Yao J, Degterev A, Xavier RJ, Yuan J (2008) Identification of a molecular signaling network that regulates a cellular necrotic cell death pathway. Cell 135 (7):1311–1323

Hoste E, Denecker G, Gilbert B, Van Nieuwerburgh F, van der Fits L, Asselbergh B, De Rycke R, Hachem J-P, Deforce D, Prens EP, Vandenabeele P, Declercq W (2013) Caspase-14-deficient mice are more prone to the development of parakeratosis. J Invest Dermatol 133(3):742–750

Huang W-X, Huang P, Hillert J (2004) Increased expression of caspase-1 and interleukin-18 in peripheral blood mononuclear cells in patients with multiple sclerosis. Mult Scler 10(5): 482–487

Hughes MA, Harper N, Butterworth M, Cain K, Cohen GM, Macfarlane M (2009) Reconstitution of the death-inducing signaling complex reveals a substrate switch that determines CD95-mediated death or survival. Mol Cell 35(3):265–279

Javle M, Curtin NJ (2011) The role of PARP in DNA repair and its therapeutic exploitation. Br J Cancer 105(8):1114–1122

Jia SH, Parodo J, Kapus A, Rotstein OD, Marshall JC (2008) Dynamic regulation of neutrophil survival through tyrosine phosphorylation or dephosphorylation of caspase-8. J Biol Chem 283 (9):5402–5413

Kamens J, Paskind M, Hugunin M, Talanian RV, Allen H, Banach D, Bump N, Hackett M, Johnston CG, Li P (1995) Identification and characterization of ICH-2, a novel member of the interleukin-1 beta-converting enzyme family of cysteine proteases. J Biol Chem 270(25): 15250–15256

Kavuri SM, Geserick P, Berg D, Dimitrova DP, Feoktistova M, Siegmund D, Gollnick H, Neumann M, Wajant H, Leverkus M (2011) Cellular FLICE-inhibitory protein (cFLIP) isoforms block CD95- and TRAIL death receptor-induced gene induction irrespective of processing of caspase-8 or cFLIP in the death-inducing signaling complex. J Biol Chem 286 (19):16631–16646

Kayagaki N, Warming S, Lamkanfi M, Vande Walle L, Louie S, Dong J, Newton K, Qu Y, Liu J, Heldens S, Zhang J, Lee WP, Roose-Girma M, Dixit VM (2011) Non-canonical inflammasome activation targets caspase-11. Nature 479(7371):117–121

Keller N, Mares J, Zerbe O, Grütter MG (2009) Structural and biochemical studies on procaspase-8: new insights on initiator caspase activation. Structure 17(3):438–448

Kerr JF, Wyllie AH, Currie AR (1972) Apoptosis: a basic biological phenomenon with wide-ranging implications in tissue kinetics. Br J Cancer 26(4):239–257

Kersse K, Verspurten J, Vanden Berghe T, Vandenabeele P (2011) The death-fold superfamily of homotypic interaction motifs. Trends Biochem Sci 36(10):541–552

Kischkel FC, Hellbardt S, Behrmann I, Germer M, Pawlita M, Krammer PH, Peter ME (1995) Cytotoxicity-dependent APO-1 (Fas/CD95)-associated proteins form a death-inducing signaling complex (DISC) with the receptor. EMBO J 14(22):5579–5588

Kitazumi I, Tsukahara M (2011) Regulation of DNA fragmentation: the role of caspases and phosphorylation. FEBS J 278(3):427–441

Koenig U, Eckhart L, Tschachler E (2001) Evidence that caspase-13 is not a human but a bovine gene. Biochem Biophys Res Commun 285(5):1150–1154

Krijnen PAJ, Sipkens JA, Molling JW, Rauwerda JA, Stehouwer CDA, Muller A, Paulus WJ, van Nieuw Amerongen GP, Hack CE, Verhoeven AJ, van Hinsbergh VWM, Niessen HWM (2010) Inhibition of Rho-ROCK signaling induces apoptotic and non-apoptotic PS exposure in cardiomyocytes via inhibition of flippase. J Mol Cell Cardiol 49(5):781–790

Krippner-Heidenreich A, Talanian RV, Sekul R, Kraft R, Thole H, Ottleben H, Lüscher B (2001) Targeting of the transcription factor Max during apoptosis: phosphorylation-regulated cleavage by caspase-5 at an unusual glutamic acid residue in position P1. Biochem J 358(Pt 3):705–715

Krueger A, Schmitz I, Baumann S, Krammer PH, Kirchhoff S (2001) Cellular FLICE-inhibitory protein splice variants inhibit different steps of caspase-8 activation at the CD95 death-inducing signaling complex. J Biol Chem 276(23):20633–20640

Kumar S, Doumanis J (2000) The fly caspases. Cell Death Differ 7(11):1039–1044

Kuwana T, Mackey MR, Perkins G, Ellisman MH, Latterich M, Schneiter R, Green DR, Newmeyer DD (2002) Bid, Bax, and lipids cooperate to form supramolecular openings in the outer mitochondrial membrane. Cell 111(3):331–342

Lamkanfi M, Walle LV, Kanneganti T-D (2011) Deregulated inflammasome signaling in disease. Immunol Rev 243(1):163–173

Larsen BD, Rampalli S, Burns LE, Brunette S, Dilworth FJ, Megeney LA (2010) Caspase 3/caspase-activated DNase promote cell differentiation by inducing DNA strand breaks. Proc Natl Acad Sci U S A 107(9):4230–4235

Lazebnik YA, Kaufmann SH, Desnoyers S, Poirier GG, Earnshaw WC (1994) Cleavage of poly (ADP-ribose) polymerase by a proteinase with properties like ICE. Nature 371(6495):346–347

Lewis EM, Wilkinson AS, Davis NY, Horita DA, Wilkinson JC (2011) Nondegradative ubiquitination of apoptosis inducing factor (AIF) by X-linked inhibitor of apoptosis at a residue critical for AIF-mediated chromatin degradation. Biochemistry 50(51):11084–11096

Lüthi AU, Cullen SP, Mcneela EA, Duriez PJ, Afonina IS, Sheridan C, Brumatti G, Taylor RC, Kersse K, Vandenabeele P, Lavelle EC, Martin SJ (2009) Suppression of interleukin-33 bioactivity through proteolysis by apoptotic caspases. Immunity 31(1):84–98

Mandal D, Moitra PK, Saha S, Basu J (2002) Caspase 3 regulates phosphatidylserine externalization and phagocytosis of oxidatively stressed erythrocytes. FEBS Lett 513(2–3):184–188

Mariathasan S, Newton K, Monack DM, Vucic D, French DM, Lee WP, Roose-Girma M, Erickson S, Dixit VM (2004) Differential activation of the inflammasome by caspase-1 adaptors ASC and Ipaf. Nature 430(6996):213–218

Martin DA, Siegel RM, Zheng L, Lenardo MJ (1998) Membrane oligomerization and cleavage activates the caspase-8 (FLICE/MACHalpha1) death signal. J Biol Chem 273(8):4345–4349

Martin SJ, Henry CM, Cullen SP (2012) A perspective on mammalian caspases as positive and negative regulators of inflammation. Mol Cell 46(4):387–397

Martinon F, Tschopp J (2004) Inflammatory caspases: linking an intracellular innate immune system to autoinflammatory diseases. Cell 117(5):561–574

Martinon F, Tschopp J (2005) NLRs join TLRs as innate sensors of pathogens. Trends Immunol 26 (8):447–454

Martinon F, Burns K, Tschopp J (2002) The inflammasome: a molecular platform triggering activation of inflammatory caspases and processing of proIL-beta. Mol Cell 10(2):417–426

McStay GP, Salvesen GS, Green DR (2008) Overlapping cleavage motif selectivity of caspases: implications for analysis of apoptotic pathways. Cell Death Differ 15(2):322–331

Meergans T, Hildebrandt AK, Horak D, Haenisch C, Wendel A (2000) The short prodomain influences caspase-3 activation in HeLa cells. Biochem J 349(Pt 1):135–140

Miao EA, Mao DP, Yudkovsky N, Bonneau R, Lorang CG, Warren SE, Leaf IA, Aderem A (2010) Innate immune detection of the type III secretion apparatus through the NLRC4 inflammasome. Proc Natl Acad Sci U S A 107(7):3076–3080

Micheau O, Thome M, Schneider P, Holler N, Tschopp J, Nicholson DW, Briand C, Grütter MG (2002) The long form of FLIP is an activator of caspase-8 at the Fas death-inducing signaling complex. J Biol Chem 277(47):45162–45171

Nagata S, Nagase H, Kawane K, Mukae N, Fukuyama H (2003) Degradation of chromosomal DNA during apoptosis. Cell Death Differ 10(1):108–116

Oberst A, Dillon CP, Weinlich R, Mccormick LL, Fitzgerald P, Pop C, Hakem R, Salvesen GS, Green DR (2011) Catalytic activity of the caspase-8-FLIP(L) complex inhibits RIPK3-dependent necrosis. Nature 471(7338):363–367

DOI: 10.1007/978-3-7091-0885-7_8,

Olsson M, Zhivotovsky B (2011) Caspases and cancer. Cell Death Differ 18(9):1441–1449
Pan G, O'Rourke K, Chinnaiyan AM, Gentz R, Ebner R, Ni J, Dixit VM (1997) The receptor for the cytotoxic ligand TRAIL. Science 276(5309):111–113
Park HH, Logette E, Raunser S, Cuenin S, Walz T, Tschopp J, Wu H (2007) Death domain assembly mechanism revealed by crystal structure of the oligomeric PIDDosome core complex. Cell 128 (3):533–546
Pop C, Timmer J, Sperandio S, Salvesen GS (2006) The apoptosome activates caspase-9 by dimerization. Mol Cell 22(2):269–275
Pop C, Fitzgerald P, Green DR, Salvesen GS (2007) Role of proteolysis in caspase-8 activation and stabilization. Biochemistry 46(14):4398–4407
Qi S, Pang Y, Hu Q, Liu Q, Li H, Zhou Y, He T, Liang Q, Liu Y, Yuan X, Luo G, Li H, Wang J, Yan N, Shi Y (2010) Crystal structure of the Caenorhabditis elegans apoptosome reveals an octameric assembly of CED-4. Cell 141(3):446–457
Rao L, Perez D, White E (1996) Lamin proteolysis facilitates nuclear events during apoptosis. J Cell Biol 135(6 Pt 1):1441–1455
Rathinam VAK, Vanaja SK, Fitzgerald KA (2012) Regulation of inflammasome signaling. Nat Immunol 13(4):333–342
Rawlings ND, Barrett AJ, Bateman A (2012) MEROPS: the database of proteolytic enzymes, their substrates and inhibitors. Nucleic Acids Res 40:D343–D350
Reubold TF, Wohlgemuth S, Eschenburg S (2011) Crystal structure of full-length Apaf-1: how the death signal is relayed in the mitochondrial pathway of apoptosis. Structure 19(8):1074–1083
Riedl SJ, Fuentes-Prior P, Renatus M, Kairies N, Krapp S, Huber R, Salvesen GS, Bode W (2001a) Structural basis for the activation of human procaspase-7. Proc Natl Acad Sci U S A 98(26): 14790–14795
Riedl SJ, Renatus M, Schwarzenbacher R, Zhou Q, Sun C, Fesik SW, Liddington RC, Salvesen GS (2001b) Structural basis for the inhibition of caspase-3 by XIAP. Cell 104(5):791–800
Rohn TT (2010) The role of caspases in Alzheimer's disease; potential novel therapeutic opportunities. Apoptosis 15(11):1403–1409
Rohn TT, Vyas V, Hernandez-Estrada T, Nichol KE, Christie L-A, Head E (2008) Lack of pathology in a triple transgenic mouse model of Alzheimer's disease after overexpression of the anti-apoptotic protein Bcl-2. J Neurosci 28(12):3051–3059
Roschitzki-Voser H, Schroeder T, Lenherr ED, Frölich F, Schweizer A, Donepudi M, Ganesan R, Mittl PRE, Baici A, Grütter MG (2012) Human caspases in vitro: expression, purification and kinetic characterization. Protein Expr Purif 84(2):236–246
Rubinsztein DC, Shpilka T, Elazar Z (2012) Mechanisms of autophagosome biogenesis. Curr Biol 22(1):R29–R34
Safa AR (2012) c-FLIP, a master anti-apoptotic regulator. Exp Oncol 34(3):176–184
Sahoo M, Ceballos-Olvera I, Del Barrio L, Re F (2011) Role of the inflammasome, IL-1β, and IL-18 in bacterial infections. Scientific World J 11:2037–2050
Saleh M, Vaillancourt JP, Graham RK, Huyck M, Srinivasula SM, Alnemri ES, Steinberg MH, Nolan V, Baldwin CT, Hotchkiss RS, Buchman TG, Zehnbauer BA, Hayden MR, Farrer LA, Roy S, Nicholson DW (2004) Differential modulation of endotoxin responsiveness by human caspase-12 polymorphisms. Nature 429(6987):75–79
Salvesen GS, Dixit VM (1999) Caspase activation: the induced-proximity model. Proc Natl Acad Sci U S A 96(20):10964–10967
Scaffidi C, Schmitz I, Krammer PH, Peter ME (1999) The role of c-FLIP in modulation of CD95-induced apoptosis. J Biol Chem 274(3):1541–1548
Schile AJ, García-Fernández M, Steller H (2008) Regulation of apoptosis by XIAP ubiquitin-ligase activity. Genes Dev 22(16):2256–2266
Schroeder T, Barandun J, Flütsch A, Briand C, Mittl PRE, Grütter MG (2013) Specific inhibition of caspase-3 by a competitive DARPin: molecular mimicry between native and designed inhibitors. Structure 21(2):277–289

Schweizer A, Roschitzki-Voser H, Amstutz P, Briand C, Gulotti-Georgieva M, Prenosil E, Binz HK, Capitani G, Baici A, Plückthun A, Grütter MG (2007) Inhibition of caspase-2 by a designed ankyrin repeat protein: specificity, structure, and inhibition mechanism. Structure 15(5):625–636

Scott FL, Stec B, Pop C, Dobaczewska MK, Lee JJ, Monosov E, Robinson H, Salvesen GS, Schwarzenbacher R, Riedl SJ (2009) The Fas-FADD death domain complex structure unravels signalling by receptor clustering. Nature 457(7232):1019–1022

Seeger MA, Mittal A, Velamakanni S, Hohl M, Schauer S, Salaa I, Grütter MG, Van Veen HW (2012) Tuning the drug efflux activity of an ABC transporter in vivo by in vitro selected DARPin binders. PLoS One 7(6):e37845

Shiozaki EN, Chai J, Rigotti DJ, Riedl SJ, Li P, Srinivasula SM, Alnemri ES, Fairman R, Shi Y (2003) Mechanism of XIAP-mediated inhibition of caspase-9. Mol Cell 11(2):519–527

Soares J, Lowe MM, Jarstfer MB (2011) The catalytic subunit of human telomerase is a unique caspase-6 and caspase-7 substrate. Biochemistry 50(42):9046–9055

Sollberger G, Strittmatter GE, Kistowska M, French LE, Beer H-D (2012) Caspase-4 is required for activation of inflammasomes. J Immunol 188(4):1992–2000

Steiner D, Forrer P, Plückthun A (2008) Efficient selection of DARPins with sub-nanomolar affinities using SRP phage display. J Mol Biol 382(5):1211–1227

Steller H (2008) Regulation of apoptosis in Drosophila. Cell Death Differ 15(7):1132–1138

Stennicke HR, Deveraux QL, Humke EW, Reed JC, Dixit VM, Salvesen GS (1999) Caspase-9 can be activated without proteolytic processing. J Biol Chem 274(13):8359–8362

Suzuki Y, Nakabayashi Y, Takahashi R (2001) Ubiquitin-protein ligase activity of X-linked inhibitor of apoptosis protein promotes proteasomal degradation of caspase-3 and enhances its anti-apoptotic effect in Fas-induced cell death. Proc Natl Acad Sci U S A 98(15):8662–8667

Thome M, Schneider P, Hofmann K, Fickenscher H, Meinl E, Neipel F, Mattmann C, Burns K, Bodmer JL, Schröter M, Scaffidi C, Krammer PH, Peter ME, Tschopp J (1997) Viral FLICE-inhibitory proteins (FLIPs) prevent apoptosis induced by death receptors. Nature 386(6624): 517–521

Thornberry NA, Bull HG, Calaycay JR, Chapman KT, Howard AD, Kostura MJ, Miller DK, Molineaux SM, Weidner JR, Aunins J (1992) A novel heterodimeric cysteine protease is required for interleukin-1 beta processing in monocytes. Nature 356(6372):768–774

Thornberry NA, Rano TA, Peterson EP, Rasper DM, Timkey T, Garcia-Calvo M, Houtzager VM, Nordstrom PA, Roy S, Vaillancourt JP, Chapman KT, Nicholson DW (1997) A combinatorial approach defines specificities of members of the caspase family and granzyme B. Functional relationships established for key mediators of apoptosis. J Biol Chem 272(29):17907–17911

Timmer JC, Salvesen GS (2007) Caspase substrates. Cell Death Differ 14(1):66–72

Tinel A, Tschopp J (2004) The PIDDosome, a protein complex implicated in activation of caspase-2 in response to genotoxic stress. Science 304(5672):843–846

Tinel A, Janssens S, Lippens S, Cuenin S, Logette E, Jaccard B, Quadroni M, Tschopp J (2007) Autoproteolysis of PIDD marks the bifurcation between pro-death caspase-2 and pro-survival NF-kappaB pathway. EMBO J 26(1):197–208

Tsiatsiani L, Van Breusegem F, Gallois P, Zavialov A, Lam E, Bozhkov PV (2011) Metacaspases. Cell Death Differ 18(8):1279–1288

Vaughn DE, Rodriguez J, Lazebnik Y, Joshua-Tor L (1999) Crystal structure of Apaf-1 caspase recruitment domain: an alpha-helical Greek key fold for apoptotic signaling. J Mol Biol 293 (3):439–447

Vaux DL, Silke J (2005) IAPs, RINGs and ubiquitylation. Nat Rev Mol Cell Biol 6(4):287–297

Verhagen AM, Ekert PG, Pakusch M, Silke J, Connolly LM, Reid GE, Moritz RL, Simpson RJ, Vaux DL (2000) Identification of DIABLO, a mammalian protein that promotes apoptosis by binding to and antagonizing IAP proteins. Cell 102(1):43–53

Verhagen AM, Silke J, Ekert PG, Pakusch M, Kaufmann H, Connolly LM, Day CL, Tikoo A, Burke R, Wrobel C, Moritz RL, Simpson RJ, Vaux DL (2002) HtrA2 promotes cell death through its serine protease activity and its ability to antagonize inhibitor of apoptosis proteins. J Biol Chem 277(1):445–454

DOI: 10.1007/978-3-7091-0885-7_8,

Vucic D, Franklin MC, Wallweber HJA, Das K, Eckelman BP, Shin H, Elliott LO, Kadkhodayan S, Deshayes K, Salvesen GS, Fairbrother WJ (2005) Engineering ML-IAP to produce an extraordinarily potent caspase 9 inhibitor: implications for Smac-dependent anti-apoptotic activity of ML-IAP. Biochem J 385(Pt 1):11–20

Vucic D, Dixit VM, Wertz IE (2011) Ubiquitylation in apoptosis: a post-translational modification at the edge of life and death. Nat Rev Mol Cell Biol 12(7):439–452

Wachmann K, Pop C, Van Raam BJ, Drag M, Mace PD, Snipas SJ, Zmasek C, Schwarzenbacher R, Salvesen GS, Riedl SJ (2010) Activation and specificity of human caspase-10. Biochemistry 49(38):8307–8315

Walczak H, Degli-Esposti MA, Johnson RS, Smolak PJ, Waugh JY, Boiani N, Timour MS, Gerhart MJ, Schooley KA, Smith CA, Goodwin RG, Rauch CT (1997) TRAIL-R2: a novel apoptosis-mediating receptor for TRAIL. EMBO J 16(17):5386–5397

Wang L, Yang JK, Kabaleeswaran V, Rice AJ, Cruz AC, Park AY, Yin Q, Damko E, Jang SB, Raunser S, Robinson CV, Siegel RM, Walz T, Wu H (2010) The Fas-FADD death domain complex structure reveals the basis of DISC assembly and disease mutations. Nat Struct Mol Biol 17(11):1324–1329

Wilson KP, Black JA, Thomson JA, Kim EE, Griffith JP, Navia MA, Murcko MA, Chambers SP, Aldape RA, Raybuck SA (1994) Structure and mechanism of interleukin-1 beta converting enzyme. Nature 370(6487):270–275

Yang Z, Klionsky DJ (2009) An overview of the molecular mechanism of autophagy. Curr Top Microbiol Immunol 335:1–32

Yin XM, Wang K, Gross A, Zhao Y, Zinkel S, Klocke B, Roth KA, Korsmeyer SJ (1999) Bid-deficient mice are resistant to Fas-induced hepatocellular apoptosis. Nature 400 (6747):886–891

Yu JW, Jeffrey PD, Shi Y (2009) Mechanism of procaspase-8 activation by c-FLIPL. Proc Natl Acad Sci U S A 106(20):8169–8174

Yuan J, Shaham S, Ledoux S, Ellis HM, Horvitz HR (1993) The C. elegans cell death gene ced-3 encodes a protein similar to mammalian interleukin-1 beta-converting enzyme. Cell 75(4): 641–652

Yuan S, Yu X, Topf M, Ludtke SJ, Wang X, Akey CW (2010) Structure of an apoptosome-procaspase-9 CARD complex. Structure 18(5):571–583

Yuan S, Yu X, Asara JM, Heuser JE, Ludtke SJ, Akey CW (2011) The holo-apoptosome: activation of procaspase-9 and interactions with caspase-3. Structure 19(8):1084–1096

Zhang Y-w, Thompson R, Zhang H, Xu H (2011) APP processing in Alzheimer's disease. Mol Brain 4:3

Zhang Y, Center DM, Wu DM, Cruikshank WW, Yuan J, Andrews DW, Kornfeld H (1998) Processing and activation of pro-interleukin-16 by caspase-3. J Biol Chem 273(2):1144–1149

Ziegler U, Groscurth P (2004) Morphological features of cell death. News Physiol Sci 19:124–128

1.2 Designed Ankyrin Repeat Proteins

1.2.1 Development and scaffold design

In 2003, Binz *et al.* reported a novel scaffold for potential binding proteins that were later named Designed Ankyrin Repeat Proteins (DARPins).[1,3] The intended design of those proteins was based on a repetitive module that has been observed in ankyrin proteins. Such ankyrin repeat motives consist of a β-turn and two antiparallel α-helices and their involvement has been observed in various protein-protein interactions.[4] Sequence alignments of various ankyrin repeat proteins revealed a consensus sequence for the designed molecule: Invariant, conserved resides were defined as framework residues whereas non-conserved residues were subjected to randomization. Randomized positions were chosen primarily in the β-turn of the module (**figure 1a**) to ensure the overall stability of the module. In addition, N- and C-terminal repeats were developed to increase the proteins' thermodynamic stability by covering the hydrophobic core of the repeat modules with a hydrophilic protein surface. Thus, the resulting DARPin scaffold consists in general of 2 - 3 internal repeats flanked by a N- and C-terminal capping module usually referred to NI_2C and NI_3C DARPins (**figure 1b**).

Six randomized positions were intended to be any of the natural amino acids (except cysteine, glycine and proline) whereas one backbone residue (position z in **figure 1a**)

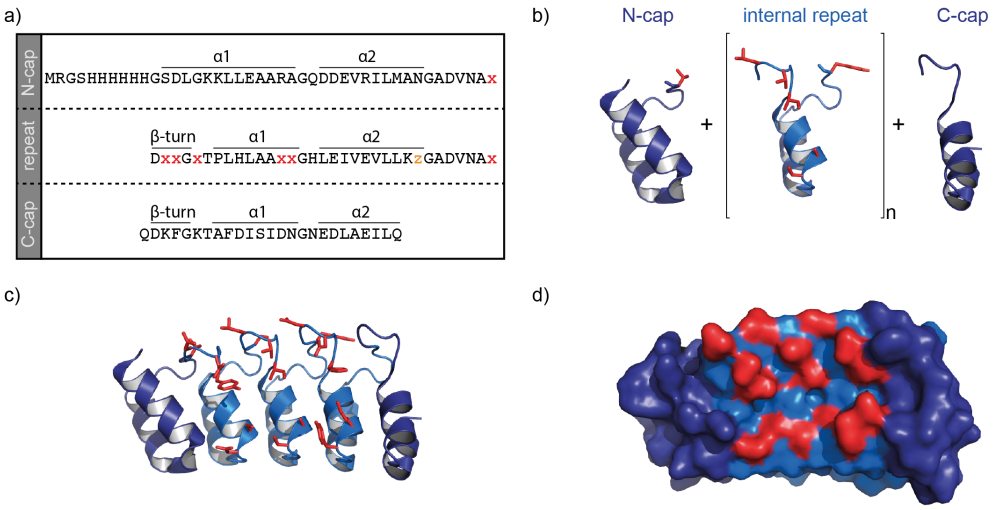

Figure 1: Designed Ankyrin Repeat Proteins
a) Consensus sequence of the capping and internal repeats. b) Internal repeat with randomized position shown as red sticks. c) Three internal repeats flanked by capping repeats form a NI3C DARPin (pdb: 1MJ0) d). Surface representation visualizes the DARPin binding interface.

was subjected to be asparagine, histidine or tyrosine.[3] Assembly into a library leads to a theoretical diversity of about $5.2 \cdot 10^{15}$ and $3.8 \cdot 10^{23}$ molecules in case of a NI_2C and NI_3C library, respectively.[3] However, the practical diversity is typically estimated to be between 10^9 and 10^{12} depending on the amount of DNA recovered in the last assembly step.

The first structure determination of an unselected DARPin (E3_5) in combination with unfolding measurements unraveled a highly stable protein with a slight curvature and a protein surface that can be randomized to provoke interactions with a desired target protein (**figure 1c,d**).[5] Furthermore, these proteins could be expressed in large amounts and purification with immobilized metal affinity chromatography (Ni^{2+}-NTA) yielded highly pure proteins.[1, 3] Overall the first initial studies on this novel scaffold already emphasized the today well-known benefits of the DARPins: A highly stable protein with binding properties to a selected target, which can be expressed in large amounts and easily be purified.

Recently, a thorough analysis of DARPin-protein interfaces solved by X-ray crystallography resulted in a second generation DARPin library with reduced hydrophobicity (see also **chapter 5**).[6] This newly generated library is based on the very same scaffold although it includes a different randomization strategy and a modified C-terminal capping repeat. Since the initial design of this terminal repeat has been shown to be the least stable module, an improved version has been developed that is more tightly packed to the adjacent internal repeat.[7, 8]

1.2.2 Selection and target prerequisites

Assembled DARPin libraries can be applied for *in-vitro* selection of specific binders using either phage-[9] or ribosome display.[10] Both selection techniques require a highly pure target protein to prevent selection against impurities. In addition, the protein has to be stable over the time of selection to exclude the enrichment of DARPins that will interact with degradation products. Immobilization of the target protein is a crucial step for *in-vitro* selection and is generally performed using neutravidine coated beads or surfaces.[11] For that purpose, the target protein needs to be biotinylated, either chemically or enzymatically.

Since the DARPin scaffold has been successfully applied many times in ribosome display selections,[3, 12-20] we have chosen to use this technique for the selection of caspase specific DARPins (see **chapter 2 - 4**). However, high affinity binders have also been reported using a modified variant of phage display that is designed for the signal recognition particle secretion system.[21, 22]

The fundamental principal of a selection round by ribosome display is depicted in **figure 2**: A DARPin library is transcribed into mRNA **(a)** and translated to the nascent protein **(b)**. Due to a missing stop codon, the genetic information on the mRNA is coupled via the ribosome to the translated polypeptide chain **(c)**. These ternary complexes are then applied to immobilized target proteins **(d)** and after a washing step **(e)**, specific binders will be retained **(f)**. An elution step **(g)** followed by reverse transcription of the mRNA **(h)** leads to an enriched DARPin library for a particular target protein **(i)**. High affine DARPins can be obtained by performing these procedure 3 to 4 times. Furthermore, adding a pre-panning step with homologous proteins can increase the specificity of a selected DARPin for a protein with closely related family members. This has been successfully applied in case of caspase-specific DARPins (see also **chapter 2 - 4**).[14, 23]

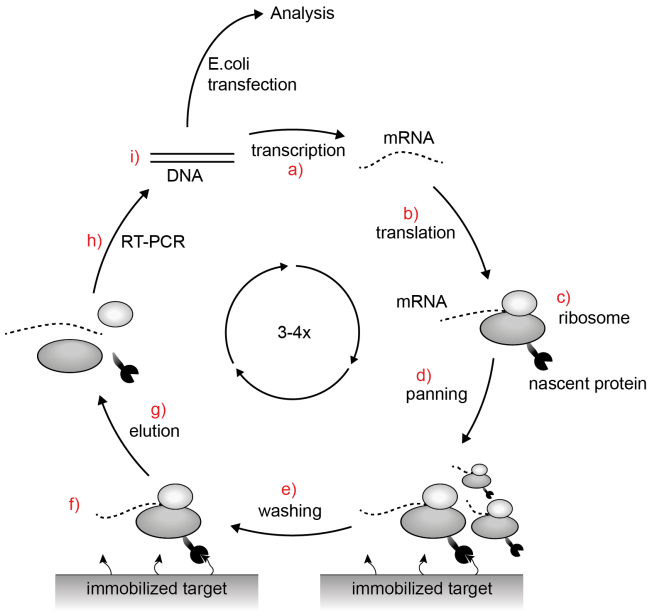

Figure 2: Ribosome display selection procedure
Schematic representation adapted from Ref 2. See main text for further explanations.

1.2.3 Selected DARPins and their application

The DARPin scaffold has been used several times to obtain high affine binders for proteins of interest. Besides their application as crystallization aids[18, 24, 25], selected DARPins were utilized as modulators of active proteins such as drug transporters[25],

kinases[26] and proteases.[14, 23] Furthermore, these binding proteins were successfully used as entry inhibitors of HIV[16, 27] as well as for tumor diagnostics[28] and tumor targeting.[17, 29-31] Recently, DARPins have also been suggested as potential anti-allergic drugs, since a DARPin demonstrated an accelerated disassembly of an IgE-receptor complex.[32] The cysteine-free framework of these binders is beneficial for intracellular applications rendering these binders to be attractive molecules for fluorescent-based biosensors.[33, 34] Besides that, the combination of high stability, high expression rates and simple purification emerges DARPins as potential candidates in clinical studies where first promising results have been achieved.[35] For further information about therapeutic strategies, the reader is referred to a recently published review.[36]

1.2.4 Concluding remarks

A decade ago, DARPins have been developed based on natural occurring ankyrin proteins using a consensus approach. The designed scaffold has been extensively studied leading to improved thermodynamic stability. Besides that, selections against numerous different target proteins have verified the intended scaffold in shaping high quality binding molecules. DARPins with high affinity and high specificity are now widely used to answer various scientific questions while a first clinical trial is approaching phase 3 thereby forecasting a promising future of those proteins.

1.2.5 Literature

1. Binz HK, Stumpp MT, Forrer P, Amstutz P, Plückthun A. Designing repeat proteins: well-expressed, soluble and stable proteins from combinatorial libraries of consensus ankyrin repeat proteins. *J Mol Biol* 2003 Sep 12; **332**(2)**:** 489-503.
2. Amstutz P, Forrer P, Zahnd C, Plückthun A. In vitro display technologies: novel developments and applications. *Curr Opin Biotechnol* 2001 Aug; **12**(4)**:** 400-405.
3. Binz HK, Amstutz P, Kohl A, Stumpp MT, Briand C, Forrer P*, et al.* High-affinity binders selected from designed ankyrin repeat protein libraries. *Nat Biotechnol* 2004 May; **22**(5)**:** 575-582.
4. Bork P. Hundreds of ankyrin-like repeats in functionally diverse proteins: mobile modules that cross phyla horizontally? *Proteins* 1993 Dec; **17**(4)**:** 363-374.
5. Kohl A, Binz HK, Forrer P, Stumpp MT, Plückthun A, Grütter MG. Designed to be stable: crystal structure of a consensus ankyrin repeat protein. *Proc Natl Acad Sci U S A* 2003 Feb 18; **100**(4)**:** 1700-1705.
6. Seeger MA, Zbinden R, Flütsch A, Gutte PG, Engeler S, Roschitzki-Voser H*, et al.* Design, construction, and characterization of a second-generation DARPin library with reduced hydrophobicity. *Protein Sci* 2013 Jul 19.
7. Interlandi G, Wetzel SK, Settanni G, Plückthun A, Caflisch A. Characterization and further stabilization of designed ankyrin repeat proteins by combining molecular dynamics simulations and experiments. *J Mol Biol* 2008 Jan 18; **375**(3)**:** 837-854.
8. Kramer MA, Wetzel SK, Plückthun A, Mittl PR, Grutter MG. Structural determinants for improved stability of designed ankyrin repeat proteins with a redesigned C-capping module. *J Mol Biol* 2010 Dec 3; **404**(3)**:** 381-391.
9. Smith GP. Filamentous fusion phage: novel expression vectors that display cloned antigens on the virion surface. *Science* 1985 Jun 14; **228**(4705)**:** 1315-1317.
10. Hanes J, Plückthun A. In vitro selection and evolution of functional proteins by using ribosome display. *Proc Natl Acad Sci U S A* 1997 May 13; **94**(10)**:** 4937-4942.
11. Zahnd C, Amstutz P, Plückthun A. Ribosome display: selecting and evolving proteins in vitro that specifically bind to a target. *Nat Methods* 2007 Mar; **4**(3)**:** 269-279.
12. Kohl A, Amstutz P, Parizek P, Binz HK, Briand C, Capitani G*, et al.* Allosteric inhibition of aminoglycoside phosphotransferase by a designed ankyrin repeat protein. *Structure* 2005 Aug; **13**(8)**:** 1131-1141.
13. Amstutz P, Koch H, Binz HK, Deuber SA, Plückthun A. Rapid selection of specific MAP kinase-binders from designed ankyrin repeat protein libraries. *Protein Eng Des Sel* 2006 May; **19**(5)**:** 219-229.
14. Schweizer A, Roschitzki-Voser H, Amstutz P, Briand C, Gulotti-Georgieva M, Prenosil E*, et al.* Inhibition of caspase-2 by a designed ankyrin repeat protein: specificity, structure, and inhibition mechanism. *Structure* 2007 May; **15**(5)**:** 625-636.
15. Zahnd C, Wyler E, Schwenk JM, Steiner D, Lawrence MC, McKern NM*, et al.* A designed ankyrin repeat protein evolved to picomolar affinity to Her2. *J Mol Biol* 2007 Jun 15; **369**(4)**:** 1015-1028.
16. Schweizer A, Rusert P, Berlinger L, Ruprecht CR, Mann A, Corthesy S*, et al.* CD4-specific designed ankyrin repeat proteins are novel potent HIV entry inhibitors with unique characteristics. *PLoS Pathog* 2008 Jul; **4**(7)**:** e1000109.
17. Winkler J, Martin-Killias P, Plückthun A, Zangemeister-Wittke U. EpCAM-targeted delivery of nanocomplexed siRNA to tumor cells with designed ankyrin repeat proteins. *Mol Cancer Ther* 2009 Sep; **8**(9)**:** 2674-2683.
18. Grubisha O, Kaminska M, Duquerroy S, Fontan E, Cordier F, Haouz A*, et al.* DARPin-assisted crystallography of the CC2-LZ domain of NEMO reveals a coupling between dimerization and ubiquitin binding. *J Mol Biol* 2010 Jan 8; **395**(1)**:** 89-104.
19. Pecqueur L, Duellberg C, Dreier B, Jiang Q, Wang C, Plückthun A*, et al.* A designed ankyrin repeat protein selected to bind to tubulin caps the microtubule plus end. *Proc Natl Acad Sci U S A* 2012 Jul 24; **109**(30)**:** 12011-12016.

20. Kummer L, Parizek P, Rube P, Millgramm B, Prinz A, Mittl PR*, et al.* Structural and functional analysis of phosphorylation-specific binders of the kinase ERK from designed ankyrin repeat protein libraries. *Proc Natl Acad Sci U S A* 2012 Aug 21; **109**(34)**:** E2248-2257.
21. Steiner D, Forrer P, Stumpp MT, Plückthun A. Signal sequences directing cotranslational translocation expand the range of proteins amenable to phage display. *Nat Biotechnol* 2006 Jul; **24**(7)**:** 823-831.
22. Steiner D, Forrer P, Plückthun A. Efficient selection of DARPins with sub-nanomolar affinities using SRP phage display. *J Mol Biol* 2008 Oct 24; **382**(5)**:** 1211-1227.
23. Schroeder T, Barandun J, Flütsch A, Briand C, Mittl PR, Grütter MG. Specific inhibition of caspase-3 by a competitive DARPin: molecular mimicry between native and designed inhibitors. *Structure* 2013 Feb 5; **21**(2)**:** 277-289.
24. Sennhauser G, Grütter MG. Chaperone-assisted crystallography with DARPins. *Structure* 2008 Oct 8; **16**(10)**:** 1443-1453.
25. Sennhauser G, Amstutz P, Briand C, Storchenegger O, Grütter MG. Drug export pathway of multidrug exporter AcrB revealed by DARPin inhibitors. *PLoS Biol* 2007 Jan; **5**(1)**:** e7.
26. Amstutz P, Binz HK, Parizek P, Stumpp MT, Kohl A, Grütter MG*, et al.* Intracellular kinase inhibitors selected from combinatorial libraries of designed ankyrin repeat proteins. *J Biol Chem* 2005 Jul 1; **280**(26)**:** 24715-24722.
27. Mann A, Friedrich N, Krarup A, Weber J, Stiegeler E, Dreier B*, et al.* Conformation-dependent recognition of HIV gp120 by designed ankyrin repeat proteins provides access to novel HIV entry inhibitors. *J Virol* 2013 May; **87**(10)**:** 5868-5881.
28. Theurillat JP, Dreier B, Nagy-Davidescu G, Seifert B, Behnke S, Zurrer-Hardi U*, et al.* Designed ankyrin repeat proteins: a novel tool for testing epidermal growth factor receptor 2 expression in breast cancer. *Mod Pathol* 2010 Sep; **23**(9)**:** 1289-1297.
29. Zahnd C, Kawe M, Stumpp MT, de Pasquale C, Tamaskovic R, Nagy-Davidescu G*, et al.* Efficient tumor targeting with high-affinity designed ankyrin repeat proteins: effects of affinity and molecular size. *Cancer Res* 2010 Feb 15; **70**(4)**:** 1595-1605.
30. Stefan N, Martin-Killias P, Wyss-Stoeckle S, Honegger A, Zangemeister-Wittke U, Plückthun A. DARPins recognizing the tumor-associated antigen EpCAM selected by phage and ribosome display and engineered for multivalency. *J Mol Biol* 2011 Nov 4; **413**(4)**:** 826-843.
31. Martin-Killias P, Stefan N, Rothschild S, Plückthun A, Zangemeister-Wittke U. A novel fusion toxin derived from an EpCAM-specific designed ankyrin repeat protein has potent antitumor activity. *Clin Cancer Res* 2011 Jan 1; **17**(1)**:** 100-110.
32. Kim B, Eggel A, Tarchevskaya SS, Vogel M, Prinz H, Jardetzky TS. Accelerated disassembly of IgE-receptor complexes by a disruptive macromolecular inhibitor. *Nature* 2012 Nov 22; **491**(7425)**:** 613-617.
33. Brient-Litzler E, Plückthun A, Bedouelle H. Knowledge-based design of reagentless fluorescent biosensors from a designed ankyrin repeat protein. *Protein Eng Des Sel* 2010 Apr; **23**(4)**:** 229-241.
34. Kummer L, Hsu CW, Dagliyan O, Macnevin C, Kaufholz M, Zimmermann B*, et al.* Knowledge-Based Design of a Biosensor to Quantify Localized ERK Activation in Living Cells. *Chem Biol* 2013 Jun 20; **20**(6)**:** 847-856.
35. Campochiaro PA, Channa R, Berger BB, Heier JS, Brown DM, Fiedler U*, et al.* Treatment of diabetic macular edema with a designed ankyrin repeat protein that binds vascular endothelial growth factor: a phase I/II study. *Am J Ophthalmol* 2013 Apr; **155**(4)**:** 697-704, 704 e691-692.
36. Tamaskovic R, Simon M, Stefan N, Schwill M, Plückthun A. Designed ankyrin repeat proteins (DARPins) from research to therapy. *Methods Enzymol* 2012; **503:** 101-134.

2 Publication: Caspase-Specific DARPins

DE GRUYTER Biol. Chem. 2014; 395(10): 1243–1252

Andreas Flütsch[a,b], Thilo Schroeder[a,c], Jonas Barandun[a,d], Rafael Ackermann, Martin Bühlmann and Markus G. Grütter*

Specific targeting of human caspases using designed ankyrin repeat proteins

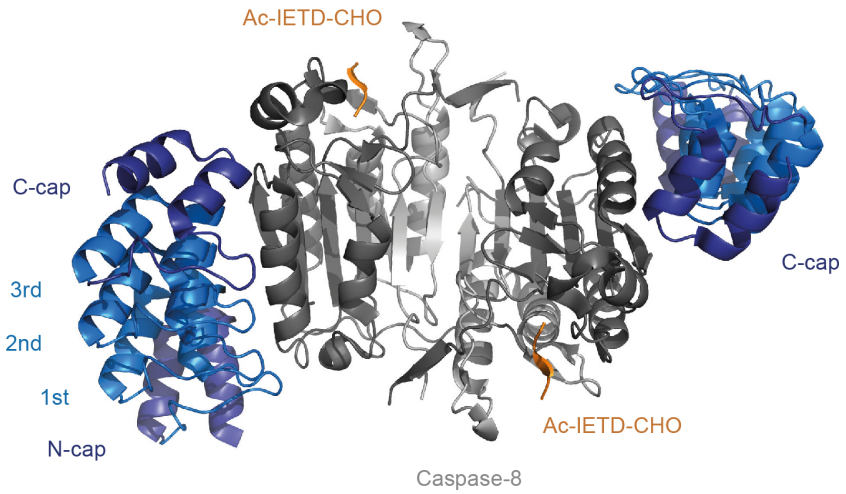

Figure 2A: Caspase-8 in complex with DARPin D8.4 (PDB: 2Y1L)

DOI: 10.1515/hsz-2014-0173,

DE GRUYTER Biol. Chem. 2014; 395(10): 1243–1252

Andreas Flütsch[a,b], Thilo Schroeder[a,c], Jonas Barandun[a,d], Rafael Ackermann, Martin Bühlmann and Markus G. Grütter*

Specific targeting of human caspases using designed ankyrin repeat proteins

Abstract: Caspases play important roles in cell death, differentiation, and proliferation. Due to their high homology, especially of the active site, specific targeting of a particular caspase using substrate analogues is very difficult. Although commercially available small molecules based on peptides are lacking high specificity due to overlapping cleavage motives between different caspases, they are often used as specific tools. We have selected designed ankyrin repeat proteins (DARPins) against human caspases 1–9 and identified high-affinity binders for the targeted caspases, except for caspase 4. Besides previously reported caspase-specific DARPins, we generated novel DARPins (D1.73, D5.15, D6.11, D8.1, D8.4, and D9.2) and confirmed specificity for caspases 1, 5, 6, and 8 using a subset of caspase family members. In addition, we solved the crystal structure of caspase 8 in complex with DARPin D8.4. This binder interacts with non-conserved residues on the large subunit, thereby explaining its specificity. Structural analysis of this and other previously published crystal structures of caspase/DARPin complexes depicts two general binding areas either involving active site forming loops or a surface area laterally at the large subunit of the enzyme. Both surface areas involve non-conserved surface residues of caspases.

Keywords: apoptosis; cell death; DARPins; specific caspase targeting; X-ray crystallography.

DOI 10.1515/hsz-2014-0173
Received March 24, 2014; accepted August 5, 2014

[a]These authors contributed equally to this work.
[b]Present address: University of California, San Diego, 9500 Gilman Drive, La Jolla, CA 92093-0629, USA.
[c]Present address: Nextech Invest Ltd., Scheuchzerstrasse 35, 8006 Zurich, Switzerland.
[d]Present address: The Rockefeller University, Laboratory of Protein and Nucleic Acid Chemistry, 1230 York Avenue, New York, NY 10065, USA.
***Corresponding author: Markus G. Grütter,** Department of Biochemistry, University of Zurich, Winterthurerstrasse 190, CH-8057 Zurich, Switzerland, e-mail: gruetter@bioc.uzh.ch
Andreas Flütsch, Thilo Schroeder, Jonas Barandun, Rafael Ackermann and Martin Bühlmann: Department of Biochemistry, University of Zurich, Winterthurerstrasse 190, CH-8057 Zurich, Switzerland

Introduction

A well-ordered removal of aberrant cells is important in multicellular animals to ensure the organism's cellular integrity. Thus, a variety of cell death pathways exist of which apoptosis is presumably one of the best-studied mechanisms, removing cells in an non-inflammatory manner thereby preventing a severe immune response in the organism (Taylor et al., 2008). Further, apoptosis plays a crucial role in embryonic development and tissue homeostasis. Although it is a highly controlled mechanism, its misregulation has been associated with severe diseases such as cancer or Alzheimer's disease (Rohn, 2010; Favaloro et al., 2012).

Proteases of the caspase family have been identified to be the major contributors of apoptosis. Caspases either induce (caspases 2, 8, 9, and 10) or execute (caspases 3, 6, and 7) the apoptotic signaling (Grütter, 2000). Furthermore, caspases 1, 4, 5, and 12 have been related to inflammatory pathways. Because all caspases share a high sequence and structural homology, specific targeting of one particular family member is limited with the contemporary available tools. The small peptide substrates or inhibitors lack specificity due to targeting of the highly conserved active site (McStay et al., 2008). Another more promising approach is the development of small molecule compounds that bind and inhibit caspases 3 and 7 outside the active site pocket, although the identified binding site for these compounds is conserved between both caspases (Hardy et al., 2004).

To increase a compound's specificity for a particular caspase, we used engineered binding proteins that provide larger binding interfaces and potentially also involve nonconserved residues. For our studies, we selected binders using a designed ankyrin repeat protein (DARPin) library. DARPins were designed based on repeat modules occurring in natural ankyrin proteins and consist of an N-terminal capping repeat (N-cap) followed by two (=NI2C) or three (=NI3C) internal and a C-terminal repeat (C-cap) (Binz et al., 2004). Each internal repeat of a DARPin harbors six randomized positions resulting in a theoretical diversity of 10^{23} different molecules in assembled DARPin libraries (Binz et al., 2004). These libraries

are generally used for binder selections against various different targets using ribosome display, an *in vitro* selection technique (Hanes and Plückthun, 1997). In addition, DARPins have also been successfully selected using phage display (Steiner et al., 2008).

Numerous DARPin selections yielding high affinity binders for particular target proteins have been reported (Amstutz et al., 2005; Sennhauser et al., 2007; Stefan et al., 2011). In the past, we used DARPin libraries to select highly specific inhibitors for caspase 2 (Schweizer et al., 2007) and caspase 3 (Schroeder et al., 2013) as well as binders for pro- and active caspase 7 that prevent procaspase 7 activation (Flütsch et al., 2014).

Here, we describe the general procedure for the selection of DARPin binders in parallel against the panel of human caspase 1–9. The selection led to high-affinity binders with the exception of caspase 4. Besides the previously reported specific DARPins for caspase 2 (Schweizer et al., 2007), caspase 3 (Schroeder et al., 2013), and caspase 7 (Flütsch et al., 2014), we report novel binders for caspases 1, 5, 6, 8, and 9. The binder's target specificity for caspases 1, 5, 6, and 8 was evaluated using a subset of caspase family members. In addition, we solved the first crystal structure of caspase 8 in complex with DARPin D8.4 and provide a comparison and analysis of the binding interface with the other three previously published caspases 2, 3, and 7/DARPin complex interfaces.

Results

Caspase purification

Because the targeted protein's purity and stability is crucial to prevent selection against impurities or degradation products, we have established purification protocols with high reproducibility for caspase 1–9 (Roschitzki-Voser et al., 2012). The kinetic characterization in combination with analysis of the oligomeric state determined by size exclusion chromatography (SEC) and the purity by SDS page ensured that the targeted caspases were properly folded and active enzymes.

Selection and characterization of caspase-targeted DARPins

DARPin selection was performed using ribosome display against caspases 1–9. We modified the selection protocol to achieve specificity and introduced pre-panning steps against the closest homologues of the targeted caspases in the first and third selection rounds (Supplementary Figure 1). Furthermore, additional washing has been performed to obtain a slow off rate using an excess of non-biotinylated targeted caspase after the panning step in the second and fourth rounds (Supplementary Figure 1). After four rounds of selection, the enriched caspase-targeted DARPin libraries have been used to analyze individual clones by crude extract ELISA. In general, binders that exhibited strong signal to the targeted caspases compared with the maltose-binding protein (MBP) control obtained a unique identifier (DX.Y), with X indicating the targeted caspases and Y the sequence of discovery. Obtained DARPins were sequenced (Supplementary Figure 2), purified, and analyzed for complex formation with the targeted caspase in solution using SEC (Figure 1A and Supplementary Figure 3). Notably, binding of the DARPins can occur to the monomeric as well as to the dimeric form of the targeted caspase. In addition, SEC traces suggest that binding of D1.73 and D8.4 may alter the oligomeric state of the targeted caspase. While first results using ultracentrifugation and D8.4 support these findings (data not shown), further experiments will be necessary to fully confirm an induced change of the oligomeric state upon DARPin binding.

Affinity of binders that displayed unambiguous sequencing results and a stable complex on SEC were analyzed using surface plasmon resonance (SPR) (e.g., caspase 8/D8.4 in Figure 1B). Following this approach, we were able to identify DARPins with affinities in the low nanomolar range to caspases 1–9 with the exception of caspase 4. Measured SPR data for these binders are summarized in Figure 1C, where we included the previously reported values of DARPins with high specificity for caspase 2 (Schweizer et al., 2007), caspase 3 (Schroeder et al., 2013), and pro- and active caspase 7 (Flütsch et al., 2014). Kinetic data have been obtained by fitting the measured data with the heterogeneous ligand model (Bravman et al., 2006), with exception of D9.2, which exhibited a very low signal. Different values of K_{d1} and K_{d2} can be explained by altered accessibility of the two binding epitopes most probably originating from the direct coating of the caspase molecules via biotin on the sensor chip. However, we cannot fully exclude a cooperative binding mechanism in case of the caspase 3 binders that exhibit a large difference between these two values.

In case of D8.4, the Langmuir model was used to fit the data (Figure 1B) obtaining a K_d of 5.2 nM. With the exception of D1.73, D8.1, and D8.4, which exhibited high χ^2 values while curve fitting, binding constants were determined by equilibrium analysis. DARPins that were selected against caspase 4 exhibited binding in the low

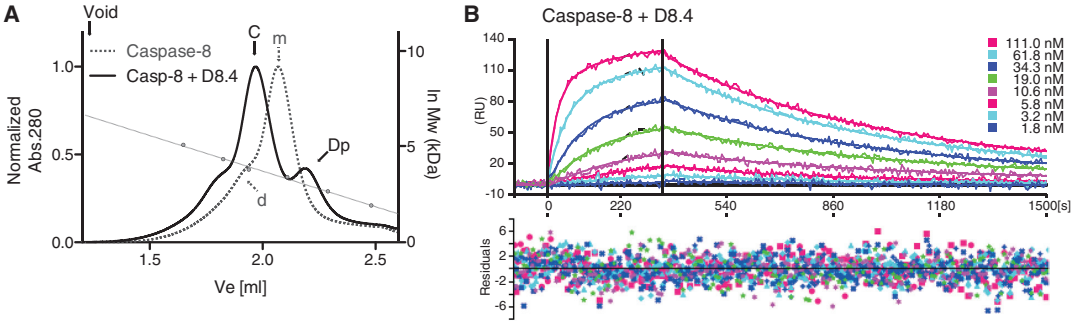

C

			Kinetic data						*Equilibrium*
DARPin	**Target**	**Ref.**	k_{a1}($M^{-1}s^{-1}$)	k_{d1}(s^{-1})	K_{d1}(M)	k_{a2}($M^{-1}s^{-1}$)	k_{d2}(s^{-1})	K_{d2}(M)	*K*d(M)
D1.73	Casp-1		1.03E+05	4.70E-04	4.54E-09	1.20E+06	1.88E-03	5.87E-09	–
AR_F8	Casp-2	(1)	–	–	4.10E-09	–	–	–	–
D3.4S76R	Casp-3	(2)	1.74E+05	4.20E-03	2.42E-08	1.62E+06	7.45E-04	4.61E-10	6.00E-09
D3.8	Casp-3	(2)	1.77E+05	2.49E-03	1.41E-08	2.44E+06	1.11E-04	4.57E-11	3.40E-09
D5.15	Casp-5		1.05E+06	1.01E-02	1.00E-08	2.85E+05	5.97E-04	2.10E-09	1.10E-08
D6.11	Casp-6		6.05E+05	1.05E-02	2.13E-08	1.55E+05	9.66E-04	6.23E-09	3.37E-08
D7.18	Casp-7	(3)	1.73E+05	1.31E-02	7.60E-08	1.08E+04	2.11E-04	1.96E-08	1.44E-07
D7.43	Casp-7	(3)	4.44E+04	9.97E-04	2.30E-08	6.65E+05	1.77E-02	2.70E-08	2.47E-08
D8.1	Casp-8		6.00E+04	1.96E-03	3.27E-08	–	–	–	–
D8.4	Casp-8		1.80E+05	9.31E-04	5.20E-09	–	–	–	–
D9.2	Casp-9		–	–	–	–	–	–	1.80E-08

Figure 1 Binding characterization of selected DARPins.
(A) Selected DARPins were analyzed on SEC for the formation of a stable complex in solution (see also Supplementary Figure 3). Caspase 8 exhibits a monomer-dimer equilibrium [marked with (m) and (d), respectively]. D8.4 binds to both the monomer and the dimeric forms of caspase 8 and elutes at earlier retention volume as a protein complex (solid lines, complex peak marked with (C) and (Dp) for DARPin excess). Calibration curve (right ordinate) was made using aldolase (158 kDa), conalbumin (75 kDa), ovalbumin (43 kDa), carbonic anhydrase (29 kDa), ribonuclease A (13.7 kDa), and aprotinin (6.5 kDa). Furthermore, (B) binding affinities were determined using SPR. (C) Binding affinities and kinetic constants of selected DARPins. Binders with two indicated kinetic constants were determined using the heterogeneous ligand model (Bravman et al., 2006). D8.1 and D8.4 kinetic data were determined using the Langmuir model. The equilibrium K_D determination for D1.73, D8.1, and D8.4 resulted in high χ^2 values and are therefore excluded. Previously reported DARPins are indicated with a gray background, and references are given with numbers: (1) Schweizer et al. (2007), (2) Schroeder et al. (2013), (3) Flütsch et al. (2014).

millimolar range, three orders of magnitude higher than the best binders we have found against the other caspases. An explanation for that observation could be that caspase 4 is less stable under selection conditions. Protein sequence and biophysical properties of the DARPins listed in Figure 1C can be found in Supplementary Table 1.

Caspase specificity of the selected DARPins was determined using SPR analysis against a representative set of caspases (caspases 1, 4, 5, 6, 7, and 8) including members of all different pre-panning groups (see Supplementary Figure 1). Caspase 3 was excluded due to its lower stability when coated on the SPR chip, whereas caspases 2 and 9 were represented by the panning group member caspase 8. Although not all caspases were tested in particular, the chosen array of different caspases is well suitable to elucidate the binder's specificity. It confirms that pre-panning during selection leads to not only specificity within a panning group (e.g., caspases 1, 4, and 5) but also across panning groups with more distantly related caspases (e.g., caspases 1, 7, and 8).

With the exception of D9.2, we tested and confirmed the binders' specificity for the targeted caspases. Caspase 8 binding specificity was tested using DARPin D8.1, which shares a very similar sequence with D8.4 with only two point mutations (Q26R and V139A, see Supplementary Figure 5) suggesting the same binding

interaction. Binding specificities for AR_F2, D3.4S76R, D3.8, D7.18, and D7.43 were reported previously (Schweizer et al., 2007; Schroeder et al., 2013; Flütsch et al., 2014).

Crystal structure of caspase 8 in complex with D8.4

To obtain a better understanding of the binding interactions between a selected DARPin and the targeted caspase, we have crystallized caspase 8 in complex with DARPin D8.4 and determined the structure at 1.8 Å resolution. Structure determination details and refinement statistics are listed in Supplementary Table 2. Crystals grew under acidic conditions at pH 4.9, indicating that the protein interaction remains intact even at low pH. This was also tested in ELISA format (data not shown) and showed that binding still occurs at acidic pH values, although a lower signal compared with neutral pH suggests a weakened binding affinity. The asymmetric unit contains a caspase 8 dimer consisting of two small and two large subunits, two bound inhibitor molecules Ac-IETD-CHO, and two bound DARPins (Figure 2A). The binding epitope is localized on the side of the large subunit of the enzyme and primarily involves residues of α-helix α2 as well as β-strand β2 (Figure 2B).

In total, 25 caspase 8 residues are involved in binding to 31 residues of the DARPin spanning a binding interface of 938 Å^2. Sixteen hydrogen bonds and 7 salt bridges surround a hydrophobic core, which is formed by amino acids Phe-56, Leu-86, Leu-89, Phe-90, and Phe-123 of the DARPin and Gln-291, Ile-295, and Ile-298 of caspase 8 (Figure 2B). Remarkably, besides the 16 non-randomized residues that are involved in binding, D8.4 possesses two unintended framework mutations (Arg-26 and Arg-85, see Supplementary Figure 5), which play a role in hydrogen bonding to caspase 8 (marked in Figure 2B, left).

As intended, the specificity of D8.4 for caspase 8 is achieved by targeting of non-conserved residues. Especially the hydrophobic interaction provided by Ile-298

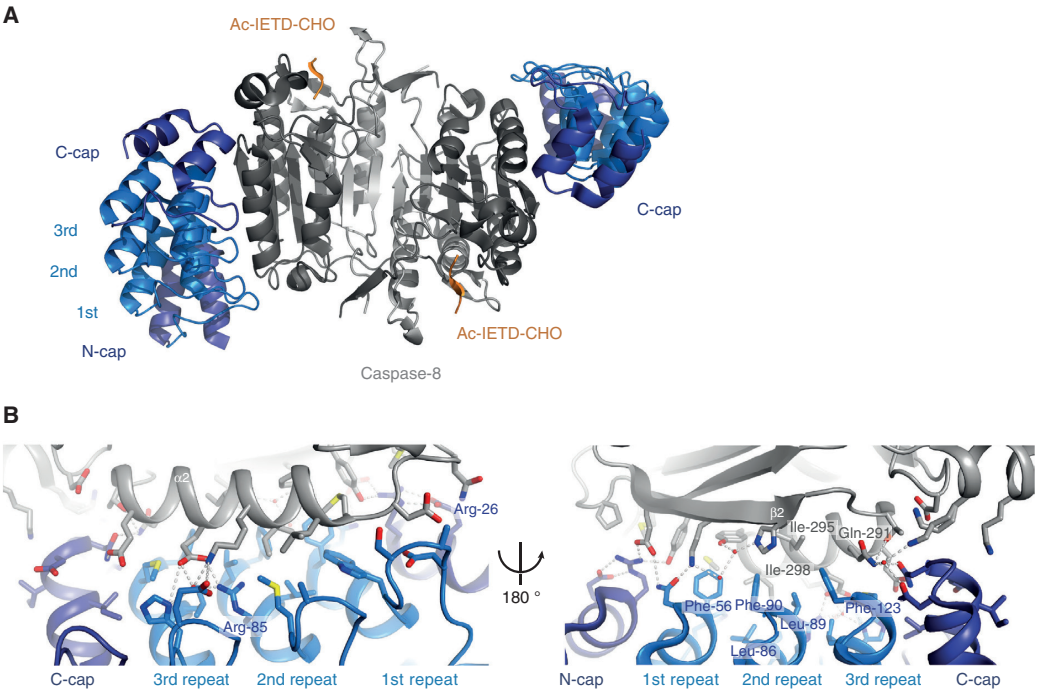

Figure 2 Caspase 8 in complex with DARPin D8.4.
(A) Standard view of caspase 8 (small subunit in light gray, large subunit in dark gray, Ac-IETD-CHO inhibitor in orange) in complex with DARPin D8.4 (N- and C-cap in dark blue, internal repeats are light blue). The DARPin binds lateral at the large subunit of the enzyme. (B) Close-up view of the caspase 8/DARPin D8.4 binding interface displaying the major interactions between the DARPin and α-helix α2 of caspase 8 (left) and the interactions of D8.4 with β-strand β2 of caspase 8 (right). Important residues are labeled in blue (DARPin) and gray (caspase 8). See also Supplementary Figure 5 for a list of interacting residues.

(Figure 2B, right) is not conserved among the apoptotic caspases, which harbor a larger and more hydrophilic residue at this position (Supplementary Figure 5). Besides that, only Thr-288 at the beginning of α-helix α1 was identified as highly conserved. Therefore, our crystal structure not only provides insights into the binding interface but also elucidates the specificity of the selected DARPin. In addition, it confirms our chosen selection procedure with the additional pre-panning steps against homologues caspases. A structural alignment of our caspase 8/DARPin-8.4 structure with the high-resolution structure of the same enzyme (1QTN; Watt et al., 1999) results in a very low root mean square deviation of about 0.7 Å, indicating no or only minor differences between the two structures. While they show no structural differences in the overall fold and the active site, several side chains in the caspase/DARPin interface adopt different conformations (e.g., Glu-290, Glu-294, Ile-298) due to the presence of the DARPin D8.4.

DARPin binding interfaces on human caspases

With the previously described crystal structures of caspases in complex with specific DARPins (Schweizer et al., 2007; Schroeder et al., 2013; Flütsch et al., 2014), we were able to compare the different DARPin epitopes for each particular caspase (Figure 3).

Based on the caspase standard view, where the five main parallel β-strands (β1–β5) of a caspase protomer are aligned with their C-termini pointing upwards, caspase 2-specific DARPin AR_F8 (Figure 3A; Schweizer et al., 2007) binds apical at the backside of loop 4 (also known as loop 381; Fuentes-Prior and Salvesen, 2004), which is involved in the formation of the active site cleft. Because this loop is not highly conserved among other caspases, it explains the high specificity of DARPin AR_F8 for caspase 2. The binding area of 799 Å^2 includes a hydrophobic core, six hydrogen bonds, and nine salt bridges. AR_F8 binding at the backside of loop 4 leads to a loop shift of 1 Å and opens the active site cleft (Schweizer et al., 2007). This finally results in a displacement of the active site cysteine (Cys-155) and structurally elucidates the allosteric mode of inhibition.

Although DARPin D3.4S76R binds in a similar way apical to caspase 3 (Figure 3B; Schroeder et al., 2013) at the active site forming loops, the epitope is only partially overlapping with that of caspases 2 and AR_F8. D3.4S76R binds directly into the active site pocket of caspases 3 and only interacts with the tip of loop 4. Its high specificity is achieved by the formation of a salt bridge between Lys-56 and the Asp-253 of caspase 3. Interestingly, the interacting DARPin residue Asp-45 occupies the S4 pocket of the enzyme, as it can be observed in binding of peptide substrates. In addition, Ile-78 of the DARPin keeps Tyr-204 of caspase 3 in a conformation that blocks the S2 binding pocket. Overall, the binding of D3.4S76R to caspase 3 prevents substrate entrance to the active site pocket and mimics an interaction seen for caspase 3 with its natural inhibitor XIAP (Schroeder et al., 2013). Enzyme kinetic analysis has classified D3.4S76R as a purely competitive inhibitor.

Besides the apical binding sites of AR_F8 and D3.4S76R, another favored caspase/DARPin epitope could be identified laterally at the large subunit of the peptidase. In addition to the above-described DARPin D8.4 that binds sideways at the large subunit (p20) primarily to residues of α-helix α2 (Figure 3D), DARPins that have been selected against caspase 7 bind at a similar epitope (Flütsch et al., 2014). For instance, the crystal structure of caspase 7 in complex with DARPin D7.18 (Figure 3C) unraveled a binding interface of 672 Å^2 that is predominantly formed by residues located on β-strand β2. In particular, two DARPin tryptophans (Trp-46 and Trp-78) are deeply buried in a hydrophobic pocket shaped by non-conserved residues of caspase 7. Because this hydrophobic pocket is obstructed in other homologues, these two tryptophans are the major contributors for the high specificity of DARPin D7.18. Although there is another caspase 7/DARPin complex structure available (pdb: 4JB8; Seeger et al., 2013) with DARPin C7_16 binding laterally at the large subunit of caspases 7, we excluded this protein complex in our structural analysis. This DARPin has been selected without additional pre-panning steps and thus may lack specificity.

More interestingly, D7.43 and D7.18 also bind to pro caspase 7, thus preventing a successful activation (Flütsch et al., 2014). D8.4 with a lateral but different binding epitope would suggest a potential effect on the activation mechanism in analogy to the caspase 7 DARPins. However, the activation mechanism of caspase 8 is different compared with the caspase-mediated cleavage of procaspase 7. It occurs via autocatalytic processing after proximity-induced oligomerization (Salvesen and Dixit, 1999) and therefore is dependent on the oligomeric state of caspase 8. Complex formation on SEC (Figure 1A) and first ultracentrifugation experiments (data not shown) demonstrate that D8.4 can bind to the monomer as well as to the dimer of caspase 8 *in vitro*. Whether binding in a cellular environment to the full procaspase 8 with its two N-terminal death effector domains occurs and modulates caspase 8 activation has not been further analyzed and remains unknown.

All the complex structures display binding of one selected DARPin to one caspase protomer; thus, every

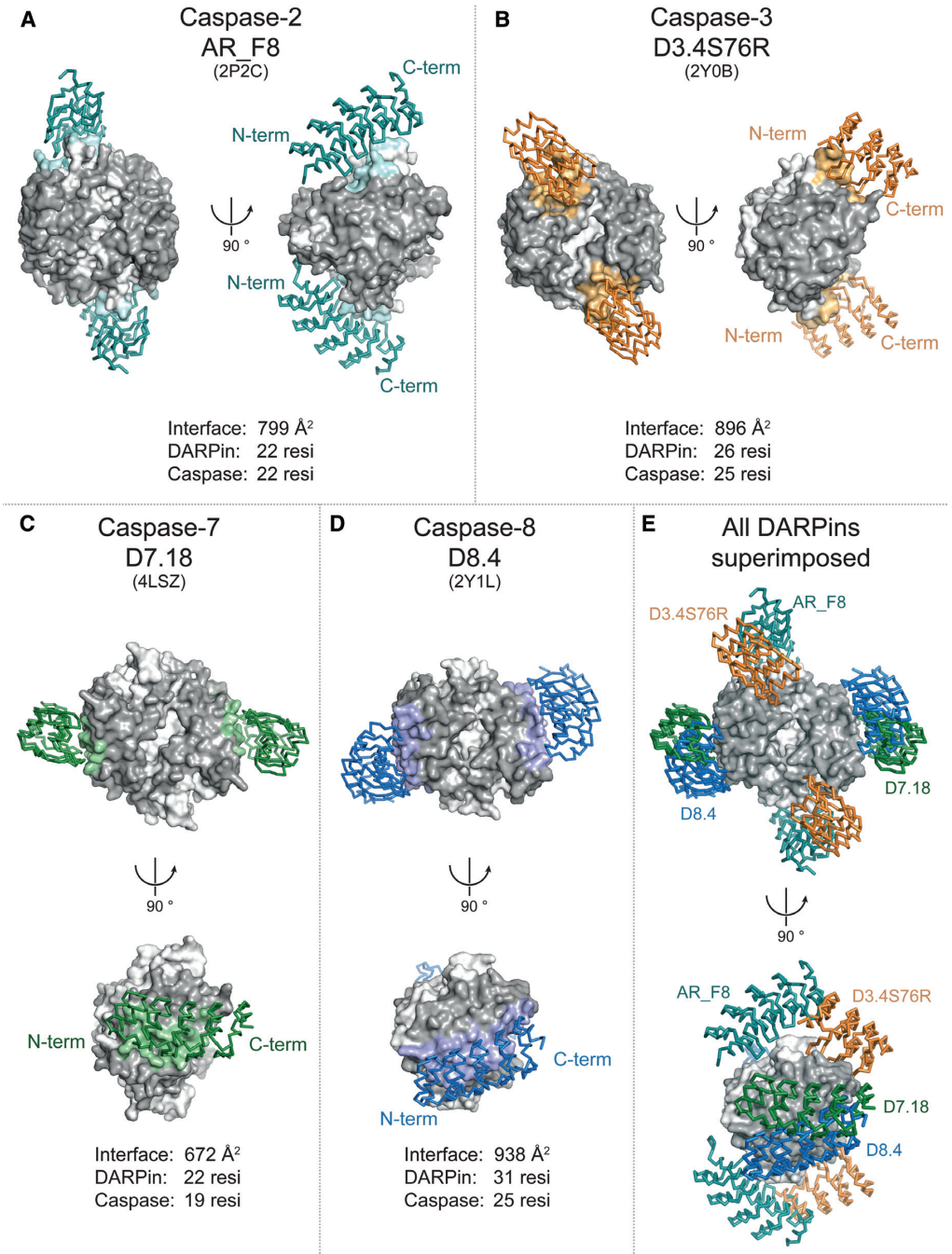

Figure 3 Caspase-specific DARPins: complex structure overview.
Currently available caspase structures in complex with specific DARPins are shown in standard view and rotated (90° around the y-axes). Interacting residues on the caspase surface are colored according to the color of the binding DARPin. (A) AR_F8 binds caspase 2 from the backside of loop 4. (B) D3.4S76R blocks the active site cleft of caspase 3. (C) D7.18 binds at the large subunit (p20) of caspase 7. (D) A similar epitope can be observed for caspase 8-specific DARPin D8.4. (E) Superposition of all DARPins on caspase 8 visualizes the different epitopes. See also Supplementary Figure 6 for a sequence alignment of all caspases and the interacting caspase residues.

caspase dimer has two DARPins bound. A superposition of all DARPins on caspase 8 shows the particular difference between the binding interfaces and emphasizes similarities (Figure 3E). While the apical epitope of DARPin AR_F8 is located at the backside of loop 4, D3.4S76R binds inside the active site cleft and completely blocks an entrance of substrate. The lateral binding at the large subunit is less distinct. DARPin D7.18 and D8.4 share a similar binding area on the caspase surface, but their position is slightly tilted by an angle of 30°. Notably, the N-terminus of all DARPins is oriented to the backside in the standard caspase representation resulting in a 'dorsal to ventral' DARPin orientation.

Comparison of these DARPin epitopes on the caspase surface suggests that binding in specific manner is more likely if it occurred at the outer rim of the enzyme rather than centrally located close to the dimer interface of two caspase protomers. However, we cannot exclude that this finding is experimentally influenced by the immobilization of the caspase molecule during the selection procedure. Random chemical biotinylation may orient the enzyme in a particular direction that binding to the outer rim is more likely. Besides that, it has been shown that the central cavity formed by two caspase protomers is conserved between caspases 3 and 7 (Hardy et al., 2004), suggesting a less favored epitope for high caspase specificity in close proximity to the cavity. In addition, exosite studies on caspase 7 revealed that surface residues located at the large subunit influence the cleavage efficiency for particular substrates (Boucher et al., 2012). For example, a caspase 7 mutant (K69L) exhibited reduced processing of the Hsp90 co-chaperone p23. More interestingly, Lys-69 is also involved in binding to DARPin D7.18, is not conserved in other caspases (see Supplementary Figure 6) and the caspase 8 homologue residue (Tyr-235) also contributes to DARPin D8.4 binding. Although very preliminary, this finding indicates that the non-conserved caspase residues involved in DARPin binding might also be of importance in providing specific binding interactions to certain caspase substrates.

Discussion

Using the here-described DARPin selection procedure including pre-panning steps against close homologues, we obtained new binders against five members of the human caspase family. We characterized these novel DARPins for caspases 1, 5, 6, 8, and 9 and included data of the previously reported specific binders for caspases 2, 3, and 7 (Schweizer et al., 2007; Schroeder et al., 2013; Flütsch et al., 2014). Caspase specificity of the new DARPins D1.73, D5.15, D.6.11, and D8.1 was tested using a subset of caspase family members (caspases 1, 4, 5, 6, 7, and 8). Although our results suggest high target specificity, binding of the DARPins to caspases 2, 3, and 9 was not tested.

The crystal structure of caspase 8 in complex with DARPin D8.4 provides insights into the binding mode of this high affine binder. D8.4 binds lateral to the large p20 subunit of the enzyme and does not interfere with the active site of the enzyme. The binding interface of caspase 8 involves a hydrophobic patch consisting of several non-conserved caspase residues and thus explains its specificity. Although the previously reported DARPins for caspases 2, 3, and 7 are binders with inhibitory function (Schweizer et al., 2007; Schroeder et al., 2013; Flütsch et al., 2014), the here newly reported DARPins do not prevent cleavage of small peptide substrates *in vitro*. If these binders can interact with the targeted procaspases and interfere with the activation process has not been tested and needs to be addressed in future experiments.

A structural comparison of all available caspase/DARPin complexes reveals two distinct binding regions on the caspase surface. One is located apical close or at the active site. Here the DARPins interact with active site forming loops or with residues in the active site and thereby inhibit the enzyme either allosterically or competitively. The other favored region is found laterally at the large subunit of the peptidase and involves α-helix α1 and α2 as well as β-strand β2. With this study, we show that specific DARPins can be selected against a particular member of a highly homologous protein family sharing a high sequence identity. Thus, these DARPins provide a molecular toolbox for functional and structural investigations either *in vitro* or in cell-based assays using mammalian expression vectors.

Materials and methods

All reagents were bought from Sigma/Fluka if not stated otherwise. Sequencing was performed at Microsynth (Balgach, Switzerland).

Caspase purification and biotinylation

Caspase 1–9 have been purified as described previously (Roschitzki-Voser et al., 2012). Ribosome display selection and ELISA experiments were performed using chemically biotinylated caspases (EZ-Link Sulfo-NHS-LC-LC-Biotin, 21338; Pierce Biotechnology, Rockford, IL, USA). After purification, 1 ml of caspase (10 μM) in phosphate buffer saline (PBS), pH 7.3, or 50 mM HEPES, pH 7.5, containing 150 mM NaCl was incubated with a molar excess (7×, 70 μM) of biotin on ice for 30 min. The reaction was quenched by adding 5 M Tris pH 7.5 (10 μl). Biotinylated proteins were purified by SEC using a Superdex 200 10/300 GL (GE Healthcare, Piscataway,

NJ, USA) equilibrated in PBS at 4°C. Fractions containing biotinylated caspases were pooled, frozen in liquid nitrogen after adding sucrose (10%), and stored at -80°C in small aliquots.

DARPin selection by ribosome display

Cloning and amplification of a DARPin library has been described previously (Binz et al., 2003) and a library containing NI3C and NI2C DARPins was used for selections by ribosome display (Hanes and Plückthun, 1997; Zahnd et al., 2007). The selection procedure was slightly modified with focus on specificity and low k_{off} rates (see Supplementary Figure 1). To prevent unspecific binding to random proteins, each round included a pre-panning step for MBP (coated 22 nM). In addition, two of the most homologues caspases were included in pre-panning steps (coated 22 nM) in rounds 1 and 3. k_{off} maturation was done by adding a 100- and 500-fold excess of unbiotinylated caspase for 5 or 10 min in rounds 2 and 4, respectively. Unbound DARPin/ribosome complexes were washed after each round with increasing stringency (Supplementary Figure 1). The enriched library was cloned after 4 selection rounds into a pQE30 vector and transfected to XL1-Blue *Escherichia coli* cells (Stratagene, La Jolla, CA, USA).

Crude extract ELISA

Single *E. coli* colonies, each expressing one selected DARPins, were picked and inoculated in 900 µl auto-inducing media (Studier, 2005) using 96-well plates (Abgene by Fisher Scientific, Wohlen, Switzerland). Cells grew over night at 37°C; 200 µl of each well were then transferred to a 96-well plate (Nunc by Thermo Fisher Scientific, Waltham, MA, USA) for plasmid preparation, and 700 µl were harvested by centrifugation. Cells were lysed using B-PER II (50 µl, 78260; Pierce Biotechnology, Rockford, IL, USA) per well (30 min, shaking at room temperature). Lysis buffer was neutralized with PBS (950 µl) and cell debris was removed by centrifugation (20 min, 4500 rpm at 4°C). A 20-µl supernatant were transferred to 384 well ELISA plates (Nunc by Thermo Fisher Scientific, Waltham, MA, USA), which were prepared in advance with either immobilized MBP or targeted caspase. For immobilization, plates were coated using NeutrAvidin solution (20 µl at 22 nM, 31000; Pierce Biotechnology, Rockford, IL, USA), followed by incubation of biotinylated proteins and extensive washing. Cell lysate supernatants containing the expressed DARPin were incubated for 1 h at room temperature. After three washing cycles (PBS), each well was incubated with mouse anti-RGS-H4 antibody (1:2000 in PBS+1% bovine serum albumin, 34650; Qiagen, Boston, MA, USA). After washing, the secondary antibody (goat α-mouse IgG alkaline phosphatase conjugate from Sigma; A3562) was incubated. After four washing cycles, the substrate (3 mM di-sodium 4-nitrophenyl phosphate in 50 mM $NaHCO_3$, 50 mM $MgCl_2$) was added and $OD_{405\,nm}$ was measured using a multiwell plate reader (Tecan Infinity M1000, Tecan, Männedorf, Switzerland). DARPins exhibited strong signals (>5-fold vs. MBP control) were sequenced.

Expression and purification of DARPins

DARPins were expressed in auto-inducing media (Studier, 2005) overnight or in 2YT (3 h at 37°C) after the induction with isopropyl β-D-1-thiogalactopyranoside (0.5 mM, IPTG) at an $OD_{600\,nm}$ between 0.6 and 1. Cells were harvested (6000 rpm, 5 min, 4°C; Biofuge primo R, Heraeus, Hanau, Germany) and lysed by ultrasonification. DARPin purification was performed by immobilized metal-affinity chromatography (gravity columns, 0.5 ml Ni^{2+}-NTA agarose beads, 30210; Qiagen, Boston, MA, USA). DARPins were eluted in PBS, 200 mM imidazole, pH 7.4. Imidazole was removed using a PD-10 desalting column (17-0435-01; GE Healthcare, Piscataway, NJ, USA). For storage at 4°C, 0.05% sodium azide (NaN_3) was added, whereas 20% glycerol was used for storage at -20°C.

Complex formation on SEC

Purified caspases were incubated with a 2-fold molar excess of selected DARPins. Protein solutions were applied on SEC using a Superdex 200 5/150 GL column (GE Healthcare, Piscataway, NJ, USA) equilibrated in 50 mM Tris, 150 mM NaCl, pH 7.5. Absorption at 280 nm was recorded and analyzed in Prism (Version 5, GraphPad Software, La Jolla, CA, USA).

SPR analysis

SPR experiments were performed using a Proteon XPR36 (Bio-Rad Laboratories, Hercules, CA, USA) and an NLC sensor chip. Sterile filtered PBS, pH 7.3, 0.005% Tween 20, was the standard buffer for all coating and kinetic measurements. Approximately 1000 RU of biotinylated caspases (5 nM) were coated on the chip at 30 µl/min. Dilution series of DARPin analytes were prepared prior to the experiment in 96-well plates and sealed to prevent evaporation or contamination. At least eight different concentrations (0–500 nM) starting with the lowest concentration were measured at 20°C. Due to the heterogeneity of the system, the chip surface was not regenerated between different analyte concentration but dissociation time could be prolonged up to 30 min. In general, experiments were performed at flow rates of 100 µl/min with 5-min association phases and 20 min dissociation phases. Recorded data were processed and evaluated using ProteOn Manager 2.1.1 (Bio-Rad Laboratories, Hercules, CA, USA). Binding kinetics and affinities were determined by equilibrium analysis or curve fitting (Bravman et al., 2006).

Crystallization of caspase 8 in complex with DARPin D8.4

Caspase 8 was incubated with a 2-fold molar excess of DARPin D8.4 (10 min on ice). The formed complex was separated using a Superdex 200 10/300 GL column (GE Healthcare, Piscataway, NJ, USA), 20 mM Tris, pH 7.5 (4°C), 20 mM NaCl. Fractions containing the dimeric caspase 8/D8.4 complex were pooled and concentrated (15–21 mg/ml) using an Amicon Ultra centrifugation device (10 kDa MWCO, EMD Millipore, Darmstadt, Germany). Prior to crystallization, the protein solution was incubated with a peptide aldehyde inhibitor Ac-IETD-CHO (two inhibitors per active site). Crystals were grown at room temperature using sitting-drop vapor-diffusion method (100 mM citric acid, pH 4.9, 200 mM Li_2SO_4, and 22.4% PEG 4000). For cryoprotection, the

crystals were equilibrated in reservoir buffer containing ethylene glycol (10%–15%) and flash frozen in a nitrogen stream at -170°C.

X-ray diffraction, data collection, and structure determination

Diffraction data were collected at the Swiss Light Source (SLS, X06SA beamline) on a Pilatus 6M fast readout pixel detector. XDS (Kabsch, 2010) was used for data processing. The crystal structure was solved by molecular replacement using PHASER (McCoy et al., 2007) and the structure of caspase 8 (1QDU) (Blanchard et al., 1999) and a NI3C-DARPin (2QYJ) (Merz et al., 2008) as search model. Structure refinement was performed with REFMAC 5.5.01.09 (Murshudov et al., 1997) and binding interface analysis was done using the EPPIC server (Duarte et al., 2012) (www.eppic-web.org). Structure figures were prepared in PyMOL (http://www.pymol.org).

Accession numbers

Atomic coordinates and structure factors of caspase 8/D8.4 were deposited in the Protein Data Bank (2Y1L).

Competing financial interests

T.S. is partner at Nextech Invest Ltd. and R.A. is employed at Cilag AG. The other authors declare no competing financial interest.

Acknowledgments: Financial support of this work was provided by the Swiss National Science Foundation grant 310030-122342 to M.G.G. We thank Beat Blattmann and Céline Stutz-Ducommun from the NCCR crystallization facility for crystal screening and the staff of the X06SA beamline at the Swiss Light Source of the Paul Scherrer Institute (PSI) for their support during data collection. Dr. Christopher Weinert is acknowledged for his calibration data of the size exclusion column.

References

Amstutz, P., Binz, H.K., Parizek, P., Stumpp, M.T., Kohl, A., Grütter, M.G., Forrer, P., and Plückthun, A. (2005). Intracellular kinase inhibitors selected from combinatorial libraries of designed ankyrin repeat proteins. J. Biol. Chem. *280*, 24715–24722.

Binz, H.K., Stumpp, M.T., Forrer, P., Amstutz, P., and Plückthun, A. (2003). Designing repeat proteins: well-expressed, soluble and stable proteins from combinatorial libraries of consensus ankyrin repeat proteins. J. Mol. Biol. *332*, 489–503.

Binz, H.K., Amstutz, P., Kohl, A., Stumpp, M.T., Briand, C., Forrer, P., Grütter, M.G., and Plückthun, A. (2004). High-affinity binders selected from designed ankyrin repeat protein libraries. Nat. Biotechnol. *22*, 575–582.

Blanchard, H., Kodandapani, L., Mittl, P.R., Marco, S.D., Krebs, J.F., Wu, J.C., Tomaselli, K.J., and Grütter, M.G. (1999). The three-dimensional structure of caspase-8: an initiator enzyme in apoptosis. Structure *7*, 1125–1133.

Boucher, D., Blais, V., and Denault, J.B. (2012). Caspase-7 uses an exosite to promote poly(ADP ribose) polymerase 1 proteolysis. Proc. Natl. Acad. Sci. USA *109*, 5669–5674.

Bravman, T., Bronner, V., Lavie, K., Notcovich, A., Papalia, G.A., and Myszka, D.G. (2006). Exploring "one-shot" kinetics and small molecule analysis using the ProteOn XPR36 array biosensor. Anal. Biochem. *358*, 281–288.

Duarte, J.M., Srebniak, A., Schärer, M.A., and Capitani, G. (2012). Protein interface classification by evolutionary analysis. BMC Bioinform. *13*, 334.

Favaloro, B., Allocati, N., Graziano, V., Di Ilio, C., and De Laurenzi, V. (2012). Role of apoptosis in disease. Aging *4*, 330–349.

Flütsch, A., Ackermann, R., Schroeder, T., Lukarska, M., Hausammann, G.J., Weinert, C., Briand, C., and Grütter, M.G. (2014). Combined inhibition of caspase 3 and caspase 7 by two highly selective DARPins slows down cellular demise. Biochem. J. *461*, 279–290.

Fuentes-Prior, P. and Salvesen, G.S. (2004). The protein structures that shape caspase activity, specificity, activation and inhibition. Biochem. J. *384*, 201–232.

Grütter, M.G. (2000). Caspases: key players in programmed cell death. Curr. Opin. Struct. Biol. *10*, 649–655.

Hanes, J. and Plückthun, A. (1997). In vitro selection and evolution of functional proteins by using ribosome display. Proc. Natl. Acad. Sci. USA *94*, 4937–4942.

Hardy, J.A., Lam, J., Nguyen, J.T., O'Brien, T., and Wells, J.A. (2004). Discovery of an allosteric site in the caspases. Proc. Natl. Acad. Sci. USA *101*, 12461–12466.

Kabsch, W. (2010). Integration, scaling, space-group assignment and post-refinement. Acta Crystallogr. D Biol. Crystallogr. *66*, 133–144.

McCoy, A.J., Grosse-Kunstleve, R.W., Adams, P.D., Winn, M.D., Storoni, L.C., and Read, R.J. (2007). Phaser crystallographic software. J. Appl. Crystallogr. *40*, 658–674.

McStay, G.P., Salvesen, G.S., and Green, D.R. (2008). Overlapping cleavage motif selectivity of caspases: implications for analysis of apoptotic pathways. Cell Death Differ. *15*, 322–331.

Merz, T., Wetzel, S.K., Firbank, S., Plückthun, A., Grütter, M.G., and Mittl, P.R. (2008). Stabilizing ionic interactions in a full-consensus ankyrin repeat protein. J. Mol. Biol. *376*, 232–240.

Murshudov, G.N., Vagin, A.A., and Dodson, E.J. (1997). Refinement of macromolecular structures by the maximum-likelihood method. Acta Crystallogr. D Biol. Crystallogr. *53*, 240–255.

Rohn, T.T. (2010). The role of caspases in Alzheimer's disease; potential novel therapeutic opportunities. Apoptosis *15*, 1403–1409.

Roschitzki-Voser, H., Schroeder, T., Lenherr, E.D., Frölich, F., Schweizer, A., Donepudi, M., Ganesan, R., Mittl, P.R., Baici, A., and Grütter, M.G. (2012). Human caspases in vitro: expression, purification and kinetic characterization. Protein Expr. Purif. *84*, 236–246.

Salvesen, G.S. and Dixit, V.M. (1999). Caspase activation: the induced-proximity model. Proc. Natl. Acad. Sci. USA *96*, 10964–10967.

Schroeder, T., Barandun, J., Flütsch, A., Briand, C., Mittl, P.R., and Grütter, M.G. (2013). Specific inhibition of caspase-3 by a competitive DARPin: molecular mimicry between native and designed inhibitors. Structure *21*, 277–289.

Schweizer, A., Roschitzki-Voser, H., Amstutz, P., Briand, C., Gulotti-Georgieva, M., Prenosil, E., Binz, H.K., Capitani, G., Baici, A., Plückthun, A., et al. (2007). Inhibition of caspase-2 by a designed ankyrin repeat protein: specificity, structure, and inhibition mechanism. Structure *15*, 625–636.

Seeger, M.A., Zbinden, R., Flütsch, A., Gutte, P.G., Engeler, S., Roschitzki-Voser, H., and Grütter, M.G. (2013). Design, construction, and characterization of a second-generation DARPin library with reduced hydrophobicity. Protein Sci. *22*, 1239–1257.

Sennhauser, G., Amstutz, P., Briand, C., Storchenegger, O., and Grütter, M.G. (2007). Drug export pathway of multidrug exporter AcrB revealed by DARPin inhibitors. PLoS Biol. *5*, e7.

Stefan, N., Martin-Killias, P., Wyss-Stoeckle, S., Honegger, A., Zangemeister-Wittke, U., and Plückthun, A. (2011). DARPins recognizing the tumor-associated antigen EpCAM selected by phage and ribosome display and engineered for multivalency. J. Mol. Biol. *413*, 826–843.

Steiner, D., Forrer, P., and Plückthun, A. (2008). Efficient selection of DARPins with sub-nanomolar affinities using SRP phage display. J. Mol. Biol. *382*, 1211–1227.

Studier, F.W. (2005). Protein production by auto-induction in high density shaking cultures. Protein Expr. Purif. *41*, 207–234.

Taylor, R.C., Cullen, S.P., and Martin, S.J. (2008). Apoptosis: controlled demolition at the cellular level. Nat. Rev. Mol. Cell Biol. *9*, 231–241.

Watt, W., Koeplinger, K.A., Mildner, A.M., Heinrikson, R.L., Tomasselli, A.G., and Watenpaugh, K.D. (1999). The atomic-resolution structure of human caspase-8, a key activator of apoptosis. Structure *7*, 1135–1143.

Zahnd, C., Amstutz, P., and Plückthun, A. (2007). Ribosome display: selecting and evolving proteins *in vitro* that specifically bind to a target. Nat. Methods *4*, 269–279.

Supplemental Material: The online version of this article (DOI: 10.1515/hsz-2014-0173) offers supplementary material, available to authorized users.

Supplementary material for

Specific targeting of human caspases using designed ankyrin repeat proteins

Andreas Flütsch[1,2,#], Thilo Schroeder[1,3,#], Jonas Barandun[1,4,#], Rafael Ackermann[1], Martin Bühlmann[1], Markus G. Grütter[1,*]

[1]Department of Biochemistry, University of Zurich, Winterthurerstrasse 190, CH-8057 Zurich, Switzerland

[2]present address: University of California, San Diego, 9500 Gilman Drive, La Jolla, CA 92093-0629, USA

[3]present address: Nextech Invest Ltd., Scheuchzerstrasse 35, 8006 Zurich, Switzerland

[4]present address: The Rockefeller University, Laboratory of Protein and Nucleic Acid Chemistry, 1230 York Avenue, New York, NY 10065, USA

[#]These authors contributed equally to this work

MGG: Tel. +41-44-6355580, Fax. +41-44-6356834, E-mail. gruetter@bioc.uzh.ch

Supplementary Figure 1

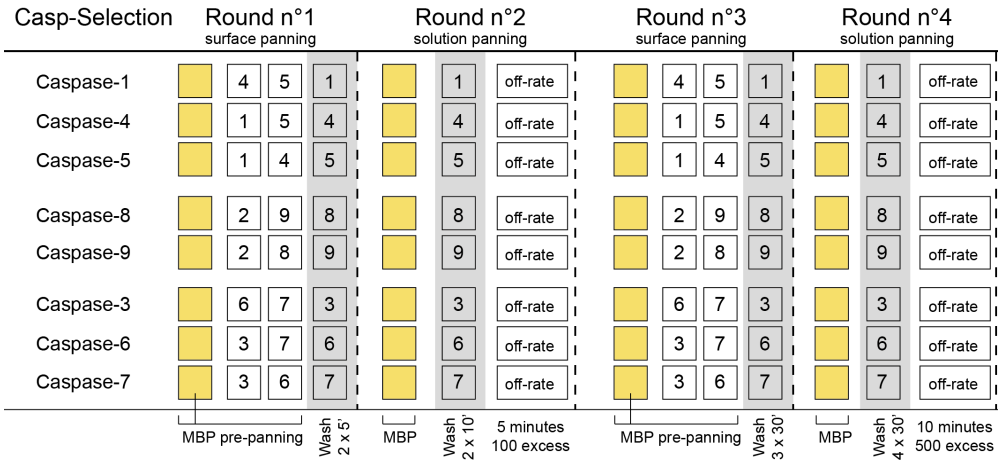

Supplementary Figure 1: Ribosome display selection strategy

To increase the binders specificity for a single caspase family member, additional pre-panning steps in round no°1 and no°3 with the closest homologues of the targeted caspase was introduced. In addition, round n°2 and n°4 was extended with k_{off} maturation steps with a final washing step containing an excess of targeted caspase.

Supplementary Figure 2

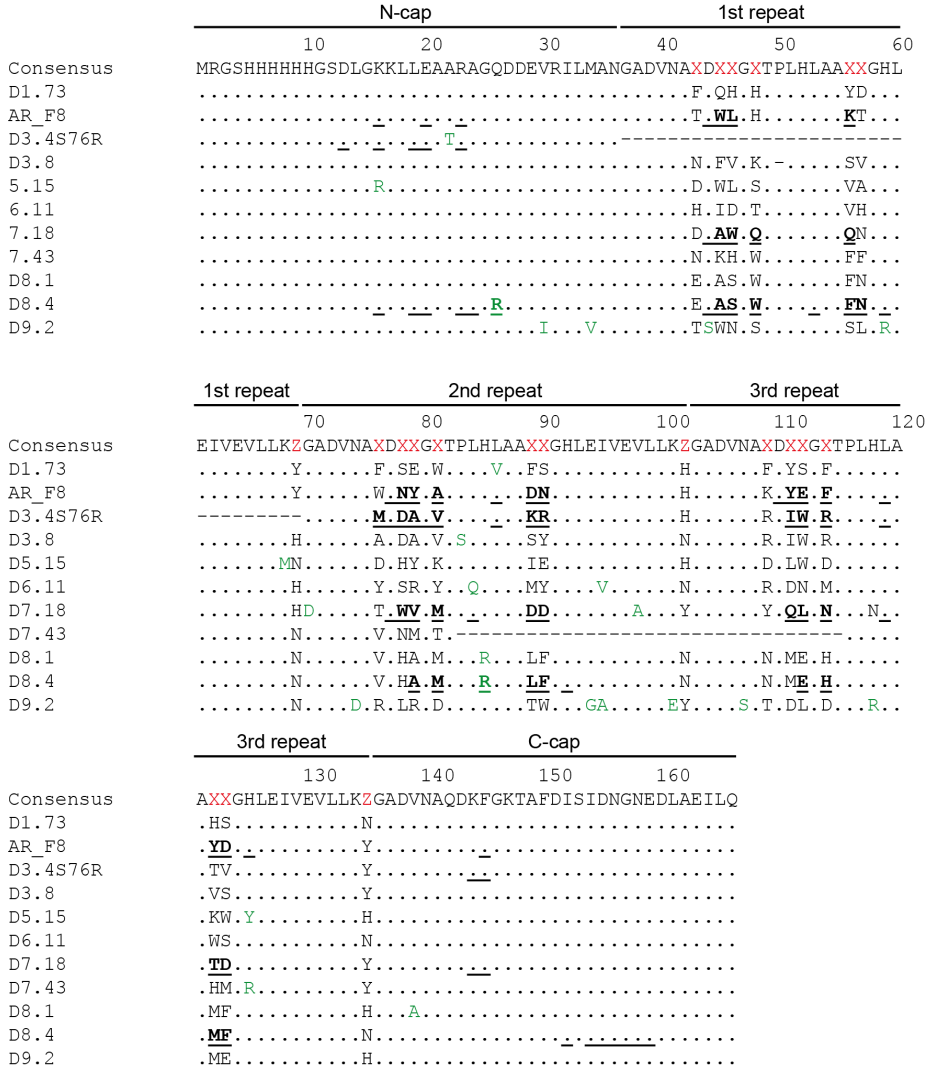

Supplementary Figure 2: Caspase-targeted DARPin sequences

The DARPin consensus sequence is shown on top in black with randomized residues in red (X = All amino acids except Cys, Gly and Pro; Z = N, H or Y). Unintended framework mutations are depicted in green. Interacting residues were determined by the EPPIC server (1) (http://www.eppicweb.org) and are marked bold and underlined.

Supplementary Table 1

DARPin	Target	Type	No# of AA	Molecular weight	Extinction coefficient	Theoretical isoelectric point	Comments	Ref.
D1.73	Casp-1	N3C	169	18358	9970	5.34	No inhibition of small substrates	
AR_F8	Casp-2	N3C	169	18417	18450	5.28	Allosteric inhibitor	(2)
D3.4S76R	Casp-3	N2C	136	14786	6690	5.56	Competitive Inhibitor	(3)
D3.8	Casp-3	N3C	168	17964	8480	5.51	Competitive Inhibitor	(3)
D5.15	Casp-5	N3C	169	18324	19480	4.99	No inhibition of small substrates	
D6.11	Casp-6	N3C	169	18300	9970	5.46	No inhibition of small substrates	
D7.18	Casp-7	N3C	169	18273	15470	4.74	Zymogen activation inhibitor	(4)
D7.43	Casp-7	N2C	136	14812	6990	5.68	Zymogen activation inhibitor	(4)
D8.1	Casp-8	N3C	169	18157	5500	5.28	No inhibition of small substrates	
D8.4	Casp-8	N3C	169	18190	5500	5.30	No inhibition of small substrates	
D9.2	Casp-9	N3C	169	18112	12490	5.01	No inhibition of small substrates	

Supplementary Table 1: Biophysical parameters of selected DARPins

Molecular weight, extinction coefficient and theoretical isoelectric point were calculated using the ProtParam Tool provided on expasy.ch (http://web.expasy.org/protparam/). Eight of eleven binders are N3C DARPins and five DARPins have reported inhibitory effects on the targeted caspase (2-4). All other selected DARPins did not show an inhibitory effect using peptide substrates. However, procaspase binding and interference with caspase activation as reported for caspase-7 DARPins (4) was not tested and thus can not be excluded.

Supplementary Figure 3

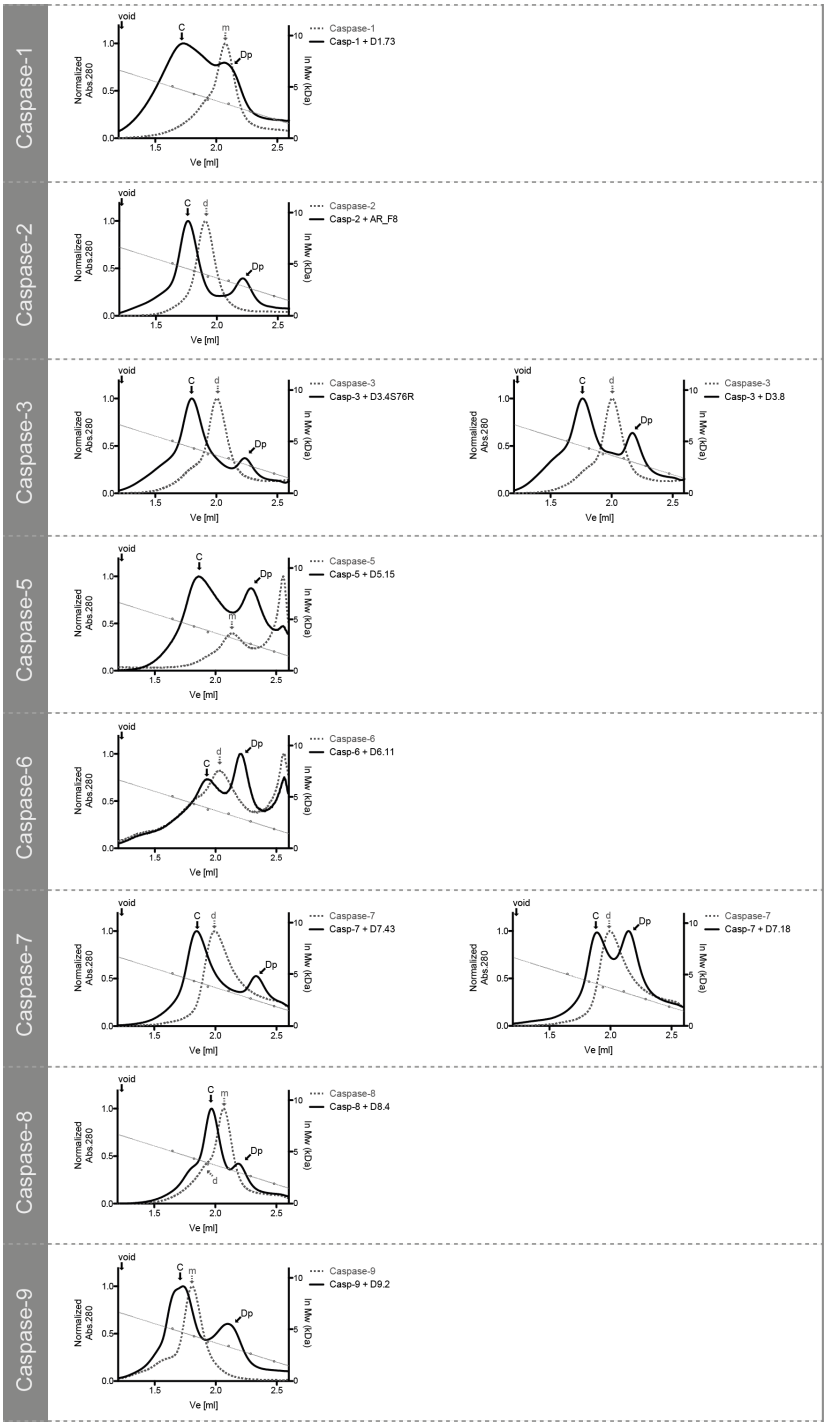

Supplementary Figure 3: Caspase-DARPin complex formation in solution

The reported DARPins form stable protein complexes with the targeted caspase in solution and can be separated on size exclusion chromatography. Without a present DARPin, Caspases-1, -5 and -9 run as monomers (dotted line, peak marked with dotted arrow and (m) for monomer), whereas caspases-2, -3, -6 and -7 run as dimers (peak marked with dotted arrow and (d) for dimer). Caspase-8 shows a monomer-dimer equilibrium (marked with (m) and (d) respectively). In presence of a selected DARPin, all caspases elute at earlier retention volumes (solid lines, complex peak marked with (C), for complex and (Dp) for DARPin excess). Caspase-5 and -6 were used directly after NiNTA purification (5) displaying an elution peak at 2.6 ml originating from imidazole. Calibration curve (right ordinate) was made using aldolase (158 kDa), conalbumin (75 kDa), ovalbumin (43 kDa), carbonic anhydrase (29 kDa), ribonuclease A (13.7 kDa) and aprotinin (6.5 kDa).

DOI: 10.1515/hsz-2014-0173,

Supplementary Table 2

Data collection	
Space group	$P2_12_12_1$
Cell dimensions	
a, *b*, *c* (Å)	61.0, 81.60, 163.20
α, β, γ (°)	90.0, 90.0, 90.0
Resolution (Å)	48.86 – 1.8
Wavelength (Å)	1.0
R_{sym} (%)	9.8 (51.5)
Completeness (%)	99.4 (98.9)
I/σ(I)	13.29 (3.76)
Refinement	
Resolution [Å]	1.8
R_{work}/R_{free}	18.0 / 21.8
No. atoms	
Protein	6246
Water	685
Ligands	$3 \cdot SO_4^{2-}$, $5 \cdot C_2H_6O_2$
B-factors	
Protein	22.9
Water	33.9
rmsd	
Bond length [Å]	0.009
Bond angle [°]	1.2
Ramachandran	
Preferred [%]	97.0
Allowed [%]	3.0
Outliers [%]	0

Supplementary Table 2: Data collection and refinement statistics

Supplementary Figure 4

a)

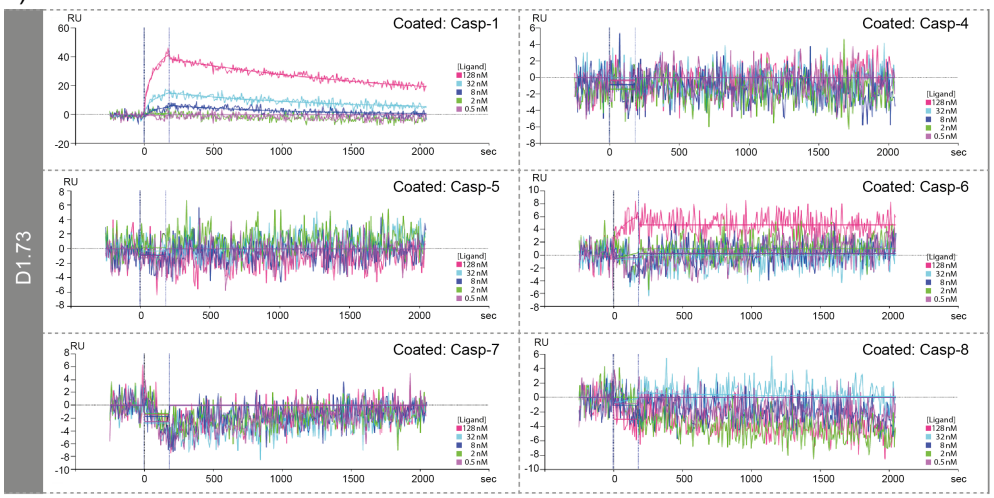

b)

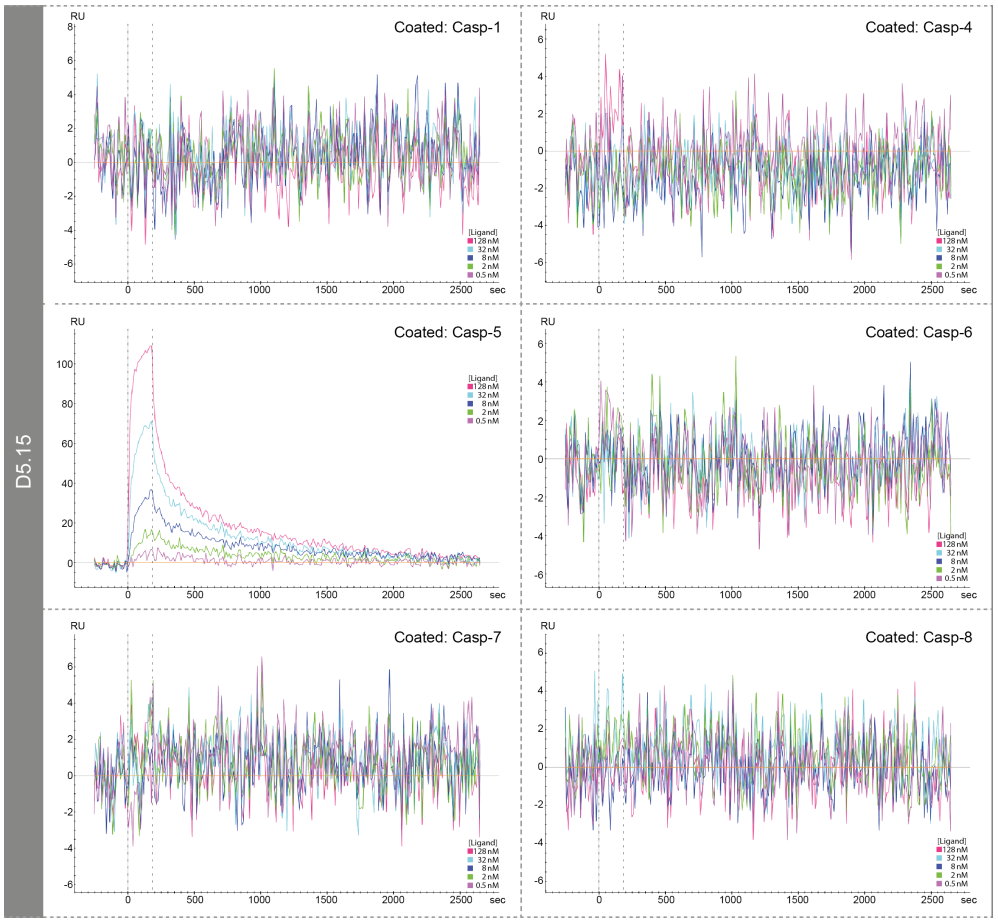

Supplementary Figure 4

c)

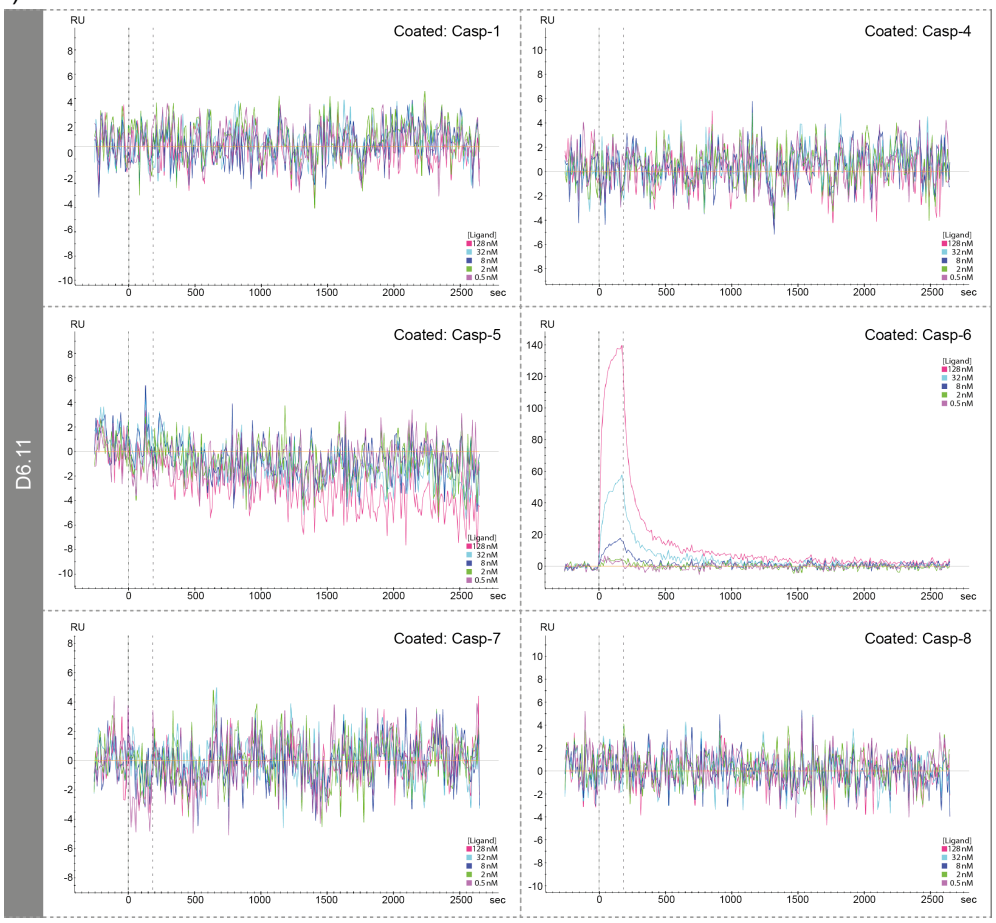

Supplementary Figure 4

d)

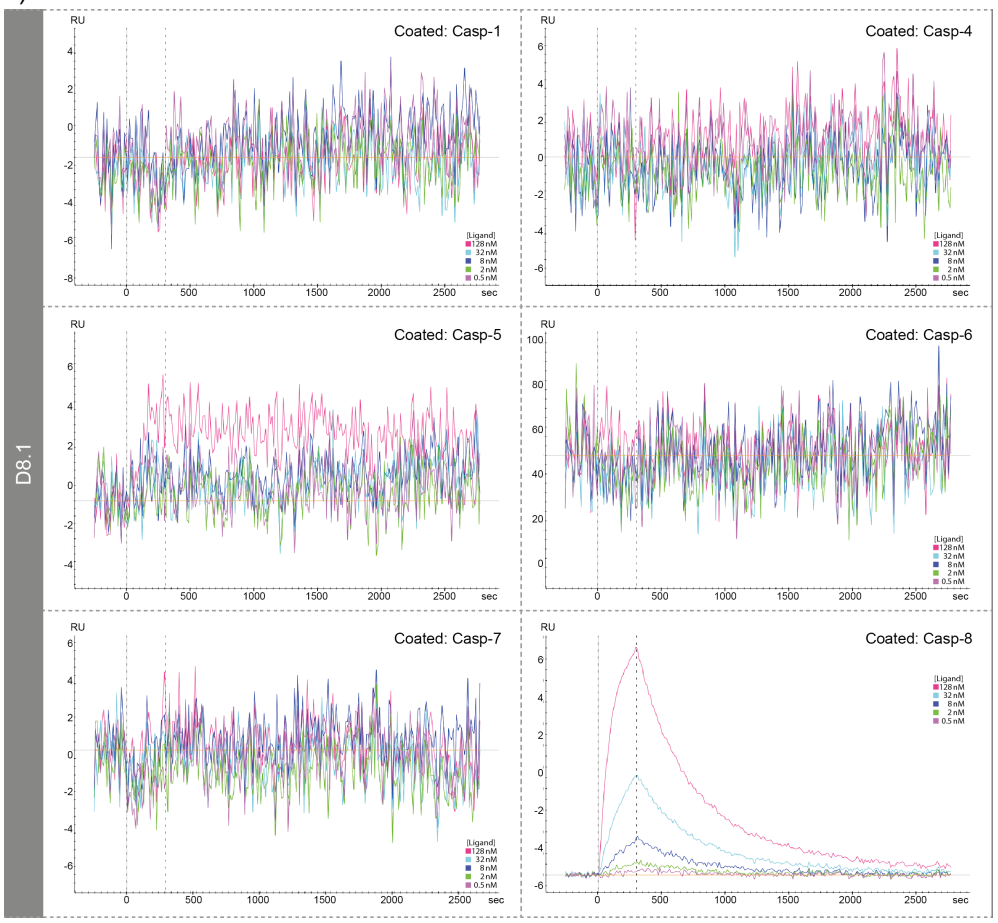

Supplementary Figure 4: Caspase specificity of selected DARPins

Caspase specificity of (a) D1.73, (b) D5.15, (c) D6.11 and (d) D8.1 was measured by surface plasmon resonance on a Proteon XPR36 (Bio-Rad Laboratories, Inc) machine using a NLC sensor chip. Six ligand channels were coated with biotinylated caspases-1, -4, -5, -6, -7 and -8 and binding of the DARPins was simultaneously observed at six different concentrations (0 nM to 128 nM). Caspase specificity of AR_F8 for caspase-2, D3.4S76R for caspase-3 and D7.18 as well as D7.43 for caspase-7 is reported elsewhere (2-4). D9.2 was not tested against other caspase family members.

Supplementary Figure 5

a)

b)

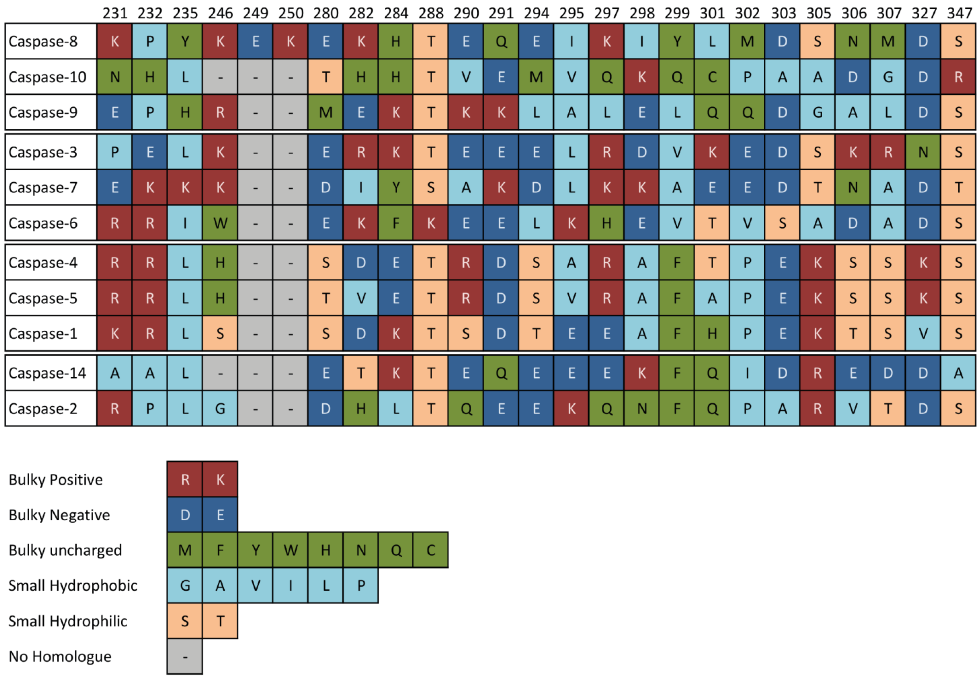

Supplementary Figure 5: DARPin D8.4/Caspase-8 interacting residues

(a) DARPin sequence D8.1 and D8.4 are aligned with the DARPin consensus sequence displaying two unintended framework mutations: H85R and V139A in D8.1; Q26R and H85R in D8.4 (marked in green). Interacting residues determined by the EPPIC server (1) (http://www.eppicweb.org) are marked in bold/underlined. In total, 18 framework and 13 randomized residues are involved in a binding interface of overall 938 $Å^2$. Notably, the D8.1 sequence is almost identical and besides Arg-26, all interacting residues of D8.4 are present in D8.1 suggesting the same interaction.

(b) Comparison of caspase-8 residues involved in D8.4 binding by sequence alignment (ClustalW2, http://www.ebi.ac.uk/Tools/msa/clustalw2/) with other human caspases. Amino acids are classified and colored in five groups. Caspase sequence accession numbers are indicated in supplementary figure 6.

Supplementary Figure 6

a)

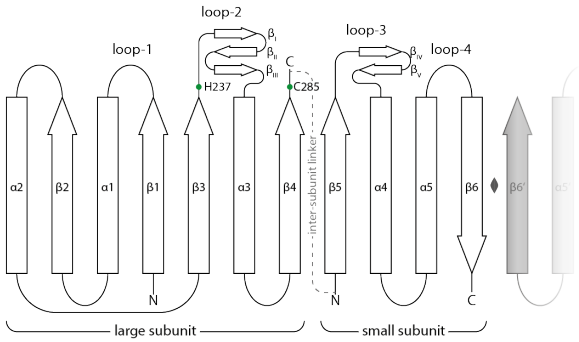

b)

```
Caspase-3  (P42574)  ----------------------------------------SYKMDYP--E  43
Caspase-7  (P55210)  ----------------------------------------TYQYNMNFE--K  66
Caspase-6  (P55212)  ---------------------------------------KYKMDHR--R  43
Caspase-8  (Q14790)  ----------------------------------SQTLDKVYQMKSK--P  232
Caspase-10 (Q92851)  KHAGSNGNRATNGAPSLVSRGMQGASANTLNSETSTKRAAVYRMNRN--H  282
Caspase-9  (P55211)  ----------------------------------NADLAYILSME--P  159
Caspase-4  (P49662)  ----------------------------------RAEEIYPIKERNNR  134
Caspase-5  (P51878)  ----------------------------------NHDEIYPIKKREDR  191
Caspase-1  (P29466)  ----------------------------------KSAEIYPIMDKSSR  161
Caspase-14 (P31944)  ----------------------------------------EKYDMSGARLA  20
Caspase-2  (P42575)  ----------------------------------HFQLAYRLQSR--P  198
                                                          * :
```

```
Caspase-3  (P42574)  MGLCIIINNKNFHKST-------GMTSRSGTDVDAANLRETFRNLKYEVR  86
Caspase-7  (P55210)  LGKCIIINNKNFDKVT-------GMGVRNGTDKDAEALTKCFRSLGFDVI  109
Caspase-6  (P55212)  RGIALIFNHERFFWHL-------TLPERRGTCADRDNLTRRFSDLGFEVK  86
Caspase-8  (Q14790)  RGYCLIINNHNFAKARDKVPKLHSIRDRNGTHLDAGALTTTFEELHFEIK  282
Caspase-10 (Q92851)  RGLCVIVNNHSFT----------SLKDRQGTHKDAEILSHVFQWLGFTVH  322
Caspase-9  (P55211)  CGHCLIINNVNFCRES-------GLRTRTGSNIDCEKLRRRFSSLHFMVE  202
Caspase-4  (P49662)  TRLALIICNTEFDHLP----------PRNGADFDITGMKELLEGLDYSVD  174
Caspase-5  (P51878)  RRLALIICNTKFDHLP----------ARNGAHYDIVGMKRLLQGLGYTVV  231
Caspase-1  (P29466)  TRLALIICNEEFDSIP----------RRTGAEVDITGMTMLLQNLGYSVD  201
Caspase-14 (P31944)  LILCVTK-------------------AREGSEEDLDALEHMFRQLRFEST  51
Caspase-2  (P42575)  RGLALVLSNVHFTGEK-------ELEFRSGGDVDHSTLVTLFKLLGYDVH  241
                           .:                  * *   *   :   :  * :
```


```
Caspase-3  (P42574)  NKNDLTREEIVELMRDVSK-EDHSKR--SSFVCVLLSHGEEG-------I  126
Caspase-7  (P55210)  VYNDCSCAKMQDLLKKASE-RDHTNA--ACFACILLSHGEEN-------V  149
Caspase-6  (P55212)  CFNDLKAEELLLKIHEVST-VSHADA--DCFVCVFLSHGEGN-------H  126
Caspase-8  (Q14790)  PHDDCIVEQIYEILKIYQL-MDHSNM--DCFICCILSHGDKG-------I  322
Caspase-10 (Q92851)  IHNNVTKVEMEMVLQKQKCNPAHADG--DCFVFCILTHGRFG-------A  363
Caspase-9  (P55211)  VKGDLTAKKMVLALLELAQ-QDHGAL--DCCVVVILSHGCQASHLQFPGA  249
Caspase-4  (P49662)  VEENLTARDMESALRAFATRPEHKSS--DSTFLVLMSHGILEG--ICGTV  220
Caspase-5  (P51878)  DEKNLTARDMESVLRAFAARPEHKSS--DSTFLVLMSHGILEG--ICGTA  277
Caspase-1  (P29466)  VKKNLTASDMTTELEAFAHRPEHKTS--DSTFLVFMSHGIREG--ICGKK  247
Caspase-14 (P31944)  MKRDPTAEQFQEELEKFQQAIDSREDPVSCAFVVLMAHGREG-------F  94
Caspase-2  (P42575)  VLCDQTAQEMQEKLQNFAQLPAHRVT--DSCIVALLSHGVEG-------A  282
                          : .  .:   :                .    :::**
```

```
Caspase-3  (P42574)   IFGTNG-PVDLKKITNFFRGDRCRSLTGKPKLFIIQACRG---------- 165
Caspase-7  (P55210)   IYGKDG-VTPIKDLTAHFRGDRCKTLLEKPKLFFIQACRG---------- 188
Caspase-6  (P55212)   IYAYDA-KIEIQTLTGLFKGDKCHSLVGKPKIFIIQACRGNQHDVPVIPL 175
Caspase-8  (Q14790)   IYGTDGQEAPIYELTSQFTGLKCPSLAGKPKVFFIQACQGDNYQKG---- 368
Caspase-10 (Q92851)   VYSSDEALIPIREIMSHFTALQCPRLAEKPKLFFIQACQGEEIQPS---- 409
Caspase-9  (P55211)   VYGTDGCPVSVEKIVNIFNGTSCPSLGGKPKLFFIQACGGEQKDHGFEVA 299
Caspase-4  (P49662)   HDEKKPDVLLYDTIFQIFNNRNCLSLKDKPKVIIVQACRGANRGELWVRD 270
Caspase-5  (P51878)   HKKKKPDVLLYDTIFQIFNNRNCLSLKDKPKVIIVQACRGEKHGELWVRD 327
Caspase-1  (P29466)   HSEQVPDILQLNAIFNMLNTKNCPSLKDKPKVIIIQACRGDSPGVVWFKD 297
Caspase-14 (P31944)   LKGEDGEMVKLENLFEALNNKNCQALRAKPKVYIIQACRGE--------- 135
Caspase-2  (P42575)   IYGVDGKLLQLQEVFQLFDNANCPSLQNKPKMFFIQACRGDETDRGVDQQ 332
                                    :   :    *  *  ***: ::*** *
                      ──►──►═══(α3)═══►──►
                      βII loop 2 βIII  α3      β4

Caspase-3  (P42574)   TELDCGIETDSG-VDDDMA--C-----------HKIPVEADFLYAYSTAP 201
Caspase-7  (P55210)   TELDDGIQADSGPINDTDANPR-----------YKIPVEADFLFAYSTVP 227
Caspase-6  (P55212)   DVVDNQTEKLDTNITEVDAASV-----------YTLPAGADFLMCYSVAE 214
Caspase-8  (Q14790)   IPVETDSEEQPYLEMDLSSPQT-----------RYIPDEADFLLGMATVN 407
Caspase-10 (Q92851)   VSIEADALNPEQAPTSLQDS---------------IPAEADFLLGLATVP 444
Caspase-9  (P55211)   STSPEDESPGSNPEPDATPFQEGLRTFDQLDAISSLPTPSDIFVSYSTFP 349
Caspase-4  (P49662)   SPASLEVASSQSSENLEEDAVY------------KTHVEKDFIAFCSSTP 308
Caspase-5  (P51878)   SPASLALISSQSSENLEADSVC------------KIHEEKDFIAFCSSTP 365
Caspase-1  (P29466)   SVGVSGNLSLPTTEEFEDDAIK------------KAHIEKDFIAFCSSTP 335
Caspase-14 (P31944)   QRDPGETVGGDEIVMVIKDSPQ------------TIPTYTDALHVYSTVE 173
Caspase-2  (P42575)   DGKNHAGSPGCEESDAGKEKLP----------KMRLPTRSDMICGYACLK 372
                                                          * :   :
                      ═══════(inter-subunit linker)═══════►──►
                                                          β5

Caspase-3  (P42574)   GYYSWRNSKDGSWFIQSLCAMLKQYA-DKLEFMHILTRVN---RKVATEF 247
Caspase-7  (P55210)   GYYSWRSPGRGSWFVQALCSILEEHG-KDLEIMQILTRVN---DRVARHF 273
Caspase-6  (P55212)   GYYSHRETVNGSWYIQDLCEMLGKYG-SSLEFTELLTLVN---RKVSQRR 260
Caspase-8  (Q14790)   NCVSYRNPAEGTWYIQSLCQSLRERCPRGDDILTILTEVN---------Y 448
Caspase-10 (Q92851)   GYVSFRHVEEGSWYIQSLCNHLKKLVPRMLKFLEKTMEIRGRKRTVWGAK 494
Caspase-9  (P55211)   GFVSWRDPKSGSWYVETLDDIFEQWAHSEDLQSLLLRVAN---------- 389
Caspase-4  (P49662)   HNVSWRDSTMGSIFITQLITCFQKYS-WCCHLEEVFRKVQ---------- 347
Caspase-5  (P51878)   HNVSWRDRTRGSIFITELITCFQKYS-CCCHLMEIFRKVQ---------- 404
Caspase-1  (P29466)   DNVSWRHPTMGSVFIGRLIEHMQEYA-CSCDVEEIFRKVR---------- 374
Caspase-14 (P31944)   GYIAYRHDQKGSCFIQTLVDVFTKRKGHILELLTEV--TR--------RM 213
Caspase-2  (P42575)   GTAAMRNTKRGSWYIFALACVFSERA-CDMHVADMLVKVN----ALIKDR 417
                            : *     *: ::  *    : :                .
                      ──►──►═══(α4)═══►═══(α5)═══►
                      loop 3 βIV βV    α4        α5

Caspase-3  (P42574)   ESFSFDATFHAKKQIPCIVSMLTKELYFYH----- 277
Caspase-7  (P55210)   ESQSDDPHFHEKKQIPCVVSMLTKELYFSQ----- 303
Caspase-6  (P55212)   VDFCKDPSAIGKKQVPCFASMLTKKLHFFPKSN-- 293
Caspase-8  (Q14790)   EVSNKDDKKNMGKQMPQPTFTLRKKLVFPSD---- 479
Caspase-10 (Q92851)   QISATSLPTAISAQTPRPPMRRWSSVS-------- 521
Caspase-9  (P55211)   ----AVSVKGIYKQMPGCFNFLRKKLFFKTS---- 416
Caspase-4  (P49662)   ---QSFETPRAKAQMPTIERLSMTRYFYLFPGN-- 377
Caspase-5  (P51878)   ---KSFEVPQAKAQMPTIERATLTRDFYLFPGN-- 434
Caspase-1  (P29466)   ---FSFEQPDGRAQMPTTERVTLTRCFYLFPGH-- 404
Caspase-14 (P31944)   AEAELVQEGKARKTNPEIQSTLRKRLYLQ------ 242
Caspase-2  (P42575)   EGYAPGTEFHRCKEMSEYCSTLCRHLYLFPGHPPT 452
                                          .
                      ═══(loop 4)═══►──►
                                  β6
```

Supplementary Figure 5: Caspase sequence alignment and interacting residues

(a) Caspase topology map with active site residues (His-237 and Cys-285) indicated with green dots. Active-site forming loops are marked with loop-1 to loop-4. They are also known as 179-loop (=loop-1), 240-loop (=loop-2), 341-loop (=loop-3) and 381-loop (=loop-4) (6).

(b) Sequence alignment (ClustalW2, http://www.ebi.ac.uk/Tools/msa/clustalw2) of all human caspase family members with sequence accession numbers as indicated in the figure. DARPin interacting residues were determined using the EPPIC server (1) (http://www.eppicweb.org) and are marked in red. Primary structure elements are indicated below the sequence and labeled according the caspase topology map depicted in panel (a). Consensus symbols are depicted below the sequence with (*) indicating fully conserved residues and conservation of strongly (:) and weakly (.) similar properties.

References

1. Duarte, J. M., Srebniak, A., Scharer, M. A., and Capitani, G. (2012) Protein interface classification by evolutionary analysis. *BMC Bioinformatics* **13**, 334
2. Schweizer, A., Roschitzki-Voser, H., Amstutz, P., Briand, C., Gulotti-Georgieva, M., Prenosil, E., Binz, H. K., Capitani, G., Baici, A., Plückthun, A., and Grütter, M. G. (2007) Inhibition of caspase-2 by a designed ankyrin repeat protein: specificity, structure, and inhibition mechanism. *Structure* **15**, 625-636
3. Schroeder, T., Barandun, J., Flütsch, A., Briand, C., Mittl, P. R., and Grütter, M. G. (2013) Specific inhibition of caspase-3 by a competitive DARPin: molecular mimicry between native and designed inhibitors. *Structure* **21**, 277-289
4. Flütsch, A., Ackermann, R., Schroeder, T., Lukarska, M., Hausammann, G. J., Weinert, C., Briand, C., and Grütter, M. G. (2014) Combined inhibition of caspase-3 and caspase-7 by two highly selective DARPins slows down cellular demise. *Biochem J*
5. Roschitzki-Voser, H., Schroeder, T., Lenherr, E. D., Frölich, F., Schweizer, A., Donepudi, M., Ganesan, R., Mittl, P. R., Baici, A., and Grütter, M. G. (2012) Human caspases in vitro: expression, purification and kinetic characterization. *Protein Expr Purif* **84**, 236-246
6. Fuentes-Prior, P., and Salvesen, G. S. (2004) The protein structures that shape caspase activity, specificity, activation and inhibition. *Biochem J* **384**, 201-232

3 Publication: Caspase-3 Directed DARPins

Structure
Article

Specific Inhibition of Caspase-3 by a Competitive DARPin: Molecular Mimicry between Native and Designed Inhibitors

Thilo Schroeder,[1,2] Jonas Barandun,[1,2,3] Andreas Flütsch,[1,2] Christophe Briand,[1] Peer R.E. Mittl,[1] and Markus G. Grütter[1,*]
[1]Department of Biochemistry, University of Zurich, Winterthurerstrasse 190, CH-8057 Zürich, Switzerland
[2]These authors contributed equally to this work
[3]Present address: Institute of Molecular Biology and Biophysics, Schafmattstrasse 20, ETH Zürich, CH-8093 Zürich, Switzerland
*Correspondence: gruetter@bioc.uzh.ch
http://dx.doi.org/10.1016/j.str.2012.12.011

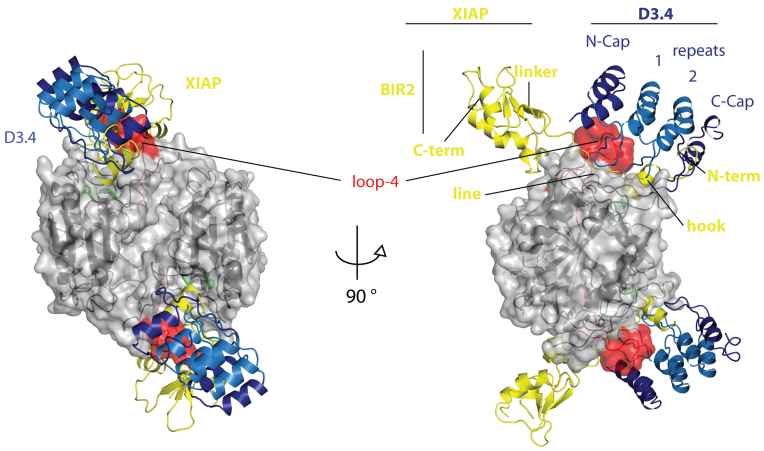

Figure 4C: Caspase-3 in complex with DARPin D3.4 (PDB: 2XZD) compared to caspase-3/XIAP complex structure (PDB: 1I3O)

Structure
Article

Specific Inhibition of Caspase-3 by a Competitive DARPin: Molecular Mimicry between Native and Designed Inhibitors

Thilo Schroeder,[1,2] Jonas Barandun,[1,2,3] Andreas Flütsch,[1,2] Christophe Briand,[1] Peer R.E. Mittl,[1] and Markus G. Grütter[1,*]
[1]Department of Biochemistry, University of Zurich, Winterthurerstrasse 190, CH-8057 Zürich, Switzerland
[2]These authors contributed equally to this work
[3]Present address: Institute of Molecular Biology and Biophysics, Schafmattstrasse 20, ETH Zürich, CH-8093 Zürich, Switzerland
*Correspondence: gruetter@bioc.uzh.ch
http://dx.doi.org/10.1016/j.str.2012.12.011

SUMMARY

Dysregulation of apoptosis is associated with several human diseases. The main apoptotic mediators are caspases, which propagate death signals to downstream targets. Executioner caspase-3 is responsible for the majority of cleavage events and its therapeutic potential is of high interest with to date several available active site peptide inhibitors. These molecules inhibit caspase-3, but also homologous caspases. Here, we describe caspase-3 specific inhibitors D3.4 and D3.8, which have been selected from a library of designed ankyrin repeat proteins (DARPins). The crystal structures of D3.4 and mutants thereof show how high specificity and inhibition is achieved. They also show similarities in the binding mode with that of the natural caspase inhibitor XIAP (X-linked inhibitor of apoptosis). The kinetic data reveal a competitive inhibition mechanism. D3.4 is specific for caspase-3 and does not bind the highly homologous caspase-7. D3.4 therefore is an excellent tool to define the precise role of caspase-3 in the various apoptotic pathways.

INTRODUCTION

Apoptosis is a central process for the development and tissue homeostasis of multicellular organisms. It is characterized by morphological changes such as nuclear fragmentation, membrane blebbing, or the formation of apoptotic bodies (Wyllie et al., 1980). In multicellular organisms including humans, improper regulation of apoptosis leads to a variety of pathologies such as cancer, autoimmune diseases, and neurodegenerative disorders (Riedl and Shi, 2004). Apoptosis is triggered by various internal and external stimuli, which are propagated by different pathways. Common to all apoptotic pathways are caspases (Fuentes-Prior and Salvesen, 2004; Grütter, 2000; Riedl and Shi, 2004). These proteins are synthesized as inactive proenzymes and activated upon triggering of the cell death machinery: The activation of initiator caspases occurs through dimerization (induced proximity model; Boatright et al., 2003; Muzio et al., 1998), followed by autoproteolytic cleavage of the prodomain and the linker between the two subdomains. Executioner caspases exist as dimeric zymogens and are activated by proteolytic cleavage of the N-terminal pro-peptide and the intersubunit linker (Fuentes-Prior and Salvesen, 2004). Active caspases are dimers of two catalytic domains with a small p10 and a large p20 chain.

Of the 11 known human caspases, caspase-3 plays a prominent role in the apoptotic cascade. Caspase-3 is activated by intrinsic and/or extrinsic death signals and it executes cell death by the cleavage of downstream key mediators of apoptosis (Timmer and Salvesen, 2007). Because apoptosis is a dangerous process for the cell, caspase activation is strictly controlled and all apoptotic signaling pathways are tightly regulated. All caspases recognize tetrapeptide sequences, which are characterized by an aspartic acid at the C terminus (P1 position) and either tryptophan, aspartic acid or leucine residues at the N terminus (P4 position) conferring selectivity for caspase-1, -3, and -8, respectively. The P4 selectivity has been attributed to different interactions with residues in loops flanking the P4 binding pocket (Mittl et al., 1997; Rotonda et al., 1996). However, the selectivity of short peptidic substrates remains controversial. It has been reported that the in vitro selectivity of caspase-3 for a substrate harboring a P4 aspartic acid is at least 100-fold higher than that for a glutamate or an asparagine (Stennicke et al., 2000). Despite this finding, commercially available peptide substrates failed to exhibit the expected caspase selectivity (McStay et al., 2008). Caspase-3 is the most unrestrained and efficient caspase and it is often more active in cleaving short peptide substrates than the caspase for which the peptide substrate was designed for (McStay et al., 2008). This analysis raised doubt regarding the use of short peptides to dissect signaling cascades leading to apoptosis. The observation that naturally occurring caspase inhibitors, such as X-linked inhibitor of apoptosis (XIAP), are highly specific for caspase-3 and -7 (Deveraux et al., 1997; Roy et al., 1997) suggests that specificity can be gained by extending the size of the inhibitor. Caspases are attractive drug targets because they are implicated in various diseases. Therefore, selective and potent caspase-specific inhibitors are highly desirable.

To develop a caspase-3 specific inhibitor, we used the Designed Ankyrin Repeat Protein (DARPin) technology (Binz et al., 2003). From a highly diverse library of DARPin molecules, binders that recognize the target molecule can be selected by

Structure
Caspase-3 Directed DARPins

Figure 1. Sequence Alignment of Caspase-3-Specific DARPin Binders

The general DARPin sequence is shown with the consensus sequence in black and the randomized amino acid positions in red (X, any of the 20 natural amino acids except cysteine, glycine, or proline; Z, any of the amino acids asparagine, histidine, or tyrosine). Four DARPin sequences are aligned to the consensus sequence with identical residues represented as a dot. Amino acids involved in the interaction with caspase-3 are colored in orange. Differences among the D3.4 and D3.8 sequences are highlighted in green. The D3.4_S76R mutation is marked by a red box. The sequence number is based on D3.4, a N2C DARPin that lacks the first internal repeat.

either ribosome- or phage display (Steiner et al., 2006; Zahnd et al., 2007). DARPins consist of N- and C-terminal capping repeats and two or three internal repeats. These internal repeats recognize the target molecule by means of specific amino acids that are randomized in the DARPin library. DARPins possess several beneficial properties that make them attractive for biotechnological applications. They are thermodynamically stable, easily produced, and do not contain cysteine residues allowing intracellular applications (Binz et al., 2005). Highly selective DARPins have been successfully selected and described for a variety of different target proteins such as caspase-2 (Schweizer et al., 2007) or kinase inhibitors (Amstutz et al., 2005), crystallization chaperones (Sennhauser et al., 2007), HIV inhibitors (Schweizer et al., 2008), and tumor-targeting binding molecules (Zahnd et al., 2010).

Here, we report the selection and characterization of DARPins that bind to active caspase-3. Kinetic and binding experiments revealed that DARPins D3.4 and D3.8 are competitive caspase-3 inhibitors that do not recognize other members of the caspase family at all (D3.4) or only extremely weakly caspase-7 (D3.8). The structure of the caspase-3/D3.4 complex reveals the critical interactions leading to high specificity and tight binding and analogies to XIAP inhibition.

RESULTS

Selection of Caspase-3-Specific DARPin Binders

A DNA library containing NI_2C and NI_3C DARPins was used to select caspase-3 binders by ribosome display (Zahnd et al., 2007). After four selection rounds, 768 putative binders were screened by crude cell extract ELISA yielding 29 clones that possessed submicromolar affinities for caspase-3. These high affinity binders were individually expressed, purified, and their binding affinities for caspase-3 were determined by surface plasmon resonance (SPR) analysis. Four of the selected DARPins showed affinities below 10 nM (Figure S1 available online). Their sequences were aligned and are shown in Figure 1. Although DARPins D3.4 and D3.8 contain 2 and 3 internal repeats, respectively, they possess the highest sequence similarity. Of the 14 randomized positions of the internal repeats seven residues are identical. When comparing the sequences of DARPin D3.6 and D3.13 only four residues in a total of 21 randomized positions are identical. Despite the different numbers of internal repeats all four DARPins possess very high affinities for caspase-3. SPR analysis revealed that D3.4, D3.6, D3.8 and D3.13 bind caspase-3 with K_D values of 9.6 ± 1.1 nM, 8.8 ± 2.0 nM, 3.4 ± 0.4 nM, and 7.7 ± 0.4 nM, respectively (Table 1). These K_D values were determined based on equilibrium analyses of the SPR signal. We used the heterogeneous ligand model to determine the kinetic values (Table 1), which suggests two epitopes with substantially different binding affinities (Morton et al., 1995).

Inhibition of Caspase-3 by DARPins D3.4 and D3.8

The inhibitory properties of the purified DARPins were analyzed using two different approaches. Initially the ability of the DARPins to inhibit the hydrolysis of the short chromogenic caspase-3 substrate Ac-DEVD-AMC was measured. These initial tests revealed that D3.4 and D3.8 inhibit the hydrolysis of the standard caspase-3 substrate with K_i values of 16.8 ± 0.3 nM and 6.7 ± 0.2 nM, respectively, whereas D3.6 and D3.13 showed no detectable inhibitory activities (Table 1). To characterize the mode of inhibition (competitive versus uncompetitive), specific velocity plot (Figure S2; Baici, 1981) analysis was performed, which yields the ratio between competitive and uncompetitive inhibitor constants (α) and the turnover rate of free enzyme to inhibited enzyme (β). For both DARPins we determined equal values of $\alpha = \infty$ and $\beta = 0$, demonstrating that D3.4 and D3.8 are purely competitive inhibitors of caspase-3 (Table 1).

In the past, short peptide substrates have been extensively used for the characterization of proteases, because the

DOI: 10.1016/j.str.2012.12.011,

Structure
Caspase-3 Directed DARPins

Table 1. Kinetic Constants and Characteristics of the Interaction

	Kinetic					
DARPin	$k_{on1}(M^{-1s-1})$	$k_{off1}(s^{-1})$	$K_{D1}(M)$	$k_{on2}(M^{-1s-1})$	$k_{off2}(s^{-1})$	$K_{D2}(M)$
D3.4	2.85×10^{5}	8.81×10^{-3}	3.09×10^{-8}	1.12×10^{6}	1.13×10^{-3}	1.01×10^{-9}
D3.4_S76R	1.74×10^{5}	4.20×10^{-3}	2.42×10^{-8}	1.62×10^{6}	7.45×10^{-4}	4.61×10^{-10}
D3.6	1.48×10^{5}	1.13×10^{-3}	7.63×10^{-9}	1.46×10^{6}	1.00×10^{-2}	6.88×10^{-9}
D3.8	1.77×10^{5}	2.49×10^{-3}	1.41×10^{-8}	2.44×10^{6}	1.11×10^{-4}	4.57×10^{-11}
D3.13	2.74×10^{5}	1.24×10^{-3}	4.51×10^{-9}	2.31×10^{6}	7.86×10^{-3}	3.41×10^{-9}

	Equlibrium	Inhibition			Interaction		
DARPin	K_D(nM)	K_i(nM)	α	β	SC	Å^2	Δ^iG kcal/mol
D3.4	9.6 ± 1.1	16.8	∞	0	0.740	875.95	−6.1
D3.4_S76R	6.0 ± 0.5	3.5	∞	0	0.725	907.55	−7.1
D3.6	8.8 ± 2.0	–	–	–	–	–	–
D3.8	3.4 ± 0.4	6.7	∞	0	nd	nd	nd
D3.13	7.7 ± 0.4	–	–	–	–	–	–

See also Figures S1 and S2. nd, not determined.

determination of rate constants is straightforward in those experiments. On the other hand, short peptide substrates represent a rather artificial situation because these substrates utilize a very limited number of binding interactions. Natural protease substrates are significantly larger and consequently their binding is guided by a broader set of interactions. Therefore, we tested whether the selected DARPins also inhibit the processing of PARP-1, one of the best-characterized caspase-3 substrates. The 116-kDa PARP-1 is specifically cleaved by caspases-3 and -7 on the C-terminal side of Asp216 into an 85-kDa and a 31-kDa fragment (Lazebnik et al., 1994). The addition of 10-fold molar excess of D3.4 or D3.8 over caspase-3 inhibited the cleavage of PARP-1 by ~90%, whereas the addition of E3_5, a DARPin that does not bind caspase-3, showed no effect on the cleavage of PARP-1 (Figure 2). In addition, a 50-fold molar excess of the caspase-3 DARPin inhibitors completely abolishes PARP-1 cleavage (Figure 2).

Specificity of DARPins D3.4 and D3.8

All commercially available caspase inhibitors are capable of inhibiting both caspases-3 and -7 equally well (McStay et al., 2008). We investigated the caspase selectivity of D3.4 and D3.8 by measuring the binding affinity and inhibitory activity against caspase-7 (56% sequence identity with caspase-3) and the more distantly related caspase-6 (41% sequence identity). SPR analysis did not show any detectable binding of the caspase-3 directed DARPins D3.4 and D3.8 to caspases-6 or -7 (Figure S3), suggesting that both DARPins are highly specific for caspase-3. These results are consistent with the activity measurements where D3.4 and D3.8 were also unable to inhibit PARP-1 cleavage by caspase-7 (Figure 2). Probing the ability of D3.4 and D3.8 to inhibit the hydrolysis of chromogenic tetrapeptide substrates by caspases-1, -2, -4, -5, -6, -7, -8, and -9 revealed that D3.4 is highly specific for caspase-3 and cannot inhibit any other tested caspase, whereas D3.8 has a moderate inhibitory activity against caspase-7 (Figures 3 and S4). A 1,000-fold excess of D3.8 decreases the activity of caspase-7 to approximately 40%.

Crystal Structure Analysis of the Caspase-3/DARPin D3.4 Complex

To understand the structural basis for the inhibition mechanism of caspase-3 by DARPins the crystal structure of the caspase-3/D3.4 complex was determined at 2.1 Å resolution. The details of the structure determination (data collection and refinement) are listed in Table 2. In the crystal structure the asymmetric unit contains one $(p12, p17)_2$ caspase-3 heterotetramer and two D3.4 molecules (Figure 4A). In the complex every DARPin buries a surface area of 876 Å^2. A surface complementarity index of 0.74 indicates a good fit between D3.4 and caspase-3 (Table 1). The interface involves residues from the N-terminal capping repeat and the two internal repeats of the DARPin, which form specific hydrogen bonds and hydrophobic interactions with the caspase (Figure 4A). The crystal structure reveals first of all that D3.4 binds in the active site pocket of caspase-3 and prevents substrate molecules from accessing the catalytic residues (Figure 4A). The β-turns of D3.4 point toward the β strand of caspase-3 that is responsible for the recognition of the substrate by main chain hydrogen bonds (residues 205 to 207). This observation agrees very well with the kinetic analysis of the inhibition mechanism, where no uncompetitive contribution was observed ($\alpha = \infty$). Therefore, structural and kinetic analyses consistently classify D3.4 as a purely competitive caspase-3 inhibitor (Figure S2).

When comparing the caspase-3/D3.4 complex with previously published caspase/protein complexes, such as the caspase-2/AR_F8 (Schweizer et al., 2007) or the natural caspase-3/XIAP complexes (Riedl et al., 2001), the following features can be highlighted: (1) DARPins AR_F8 and D3.4 both bind to loop-4 (also termed 381-loop). However, AR_F8 binds from the backside and inhibits caspase-2 by an allosteric mechanism (Figure 4B). (2) D3.4 and XIAP are competitive caspase-3 inhibitors, but the main chains of D3.4 and the N-terminal extension loop of XIAP run in opposite directions (Figure 4C).

The binding mode of D3.4 shows similarities to the binding of natural substrates (based on inhibitor structures) and the natural inhibitor XIAP. Asp45 of D3.4 is located in the β-turn that

Structure
Caspase-3 Directed DARPins

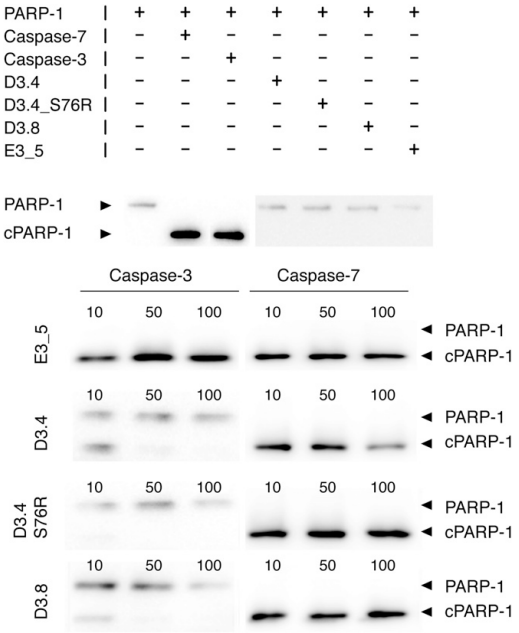

Figure 2. Inhibition of Caspase-3-Dependent PARP-1 Cleavage by DARPin Inhibitors

The cleavage of PARP-1 by caspase-3 (40 nM) and -7 (150 nM) was analyzed by SDS-PAGE (upper panel). Full length and cleaved PARP-1 (cPARP-1) were detected by a specific antibody that recognizes both forms. None of the selected DARPins cleave PARP-1 themselves. DARPins were added at 10-, 50-, and 100-fold molar excess per active site (lower panel).

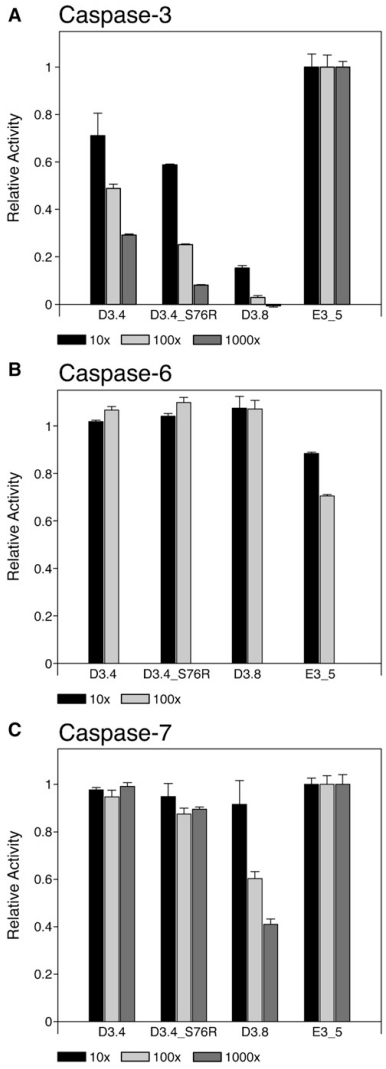

Figure 3. Specificity and Inhibition of Selected DARPins for Caspase-3, -6, and -7

(A–C) The relative enzymatic activity of caspase-3 is shown in the presence of D3.4, D3.4_S76R, D3.8, and E3_5 (control DARPin). Each DARPin was added at three different concentrations: 10- (black), 100- (light gray), and 1,000-fold molar excess (gray). All DARPins inhibit the activity of caspase-3 with the exception of E3_5. Shown are the relative enzymatic activities of caspase-6 (B) and −7 (C) in presence of four DARPins as described above. The 1000-fold molar excess of DARPin was not measured for caspase-6 because no inhibition was observed at 100-fold molar excess. D3.8 shows a moderate inhibition of caspase-7; all other DARPins are specific for caspase-3. Error bars represent the standard deviation of three independent experiments.
See also Figures S3 and S4.

connects the N-terminal capping repeat and the first internal repeat of D3.4, and its side chain occupies the S4 pocket of caspase-3 (Figure 5A). It forms a direct hydrogen bond with Asn208-ND2 and two water-mediated hydrogen bonds with Trp214-NE1 and Phe250-N (Figures 5A and S5). The main chain carbonyl oxygen of Asp45 forms another water-mediated (Wat10) hydrogen bond with Arg207-N of caspase-3. In other caspase-3 structures Arg207-N participates in an antiparallel β sheet with the substrate main chain. A water molecule (water 10) forms a third hydrogen bond with the hydroxyl group of-Tyr204. As a consequence, Thr166 moves toward the active site pocket and forms hydrogen bonds with Trp79-NE1 and Lys111-NZ from D3.4 (Figures 5A and 6A).

The tip of loop-4 of caspase-3 is recognized by the concave surface of D3.4 (Figures 5B and 5C). The side chain of Asp44 of D3.4 is buried in the interface and forms two hydrogen bonds with Ser251-OG and Phe252-N. In contrast, the side chains of Lys56 and Arg81 of D3.4 are solvent exposed and form salt bridges with the Asp253 side chain of caspase-3. Hydrophobic interactions seem to play equally important roles. The side chain of Phe256 of caspase-3 fits into a pocket that is formed by Ala46, Val48, Ile78, and Trp79 of D3.4. The benzyl ring of Phe256 of caspase-3 forms T-stacking interactions with the indole ring of D3.4

Structure
Caspase-3 Directed DARPins

Table 2. X-Ray Data Collection and Model Refinement Statistics

	Caspase-3/ D3.4 (2XZD)	Caspase-3/ D3.4_S76R (2Y0B)
Data Collection		
Frame width (°)	0.25	0.2
Space group	$P3_121$	$P3_121$
Unit cell parameter	a = 98 Å	a = 98 Å
	b = 98.0 Å	b = 98.0 Å
	c = 193.6 Å	c = 192.9 Å
	α = β = 90.0° γ = 120.0°	α = β = 90.0° γ = 120.0°
Resolution (Å)	49.0–2.1	49.0–2.1
Wavelength (Å)	1.000	0.92
R_{sym} (%)	4.2 (60.4)	4.9 (60.9)
Completeness (%)	99.3 (99.5)	99.2 (99.5)
I/σ(I)	15.59 (1.92)	12.94 (1.96)
Refinement		
Resolution (Å)	2.1	2.1
R_f/R_{free} (%)	18.5/21.8	19.1/21.7
No. of protein atoms	5,616	5,622
No. of water atoms	247	345
Average B-factor (Å^2)	35.3	35.8
Root Mean Square Deviations		
Bond length (Å)	0.011	0.006
Bond angles (°)	1.192	0.941

Trp79 (Figure 5C). Although the Phe256 binding pocket is mainly hydrophobic, the side chain of Asp77 is located at the bottom of this pocket and forms an intramolecular salt bridge with Arg81 and a hydrogen bond with Wat26 (Figure 5C).

Comparison of the Caspase-3/D3.4 Structure with Caspase-3 in Complex with XIAP and DEVD

The overall structure of caspase-3 is identical to several other caspase structures. Superposition of the caspase-3/D3.4 structure with the caspase-3/z-DEVD-cmk (2DKO; Ganesan et al., 2006) and the caspase-3/XIAP complex structures (1I3O; Riedl et al., 2001) reveals rmsd values of 0.39 Å and 0.35 Å, respectively. Differences between caspase-3/D3.4 and the caspase-3/z-DEVD-cmk structures are observed in the active site pocket. In the caspase-3/D3.4 structure loop-4 of caspase-3 has moved approximately 1 Å out of the active site, whereas Thr166 has moved into the active site compared to the caspase-3/z-DEVD-cmk structure (Figure 6A). The movement of Thr166 is a consequence of the 120° rotation of the Tyr204 side chain. In the caspase-3/z-DEVD-cmk structure Tyr204 points toward Thr166, whereas in the caspase-3/D3.4 complex the Tyr204 side chain occupies the S2 pocket (Figure 6A).

The conformations of Tyr204 and loop-4 in the caspase-3/D3.4 complex structure resemble the conformations seen in the caspase-3/XIAP structure (1I3O) (Figure 6B). In both complexes, Tyr204 occupies the S2 pocket (Riedl et al., 2001). Furthermore, Tyr204 rests against a hydrophobic patch of the inhibitor, which is formed by Leu141 and Val146 in XIAP and by Ala46 and Ile78 in D3.4 (Figure 6B).

Modeling the Caspase-3/D3.8 Complex Structure

Based on the sequence alignment and the competitive inhibition we assume that D3.4 and D3.8 bind to the same epitope with similar interactions. We were not able to crystallize the caspase-3/D3.8 complex and thus calculated a homology model of D3.8 based on a N3C DARPin E3_5 structure (1MJ0; Kohl et al., 2003). This homology model was superimposed on D3.4 in the caspase-3/D3.4 crystal structure (Figure 6C). The N2C DARPin D3.4 lacks the first internal repeat so that the N-cap of D3.4 superimposes on the first internal repeat of the N3C DARPin D3.8 (Figure 6C). Furthermore, D3.8 has two critical mutations compared to D3.4. Mutations Lys56Ser and Ser76Arg are located in the caspase/DARPin interface, whereas all other amino acid changes between D3.4 and D3.8 are located more than 4 Å away from caspase-3. The homology model showed that the salt bridge between Lys56 and Asp253 is absent in the D3.8/caspase-3 complex (Figure 6D). In D3.8 the corresponding Ser56 is unable to form a salt bridge as observed in the caspase-3/D3.4 structure. Furthermore, the positive charge of Lys56 in D3.4 could cause repulsive interactions with His255 at the top of loop-4 of caspase-7 (Figure 6D). These repulsive interactions could explain why D3.4 does not show any affinity for caspase-7, whereas D3.8 possesses weak affinity for caspase-7 due to the Lys56Ser mutation.

D3.4 Mutant Ser76Arg

D3.8 binds caspase-3 with higher affinity and has a lower inhibition constant (K_i = 6.7 nM) compared to D3.4 (Table 1). Residue Ser76 in D3.4 is located in proximity to the interface but does not interact with caspase-3. The caspase-3/D3.8 model suggests that a bulkier side chain, such as arginine, could participate in an extended DARPin/caspase-3 interface. To test this hypothesis we generated the D3.4 Ser76Arg mutant (D3.4_S76R) and characterized its functional and structural properties. D3.4_S76R revealed dissociation and inhibitory constants of K_D^{S76R} = 6.0 ± 0.5 nM and K_i^{S76R} = 3.49 ± 0.03 nM, respectively. Thus, D3.4_S76R shows an equally low inhibitory constant for caspase-3 compared to D3.8 (Table 1).

The 2.1 Å resolution crystal structure of the caspase-3/D3.4_S76R complex revealed that although the overall structure is identical to the caspase-3/D3.4 structure (rmsd of 0.198 Å), the C-terminal capping repeat has shifted by approximately 2 Å (Figure 6E). The side chain of the newly introduced Arg76 forms two intramolecular hydrogen bonds with Gly80-O and Gln109-O of the C-terminal capping repeat and an intermolecular hydrogen bond with Gly60-O of caspase-3 (Figure 6E). In addition, the weak hydrogen bond between Lys111 and Thr166 as it is seen in the parent structure is broken and the Lys111 side chain points into the active site forming a water-mediated hydrogen bond with Gly165-O of caspase-3 and an intramolecular hydrogen bond with Ile78-O from the preceding DARPin repeat. The mediating water molecule is located in direct vicinity of the active site Cys163 (Figure 6E).

DISCUSSION

The development of specific caspase inhibitors has remained a challenging task due to the similarity between the active sites of caspases. Although the selectivity of caspases for short

Structure
Caspase-3 Directed DARPins

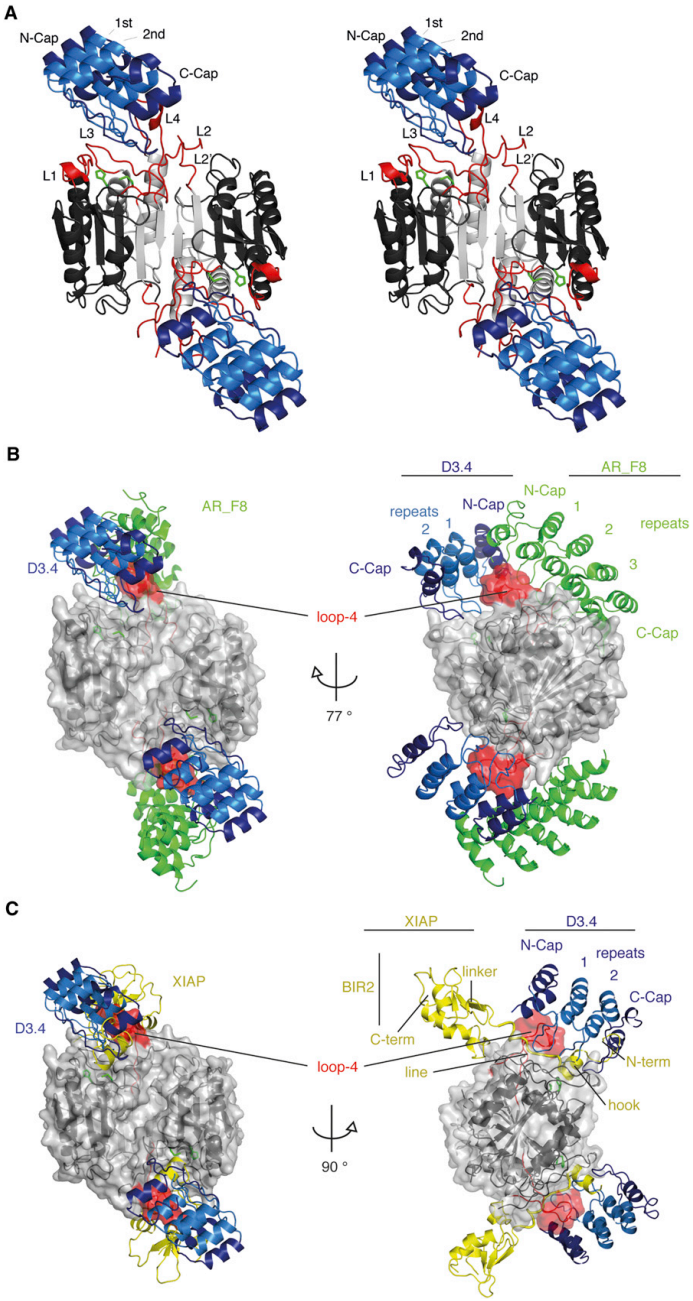

Figure 4. Structures of Caspase-3 in Complex with Different Inhibitors

(A) Stereo view of the caspase-3/D3.4 complex structure as a ribbon cartoon. The two chains of caspase-3 are colored in dark (p17) and light gray (p12). The active site L1, L2, and L4 loops and the catalytic residues are highlighted in red and green, respectively. D3.4 consists of N- and C-terminal capping repeats (dark blue) and two internal repeats (light blue). D3.4 binds in the active site and interacts mainly with loop-4 of caspase-3.

(B) The superposition of the caspase-2 specific DARPin AR_F8 (green, 2P2C) on the caspase-3/D3.4 structure is shown in two different views. Caspases are shown as a gray surface. Darpins D3.4 (blue) and AR_F8 (green) recognize the active site loop-4 (red), albeit from different sides.

(C) The caspase-3/XIAP structure (yellow, 1I3O) was superimposed on the caspase-3/D3.4 structure. The C-terminal BIR2 domain of XIAP binds outside the active side cleft and inhibits the enzyme with the N-terminal tail.

DOI: 10.1016/j.str.2012.12.011,

Structure
Caspase-3 Directed DARPins

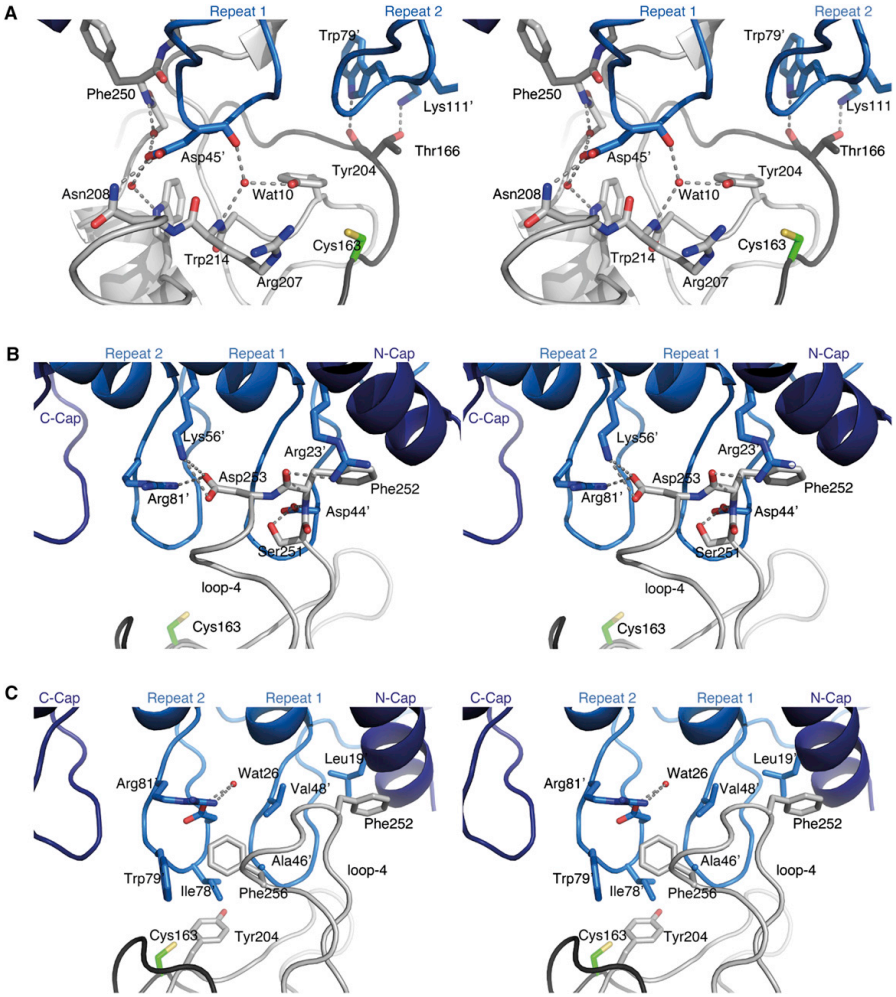

Figure 5. Binding Interface of Caspase-3 with D3.4

Close-up views of the caspase-3/D3.4 interaction in stereo. D3.4 (blue) interacts with caspase-3 (p17, dark gray; p12, light gray) via hydrogen bonds (dotted lines) and hydrophobic interactions. Amino acids from the DARPin are labeled by an additional '. The active site cysteine is shown in green.

(A) Active site standard view: Asp45' forms several hydrogen bonds in the S4 pocket of caspase-3. Thr166, which is located close to the active site Cys163, forms two hydrogen bonds with the second repeat of D3.4.

(B and C) View from the backside of loop-4: The concave site of D3.4 recognizes the tip of loop-4 by several hydrogen bonds (B). The hydrophobic interactions in the interface between caspase-3 and D3.4. Phe256 from caspase-3 binds into a hydrophobic pocket of D3.4 and forms T-stacking interactions with Trp79' (C). See also Figure S5.

peptide inhibitors that differ in the P4 positions is well established (Thornberry et al., 1997), their selectivity is often insufficient considering the different amounts of active caspases in cells undergoing apoptosis (Berger et al., 2006). In 2007, Schweizer et al. published the first truly specific caspase inhibitor (AR_F8) that inhibits caspase-2 with an allosteric mechanism by interacting with loop-4 (Schweizer et al., 2007).

Using the same technology (Binz et al., 2003), we identified four caspase-3 DARPins, two of which specifically inhibited the enzyme. Kinetic analysis characterized D3.4 and D3.8 as purely competitive inhibitors, which is in agreement with the structural data. In the caspase-3/D3.4 structure, the DARPin occupies the active site pocket and recognizes loop-4 of caspase-3. The caspase-2-directed DARPin AR_F8 also recognizes loop-4,

Structure
Caspase-3 Directed DARPins

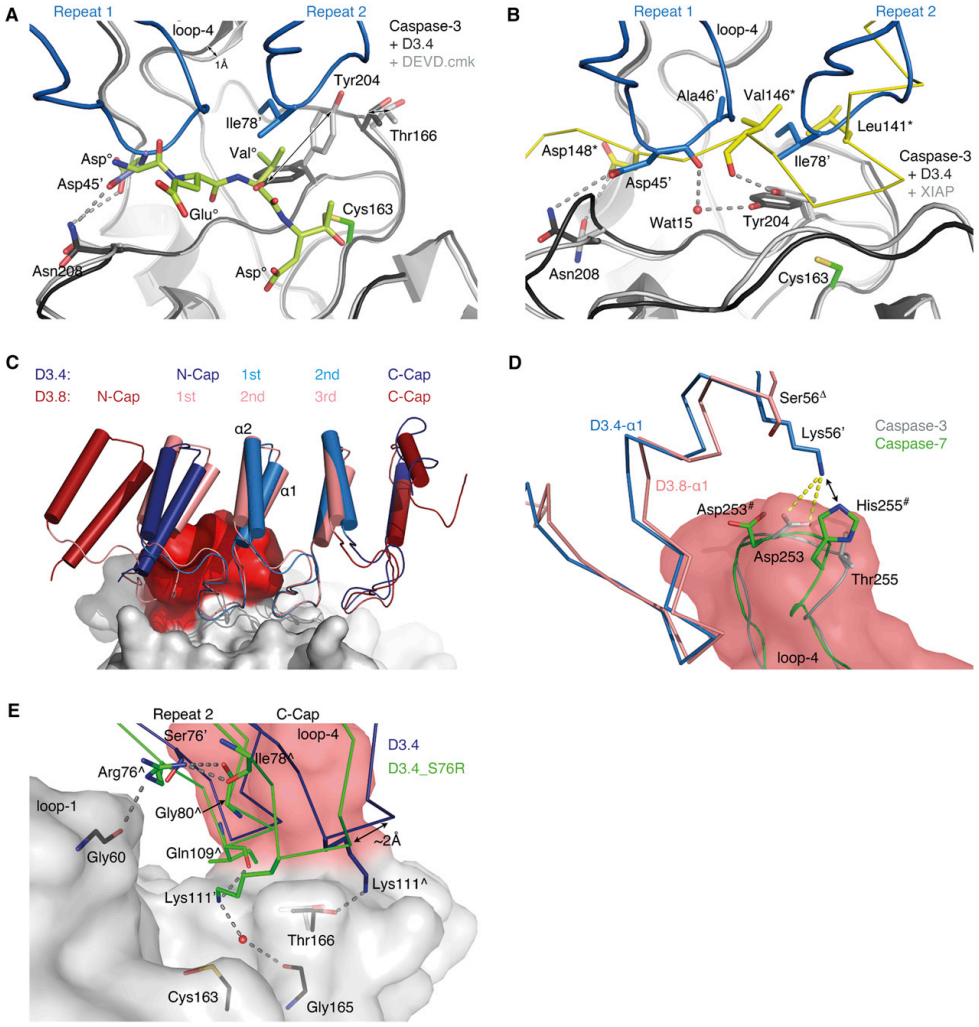

Figure 6. Structural Comparison of Caspase-3 Inhibitors

With the exception of caspase-3, the labels of all amino acids contain unique identifiers: D3.4 ('), DEVD (°), XIAP (*), D3.4_S76R (^), D3.8 ($^{\Delta}$), and caspase-7 ($^{\#}$).

(A) Superposition of caspase-3/z-DEVD-fmk (light green and gray, 2DKO) on the caspase-3/D3.4 structure (dark gray and blue). Tyr204 is rotated by approximately 120° in the DARPin bound structure. As a consequence of this rotation Thr166 is shifted away from the active site. Movements are indicated by black arrows.

(B) Superposition of caspase-3/XIAP (gray and yellow, 1I3O) on the caspase-3/D3.4 structure (dark gray and blue) indicating a similar orientation of Tyr204 in a subsite S2-blocking position.

(C) The D3.8 model (dark red and salmon represent the capping and internal repeats, respectively) superimposed on D3.4 (dark and light blue) with numbered α helices in repeat 2 (D3.8) and 1 (D3.4), respectively. Caspase-3 is shown as a gray surface with loop-4 highlighted in red.

(D) Close-up view of the modeled interaction between either D3.4 (blue) or D3.8 (salmon) and either caspase-3 (gray) or caspase-7 (green). Shown are the α helices 1 of the first internal repeat of D3.4 and the second internal repeat of the D3.8 model. In the caspase-3/D3.4 complex Lys56' forms a salt bridge with Asp253. In caspase-7, this position is occupied by His255$^{\#}$. In D3.8 Ser56$^{\Delta}$ cannot form the salt bridge with caspase-3 and does not exert repulsive interactions with His255$^{\#}$ in caspase-7.

(E) Superposition of the caspase-3/D3.4 on the caspase-3/D3.4_S76R structure. Caspase-3 is shown as a gray surface with loop-4 colored in red, whereas D3.4 and D3.4_S76R are shown as dark blue and green Cα-traces. Interacting side chains are highlighted. Hydrogen bonds are indicated as gray dotted lines. In the caspase-3/D3.4_S76R structure the side chain of Arg76^, Ile78^, and Lys111^ form hydrogen bonds that are not seen in the parent structure (Table 3) and cause a shift of the C-cap.

DOI: 10.1016/j.str.2012.12.011,

Structure
Caspase-3 Directed DARPins

Table 3. Hydrogen Bonds in the Caspase-3/D3.4 Interface

DARPin	Distance	Caspase-3
D:ARG 23 [NH1]	3.19	C:PHE 252 [O][a]
D:ASP 44 [OD2]	2.69	C:SER 251 [OG][a]
D:ASP 44 [OD2]	2.97	C:PHE 252 [N][a]
D:ASP 45 [OD1]	3.1	C:ASN 208 [ND2][b]
D:ASP 45 [O]	2.5/2.8	C:Wat 10 - TYR 204 [OH][b]
D:ASP 45 [OD2]	2.6/2.7	C:Wat 12 - PHE 250 [N][a]
D:ASP 45 [OD2]	2.6/2.9	C:Wat 11 - TRP 214 [NE1][b]
D:LYS 56 [NZ]	3.38	C:ASP 253 [OD1][a]
D:LYS 56 [NZ]	–	C:ASP 253 [OD2][a]
D:TRP 79 [NE1]	2.87	C:THR 166 [O][a]
D:ARG 81 [NH2]	2.79	C:ASP 253 [OD2][a]
D:LYS 111 [NZ]	3.75	C:GLU 167 [OE2][a]
D:LYS 111 [NZ][c]	2.68	C:THR 166 [OG1][a]
D3.4_S76R		
D:ARG 76 [NE]	3.3	C:GLY 60 [O][a]
D:LYS 111 [NZ]	2.7/3.2	C:Wat - GLY 165 [O][a]

[a]Caspase residues, not involved in subsite formation.
[b]Caspase residues, forming substrate binding pockets S4–S1.
[c]Not present in D3.4_S76R.

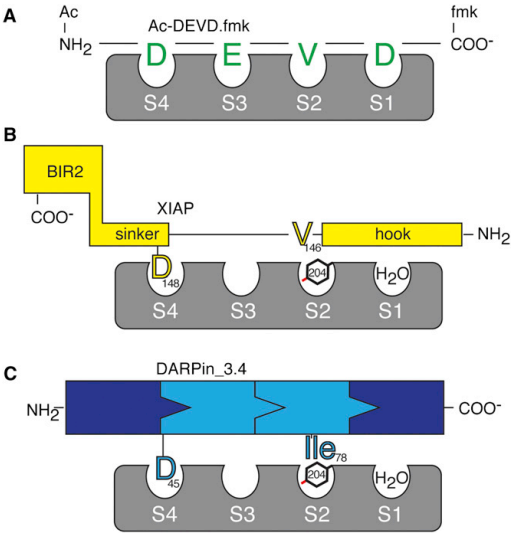

Figure 7. Schematic Caspase-3 Inhibition
(A) The peptide inhibitor Ac-DEVD-fmk occupies four substrate binding pockets of caspase-3 (S1–S4).
(B) The BIR2 domain of XIAP occupies the S4 pocket of caspase-3 with Asp146 and Val146 keeps Tyr204 at a position, which blocks the S2 pocket. S1 is filled with water molecules. Compared to Ac-DEVD-fmk the XIAP main chain runs in the opposite direction.
(C) D3.4 uses a caspase-3 inhibition mechanism that shares features of XIAP and Ac-DEVD-fmk. The S4 pocket is also occupied (Asp45), Ile78 keeps Tyr204 in a locked conformation and the S1 pocket is filled with water, but the D3.4 main chain runs in the same direction like in Ac-DEVD-fmk.

however from a different direction than the caspase-3-directed DARPin D3.4. Its kinetic characterization using the specific velocity plot demonstrated a mixed type inhibition with a significant part of uncompetitive inhibition. The different inhibition modes of D3.4 and AR_F8 can be explained by the different epitopes on the caspases. AR_F8 recognizes caspase-2 from the backside of loop-4 and stabilizes a distinct conformation, which is not able to bind the substrate, whereas D3.4 binds straight into the active site of caspase-3. Our analysis further showed that D3.4 prevents substrates from accessing the catalytic Cys163 and leaves the conformation of loop-4 almost undisturbed when compared to the caspase-3 inhibitor structure.

Another finding is the superior inhibition of caspase-3 by the closely related D3.8, which inhibits caspase-3 even better than D3.4. DARPin molecules D3.6 and D3.13 bind caspase-3 but do not inhibit hydrolysis and were thus not further analyzed. D3.4 does not inhibit the closely related caspase-7 but from the data given in Figure 2 the IC_{50} value for the inhibition of caspase-7 by D3.8 can be estimated to be in the lower micro-molar range. This residual activity is probably resulting from the replacement of Lys56 in D3.4 to Ser56 in D3.8. Lys56 in D3.4 forms a salt bridge with Asp253 from caspase-3 and at the same time could enforce a repulsive effect to His255 from caspase-7 to ensure specificity for caspase-3. The model of the less specific D3.8 does not show this repulsion at caspase-7, which could explain the slight binding ability of D3.8 for caspase-7. Thus, even inhibitors with significantly extended interaction surfaces compared to tetrapeptide inhibitors can recognize closely related caspases, albeit with affinity constants that differ by at least three orders of magnitude.

Our inhibition studies using PARP-1 as a caspase substrate revealed that the selected DARPins (D3.4, D3.4_S76R and D3.8) inhibit PARP-1-cleavage by caspase-3 completely using a 50-fold molar excess. In contrast, caspase-7 cleavage is not influenced even with a 100-fold excess of D3.4, D3.4_S76R, or D3.8, respectively.

Our data suggest that D3.4 and D3.8 bind to the same caspase-3 epitope because residues that seem to be crucial for the recognition of this epitope, such as Asp45, Ala46, Val48, Ile78, Trp79, and Arg81, are conserved in both molecules. The crystal structure revealed that D3.4 recognizes caspase-3 by a set of specific hydrogen bonds, salt bridges and hydrophobic contacts (Table 3). Particularly interesting are the interactions formed by Asp45, which occupies the S4 pocket. So far all structurally characterized caspase-3 specific peptide inhibitors harbor an aspartic acid that occupies this pocket (Figure 7). Although the hydrogen bonding networks are different in the structures of caspase-3 in complex with D3.4, z-DEVD-cmk or XIAP, the positive electrostatic potential explains the preference for a small and negatively charged hydrogen bonding partner like aspartate. Further similarities between the complex structures of caspase-3 with D3.4 and XIAP are seen for Tyr204 (Figure 7). In both structures the Tyr204 side chain points toward Arg341, placing the phenyl ring at van der Waals distance to Cys163-$S\gamma$. On the opposite side the Tyr204 phenyl ring rests against a hydrophobic core, which is composed of caspase-3 residues Leu168 and Phe256 and the side chains of Ala46 and Ile78 from D3.4 or Leu141 and Val146 from XIAP. D3.4 and XIAP are

Structure
Caspase-3 Directed DARPins

both lacking an aspartic acid that could occupy the S1 pocket of caspase-3, which consequently is filled by water molecules. The same conformation of Tyr204 is also seen in several other structures of caspase-3 in complex with low molecular weight inhibitors that are lacking a P1 aspartate (Agniswamy et al., 2009; Ganesan et al., 2011) as well as in unliganded caspase-3 (Ni et al., 2003). Conversely, this conformation is different from structures with classical tetrapeptide inhibitors, where the Tyr204 side chain rests against the side chain of Thr166 (Ganesan et al., 2006).

The main chains of the small peptide inhibitor z-DEVD.cmk and D3.4 run antiparallel to caspase-3 residues 204–208. The S4 pocket of caspase-3 is occupied by Asp1 and Asp45 of z-DEVD.cmk and D3.4, respectively. In contrast to that the main chain of XIAP runs parallel to caspase-3 with Val146 and Asp148 binding into the S2- and the S4 pocket, respectively. Although the main chains of D3.4 and XIAP run in opposite directions, both inhibitors use very similar interactions to inhibit caspase-3 (Figure 7). Thus, the comparison of the caspase-3/D3.4 crystal structure with the caspase-3/XIAP crystal structure provides an interesting example for the molecular mimicry of natural and designed caspase-3 inhibitors.

In summary, our study presents the selection and characterization of caspase-3-directed DARPin inhibitors with implications for specificity and inhibition mechanism. The selected DARPins D3.4 and D3.8 are pure competitive inhibitors. D3.4 and the improved variant D3.4_S76R are the first truly specific caspase-3 inhibitors and do not bind caspase-7, a close caspase-3 paralog, or any other human caspase. Such highly specific binders/inhibitors are a prerequisite for the analysis of the function of any enzyme involved in signaling pathways. In the particular case of caspase-3 and its role in apoptotic signaling, D3.4_S76R is the best molecule for such an analysis. Remarkably D3.4 inhibits caspase-3 with a similar mechanism compared to XIAP, the natural caspase-3 inhibitor that also inhibits caspase-7. It has previously been postulated that specificity is achieved by two key factors, allosteric regulation and scanning of large volumes of conformational space (Salvesen and Riedl, 2007). While the second aspect holds true, we demonstrate here that specificity can be achieved even when the conserved substrate binding pockets are targeted, provided this is combined with specific surface recognition of non-subsite residues, which are unique to the targeted protein.

EXPERIMENTAL PROCEDURES

DARPin Selection with Ribosome Display

We performed four rounds of ribosome display to enrich caspase-3 specific binders based on a NI3C and NI2C library as described before (Binz et al., 2004; Zahnd et al., 2007). Prior to each selection the DARPin-ribosome-mRNA complex was incubated with the closest homologous of caspase-3 (caspase-6 and -7) and streptavidin for 30 min at 4°C to avoid selection of unspecific DARPins. Biotinylated caspase-3 was immobilized on magnetic particles (Dynabeads, Invitrogen) for solution panning. DARPin selection was performed in the absence of a caspase-3 inhibitor. The DARPin-ribosome-mRNA complex was incubated with 20 µl of beads for 30 min at 4°C in a tube that was previously blocked with TBST-BSA (50 mM Tris-HCl pH 7.4, 150 mM sodium chloride, 0.05% Tween-20, 0.1% BSA). The incubation was followed by four washing cycles in 50 mM Tris-acetate pH 7.4, 150 mM sodium chloride, 50 mM magnesium acetate, and 0.05% Tween-20. The RNA was eluted in 50 mM Tris-acetate pH 7.4, 150 mM sodium chloride, and 25 mM EDTA and transcribed into DNA for amplification. In rounds three and four, we added a 1000-fold excess of unbiotinylated caspase-3 for 10 min during the selection to favor the enrichment of DARPins with slow k_{off} rates. After four rounds of selection, we cloned the DARPin library in a pQE30 vector (-QIAGEN), transformed competent XL1 blue cells (Stratagene), and continued with crude cell extract ELISA.

Crude Cell Extract ELISA

Single colonies each containing one DARPin clone of the selected library were picked and inoculated in 0.9 ml auto-inducing media 5052 (Studier, 2005) containing deep 96-well plates (Abgene, UK). The cells were grown over night at 37°C while shaking at 300 rpm in a shaker (TH15, Edmund Bühler GmbH). Then 200 µl of each well were transferred into a sterile 96-well plate (449824, Nunc) as a backup for further protein expression and plasmid preparation. The remaining 700 µl of cell-suspension was harvested by centrifugation and the cell pellet was lysed with 50 µl B-PER II (Pierce, 78260) per well for 30 min shaking at room temperature. The lysed cells were resuspended by adding 950 µl PBS, pH 7.3, and cell debris were removed by centrifugation (20 min, 4500 rpm at 4°C) in a tabletop centrifuge (Eppendorf). We now took 20 µl of the supernatant of four 96 well plates and transferred it to one 384-well ELISA plate (Nunc, 464718). This plate was previously coated with 20 µl of a 22 nM neutravidin solution (Pierce, 31000) and biotinylated caspase-3, followed by extensive washing. After 1 hr of incubation at room temperature and three washing cycles, the plate was incubated with mouse anti-RGS-H_4 antibody (QIAGEN, 34650) at a dilution of 1:2000 in PBS 1% BSA. After adding the secondary antibody (goat-α-mouse IgG alkaline phosphatase conjugate, Sigma, A3562) and four washing steps the amount of bound DARPin was quantified by adding the substrate buffer (3 mM di-sodium 4-nitrophenyl phosphate, 50 mM sodium bicarbonate, 50 mM magnesium chloride). The optical density (OD) was measured at 405 nm using a multiwell plate reader (Infinite M1000, Tecan).

Expression, Purification, and Biotinylation of Proteins

All DARPins were expressed in auto-inducing media (Studier, 2005) or lysogeny broth media (Binz et al., 2003). The expressed DARPin was purified by IMAC using a self-made gravity column (Supelco, 57024) containing 0.5 ml bead volume of Ni^{2+}-NTA agarose (QIAGEN, 30210). The DARPins were eluted in PBS complemented with 200 mM imidazole. The imidazole was removed with a PD-10 desalting column (GE Helthcare, 17-0435-01). We added sodium azide to a final concentration of 0.03% to prevent growth of bacteria and fungi. The DARPin solutions were stored at 4°C. Caspase-1 to caspase-9 were expressed and purified as described elsewhere (Roschitzki-Voser et al., 2012). Expression plasmids for caspase-6, -7, and -9 have been obtained from Dr. Guy Salvesen, the Burnham Institute, La Jolla, CA, USA (Denault and Salvesen, 2003).

For chemical biotinylation of caspases, we used the linker EZ-Link Sulfo-NHS-LC-LC-Biotin (Pierce, 21338), containing a reactive group, a 3.05-nm long linker, and a biotin moiety. After purification, 1 ml of 10 µM caspase in PBS, pH 7.3 was incubated with a 7-fold molar excess (1 ml of a 70 µM solution) of biotin on ice for 30 min. The reaction was quenched by adding 10 µl of 5 M Tris-HCl, pH 7.5. The biotinylated protein was purified by size exclusion chromatography, using a Superdex 200 10/300 GL (GE Healthcare) in PBS at 4°C. Fractions containing biotinylated caspase were pooled and frozen in liquid nitrogen after adding sucrose to a final concentration of 10%.

Crystallization

The caspase/DARPin complexes were formed by incubating caspase-3 with a 2-fold molar excess of each DARPin for 10 min on ice. The complex was purified by size exclusion chromatography (Superdex 200 HR 10/30, Amersham Pharmacia, Sweden) in 50 mM Tris-HCl, pH 8.0 (4°C), 50 mM sodium chloride. Fractions containing caspase/DARPin were concentrated to 5 mg/ml and 10 mg/ml for D3.4 and D3.4_S76R, respectively, using an ultrafiltration device with a molecular weight limit of 15 kDa (Amicon Ultra, Millipore).

Crystals were grown at room temperature using the vapor-diffusion method. Two microliters of concentrated protein solution were mixed with 1 µl of reservoir solution containing 100 mM HEPES, pH 7.3, 70% (v/v) 2-methyl-2,4-pentanediol. Crystallization plates were stored at 20°C. Crystals appeared within 24 hr.

DOI: 10.1016/j.str.2012.12.011,

Structure
Caspase-3 Directed DARPins

Data Collection, Structure Determination, and Refinement

For X-ray diffraction analysis, crystals were flash-frozen in liquid nitrogen and data were collected (100 K) at beamline X06SA (Swiss Light Source, Villigen, Switzerland). No cryoprotectant was necessary for data collection. The beamline was equipped with a Pilatus 6M fast readout pixel detector (Dectris, Switzerland). The program XDS was used for data processing and data were scaled with XSCALE (Kabsch, 2010; Potterton et al., 2003). Both complexes crystallized in space group $P3_121$. Unit cell dimensions are listed in Table 2. The structures were solved by molecular replacement with the program PHASER (McCoy et al., 2007) using a high-resolution structure of caspase-3 (2DKO; Ganesan et al., 2006) and a model of the N2C DARPin, which was generated by homology modeling (MODELER 9v8; Eswar et al., 2007) using the N3C DARPin E3_5 (1MJ0; Kohl et al., 2003) as a template. The crystals have a solvent content of 59% (Matthews coefficient of 3.0 $Å^3$/Da) (Collaborative Computational Project, Number 4, 1994) with one (p12, p17, D3.4)$_2$ complex in the asymmetric unit. Alternating rounds of manual model building using COOT (Emsley et al., 2010) and restrained refinement using REFMAC version 5.5.01.09 (Murshudov et al., 1997) yielded R_F/R_{free} values of 0.185/0.217 for the caspase-3/D3.4 and 0.174/0.214 for the caspase-3/D3.4_S76R complex. Data collection and structure refinement statistics are listed in Table 2. Structures were superimposed using COOT (Emsley et al., 2010) and figures were prepared using PyMOL (Schrodinger, 2010).

Site-Directed Mutagenesis

We used the QuikChange Site Directed Mutageneis Kit (Stratagene) to incorporate mutations in the DARPin sequence. The following primers were used to introduce the Ser76Arg mutation in D3.4: 5′-GGT GCT GAC GTT AAC GCT CGT GAC ATT TGG GGT CGT ACT-3′ (fwd) and 5′-AGT ACG ACC CCA AAT GTC ACG AGC GTT AAC GTC AGC ACC-3′ (rev). The underlined codons indicate the mutation.

Surface Plasmon Resonance Analysis

For SPR experiments we used the Proteon XPR36^{TM} (Biorad Laboratories) and a NLC sensor chip (Biorad Laboratories). Sterile filtered PBS, pH 7.3, and 0.005% Tween-20 were used as the standard buffer for all coating and kinetic analysis steps. A 5-nM solution of biotinylated, fully processed caspase was coated in the absence of caspase inhibitors on the sensor chip at a flow rate of 30 μl per minute. The coating procedure was stopped when 1000 relative units were immobilized on the chip. Dilution series of DARPins were pipetted in 96-deep well plates (Biorad, 176-6023), which were sealed to prevent evaporation and contamination with dust particles. Starting with the lowest concentration we measured the binding of DARPins at 0, 0.176, 0.52, 1.58, 4.47, 14.2, 42.6, and 128 nM concentrations. All experiments were performed at 20°C. Flow rates of 100 μl per minute, association times of 3 min and dissociation times of 20 min were used. Data were recorded and kinetic binding data were determined with the ProteOn Manager 2.1.1 software (Biorad) using the heterogeneous ligand model (Bravman et al., 2006).

Caspase Activity Measurements

Specific inhibition of caspase-1 to caspase-9 was measured using peptide substrates from Peptide Institute (Osaka, Japan). We used Ac-DEVD-amc for caspase-3, -6, -7, and -8; Ac-WEHD-amc for caspase-1, -4, and -5; Ac-VDVAD-amc for caspase-2; and Ac-LEHD-amc for caspase-9. Enzyme and substrate concentrations in the assay were as follows: caspase-1 (10 nM enzyme; 150 μM substrate), caspase-2 (25 nM; 150 μM), caspase-3 (0.5 nM; 150 μM), caspase-4 (200 nM; 600 μM), caspase-5 (10 nM; 150 μM), caspase-6 (10 nM; 600 μM), caspase-7 (2 nM, 400 μM), caspase-8 (10 nM; 150 μM), and caspase-9 (25 nM, 600 μM) considering all caspases as hetero-tetramers. DARPins were added assuming that one DARPin binds to every caspase active site. The following assay buffers were used: caspase-2, 100 mM MES, pH 6.5, 10% PEG600 (w/v), 0.1% CHAPS (w/v), 10 mM DTT; caspase-9, 50 mM Tris-HCl, pH 7.5, 10% sucrose (w/v), 1.3 M sodium citrate; all other caspases, 20 mM PIPES, pH 6.5, 10% sucrose (w/v), 0.1% CHAPS (w/v), 10 mM DTT, 150 mM sodium chloride, and 1 mM EDTA. AMC release was monitored by measuring the fluorescent excitation and emission wavelengths of 360 nm and 465 nm, respectively, using an Infinite M-1000 spectrofluorometer (Tecan).

Specific Velocity Plot

Inhibition mechanism and K_i values of DARPins D3.4, D3.8, and D3.4_S76R have been determined using the specific velocity plot (Baici, 1981). The concentration of caspase-3 was determined by active site titration as described previously (Stennicke et al., 2000). The caspases inhibitor Ac-DEVD-cmk (0 to 7.6 nM), caspase-3 (0.5 nM), and the substrate Ac-DEVD-amc (100 μM) were prepared in activity buffer containing no DTT (20 mM PIPES, pH 6.5, 10% sucrose [w/v], 0.1% CHAPS [w/v], 150 mM sodium chloride, 1 mM EDTA). Concentrations of DARPins were determined using amino acid analysis at the Functional Genomic Center (Zürich, Switzerland). The initial velocities of substrate hydrolysis with 0.5 nM caspase-3 have been measured at different DARPin concentrations (D3.4, 8–32 nM; D3.4_S76R, 4–10 nM; D3.8, 2–8 nM) and substrate concentration between 0.2 and 0.8 times K_m (K_m = 24.7 ± 1.8 μM). Graphical analysis of the velocity plot was done with Prism5 (GraphPad Software). The inhibitor titration has been performed using 0.5 nM caspase-3, different DARPin concentrations (D3.4, 0–1,000 nM; D3.4_S76R, 0–1,000 nM; D3.8, 0–100 nM), and 24 μM substrate. To determine K_i values of DARPins initial velocities were fitted to the tight binding inhibition equation as described previously (Szedlacsek et al., 1988).

PARP-1 Inhibition and Western Blot Analysis

A 0.18-μM solution of PARP-1 in 50 mM Tris-HCl, pH 7.5, 150 mM sodium chloride was mixed with either 40 nM caspase-3 or 150 nM caspase-7 and the corresponding DARPin (10- to 100-fold excess per active site) as indicated in Figure 2. The mixture was incubated for 20 min at room temperature in 50 mM Tris-HCl pH 7.5, 150 mM sodium chloride, and 0.5 mM DTT, and stopped by adding SDS sample buffer (95°C for 5 min). The samples were subjected to 12% SDS-PAGE under reducing conditions and transferred to a nitrocellulose membrane (iBlot, Invitrogen). The membrane was blocked in high-TBS (50 mM Tris-HCl, pH 7.5, 500 mM sodium chloride) containing 5% (w/v) nonfat dry milk for 1 hr at room temperature. The primary PARP antibody (Cell Signaling, 9542) was incubated with the membrane at a dilution of 1:1000 in high-TBS-T (50 mM Tris-HCl, pH 7.5, 500 mM sodium chloride, 0.1% Tween-20) at 4°C overnight. After intensive washing in high-TBS-T, we incubated the membrane with anti-rabbit HRP conjugated antibody (Cell Signaling, 7074) for 1 hr at room temperature in TBS (50 mM Tris-HCl, pH 7.5, 150 mM sodium chloride). Protein bands were visualized by chemiluminescence using the SuperSignal West Pico Chemiluminescent Substrate (Pierce) in combination with a Fuji Las 3000 camera.

Modeling of D3.8

Based on the kinetic data and sequence alignments, we hypothesized that D3.8 binds to the same epitope as D3.4. Therefore, we generated a model of D3.8 in complex with caspase-3. The N3C DARPin E3_5 (1MJ0; Kohl et al., 2003) was used as a template to calculate a homology model of D3.8 using the program MODELER 9v8 (Eswar et al., 2007). The model of D3.8 was then superimposed on D3.4 in the complex structure according to the sequence alignment shown in Figure 1.

ACCESSION NUMBERS

The Protein Data Bank (PDB) accession numbers for the coordinates and structure factors of caspase-3 in complex with DARPin D3.4 and with DARPin D3.4_S76R, respectively, reported in this paper are 2XZD and 2Y0B.

SUPPLEMENTAL INFORMATION

Supplemental Information includes five figures and can be found with this article online at http://dx.doi.org/10.1016/j.str.2012.12.011.

ACKNOWLEDGMENTS

This work was supported by Swiss National Science Foundation grant 310030-122342 to M.G.G. We gratefully acknowledge the Salvesen laboratory for the expression plasmid of caspase-6 and -7 as well as Prof. M. Hottiger (University Zürich, Switzerland) for providing a sample of PARP-1 for the caspase inhibition studies. We acknowledge Prof. A. Baici for discussion

Structure
Caspase-3 Directed DARPins

and advice on the evaluation of our kinetic experiments. Crystallographic data collection was performed at the Swiss Light Source (Paul Scherrer Institute, Villigen, Switzerland). SPR data were measured at the Functional Genomics Center Zürich. T.S. is a member of the Molecular Life Science Ph.D. program at the ETH/University of Zürich. J.B. and A.F. are members of the Biomolecular Structure Ph.D. program at the ETH/University of Zürich.

Received: October 18, 2012
Revised: December 3, 2012
Accepted: December 14, 2012
Published: January 17, 2013

REFERENCES

Agniswamy, J., Fang, B., and Weber, I.T. (2009). Conformational similarity in the activation of caspase-3 and -7 revealed by the unliganded and inhibited structures of caspase-7. Apoptosis *14*, 1135–1144.

Amstutz, P., Binz, H.K., Parizek, P., Stumpp, M.T., Kohl, A., Grütter, M.G., Forrer, P., and Plückthun, A. (2005). Intracellular kinase inhibitors selected from combinatorial libraries of designed ankyrin repeat proteins. J. Biol. Chem. *280*, 24715–24722.

Baici, A. (1981). The specific velocity plot. A graphical method for determining inhibition parameters for both linear and hyperbolic enzyme inhibitors. Eur. J. Biochem. *119*, 9–14.

Berger, A.B., Sexton, K.B., and Bogyo, M. (2006). Commonly used caspase inhibitors designed based on substrate specificity profiles lack selectivity. Cell Res. *16*, 961–963.

Binz, H.K., Stumpp, M.T., Forrer, P., Amstutz, P., and Plückthun, A. (2003). Designing repeat proteins: well-expressed, soluble and stable proteins from combinatorial libraries of consensus ankyrin repeat proteins. J. Mol. Biol. *332*, 489–503.

Binz, H.K., Amstutz, P., Kohl, A., Stumpp, M.T., Briand, C., Forrer, P., Grütter, M.G., and Plückthun, A. (2004). High-affinity binders selected from designed ankyrin repeat protein libraries. Nat. Biotechnol. *22*, 575–582.

Binz, H.K., Amstutz, P., and Plückthun, A. (2005). Engineering novel binding proteins from nonimmunoglobulin domains. Nat. Biotechnol. *23*, 1257–1268.

Boatright, K.M., Renatus, M., Scott, F.L., Sperandio, S., Shin, H., Pedersen, I.M., Ricci, J.E., Edris, W.A., Sutherlin, D.P., Green, D.R., and Salvesen, G.S. (2003). A unified model for apical caspase activation. Mol. Cell *11*, 529–541.

Bravman, T., Bronner, V., Lavie, K., Notcovich, A., Papalia, G.A., and Myszka, D.G. (2006). Exploring "one-shot" kinetics and small molecule analysis using the ProteOn XPR36 array biosensor. Anal. Biochem. *358*, 281–288.

Collaborative Computational Project, Number 4 (1994). The CCP4 suite: programs for protein crystallography. Acta Crystallogr. D Biol. Crystallogr. *50*, 760–763.

Denault, J.B., and Salvesen, G.S. (2003). Expression, purification, and characterization of caspases. Curr Protoc Protein Sci., Chapter 21, Unit 21 13.

Deveraux, Q.L., Takahashi, R., Salvesen, G.S., and Reed, J.C. (1997). X-linked IAP is a direct inhibitor of cell-death proteases. Nature *388*, 300–304.

Emsley, P., Lohkamp, B., Scott, W.G., and Cowtan, K. (2010). Features and development of Coot. Acta Crystallogr. D Biol. Crystallogr. *66*, 486–501.

Eswar, N., Webb, B., Marti-Renom, M.A., Madhusudhan, M.S., Eramian, D., Shen, M.Y., Pieper, U., and Sali, A. (2007). Comparative protein structure modeling using MODELLER. Curr Protoc Protein Sci., Chapter 2, Unit 2 9.

Fuentes-Prior, P., and Salvesen, G.S. (2004). The protein structures that shape caspase activity, specificity, activation and inhibition. Biochem. J. *384*, 201–232.

Ganesan, R., Mittl, P.R., Jelakovic, S., and Grütter, M.G. (2006). Extended substrate recognition in caspase-3 revealed by high resolution X-ray structure analysis. J. Mol. Biol. *359*, 1378–1388.

Ganesan, R., Jelakovic, S., Mittl, P.R., Caflisch, A., and Grütter, M.G. (2011). In silico identification and crystal structure validation of caspase-3 inhibitors without a P1 aspartic acid moiety. Acta Crystallogr. Sect. F Struct. Biol. Cryst. Commun. *67*, 842–850.

Grütter, M.G. (2000). Caspases: key players in programmed cell death. Curr. Opin. Struct. Biol. *10*, 649–655.

Kabsch, W. (2010). Integration, scaling, space-group assignment and post-refinement. Acta Crystallogr. D Biol. Crystallogr. *66*, 133–144.

Kohl, A., Binz, H.K., Forrer, P., Stumpp, M.T., Plückthun, A., and Grütter, M.G. (2003). Designed to be stable: crystal structure of a consensus ankyrin repeat protein. Proc. Natl. Acad. Sci. USA *100*, 1700–1705.

Lazebnik, Y.A., Kaufmann, S.H., Desnoyers, S., Poirier, G.G., and Earnshaw, W.C. (1994). Cleavage of poly(ADP-ribose) polymerase by a proteinase with properties like ICE. Nature *371*, 346–347.

McCoy, A.J., Grosse-Kunstleve, R.W., Adams, P.D., Winn, M.D., Storoni, L.C., and Read, R.J. (2007). Phaser crystallographic software. J. Appl. Cryst. *40*, 658–674.

McStay, G.P., Salvesen, G.S., and Green, D.R. (2008). Overlapping cleavage motif selectivity of caspases: implications for analysis of apoptotic pathways. Cell Death Differ. *15*, 322–331.

Mittl, P.R.E., Di Marco, S., Krebs, J.F., Bai, X., Karanewsky, D.S., Priestle, J.P., Tomaselli, K.J., and Grütter, M.G. (1997). Structure of recombinant human CPP32 in complex with the tetrapeptide acetyl-Asp-Val-Ala-Asp fluoromethyl ketone. J. Biol. Chem. *272*, 6539–6547.

Morton, T.A., Myszka, D.G., and Chaiken, I.M. (1995). Interpreting complex binding kinetics from optical biosensors: a comparison of analysis by linearization, the integrated rate equation, and numerical integration. Anal. Biochem. *227*, 176–185.

Murshudov, G.N., Vagin, A.A., and Dodson, E.J. (1997). Refinement of macromolecular structures by the maximum-likelihood method. Acta Crystallogr. D Biol. Crystallogr. *53*, 240–255.

Muzio, M., Stockwell, B.R., Stennicke, H.R., Salvesen, G.S., and Dixit, V.M. (1998). An induced proximity model for caspase-8 activation. J. Biol. Chem. *273*, 2926–2930.

Ni, C.Z., Li, C., Wu, J.C., Spada, A.P., and Ely, K.R. (2003). Conformational restrictions in the active site of unliganded human caspase-3. J. Mol. Recognit. *16*, 121–124.

Potterton, E., Briggs, P., Turkenburg, M., and Dodson, E. (2003). A graphical user interface to the CCP4 program suite. Acta Crystallogr. D Biol. Crystallogr. *59*, 1131–1137.

Riedl, S.J., and Shi, Y. (2004). Molecular mechanisms of caspase regulation during apoptosis. Nat. Rev. Mol. Cell Biol. *5*, 897–907.

Riedl, S.J., Renatus, M., Schwarzenbacher, R., Zhou, Q., Sun, C., Fesik, S.W., Liddington, R.C., and Salvesen, G.S. (2001). Structural basis for the inhibition of caspase-3 by XIAP. Cell *104*, 791–800.

Roschitzki-Voser, H., Schroeder, T., Lenherr, E.D., Frölich, F., Schweizer, A., Donepudi, M., Ganesan, R., Mittl, P.R., Baici, A., and Grütter, M.G. (2012). Human caspases in vitro: expression, purification and kinetic characterization. Protein Expr. Purif. *84*, 236–246.

Rotonda, J., Nicholson, D.W., Fazil, K.M., Gallant, M., Gareau, Y., Labelle, M., Peterson, E.P., Rasper, D.M., Ruel, R., Vaillancourt, J.P., et al. (1996). The three-dimensional structure of apopain/CPP32, a key mediator of apoptosis. Nat. Struct. Biol. *3*, 619–625.

Roy, N., Deveraux, Q.L., Takahashi, R., Salvesen, G.S., and Reed, J.C. (1997). The c-IAP-1 and c-IAP-2 proteins are direct inhibitors of specific caspases. EMBO J. *16*, 6914–6925.

Salvesen, G.S., and Riedl, S.J. (2007). Caspase inhibition, specifically. Structure *15*, 513–514.

Schrodinger, LLC (2010). The AxPyMOL Molecular Graphics Plugin for Microsoft PowerPoint, Version 1.0.

Schweizer, A., Roschitzki-Voser, H., Amstutz, P., Briand, C., Gulotti-Georgieva, M., Prenosil, E., Binz, H.K., Capitani, G., Baici, A., Plückthun, A., and Grütter, M.G. (2007). Inhibition of caspase-2 by a designed ankyrin repeat protein: specificity, structure, and inhibition mechanism. Structure *15*, 625–636.

Schweizer, A., Rusert, P., Berlinger, L., Ruprecht, C.R., Mann, A., Corthésy, S., Turville, S.G., Aravantinou, M., Fischer, M., Robbiani, M., et al. (2008).

Structure

Caspase-3 Directed DARPins

CD4-specific designed ankyrin repeat proteins are novel potent HIV entry inhibitors with unique characteristics. PLoS Pathog. *4*, e1000109.

Sennhauser, G., Amstutz, P., Briand, C., Storchenegger, O., and Grütter, M.G. (2007). Drug export pathway of multidrug exporter AcrB revealed by DARPin inhibitors. PLoS Biol. *5*, e7.

Steiner, D., Forrer, P., Stumpp, M.T., and Plückthun, A. (2006). Signal sequences directing cotranslational translocation expand the range of proteins amenable to phage display. Nat. Biotechnol. *24*, 823–831.

Stennicke, H.R., Renatus, M., Meldal, M., and Salvesen, G.S. (2000). Internally quenched fluorescent peptide substrates disclose the subsite preferences of human caspases 1, 3, 6, 7 and 8. Biochem. J. *350*, 563–568.

Studier, F.W. (2005). Protein production by auto-induction in high density shaking cultures. Protein Expr. Purif. *41*, 207–234.

Szedlacsek, S.E., Ostafe, V., Serban, M., and Vlad, M.O. (1988). A re-evaluation of the kinetic equations for hyperbolic tight-binding inhibition. Biochem. J. *254*, 311–312.

Thornberry, N.A., Rano, T.A., Peterson, E.P., Rasper, D.M., Timkey, T., Garcia-Calvo, M., Houtzager, V.M., Nordstrom, P.A., Roy, S., Vaillancourt, J.P., et al. (1997). A combinatorial approach defines specificities of members of the caspase family and granzyme B. Functional relationships established for key mediators of apoptosis. J. Biol. Chem. *272*, 17907–17911.

Timmer, J.C., and Salvesen, G.S. (2007). Caspase substrates. Cell Death Differ. *14*, 66–72.

Wyllie, A.H., Kerr, J.F., and Currie, A.R. (1980). Cell death: the significance of apoptosis. Int. Rev. Cytol. *68*, 251–306.

Zahnd, C., Amstutz, P., and Plückthun, A. (2007). Ribosome display: selecting and evolving proteins in vitro that specifically bind to a target. Nat. Methods *4*, 269–279.

Zahnd, C., Kawe, M., Stumpp, M.T., de Pasquale, C., Tamaskovic, R., Nagy-Davidescu, G., Dreier, B., Schibli, R., Binz, H.K., Waibel, R., and Plückthun, A. (2010). Efficient tumor targeting with high-affinity designed ankyrin repeat proteins: effects of affinity and molecular size. Cancer Res. *70*, 1595–1605.

Structure, Volume *21*

Supplemental Information

Specific Inhibition of Caspase-3 by a Competitive DARPin: Molecular Mimicry between Native and Designed Inhibitors

Thilo Schroeder, Jonas Barandun, Andreas Flütsch, Christophe Briand, Peer R.E. Mittl, and Markus G. Grütter

Inventory of Supplemental Information

DOI: 10.1016/j.str.2012.12.011,

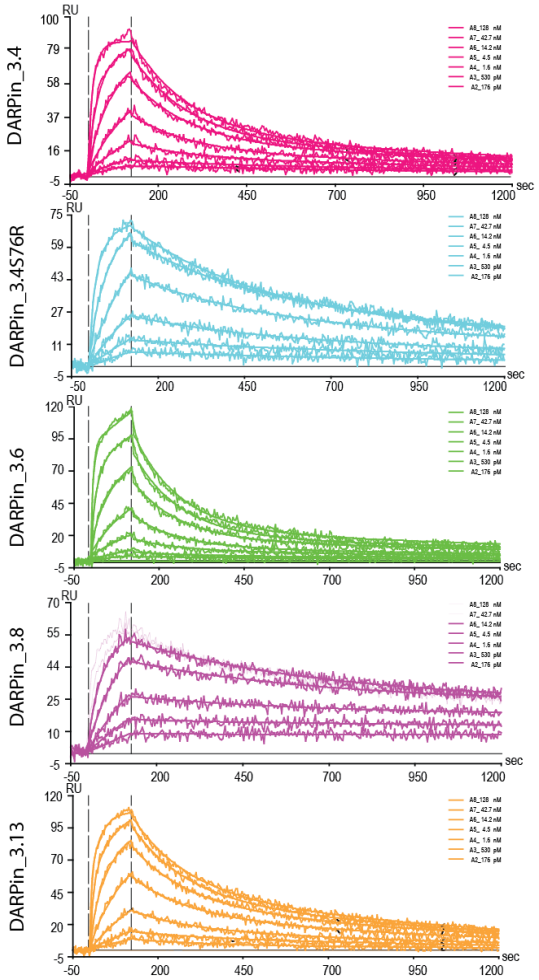

Supplementary Figure S1 related to Table 1

SPR analysis of five caspase-3 directed DARPins. Eight different concentrations (0, 0.176, 0.53, 1.6, 4.5, 14.2, 42.7, 128 nM) have been measured. The relative units (RU) were recorded for the association (3 minutes) and dissociation phase (20 minutes).

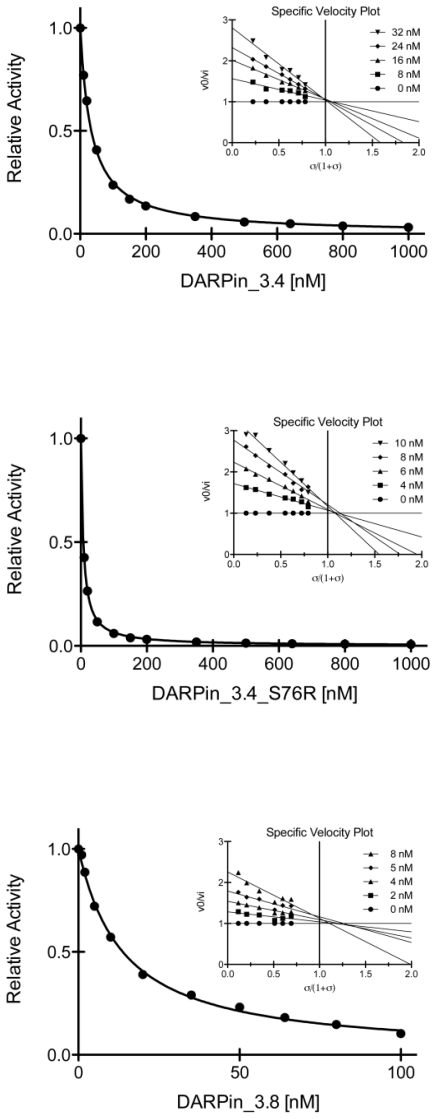

Supplementary Figure S2 kinetic analysis of inhibitor mechanism, related to Table 1

Characterization of the inhibition types of caspase-3 directed DARPins. The initial velocities and the specific velocity plots (small figure) are shown. The specific velocity plots reveal the behaviors of competitive inhibitors with $\alpha = \infty$ and $\beta = 0$.

DOI: 10.1016/j.str.2012.12.011,

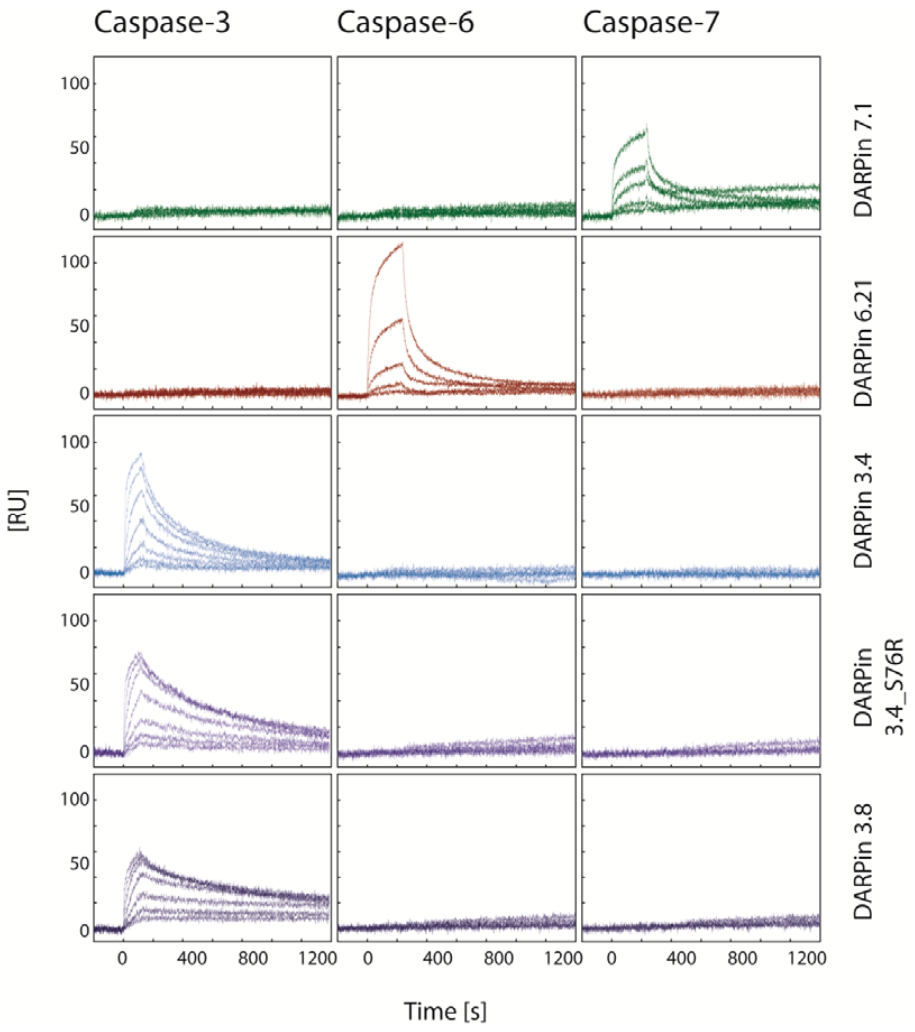

Supplementary Figure S3: Specificity for other caspases on SPR, related to Figure 3

SPR analysis of selected DARPins. Caspase-3 specific DARPins have been tested on binding against the close homologs caspase-6 and -7. All three caspases have been coated on the Proteon XPR36 NLC chips followed by testing of five DARPins. DARPin_6.21 and DARPin_7.1 were generated against caspase-6 and -7, respectively. They serve as positive controls, to show that the caspases are functional on the surface on the chip. All analyzed DARPins bind exclusively to one caspase only, indicating that they are all very specific for their target proteins.

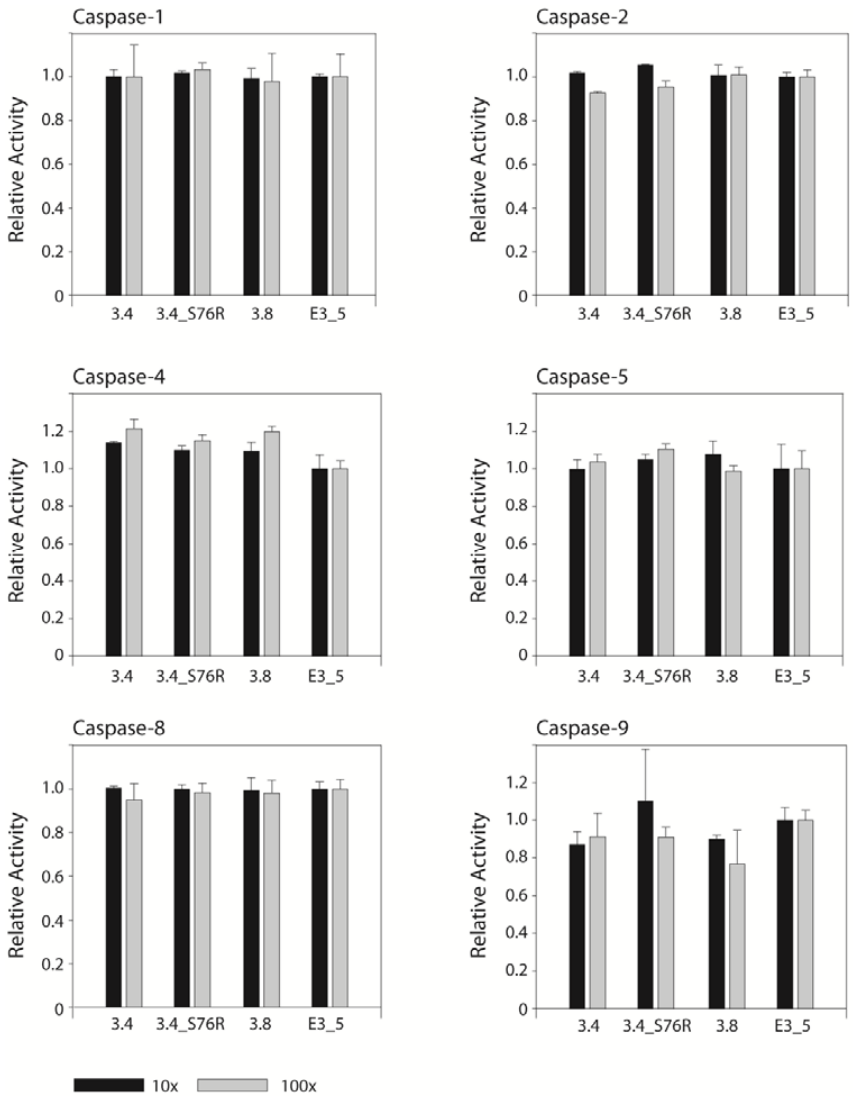

Supplementary Figure S4 related to Figure 3

Enzymatic activities of caspases in the presence of caspase-3 directed DARPins. Assays were performed as described in Materials and Methods and Figure 3, using caspase-1, -2, -4, -5, -8 and -9 instead of caspase-3. Error bars represent the standard deviation of three independent experiments.

DOI: 10.1016/j.str.2012.12.011,

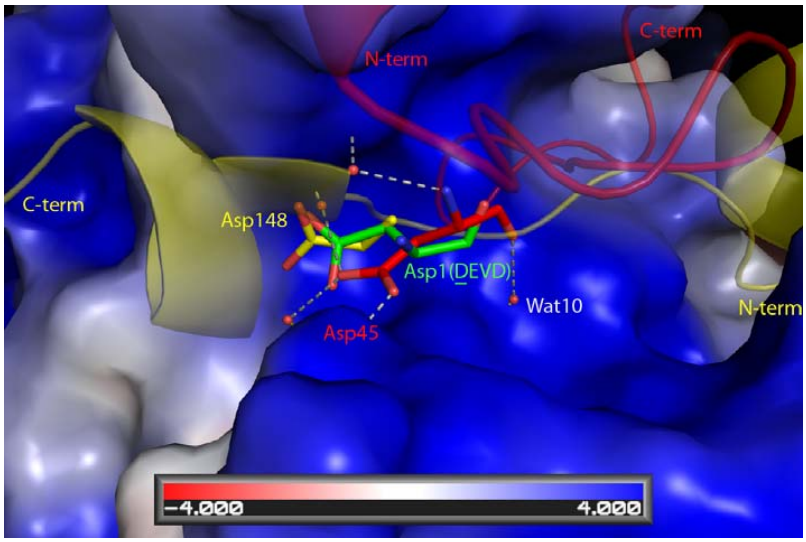

Supplementary Figure S5 related to Figure 5

Binding of Asp45 in the S4 pocket of caspase-3. Surface of the caspase-3 active site is shown with three different inhibitors superimposed. The peptide inhibitors DEVD (green), XIAP (yellow) and D3.4 (red) occupy the S4 pocket with an aspartic acid.

4 Publication: Caspase-7 Directed DARPins

BJ ChemBio

Biochem. J. (2014) **461**, 279–290 (Printed in Great Britain) doi:10.1042/BJ20131456

279

Combined inhibition of caspase 3 and caspase 7 by two highly selective DARPins slows down cellular demise

Andreas FLÜTSCH*[1], Rafael ACKERMANN*[2], Thilo SCHROEDER*[2,3], Maria LUKARSKA*[4], Georg J. HAUSAMMANN*, Christopher WEINERT*, Christophe BRIAND*[5] and Markus G. GRÜTTER*[6]

*Department of Biochemistry, University of Zurich, Winterthurerstrasse 190, CH-8057 Zurich, Switzerland

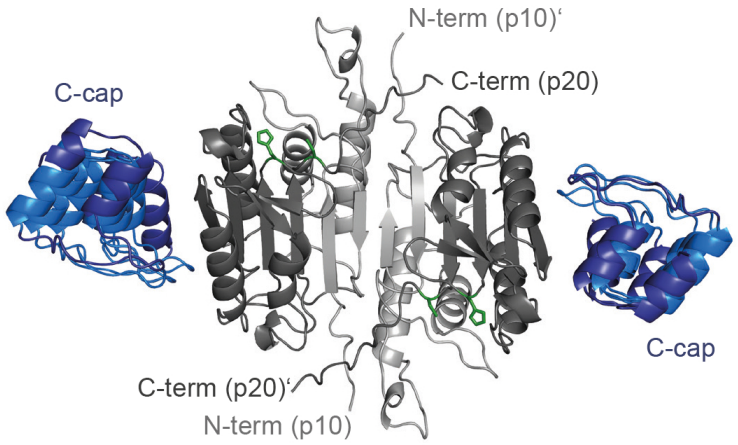

Figure 2A: Caspase-7 in complex with DARPin D7.18 (PDB: 4LSZ)

Biochem. J. (2014) **461**, 279–290 (Printed in Great Britain) doi:10.1042/BJ20131456

Combined inhibition of caspase 3 and caspase 7 by two highly selective DARPins slows down cellular demise

Andreas FLÜTSCH*[1], Rafael ACKERMANN*[2], Thilo SCHROEDER*[2,3], Maria LUKARSKA*[4], Georg J. HAUSAMMANN*, Christopher WEINERT*, Christophe BRIAND*[5] and Markus G. GRÜTTER*[6]

*Department of Biochemistry, University of Zurich, Winterthurerstrasse 190, CH-8057 Zurich, Switzerland

Caspases play important roles during apoptosis, inflammation and proliferation. The high homology among family members makes selective targeting of individual caspases difficult, which is necessary to precisely define the role of these enzymes. We have selected caspase-7-specific binders from a library of DARPins (designed ankyrin repeat proteins). The DARPins D7.18 and D7.43 bind specifically to procaspase 7 and active caspase 7, but not to other members of the family. Binding of the DARPins does not affect the active enzyme, but interferes with its activation by other caspases. The crystal structure of the caspase 7–D7.18 complex elucidates the high selectivity and the mode of inhibition. Combining these caspase-7-specific DARPins with the previously reported caspase-3-inhibitory DARPin D3.4S76R reduces the activity of caspase 3 and 7 in double-transfected HeLa cells during apoptosis. In addition, these cells showed less susceptibility to TRAIL (tumour-necrosis-factor-related apoptosis-inducing ligand)-induced apoptosis in living cell experiments. D7.18 and D7.43 are therefore novel tools for *in vitro* studies on procaspase 7 activation as well as for clarifying the role of its activation in different cellular processes. If applied in combination with D3.4S76R, they represent an excellent instrument to increase our understanding of these enzymes during various cellular processes.

Key words: caspase inhibition, caspase targeting, designed ankyrin repeat protein (DARPin), procaspase 7 activation, tumour-necrosis-factor-related apoptosis-inducing ligand (TRAIL)-induced apoptosis.

INTRODUCTION

To ensure the correct development of a multicellular organism, a variety of distinctive death pathways have evolved. These processes guarantee an accurate tissue maintenance and homoeostasis by the removal of aberrant cells. One of the well-studied cellular death pathways is termed apoptosis, which is primarily executed by proteolytic enzymes of the caspase family and triggered by either intra- or extra-cellular stimuli [1–3]. Once initiated, apoptosis leads to distinct morphological changes (e.g. rapid cell shrinkage, nuclear fragmentation or membrane blebbing) and non-inflammatory elimination of the cell by the recruitment of macrophages [4–6]. To prevent accidental apoptosis, various redundant regulatory systems have evolved. However, down- or up-regulation is related to severe pathological diseases such as tumour development, Parkinson's disease or Alzheimer's disease [2,7].

A crucial regulatory mechanism of apoptosis is the expression of caspases as inactive zymogens, which are activated upon certain death stimuli. The activation of initiator caspases requires dimerization at recruitment platforms followed by autoproteolytic cleavage of the prodomain and intersubunit linkers. The zymogens of the executioner procaspases are expressed as stable dimeric proteins and activated by partial proteolysis at the N-terminal propeptide and between the two subunits either by initiating or executing family members. After successful activation, all caspases consist of two catalytic domains, each formed by a large (p20) and a small (p10) subunit. Once initiated, the caspase cascade leads to numerous proteolytic cleavage events at downstream proteins, mainly performed by the executioner caspases, i.e. caspases 3, 6 and 7. Although these enzymes share a very high sequence identity of up to 50 %, their executing role during apoptosis has been proposed as similar, but non-redundant [8,9].

Targeting a well-conserved active site as observed in the caspase family is a challenging task. For example, the commercially available specific caspase substrates lack specificity owing to overlapping sequence recognition and cleavage by other caspases [10]. Besides targeting the active site, the selection of binding proteins with larger protein–protein interaction surfaces seems to be more promising. Such binding interfaces may involve non-conserved residues that would increase the binding specificity for the targeted enzyme. We therefore decided to screen for caspase-specific binders using a library of DARPins (designed ankyrin repeat proteins).

The intended DARPin design is based on the scaffold of ankyrin proteins [11]: located between a N- and C-terminal capping repeat, DARPins contain two (= NI2C) or three (= NI3C) internal repeats that each harbour six randomized positions. This results in a library with a theoretical diversity

Abbreviations: Ac, acetyl; cmk, chloromethylketone; DARPin, designed ankyrin repeat protein; DMEM, Dulbecco's modified Eagle's medium; IMAC, immobilized metal-ion-affinity chromatography; NA, numerical aperture; PARP-1, poly(ADP-ribose) polymerase 1; SEC, size-exclusion chromatography; SPR, surface plasmon resonance; TRAIL, tumour-necrosis-factor-related apoptosis-inducing ligand; Z, benzyloxycarbonyl.

[1] Present address: University of California, San Diego, 9500 Gilman Drive; M/C 0322, La Jolla, CA 92093, U.S.A.
[2] Rafael Ackermann is an employee of Cilag AG, and Thilo Schroeder is employed at Nextech Invest Ltd.
[3] Present address: Nextech Invest Ltd, Scheuchzerstrasse 35, 8006 Zurich, Switzerland.
[4] Present address: European Molecular Biology Laboratory, 38042 Grenoble Cedex 9, France.
[5] Present address: ETH Zurich, Light Microscopy and Screening Center, Schafmattstrasse 18, 8093 Zurich, Switzerland.
[6] To whom correspondence should be addressed (email gruetter@bioc.uzh.ch).

Structure factors and co-ordinates of the caspase 7–DARPin D7.18 complex were deposited in the PDB under code 4LSZ.

of up to 10^{23} different molecules, which can be used in phage or ribosome display selection procedures [12,13]. Besides their straightforward purification, these molecules combine high thermodynamic stability with a cysteine-free framework, rendering them highly attractive for intracellular applications.

Successful DARPin selections have been reported for numerous target proteins [14–17]. We highlight the caspase-2-specific [18] and the recently reported caspase-3-specific [19] inhibitory DARPins that are of importance to the present study. Whereas the caspase-2-targeted DARPin AR_F8 inhibits the enzyme in a highly specific and allosteric manner, the caspase-3-selected DARPin D3.4S76R is a highly specific competitive inhibitor.

To increase the availability of such caspase-specific and potentially inhibitory DARPins, we have performed DARPin selection to target human caspase 7. The DARPins D7.18 and D7.43, reported in the present paper, share an overlapping epitope and are highly selective binders for the active and the zymogenic form of caspase 7. Although both DARPins do not affect the function of the active enzyme, their binding to the zymogen interferes with its proteolytic activation. A crystal structure of the caspase 7–D7.18 complex unravels a potential mechanism of caspase 7 inhibition, which has been tested *in vitro* as well as in transfected HeLa cells.

MATERIALS AND METHODS

Reagents

All chemicals and growth media (including additives) were purchased from Sigma/Fluka if not mentioned otherwise. Primers were obtained from Microsynth, restriction enzymes and polymerases were from New England Biolabs (NEB) and T4 DNA ligase was purchased from Thermo Scientific. DARPin E3_5 is an unselected non-binding DARPin, widely used as a control and is described elsewhere [20].

DARPin selection by ribosome display and crude extract ELISA

Caspase-7-specific DARPin selection was performed as described in [19] using a library containing NI3C and NI2C DARPins [11,21]. Notably, before the caspase-7-panning step, the *in vitro* translation ribosomal complex was incubated with the closest homologues, caspases 3 and 6, for 30 min at 4 °C avoiding the selection of cross-specific binders. In addition, off-rate maturation was performed in rounds 3 and 4 by adding a 1000-fold excess of unbiotinylated caspase 7 for 10 min. The full selection was performed in the absence of caspase active-site inhibitors. Selected DARPins were then probed against caspase 7 using crude extract ELISA as described in [19], and DARPins surpassing a signal over control of 5 were sequenced by Microsynth.

Protein expression and purification

Expression and purification of caspases 3, 6, 7 and 8 was performed as described previously [22]. Purified enzymes were frozen in liquid nitrogen and stored at −80 °C.

DARPin D7.18 and D7.43 were expressed in *Escherichia coli* XL-1-Blue cells inoculated in 2YT medium (Bacto tryptone and Bacto yeast extract from Becton Dickinson). Expression time varied from 4–6 h up to overnight expression for crystallization trials. After cell lysis, DARPins were purified by IMAC (immobilized metal-ion-affinity chromatography) using Ni-NTA (Ni^{2+}-nitrilotriacetate) resins in gravity columns. Standard IMAC wash and elution buffers were 50 mM Tris/HCl (pH 7.5), 400 mM NaCl and 20 mM or 200 mM imidazole respectively. These buffers were adapted according to the intended use of the proteins, which are mentioned below. Eluted DARPins were stored at 4 °C after the addition of sodium azide to a final concentration of 0.05 %.

Production of procaspase 7

Procaspase 7 was obtained by mutagenesis of the active-site cysteine residue (C186A) [23,24] using a QuikChange® site-directed mutagenesis kit (Stratagene) and the primers 5′-CATTCAGGCTGCCCGAGGGACC-3′ and 5′-GGTCCCTCGGGCAGCCTGAATG-3′.

Expression and purification of procaspase 7 was performed using the procedure for active caspase 7 [22].

Biotinylation of procaspase 7 and active caspase 7

Before chemical biotinylation, caspase 7 and its zymogenic form were subjected to buffer exchange on a Superdex 200 10/300 GL column (GE Healthcare), equilibrated in PBS (pH 7.4) containing 10 % (w/v) sucrose. Protein-containing fractions were pooled and subsequently used for chemical biotinylation using a 4-fold molar excess of EZ-Link sulfo-NHS-LC-LC-biotin [sulfosuccinimidyl-6′-(biotinamido)-6-hexanamido hexanoate] (Pierce). Coupling mixtures of 700 μl of procaspase 7 (95 μM) or 700 μl of caspase 7 (62 μM) plus the calculated amount of biotin were incubated for 15 min on ice. The reaction was then quenched by the addition of Tris/HCl to a final concentration of 2.8 mM. Free biotin was removed with an additional SEC (size-exclusion chromatography) step using the same column and buffer as mentioned above. Chemically biotinylated enzymes were frozen in liquid nitrogen and stored in aliquots of 100 μl at −80 °C.

SPR (surface plasmon resonance) analysis

Binding affinities of DARPin D7.18 and D7.43 to caspase 7 and procaspase 7 were determined by SPR analysis using a NeutrAvidin-coated NLC sensorchip with a ProteOn™ XPR36 machine (Bio-Rad Laboratories). Approximately 1000 RU (response units) of biotinylated enzymes (80 nM in SPR buffer: PBS and 0.005 % Tween 20, filtered through a 0.22 μm pore-size filter) were immobilized on the chip at a flow rate of 30 μl/min. Analyte solutions of a DARPin 2-fold dilution series, from 512 nM to 8 nM, were injected beginning with the lowest concentration. Each measurement was performed at 20 °C using a flow rate of 60 μl/min with a contact time of 400 s and a dissociation time of 1800 s. Obtained sensorgrams were processed and analysed with the ProteOn Manager Software (version 3.1.0.6, Bio-Rad Laboratories). Binding affinities were determined by equilibrium analysis and kinetic data was obtained by curve-fitting using the heterogeneous ligand model [25].

In vitro procaspase 7 cleavage assay

The caspase 7 zymogen processing in presence of DARPins D7.18, D7.43 and E3_5 was monitored by incubation of chemically biotinylated procaspase 7 (2.5 μM) with the corresponding DARPins in a 10-fold excess. The reaction was started by the addition of the cleaving enzymes caspases 3, 7 or 8 (all 500 nM) or caspase 9 (5 μM) and was performed in PBS (pH 7.4) on ice for 48 h. Reactions with the cleaving enzyme caspase 9 were incubated on ice for 62 h. Enzymatic reactions were stopped by adding reducing SDS sample buffer and subsequent boiling at 95 °C for 5 min. Reaction mixtures were applied to SDS/PAGE (15 %) and blotted on to nitrocellulose

membranes using the Mini Trans-Blot® system (Bio-Rad Laboratories). Membranes were blocked in PBS containing 5 % (w/v) non-fat dried skimmed milk powder for 60 min at room temperature or overnight at 4 °C. After extensive washes with PBS, streptavidin-conjugated horseradish peroxidase (Pierce, 1:2000 dilution in PBS) was incubated for 60 min at room temperature. Protein bands were finally digitized at different exposure times on a Fuji Las 4000 system using the SuperSignal Pico Chemiluminescent Substrate (Pierce).

Crystallization of caspase 7 in complex with DARPin D7.18

Protein purification protocols were slightly modified for crystallization: caspase 7 and DARPin D7.18 were both purified by IMAC using 50 mM Hepes (pH 7.5), 400 mM NaCl and 20 mM or 200 mM imidazole for wash and elution respectively. Then, complex formation was initiated by incubation of caspase 7 with DARPin D7.18 at a molar ratio of 1:5 for 10 min at 4 °C. The protein complex was separated from DARPin excess by SEC using a Superdex 200 10/300 GL column (GE Healthcare) equilibrated in 50 mM Hepes (pH 7.5) and 150 mM NaCl. Fractions corresponding to the caspase–DARPin complex were pooled, concentrated to ∼16 mg/ml and applied to crystallization using the sitting-drop vapour-diffusion method.

Initial crystal hits appeared in 100 mM Tris/HCl (pH 7.5), 200 mM Li_2SO_4 and 25 % PEG 2000 monomethyl ether, and could be improved by additive screens to the final conditions of 100 mM Tris/HCl (pH 7.6), 0.8 M sodium formate and 13 % PEG 4000. Crystals were stored in liquid nitrogen after addition of 20 % ethylene glycol for cryoprotection until data collection.

Data collection, structure determination and refinement

Data collection was performed at the synchrotron beamline X06SA (Swiss Light Source, Villigen, Switzerland), and data processing and scaling were carried out using XDS and XSCALE [26]. To solve the complex structure, the PDB codes 3IBC [27] for caspase 7 and 2P2C [18] for DARPin were applied for molecular replacement using Phaser [28]. Final model building was performed manually in Coot [29] with alternating refinement steps by PHENIX [30] including TLS (Translation–Libration–Screw-rotation) refinement [31]. For caspase–DARPin interface analysis, the EPPIC server [32] (http://www.eppic-web.org) was used and structure Figures were made using PyMOL (http://www.pymol.org).

Modelling of the procaspase 7 interdomain linker

For better visualization of the flexible interdomain linker of procaspase 7, a model was generated using the program MODELLER 9.12 [33]. Co-ordinates of chain A of the procaspase 7 structure (PDB code 1K88) [23] were used as a template to calculate 20 different models containing the interdomain linker. A crystal structure of caspase 8 (PDB code 1QTN) [34] was aligned with its substrate-binding cleft to the linker cleavage site. For that purpose, the caspase-8-bound peptide inhibitor (Ac-IETD-aldehyde, where Ac is acetyl) was mutated to the caspase 7 cleavage sequence (IQAD) using PyMOL's mutagenesis wizard.

Cloning of DARPin constructs for mammalian expression

The production of fluorescent DARPins for mammalian expression was performed in two cloning steps. First, DARPins D7.18, D7.43 and E3_5 were amplified by PCR using Vent polymerase and the primers 5′-TTCCTCCATGGGTATGAGA-GGATCGCATCACCATCACCATCACGGATCCGACCTGGG-3′ and 5′-CCCAAGCTTCTGCAGGATTTCAGCCAG-3′. PCR products were purified by (1 %, w/v) agarose gel electrophoresis, digested using BamHI and HindIII for 2 h at 37 °C, and ligated into a custom-made pQe vector containing the fluorescent proteins, which was double digested by BamHI and HindIII as well as dephosphorylated by rAPid alkaline phosphatase (Roche). Ligation with T4 ligase led to a fusion protein of the DARPin with a C-terminal eGFP or mCherry and a C-terminal Myc tag.

In the second cloning step, the fusion proteins were transferred by FX-cloning [35] into a FX-ready mammalian expression vector based on the pcDNA5 vector (Invitrogen) using the primers 5′-ATATATGCTCTTCTAGTAGAGGATCGCATCACCATCACC-ATCAC-3′ and 5′-TATATAGCTCTTCATGCTCATTATTCATT-CAAGTCCTCTTCAGA-3′. DNA for mammalian expression was purified using a PureYield™ Plasmid Midiprep System (Promega) and sequenced by Microsynth (Supplementary Figure S1a at http://www.biochemj.org/bj/461/bj4610279add.htm).

Cell culturing and transfection of HeLa cells

HeLa cells were cultured in a humidified incubator with a 5 % CO_2 atmosphere using DMEM (Dulbecco's modified Eagle's medium high glucose; Sigma #6429). Medium was supplemented with 10 % (v/v) FBS, 100 units/ml penicillin and 100 μg/ml streptomycin.

For transient expression of fluorescent DARPins, HeLa cells were seeded on to six-well plates and grown to 80 % confluence. For transfection, the medium was replaced by 1.2 ml of fresh DMEM containing 2 % (v/v) FCS and antibiotics. Each transfection mixture consisted of a total amount of 3.4 μg of DARPin–DNA and 5.1 μg of branched PEI (polyethyleneimine) (25 kDa) mixed in 500 μl of DMEM without FCS and antibiotics. In the case of double transfections, the molar ratio of each construct was 1:1. After 20 min of incubation at room temperature, the transfection mixture was added dropwise to the cells. Successful transfection was determined 24 h after transfection using a Nikon Eclipse TE300 inverted microscope equipped with a xenon lamp and a Plan Fluor × 10/0.30 NA (numerical aperture) objective (Nikon) (Supplementary Figure S2 at http://www.biochemj.org/bj/461/bj4610279add.htm). Transfer to either 96-well plates (six wells per experiment) or chambered coverglass (Nunc® Lab-Tek® II) was performed by trypsinization with 0.1 % trypsin/EDTA solution and a splitting rate of 1:5. The cells were then grown in Phenol Red-free and Hepes-buffered (25 mM) DMEM (high glucose from Gibco) supplemented with 10 % (v/v) FBS and antibiotics.

Caspase activity measurements

The activity of caspase 3 and 7 was measured using the Caspase Glo® 3/7 assay (Promega) according to the manufacturer's protocol with minor modifications. The medium of transfected cells grown on 96-well plates was exchanged to fresh Phenol Red-free DMEM (see above) containing one of the following well-known apoptosis inducers [36–41]: TRAIL (tumour-necrosis-factor-related apoptosis-inducing ligand) (100 ng/ml; Gibco), etoposide (100 μM) and cisplatin (100 μM). Half of the cells per experiment (i.e. three wells) were grown in apoptosis-inducer-free medium and served as a control. Treated cells were incubated for 3 h (TRAIL) or 24 h (etoposide and cisplatin) at 37 °C. Then, 100 μM caspase inhibitor Z-DEVD-cmk (where Z is

Table 1 DARPin affinities and kinetic constants

(a) Kinetic data

Target	DARPin	$k_{a\,1}$ ($M^{-1} \cdot s^{-1}$)	$k_{d\,1}$ (s^{-1})	$K_{d\,1}$ (nM)	$k_{a\,2}$ ($M^{-1} \cdot s^{-1}$)	$k_{d\,2}$ (s^{-1})	$K_{d\,2}$ (nM)	χ^2 of R_{max} (%)
Caspase 7	D7.18	1.73×10^5	1.31×10^{-2}	76	1.08×10^4	2.11×10^{-4}	19.60	3.7
	D7.43	4.44×10^4	9.97×10^{-4}	23	6.65×10^5	1.77×10^{-2}	27	7.2
Procaspase 7	D7.18	1.01×10^5	1.44×10^{-2}	142	9.07×10^3	1.75×10^{-4}	19	3.0
	D7.43	2.99×10^4	1.41×10^{-3}	47	4.73×10^5	2.39×10^{-2}	51	4.9

(b) Equilibrium

Target	DARPin	K_d (nM)
Caspase 7	D7.18	144.0 ± 35.7
	D7.43	24.7 ± 4.9
Procaspase 7	D7.18	295.0 ± 84.3
	D7.43	32.2 ± 7.0

benzyloxycarbonyl and cmk is chloromethylketone) (Bachem) was added to non-transfected control cells and incubated for 10 min at room temperature. Caspase Glo® 3/7 reagent was added to cells and mixed gently by pipetting. After incubation for 40 min at room temperature, 50 μl of reaction mixture was transferred to white 96-well plates (half area, Corning) to measure the luminescence of each reaction on a multi-well plate reader (Tecan Infinity M1000). The signal-to-noise ratio was calculated using eqn (1) and statistical comparisons between the inhibitory DARPin-expressing cells (D7.43/D3.4S76R, D7.43/E3_5 and D3.4S76R/E3_5) were performed by one-way ANOVA and Tukey's post-hoc test in GraphPad Prism version 5.

$$\text{Signal-to-noise ratio} = \frac{\text{signal} - \text{background average}}{\text{S.D. of background}} \quad (1)$$

Live-cell imaging

Fluorescent time-lapse experiments were performed using a confocal laser-scanning microscope (Leica SP5) equipped with a resonant scanner (8000 Hz) for fast imaging, two sensitive HyD detectors and an environmental chamber. Images (512 pixels × 512 pixels, 12 bits) were taken using a HCX PL APO CS × 40/1.25 NA oil-immersion objective with a 3-fold line-average and a minimal zoom of 1.7. Each experiment was observed at 25 positions every 1 min with autofocusing every 15 min.

Before imaging, the culture medium of transfected cells grown on chambered coverglass (Nunc® Lab-Tek® II) was replaced with fresh medium (DMEM, Phenol Red-free, as above). Cells were imaged for approximately 20 min at 37 °C until TRAIL was added to a final concentration of 50 ng/ml to induce apoptosis. A time-lapse experiment was then performed for 5.5 h. Image analysis was carried out using ImageJ (version 1.45s, http://rsbweb.nih.gov/ij/) using the included cell counting plugin in a modified version for cell counting and manual determination of apoptotic time points. Cells that were displaying rapid shrinkage followed by membrane blebbing were considered as apoptotic and the time point of this event was noted. Cells were marked as survivors in the case of survival after incubation for 5.5 h in TRAIL-containing medium. Statistical analysis was performed using GraphPad Prism version 5.

RESULTS

Selection and characterization of caspase-7-specific DARPins

DARPin selection was performed by ribosome display as described in [19] using a NI2C and NI3C DARPin library [11]. A total of 288 individual clones were picked after the fourth round of selection and screened for binding to targeted caspase 7 by crude extract ELISA. A total of 43 binders with a strong signal were purified and subjected to SPR analysis for a preliminary binding-affinity evaluation (results not shown). The DNA of 24 high-affinity binders with a K_d below 500 nM exhibited unambiguous and unique sequencing results. Sequence alignments did not show highly conserved motifs at randomized positions as experienced previously in two different DARPin selections against caspase 3 [19,42]. Although our experience with conserved DARPin features [43] would suggest different binding interactions of the selected DARPin to caspase 7, seven of the highest affinity binders possess an overlapping epitope, as determined by competition ELISA (Supplementary Figure S3a at http://www.biochemj.org/bj/461/bj4610279add.htm, and results not shown). The selected binders were analysed further for caspase 7 inhibition as described previously [19]. None of the binders showed a detectable inhibitory effect (results not shown). DARPin D7.43 had the highest affinity for caspase 7, but only DARPin D7.18 crystallized in complex with caspase 7.

Selected DARPins bind to procaspase 7 and active caspase 7

To test whether the selected DARPins bind to the caspase 7 zymogen, complex formation with procaspase 7 was tested. Both DARPins D7.18 and D7.43 formed a stable complex with procaspase 7 in solution as detected by SEC (Supplementary Figure S4a at http://www.biochemj.org/bj/461/bj4610279add.htm). Binding affinities to procaspase 7 and active caspase 7 were determined by SPR analysis. Equilibrium analysis of the measured data led to K_d values of 144 ± 35.7 nM and 295 ± 84.3 nM in the case of binding of DARPin D7.18 to caspase 7 and procaspase 7 respectively. In line with the preliminary SPR data measured after the selection procedure, DARPin D7.43 showed a 5-fold higher affinity for caspase 7 with a K_d of 25.7 ± 4.9 nM. Notably, the affinity of D7.43 for procaspase 7 (K_d of 32.2 ± 7.0 nM) was identical compared with that of the active enzyme, which is one order of magnitude smaller than the K_d of the D7.18/procaspase 7 interaction. Binding curves (Supplementary Figures S4b and S4c) were fitted using the heterogeneous ligand model [25] and kinetic values are summarized in Table 1.

DARPin binding to procaspase 7 affects zymogen-processing *in vitro*

To address the question of whether binding of caspase-7-specific DARPins to the zymogenic form interferes with its processing,

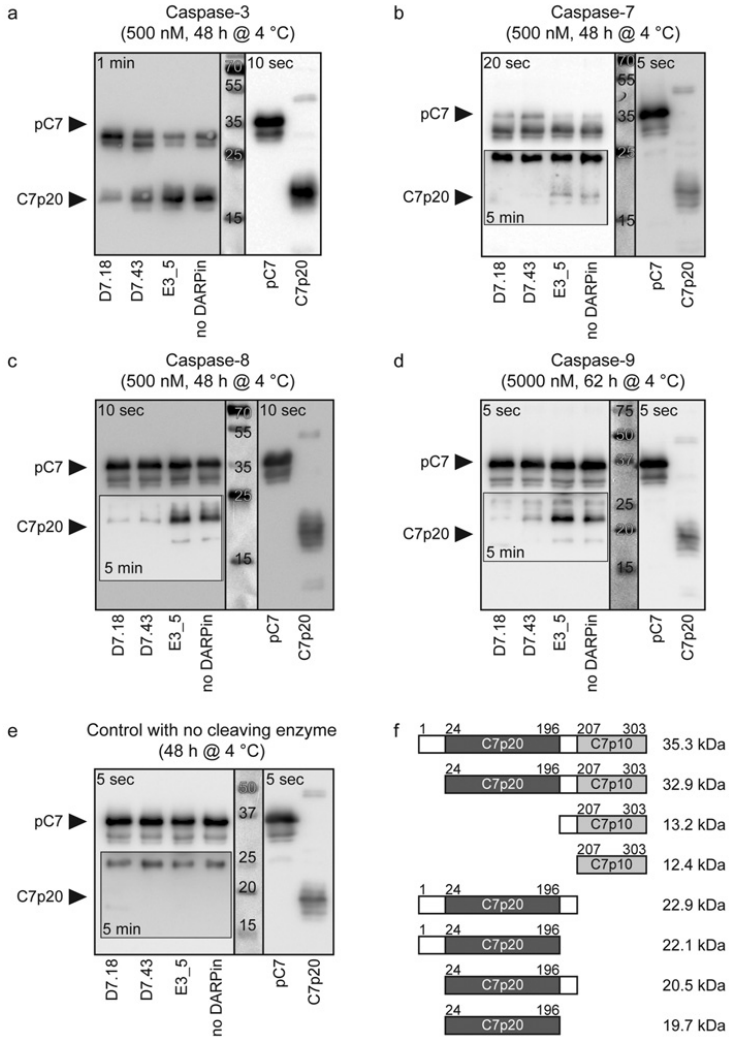

Figure 1 ***In vitro*** **inhibition of procaspase 7 activation by specific DARPins**

Processing of the zymogenic form of caspase 7 was monitored using chemically biotinylated procaspase 7 (2.5 μM), incubated with a 10-fold excess of either caspase-7-specific DARPins D7.18 and D7.43 or control DARPin E3_5, as well as without DARPin. Zymogen processing was performed using (**a**) caspase 3 (500 nM, 48 h), (**b**) caspase 7 (500 nM, 48 h), (**c**) caspase 8 (500 nM, 48 h) or (**d**) caspase 9 (5 μM, 62 h) at 4°C. All reactions are affected by caspase-7-specific DARPins and noticeably slow down the complete processing to p20. The small subunit p10 is not visible due to a very low accessibility during biotinylation. (**e**) A control without cleaving enzyme showed only small degradation of procaspase 7 over time. All blots were exposed at different exposure times ranging from 5 s to 5 min. The final blot picture was composed using different exposure times that displayed the best visibility. The particular exposure time is indicated in the different panels. Insets with black borders show exposure time of 5 min for better visibility of the processed bands. The contrast of the inset for caspase 7 (**b**) was slightly adjusted for better visibility of the faint bands. Possible cleavage products and corresponding molecular masses are depicted in (**f**).

cleavage of the interdomain linker was tested in the presence of D7.18, D7.43 and a non-binding control DARPin E3_5. Chemically biotinylated procaspase 7 was incubated with a 10-fold molar excess of DARPins and a cleaving enzyme, namely caspase 3, 7, 8 or 9. These caspase family members are well known as procaspase-7-cleaving enzymes during apoptosis [44]. Interestingly, both of the selected DARPins had an effect on zymogen processing: in the case of caspase 3 as the cleaving enzyme, the activation process was stalled considerably compared with the control reactions (Figure 1a). Cleavage by caspase 8 or 9 was abolished to approximately 90 % (Figures 1c and 1d). Whereas reactions with caspase 7 displayed no fully processed large subunit p20, a semi-processed form appeared as a fragment of approximately 25 kDa (Figure 1b). This would correspond to a caspase 7 fragment containing the full propeptide, the large subunit and the interdomain linker (Figure 1f). However, caspase

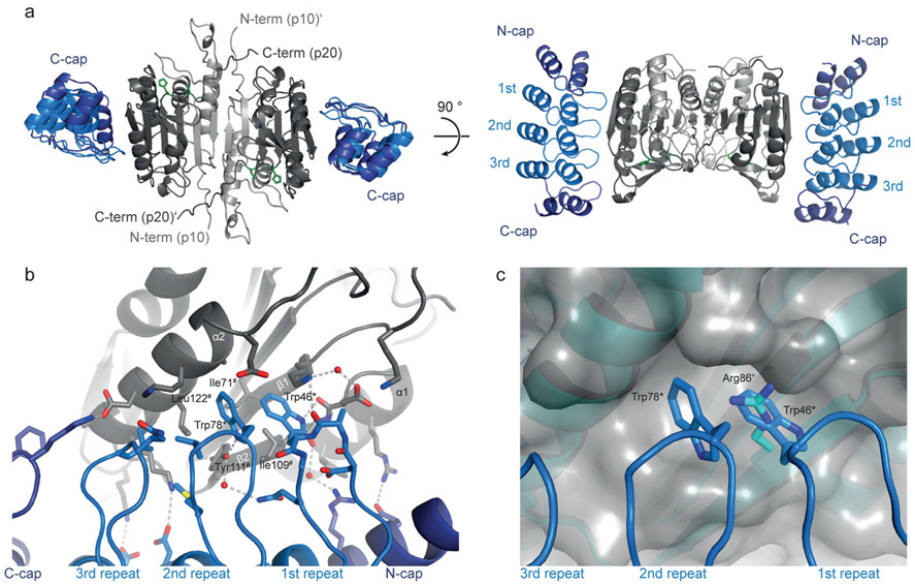

Figure 2 Crystal structure of caspase 7 in complex with D7.18

(**a**) Standard view of caspase 7 with the large subunit (p20) coloured dark grey and the small subunit (p10) in light grey. Active-site residues are displayed as green sticks. The N- and C-termini of p10 and p20 respectively are indicated; the right-hand protomer is labelled with an apostrophe ('). DARPin D7.18 with capping repeats (dark blue) and internal repeats (light blue) binds sideways at the p20 subunit. (**b**) Binding interface close-up view. Interacting residues (distance <4.5 Å) are depicted in stick representation. The major contribution for binding relies on a hydrophobic pocket shaped by caspase 7 residues (labelled #), which harbours two deeply buried DARPin tryptophan residues (labelled *). (**c**) Superimposition of caspase 3 (cyan) unravels the specificity of DARPin D7.18 for caspase 7. The hydrophobic pocket shaped by caspase 7 (grey cartoon and surface representation) is shrunk on caspase 3 due to a large Arg^{86} (labelled ") residue (depicted in stick representation).

7 was reported to primarily remove the N-terminal propeptide leading to a fragment of approximately 33 kDa [44], which can also be observed in our assay and which would prevent the formation of such a 25-kDa fragment. Since a fragment of 25 kDa also appeared in a control assay with no cleaving enzyme and procaspase 7 possesses low catalytic activity [45], we considered that this fragment originates from self-processing. Furthermore, the formation of truncated bands at 25 kDa has been observed in human brain tissues after experimental traumatic brain injury [46], suggesting a natural occurring cleavage product.

Selected DARPins do not affect procaspase 3 activation by caspases 3 and 8

Chemically biotinylated procaspase 3 incubated in the presence of D7.18, D7.43 and E3_5 was processed by active caspases 3 and 8. Neither a 50-fold molar excess of caspase-7-specific DARPins nor the control E3_5 had an effect on zymogen processing (Supplementary Figure S3b). In case of caspase 9 as the cleaving enzyme, we could not observe detectable activation of caspase 3 (Supplementary Figure S3b) even with extended incubation time and higher enzyme concentration. This can be explained by the caspase 9 monomer/dimer equilibrium and the enzyme's lower activity in buffers without kosmotropic salts [22,47].

D7.18 and D7.43 have no effect on caspase 7 activity

The inhibitory effect of caspase-7-specific DARPins was tested during the initial DARPin screening procedure using the chromogenic substrate Ac-DEVD-AMC (AMC is 7-amino-4-methylcoumarin). No reduction of activity was observed (results not shown). In addition, the influence of D7.43 on the cleavage of a natural caspase 7 substrate was analysed. We used the 116-kDa protein PARP-1 [poly(ADP-ribose) polymerase 1], which is a well-known substrate for caspase 3 and 7 that is cleaved after a canonical cleavage site (DEVD) at position 216 [48]. The resulting fragments can be observed using a PARP-1-specific antibody as described previously [19]. The cleavage assay was performed in presence of a 50-fold molar excess of D7.43 or E3_5 with no observable decrease in PARP-1 cleavage (Supplementary Figure S3c).

The caspase 7–D7.18 complex structure

Despite extensive screening with the highest-affinity binder D7.43, we were not able to obtain crystals of this DARPin in complex with caspase 7. However, crystal screening with D7.18 yielded a caspase 7–D7.18 complex structure determined at 2.26 Å (1 Å = 0.1 nm) resolution. The structure revealed a DARPin-binding epitope located laterally on the large p20 subunit of the enzyme (Figure 2a), which is substantially different from the one reported for other caspase-inhibitory DARPins [18,19].

Details of the structure determination and refinement statistics are summarized in Supplementary Table S1 (http://www.biochemj.org/bj/461/bj4610279add.htm). One caspase 7 heterotetramer $(p20, p10)_2$ and two binding DARPin molecules form the asymmetric unit of the crystal. The binding

interface comprises residues located at β-strand $\beta 2$ and α-helix $\alpha 2$ of caspase 7 and randomized positions of D7.18 (Supplementary Figure S1a). Five hydrogen bonds and five salt bridges in combination with a hydrophobic core form a total binding surface area of 672 Å^2. A significant binding contribution can be assigned to a deep hydrophobic pocket on the caspase 7 surface, shaped by Lys^{69}, Ile^{71}, Ile^{109}, Tyr^{111}, Leu^{122} and Ala^{126} located on β-strands $\beta 1$ and $\beta 2$ as well as on α-helix $\alpha 2$. The pocket accommodates two deeply buried tryptophan residues (Figure 2b) of the DARPin (Trp^{46} and Trp^{78}). Both tryptophan residues are stabilized further by hydrogen bonds with caspase 7 residues: Trp^{46} forms a hydrogen bond with the backbone carbonyl oxygen of Asp^{107}, whereas Trp^{78} is hydrogen-bonded to Tyr^{111}. This pocket not only provides a large hydrophobic binding area, but also explains the binding specificity of D7.18. Superimposition of a high-resolution structure of the closest homologue, caspase 3 (PDB code 2DKO) [49], on the caspase 7–D7.18 complex structure reveals that the Ile^{109} homologue on caspase 3 (Arg^{86}) fills the pocket to the extent that it prevents binding of D7.18 to caspase 3 (Figure 2c). This was confirmed by a caspase 7 mutant (I109R), which does not bind to D7.18 (Supplementary Figure S5f at http://www.biochemj.org/bj/461/bj4610279add.htm). In the case of caspase 6, the sequence homologue Lys^{86} shrinks the pocket and blocks a possible interaction with D7.18 (results not shown). Caspase sequence alignments show that Ile^{109} of caspase 7 is not conserved (Supplementary Figure S6a at http://www.biochemj.org/bj/461/bj4610279add.htm) and thus is, to a large extent, responsible for the binder's high specificity. However, Ile^{109} is not the only determinant for specificity between caspase 7 and D7.18, since the introduction of this isoleucine residue in caspase 3 (R86I) does not confer binding of the DARPin on caspase 3 (Supplementary Figure S5e). Clearly, other non-conserved residues (Lys^{69}, Phe^{98}, Val^{110}, Ala^{117}, Lys^{118}, Leu^{125} and Lys^{153}) of caspase 7 also contribute to the binding interface (Supplementary Figure S6).

Double transfection of D7.43 and D3.4S76R reduces caspase activity in apoptotic cells

The intracellular effect of a procaspase 7 cleavage inhibitor was tested in combination with the previously reported highly specific caspase-3-inhibitory DARPin D3.4S76R [19]. We transiently expressed D7.43 and D3.4S76R in HeLa cells and induced apoptosis with three different and well-characterized apoptotic stimuli [36–41]: TRAIL, etoposide and cisplatin. Co-transfected cells will have expression of D7.43 to prevent caspase 7 activation and D3.4S76R to inhibit activated caspase 3. After the induction of apoptosis, caspase activity can be measured using the DEVD-based Caspase Glo® 3/7 assay. It has to be noted that short peptide-based caspase substrates are not highly selective for an individual family member [10] and therefore measured values will represent an average of all cleaving proteases. Nevertheless, we expected an observable decrease in caspase activity in the case of caspase 3 and 7 inhibition, since these enzymes are known as highly active executioner caspases during apoptosis [50]. Indeed, D7.43- and D3.4S76R-co-expressing HeLa cells exhibited significantly reduced caspase activity of approximately 70–80 % after the induction of apoptosis with three different inducers (Figure 3). Control experiments were performed using double-transfected cells expressing either D7.43 and E3_5 or D3.4S76R and E3_5. Remarkably, caspase activity was reduced by approximately 30–50 % in cells expressing D3.4S76R/E3_5, whereas the expression of D7.43/E3_5 had no effect on proteolytic activity. This indicates that the additional 20–30 % reduction in activity, which has

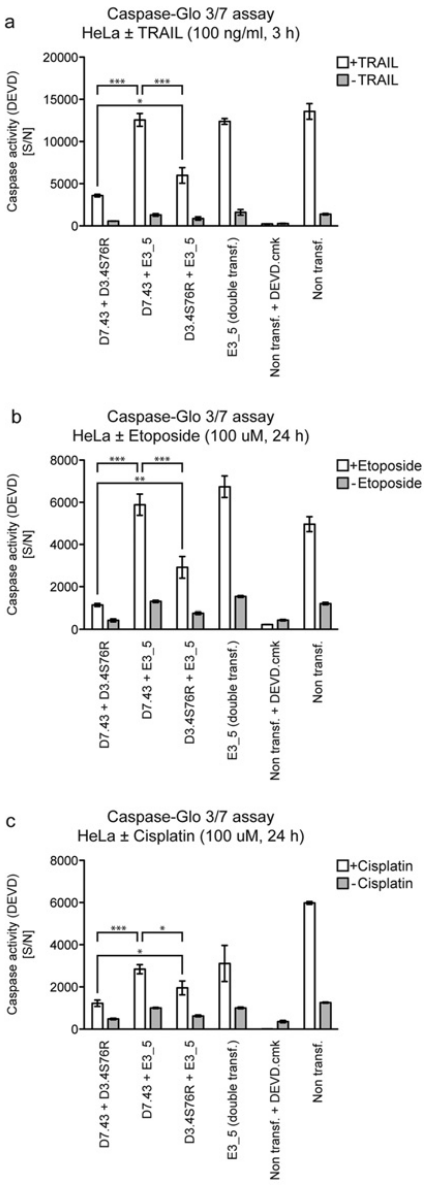

Figure 3 Caspase activity in co-transfected HeLa cells with D7.43 and D3.4S76R

Caspase activity of HeLa cells untreated (grey bar) or treated with apoptotic stimuli (white bar) measured using the Caspase Glo® 3/7 assay. Double-transfected cells expressing caspase-7-specific DARPin D7.43 and caspase-3-inhibitory DARPin D3.4S76R show a significantly reduced caspase activity after treatment with (**a**) TRAIL (100 ng/ml, 3 h), (**b**) etoposide (100 μM, 24 h) or (**c**) cisplatin (100 μM, 24 h) compared with cells which are expressing E3_5 and either D7.43 or D3.4S76R (*$P \leqslant 0.05$; **$P \leqslant 0.01$; ***$P \leqslant 0.001$). Control with non-transfected cells and Z-DEVD-cmk display complete abolishment of caspase activity. All values are signal-to-noise corrected means ± S.D. ($n = 3$).

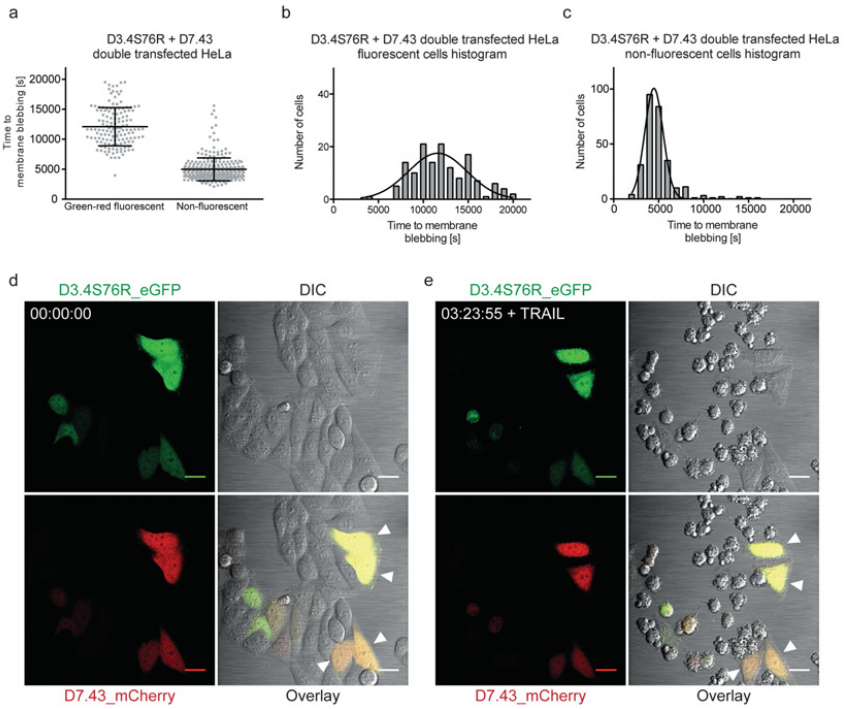

Figure 4 Time-lapse experiment following apoptosis of HeLa cells induced by TRAIL

HeLa cells were double transfected with D3.4S76R–eGFP and D7.43–mCherry leading to double-fluorescent cells in the case of successful co-transfection. (**a**) Cells expressing both DARPins (left-hand scatter plot, green/red fluorescent cells) survive for longer than non-expressing cells (right-hand scatter plot). Black lines indicate the mean ± S.D. time until cells show rapid shrinkage and membrane blebbing. Distributions of all counted cells, either double-fluorescent (**b**) or non-fluorescent (**c**), show a Gaussian distribution (bin width = 1000 s). Sample images at the beginning of the time-lapse experiment (**d**) show healthy and a few double-transfected cells. After 3 h 24 min of incubation with TRAIL (50 ng/ml) (**e**), all non-fluorescent cells died, whereas DARPin-expressing cells survived (indicated by white arrowheads) or just entered programmed cell death. The mean time for indication of cell death hallmarks of double-transfected cells was determined as 3 h 22 min (Table 2). DIC, differential interference contrast. Scale bars, 25 μm. Additional information is provided in Supplementary Figure S7, Supplementary Table S2 and Supplementary Movie S1 at http://www.biochemj.org/bj/461/bj4610279add.htm.

been observed for D7.43/D3.4S76R-expressing cells, derives from a successful inhibition of procaspase 7 activation. It underlines further the high processivity of caspase 3, which has been determined as the major executioner caspase during the demolition phase of apoptosis [9].

Live-cell imaging

Live-cell experiments were performed to directly monitor the effect of caspase inhibitory DARPins on the progression of apoptosis. The extrinsic apoptotic pathway of co-transfected HeLa cells was initiated by supplementation of the growth medium with TRAIL. After the addition of the death ligand (50 ng/ml), cells were imaged for 5.5 h using a confocal microscope. Images were analysed for observable hallmarks of apoptosis, such as rapid cell shrinkage and membrane blebbing [4]. Time points for such observations were determined for each individual cell and analysed statistically (Figure 4 and Supplementary Figure S7 at http://www.biochemj.org/bj/461/bj4610279add.htm). To distinguish between successfully transfected and non-transfected cells, expressed DARPins were fused to either eGFP or mCherry. Non-transfected cells, E3_5 double-transfected cells as well as D7.43 and D3.4S76R single-transfected cells displayed the first observable signs of apoptosis after approximately 1.5 h (Table 2, and Supplementary Table S2 at http://www.biochemj.org/bj/461/bj4610279add.htm). In contrast, D7.43- and D3.4S76R-co-expressing cells were less susceptible to TRAIL-induced apoptosis and entered apoptosis after approximately 3.3 h (Figure 4d and Supplementary Movie S1 at http://www.biochemj.org/bj/461/bj4610279add.htm). Furthermore, 23.5 % of all counted D7.43/D3.4S76R-expressing cells survived for more than 5.5 h in TRAIL-containing medium.

DISCUSSION

Specific targeting of highly homologous proteins brings along many challenges. The caspase family with a sequence identity of up to ~50 % has been thoroughly analysed using either peptide-based inhibitors or small substrates, which both target the highly conserved active site of the enzyme. Although well established, these short peptides are known for their lack of selectivity due to their consensus caspase-recognition sequence [10]. A more promising approach to target caspases more specifically has been reported by using small molecules that are binding to a region outside the active site [51–53]. These small compounds bind at an allosteric site in the central cavity of caspase 3 and 7, thereby

Table 2 Survival statistics of transfected HeLa cells after induction of apoptosis with TRAIL (50 ng/ml)

See also Supplementary Table S2 at http://www.biochemj.org/bj/461/bj4610279add.htm.

D3.4S76R + D7.43 double transfection	Number of cells	Number of survivors	Survival (%)	Mean ± S.D. time to cell death (h:min:s)
Green/red fluorescent	187	44	23.5	03:21:37 ± 00:53:09
Non-fluorescent	282	1	0.4	01:23:01 ± 00:31:47
Total	469	45	9.6	

trapping the enzymes in a zymogenic and inactive form. Larger molecules such as proteins may overcome the selectivity problem by increasing the interaction surface involving non-conserved residues. In the past, DARPins have been shown to be suitable tools for specific caspase targeting. AR_F8 was reported as the first truly specific allosteric caspase 2 inhibitor [18]. Recently, caspase 3 was specifically inhibited in a competitive manner using DARPin D3.4S76R [19].

We have selected caspase-7-specific DARPins using ribosome display [21]. By using this method, we could achieve high selectivity by introducing additional pre-panning steps, which have been performed against the closest homologues of caspase 7, namely caspases 3 and 6. The DARPins D7.18 and D7.43, reported in the present paper, share an overlapping epitope on caspase 7. Furthermore, both DARPins exhibited binding to procaspase 7, although the zymogenic form was not included during the selection procedure. This suggests a binding area apart from the active-site cleft, where no major structural rearrangements occur during zymogen activation. Interestingly, binding of D7.18 and D7.43 to procaspase 7 interferes with the interdomain linker cleavage by other caspases during activation processes. Cleavage of this linker is a prerequisite for the formation of active and mature caspase 7 [23,24]. The *in vitro* assay demonstrated that if D7.18 or D7.43 were incubated with procaspase 7, the interdomain linker cleavage by caspase 3 is significantly reduced, whereas cleavage by caspase 7, 8 or 9 is almost completely abolished. Furthermore, both DARPins do not interfere with *in vitro* processing of procaspase 3 by active caspase 3 and 8, emphasizing a high selectivity of these binders for caspase 7.

The high specificity of the selected binders can be explained by the large binding interface between the two molecules, which involves not only conserved, but also non-conserved, caspase 7 residues. In the particular case of D7.18, the protein complex structure illustrates that many non-conserved caspase 7 residues interact with the DARPin D7.18 (Supplementary Figure S6). A noteworthy binding interaction occurs between two DARPin tryptophan residues that are deeply buried in a hydrophobic pocket formed by α-helix $\alpha 1$ and β-strands $\beta 1$ and $\beta 2$ lateral on the large subunit p20. Interestingly, one of the pocket-shaping residues (Ile^{109}) is not conserved among other caspases, which possess bulkier residues at this position leading to a smaller shape of the pocket. Thus the crystal structure provides good evidence that the chosen selection procedure, which included pre-panning steps with closely related caspases, resulted in highly specific binders for caspase 7 by targeting of non-conserved amino acids. Notably, this strategy has been successfully applied in the past for a caspase-3-specific DARPin selection [19].

Although both DARPins share a similar epitope on caspase 7, the detailed molecular interactions between caspase 7 and D7.43 are different as illustrated by the binding data of a mutant caspase 7_I109R, which shows no binding to D7.18, but less effect on binding to D7.43. This does not exclude an overlapping epitope for both binders, and further mutational studies would be necessary to narrow down the interacting residues of caspase 7.

To elucidate how procaspase 7 activation is affected by the DARPins, the superimposition of the procaspase 7 crystal structure (PDB code 1K88) [23] with the caspase 7–DARPin structure (Figure 5a) provides further insights. Although slight rearrangements occur at the location of the interdomain linker, the overall α/β topology of the enzyme is kept constant, resulting in a non-altered DARPin epitope. Thus we assume that binding of the DARPin itself does not induce conformational changes that cause the observed inhibition of linker cleavage. The interdomain linker is highly flexible and not resolved in the procaspase 7 structure. For better visualization of its intrinsic flexibility, we modelled 20 interdomain linker structures and superimposed these models with the caspase 7–DARPin structure (Figure 5b). A putative cleaving complex with caspase 8 was modelled by alignment of the cleavage site of the intersubunit linker with the peptide inhibitor found in the caspase 8 structure (PDB code 1QTN) [34] (Figure 5c). This Figure visualizes that the cleaving enzyme would sterically clash with the DARPin leading to a reduced or abolished cleavage. Conclusively, DARPin binding most probably reduces the accessibility of the flexible linker for an activating caspase (Figure 5d) rendering the selected DARPins D7.18 and D7.43 highly specific inhibitors.

Once activated, caspase 7 can cleave its natural substrate PARP-1 even in presence of D7.43 (Supplementary Figure S3c), suggesting that no steric hindrance occurs between a bound DARPin and PARP-1, an example of a caspase 7 substrate. In this particular case, it is presumably due to a highly accessible cleavage site. However, this observation does not exclude the possibility that processing of other natural substrates can be affected. A caspase-7-bound DARPin could also either provide steric hindrance or potentially mask an important exosite on the surface of the enzyme.

To investigate the intracellular effect of the selected DARPins, we produced DARPins fused to fluorescent proteins and expressed them in HeLa cells. Furthermore, we included the highly specific caspase-3-inhibitory DARPin D3.4S76R [19] and focused the cellular studies on DARPin D7.43 because of its 10- and 5-fold higher affinity for procaspase 7 and active caspase 7 respectively in comparison with D7.18. D7.43 and D3.4S76R double-transfected HeLa cells exhibited a strongly reduced caspase activity after the induction of apoptosis by different stimuli. We were not able to achieve a 100 % reduction in caspase activity as shown in a control assay using the peptide-based caspase inhibitor Z-DEVD-cmk. There are two explanations for this. (i) The transient expression of DARPins. Transfection efficiency was determined to be approximately 80 %, resulting in 20 % non-transfected cells, which would be responsible for the measured residual caspase activity. (ii) Caspase activity was measured using the Caspase Glo® 3/7 assay, which is based on the short peptide DEVD. This peptide is not primarily specific for caspases 3 and 7, and is also cleaved by other caspases [10]. Notably, D7.43/E3_5-double-transfected cells showed no reduction in caspase activity, which

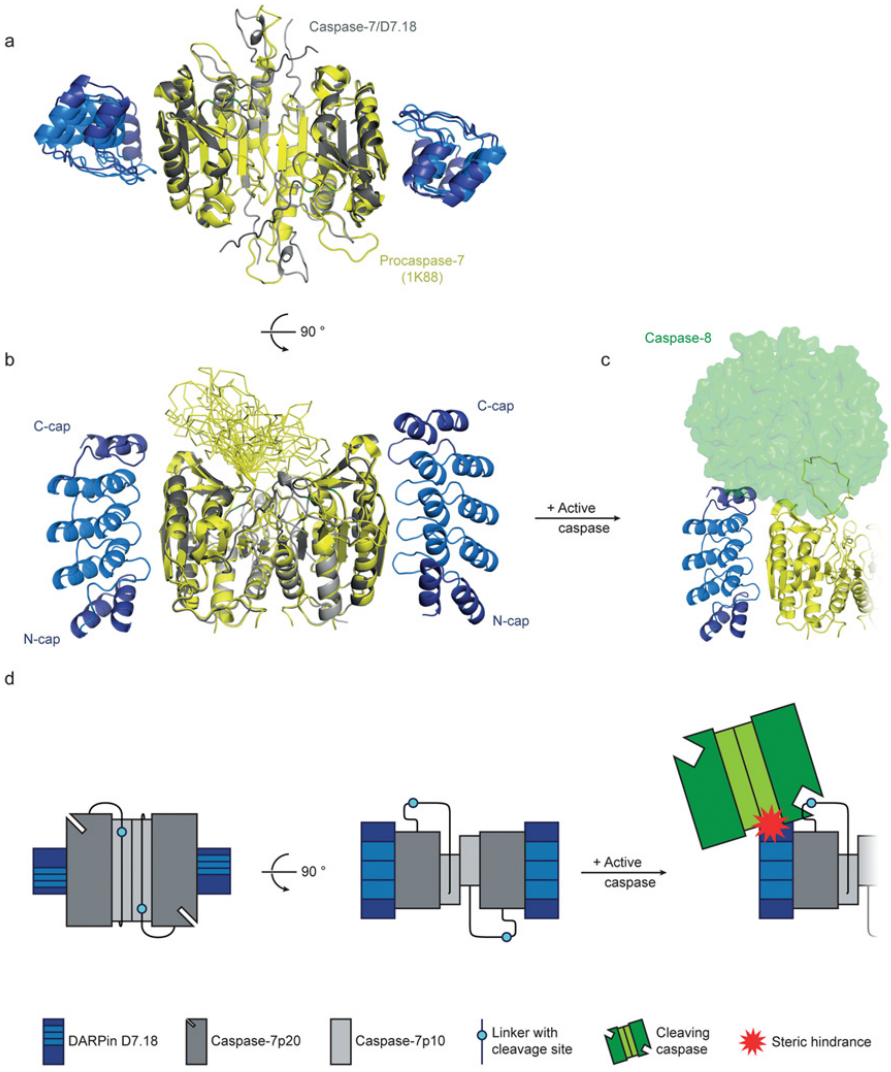

Figure 5 Superimposition of the procaspase 7 crystal structure and proposed inhibition mechanism

(**a**) The crystal structure of procaspase 7 (yellow, PDB code 1K88 [23]) is superimposed on the caspase 7–D7.18 complex structure (C7p20 is coloured dark grey, C7p10 is light grey; DARPin capping repeats are dark blue, internal repeats are light blue) and shows only small structural differences far away from the binding interface of the DARPin mainly at the N- and C-termini of p20 and p10 respectively. (**b**) Twenty calculated models of the interdomain linker (ribbon representation) of procaspase 7 are shown for better visualization of the linker flexibility. (**c**) Alignment of the active-site cleft of caspase 8 (green surface representation) with the linker cleavage site demonstrates how the cleaving enzyme would sterically clash with the caspase 7 DARPin. (**d**) Putative mechanism of zymogen-processing inhibition by caspase-7-specific DARPins. Binding of the DARPin sideways at the large subunit (p20) leads to a steric hindrance during cleavage of the interdomain linker performed by a cleaving caspase.

can be explained by the high efficiency of caspase 3 in cleavage of small peptide substrates. Double-transfected cells expressing D3.4S76R and E3_5 control DARPin showed a less prominent reduction of caspase activity compared with D7.43/D3.4S76R-transfected cells. This not only underlines the high processivity of caspase 3, but also proves the inhibitory effect of D7.43 on procaspase 7 activation.

Additional live-cell imaging experiments with D7.43- and D3.4S76R-expressing HeLa cells highlight the importance of both executioner caspases 3 and 7 during apoptosis and illustrates the potential for intracellular applications using these DARPins. D7.43/D3.4S76R-double-transfected HeLa cells were less susceptible to TRAIL-induced apoptosis compared with non-transfected cells. Furthermore, D7.43 or D3.4S76R

single-transfected cells entered apoptosis on average at the same time compared with non-transfected cells, emphasizing a functional substitution and redundancy of these two enzymes.

In summary, the present study describes the selection of two highly specific caspase 7 binders, D7.18 and D7.43, sharing an overlapping epitope on the protease. The lateral binding of DARPin D7.18 was revealed by its complex structure with caspase 7, illustrating that high specificity can be achieved by targeting a surface with non-conserved residues. Both selected DARPins can bind to the zymogen as well as to the active enzyme. In addition, pro-form binding interferes with interdomain linker cleavage *in vitro*. Thus DARPins D7.43 and D7.18 can be applied to study the process of procaspase 7 activation and autoproteolysis *in vitro*. In combination with the caspase-3-inhibitory DARPin 3.4S76R, HeLa cells show reduced caspase activity upon apoptotic stimuli and are able to escape apoptosis by surviving longer in death-ligand-supplemented growth medium. In particular, our findings demonstrate that the two DARPins, D7.43 and D3.4S76R, can be excellent intracellular tools for caspase 3 and 7 targeting. On one hand, D7.43 can be used to study the role of caspase 7 activation during various cellular processes. On the other hand, the combination of D7.43 and D3.4S76R can be used to shut down the activity of caspases 3 and 7 in a highly selective manner. For example, a stable cell line with inducible promoters for these binders will not only contribute to a better understanding of the two executioner caspases during apoptosis, but also open the door to study other remaining and less active caspases. Furthermore, these DARPins provide tools to further study bypass mechanisms of apoptosis. We believe that these molecules could serve as prototypes to develop novel therapeutics for degenerative diseases.

AUTHOR CONTRIBUTION

Markus G. Grütter supervised the study and designed the experiments together with Andreas Flütsch. Andreas Flütsch produced procaspases, performed SPR measurements and *in vitro* cleavage assays, as well as cellular caspase activity measurements and live-cell imaging. Rafael Ackermann cloned the fusion proteins and performed initial mammalian expression experiments. Thilo Schroeder performed the DARPin selection and initial characterization. Maria Lukarska improved the crystallization conditions and solved the structure together with Christophe Briand. Georg Hausammann and Christopher Weinert performed experiments on mutated caspases and procaspase 3 cleavage assays. Andreas Flütsch refined and analysed the complex structure and wrote the paper together with Markus G. Grütter.

ACKNOWLEDGEMENTS

Special thanks to the Salvesen laboratory (Sanford Burnham Medical Research Institute, La Jolla, CA, U.S.A.) for the expression plasmids of caspase 6 and 7. Professor P. Sonderegger (University of Zurich) is acknowledged for providing vectors containing fluorescent proteins (mCherry and eGFP) and Professor M. Hottiger (University of Zurich) for a sample of PARP-1 for cleavage assays. We are grateful to Martin Steger and the group of Professor A. Sartori (University of Zurich) for providing *Mycoplasma*-free HeLa cells. We thank Beat Blattmann and Céline Stutz-Ducommun from the NCCR crystallization facility for crystal screening as well as the staff of the X06SA beamline at the Swiss Light Source of the Paul Scherrer Institute (PSI) for their support during data collection. We highly appreciate the use of equipment for confocal imaging at the Center for Microscopy and Image Analysis at the University of Zurich and acknowledge U. Ziegler and his team for technical advice and maintenance of the microscopes.

FUNDING

Financial support for this work was provided by the Swiss National Science Foundation [grant number 310030-122342 (to M.G.G.)]

REFERENCES

1 Grütter, M. G. (2000) Caspases: key players in programmed cell death. Curr. Opin. Struct. Biol. **10**, 649–655 CrossRef PubMed
2 Riedl, S. J. and Shi, Y. (2004) Molecular mechanisms of caspase regulation during apoptosis. Nat. Rev. Mol. Cell Biol. **5**, 897–907 CrossRef PubMed
3 Fuentes-Prior, P. and Salvesen, G. S. (2004) The protein structures that shape caspase activity, specificity, activation and inhibition. Biochem. J. **384**, 201–232 CrossRef PubMed
4 Ziegler, U. and Groscurth, P. (2004) Morphological features of cell death. News Physiol. Sci. **19**, 124–128 PubMed
5 Shiratsuchi, A., Mori, T. and Nakanishi, Y. (2002) Independence of plasma membrane blebbing from other biochemical and biological characteristics of apoptotic cells. J. Biochem. (Tokyo) **132**, 381–386 CrossRef
6 Savill, J. and Fadok, V. (2000) Corpse clearance defines the meaning of cell death. Nature **407**, 784–788 CrossRef PubMed
7 Rohn, T. T. (2010) The role of caspases in Alzheimer's disease; potential novel therapeutic opportunities. Apoptosis **15**, 1403–1409 CrossRef PubMed
8 Slee, E. A., Adrain, C. and Martin, S. J. (2001) Executioner caspase-3, -6, and -7 perform distinct, non-redundant roles during the demolition phase of apoptosis. J. Biol. Chem. **276**, 7320–7326 CrossRef PubMed
9 Walsh, J. G., Cullen, S. P., Sheridan, C., Luthi, A. U., Gerner, C. and Martin, S. J. (2008) Executioner caspase-3 and caspase-7 are functionally distinct proteases. Proc. Natl. Acad. Sci. U.S.A. **105**, 12815–12819 CrossRef PubMed
10 McStay, G. P., Salvesen, G. S. and Green, D. R. (2008) Overlapping cleavage motif selectivity of caspases: implications for analysis of apoptotic pathways. Cell Death Differ. **15**, 322–331 CrossRef PubMed
11 Binz, H. K., Amstutz, P., Kohl, A., Stumpp, M. T., Briand, C., Forrer, P., Grütter, M. G. and Plückthun, A. (2004) High-affinity binders selected from designed ankyrin repeat protein libraries. Nat. Biotechnol. **22**, 575–582 CrossRef PubMed
12 Hanes, J. and Plückthun, A. (1997) *In vitro* selection and evolution of functional proteins by using ribosome display. Proc. Natl. Acad. Sci. U.S.A. **94**, 4937–4942 CrossRef PubMed
13 Steiner, D., Forrer, P. and Plückthun, A. (2008) Efficient selection of DARPins with sub-nanomolar affinities using SRP phage display. J. Mol. Biol. **382**, 1211–1227 CrossRef PubMed
14 Amstutz, P., Binz, H. K., Parizek, P., Stumpp, M. T., Kohl, A., Grütter, M. G., Forrer, P. and Plückthun, A. (2005) Intracellular kinase inhibitors selected from combinatorial libraries of designed ankyrin repeat proteins. J. Biol. Chem. **280**, 24715–24722 CrossRef PubMed
15 Sennhauser, G., Amstutz, P., Briand, C., Storchenegger, O. and Grütter, M. G. (2007) Drug export pathway of multidrug exporter AcrB revealed by DARPin inhibitors. PLoS Biol. **5**, e7 CrossRef PubMed
16 Schweizer, A., Rusert, P., Berlinger, L., Ruprecht, C. R., Mann, A., Corthesy, S., Turville, S. G., Aravantinou, M., Fischer, M., Robbiani, M. et al. (2008) CD4-specific designed ankyrin repeat proteins are novel potent HIV entry inhibitors with unique characteristics. PLoS Pathog. **4**, e1000109 CrossRef PubMed
17 Zahnd, C., Kawe, M., Stumpp, M. T., de Pasquale, C., Tamaskovic, R., Nagy-Davidescu, G., Dreier, B., Schibli, R., Binz, H. K., Waibel, R. and Plückthun, A. (2010) Efficient tumor targeting with high-affinity designed ankyrin repeat proteins: effects of affinity and molecular size. Cancer Res. **70**, 1595–1605 CrossRef PubMed
18 Schweizer, A., Roschitzki-Voser, H., Amstutz, P., Briand, C., Gulotti-Georgieva, M., Prenosil, E., Binz, H. K., Capitani, G., Baici, A., Plückthun, A. and Grütter, M. G. (2007) Inhibition of caspase-2 by a designed ankyrin repeat protein: specificity, structure, and inhibition mechanism. Structure **15**, 625–636 CrossRef PubMed
19 Schroeder, T., Barandun, J., Flütsch, A., Briand, C., Mittl, P. R. and Grütter, M. G. (2013) Specific inhibition of caspase-3 by a competitive DARPin: molecular mimicry between native and designed inhibitors. Structure **21**, 277–289 CrossRef PubMed
20 Kohl, A., Binz, H. K., Forrer, P., Stumpp, M. T., Plückthun, A. and Grütter, M. G. (2003) Designed to be stable: crystal structure of a consensus ankyrin repeat protein. Proc. Natl. Acad. Sci. U.S.A. **100**, 1700–1705 CrossRef PubMed
21 Zahnd, C., Amstutz, P. and Plückthun, A. (2007) Ribosome display: selecting and evolving proteins *in vitro* that specifically bind to a target. Nat. Methods **4**, 269–279 CrossRef PubMed
22 Roschitzki-Voser, H., Schroeder, T., Lenherr, E. D., Frölich, F., Schweizer, A., Donepudi, M., Ganesan, R., Mittl, P. R., Baici, A. and Grütter, M. G. (2012) Human caspases *in vitro*: expression, purification and kinetic characterization. Protein Expr. Purif. **84**, 236–246 CrossRef PubMed
23 Chai, J., Wu, Q., Shiozaki, E., Srinivasula, S. M., Alnemri, E. S. and Shi, Y. (2001) Crystal structure of a procaspase-7 zymogen: mechanisms of activation and substrate binding. Cell **107**, 399–407 CrossRef PubMed
24 Riedl, S. J., Fuentes-Prior, P., Renatus, M., Kairies, N., Krapp, S., Huber, R., Salvesen, G. S. and Bode, W. (2001) Structural basis for the activation of human procaspase-7. Proc. Natl. Acad. Sci. U.S.A. **98**, 14790–14795 CrossRef PubMed

25 Bravman, T., Bronner, V., Lavie, K., Notcovich, A., Papalia, G. A. and Myszka, D. G. (2006) Exploring "one-shot" kinetics and small molecule analysis using the ProteOn XPR36 array biosensor. Anal. Biochem. **358**, 281–288 CrossRef PubMed

26 Kabsch, W. (2010) Xds. Acta Crystallogr. D Biol. Crystallogr. **66**, 125–132 CrossRef PubMed

27 Agniswamy, J., Fang, B. and Weber, I. T. (2009) Conformational similarity in the activation of caspase-3 and -7 revealed by the unliganded and inhibited structures of caspase-7. Apoptosis **14**, 1135–1144 CrossRef PubMed

28 McCoy, A. J., Grosse-Kunstleve, R. W., Adams, P. D., Winn, M. D., Storoni, L. C. and Read, R. J. (2007) Phaser crystallographic software. J. Appl. Crystallogr. **40**, 658–674 CrossRef PubMed

29 Emsley, P., Lohkamp, B., Scott, W. G. and Cowtan, K. (2010) Features and development of Coot. Acta Crystallogr. D Biol. Crystallogr. **66**, 486–501 CrossRef PubMed

30 Adams, P. D., Afonine, P. V., Bunkoczi, G., Chen, V. B., Davis, I. W., Echols, N., Headd, J. J., Hung, L. W., Kapral, G. J., Grosse-Kunstleve, R. W. et al. (2010) PHENIX: a comprehensive Python-based system for macromolecular structure solution. Acta Crystallogr. D Biol. Crystallogr. **66**, 213–221 CrossRef PubMed

31 Painter, J. and Merritt, E. A. (2006) Optimal description of a protein structure in terms of multiple groups undergoing TLS motion. Acta Crystallogr. D Biol. Crystallogr. **62**, 439–450 CrossRef PubMed

32 Duarte, J. M., Srebniak, A., Scharer, M. A. and Capitani, G. (2012) Protein interface classification by evolutionary analysis. BMC Bioinformatics **13**, 334 CrossRef PubMed

33 Eswar, N., Webb, B., Marti-Renom, M. A., Madhusudhan, M. S., Eramian, D., Shen, M. Y., Pieper, U. and Sali, A. (2006) Comparative protein structure modeling using Modeller. Curr. Protoc. Bioinformatics, **Chapter 5**, Unit 5.6 CrossRef PubMed

34 Watt, W., Koeplinger, K. A., Mildner, A. M., Heinrikson, R. L., Tomasselli, A. G. and Watenpaugh, K. D. (1999) The atomic-resolution structure of human caspase-8, a key activator of apoptosis. Structure **7**, 1135–1143 CrossRef PubMed

35 Geertsma, E. R. and Dutzler, R. (2011) A versatile and efficient high-throughput cloning tool for structural biology. Biochemistry **50**, 3272–3278 CrossRef PubMed

36 Pitti, R. M., Marsters, S. A., Ruppert, S., Donahue, C. J., Moore, A. and Ashkenazi, A. (1996) Induction of apoptosis by Apo-2 ligand, a new member of the tumor necrosis factor cytokine family. J. Biol. Chem. **271**, 12687–12690 CrossRef PubMed

37 LeBlanc, H. N. and Ashkenazi, A. (2003) Apo2L/TRAIL and its death and decoy receptors. Cell Death Differ. **10**, 66–75 CrossRef PubMed

38 Karpinich, N. O., Tafani, M., Rothman, R. J., Russo, M. A. and Farber, J. L. (2002) The course of etoposide-induced apoptosis from damage to DNA and p53 activation to mitochondrial release of cytochrome *c*. J. Biol. Chem. **277**, 16547–16552 CrossRef PubMed

39 Qin, L. F. and Ng, I. O. (2002) Induction of apoptosis by cisplatin and its effect on cell cycle-related proteins and cell cycle changes in hepatoma cells. Cancer Lett. **175**, 27–38 CrossRef PubMed

40 Tanida, S., Mizoshita, T., Ozeki, K., Tsukamoto, H., Kamiya, T., Kataoka, H., Sakamuro, D. and Joh, T. (2012) Mechanisms of cisplatin-induced apoptosis and of cisplatin sensitivity: potential of BIN1 to act as a potent predictor of cisplatin sensitivity in gastric cancer treatment. Int. J. Surg. Oncol. **2012**, 862879 PubMed

41 Manzl, C., Krumschnabel, G., Bock, F., Sohm, B., Labi, V., Baumgartner, F., Logette, E., Tschopp, J. and Villunger, A. (2009) Caspase-2 activation in the absence of PIDDosome formation. J. Cell Biol. **185**, 291–303 CrossRef PubMed

42 Seeger, M. A., Zbinden, R., Flütsch, A., Gutte, P. G., Engeler, S., Roschitzki-Voser, H. and Grütter, M. G. (2013) Design, construction and characterization of a second-generation DARPin library with reduced hydrophobicity. Protein Sci. **22**, 1239–1257 CrossRef PubMed

43 Monroe, N., Sennhauser, G., Seeger, M. A., Briand, C. and Grütter, M. G. (2011) Designed ankyrin repeat protein binders for the crystallization of AcrB: plasticity of the dominant interface. J. Struct. Biol. **174**, 269–281 CrossRef PubMed

44 Van de Craen, M., Declercq, W., Van den brande, I., Fiers, W. and Vandenabeele, P. (1999) The proteolytic procaspase activation network: an *in vitro* analysis. Cell Death Differ. **6**, 1117–1124 CrossRef PubMed

45 Thomsen, N. D., Koerber, J. T. and Wells, J. A. (2013) Structural snapshots reveal distinct mechanisms of procaspase-3 and -7 activation. Proc. Natl. Acad. Sci. U.S.A. **110**, 8477–8482 CrossRef PubMed

46 Zhang, X., Alber, S., Watkins, S. C., Kochanek, P. M., Marion, D. W., Graham, S. H. and Clark, R. S. (2006) Proteolysis consistent with activation of caspase-7 after severe traumatic brain injury in humans. J. Neurotrauma **23**, 1583–1590 CrossRef PubMed

47 Pop, C., Salvesen, G. S. and Scott, F. L. (2008) Caspase assays: identifying caspase activity and substrates *in vitro* and *in vivo*. Methods Enzymol. **446**, 351–367 CrossRef PubMed

48 Lazebnik, Y. A., Kaufmann, S. H., Desnoyers, S., Poirier, G. G. and Earnshaw, W. C. (1994) Cleavage of poly(ADP-ribose) polymerase by a proteinase with properties like ICE. Nature **371**, 346–347 CrossRef PubMed

49 Ganesan, R., Mittl, P. R., Jelakovic, S. and Grütter, M. G. (2006) Extended substrate recognition in caspase-3 revealed by high resolution X-ray structure analysis. J. Mol. Biol. **359**, 1378–1388 CrossRef PubMed

50 Lakhani, S. A., Masud, A., Kuida, K., Porter, Jr, G. A., Booth, C. J., Mehal, W. Z., Inayat, I. and Flavell, R. A. (2006) Caspases 3 and 7: key mediators of mitochondrial events of apoptosis. Science **311**, 847–851 CrossRef PubMed

51 Hardy, J. A. and Wells, J. A. (2004) Searching for new allosteric sites in enzymes. Curr. Opin. Struct. Biol. **14**, 706–715 CrossRef PubMed

52 Hardy, J. A., Lam, J., Nguyen, J. T., O'Brien, T. and Wells, J. A. (2004) Discovery of an allosteric site in the caspases. Proc. Natl. Acad. Sci. U.S.A. **101**, 12461–12466 CrossRef PubMed

53 Hardy, J. A. and Wells, J. A. (2009) Dissecting an allosteric switch in caspase-7 using chemical and mutational probes. J. Biol. Chem. **284**, 26063–26069 CrossRef PubMed

Received 7 November 2013/22 April 2014; accepted 30 April 2014
Published as BJ Immediate Publication 30 April 2014, doi:10.1042/BJ20131456

Biochem. J. (2014) **461**, 279–290 (Printed in Great Britain) doi:10.1042/BJ20131456

online data multimedia

SUPPLEMENTARY ONLINE DATA

Combined inhibition of caspase 3 and caspase 7 by two highly selective DARPins slows down cellular demise

Andreas FLÜTSCH*[1], Rafael ACKERMANN*[2], Thilo SCHROEDER*[2,3], Maria LUKARSKA*[4], Georg J. HAUSAMMANN*, Christopher WEINERT*, Christophe BRIAND*[5] and Markus G. GRÜTTER*[6]

*Department of Biochemistry, University of Zurich, Winterthurerstrasse 190, CH-8057 Zurich, Switzerland

See the following pages for Figures S1–S7 and Tables S1 and S2.

[1] Present address: University of California, San Diego, 9500 Gilman Drive; M/C 0322, La Jolla, CA 92093, U.S.A.
[2] Rafael Ackermann is an employee of Cilag AG, and Thilo Schroeder is employed at Nextech Invest Ltd.
[3] Present address: Nextech Invest Ltd, Scheuchzerstrasse 35, 8006 Zurich, Switzerland.
[4] Present address: European Molecular Biology Laboratory, 38042 Grenoble Cedex 9, France.
[5] Present address: ETH Zurich, Light Microscopy and Screening Center, Schafmattstrasse 18, 8093 Zurich, Switzerland.
[6] To whom correspondence should be addressed (email gruetter@bioc.uzh.ch).
Structure factors and co-ordinates of the caspase 7–DARPin D7.18 complex were deposited in the PDB under code 4LSZ.

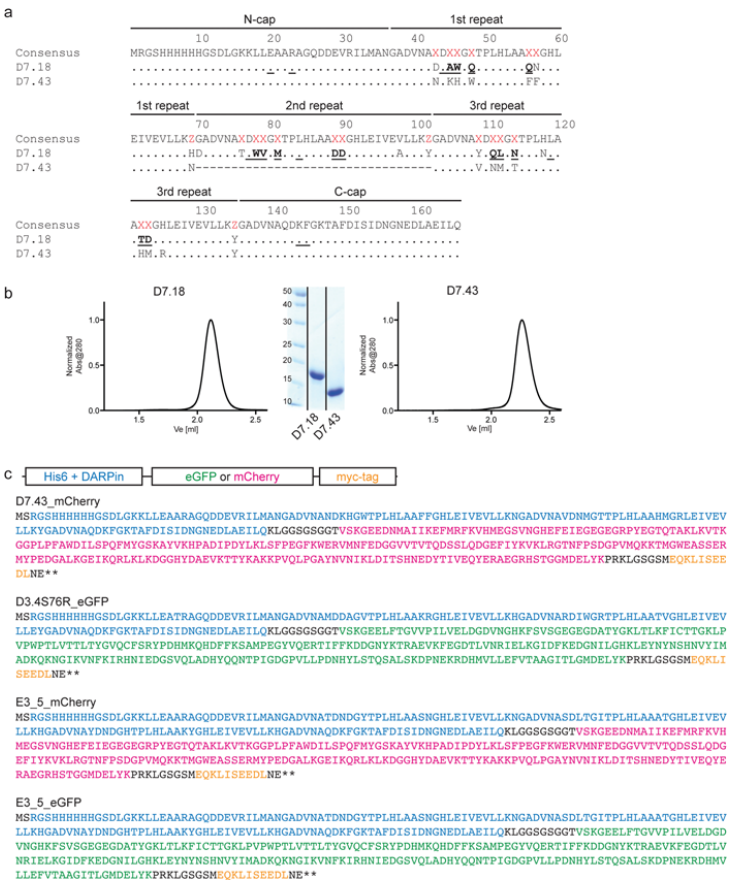

Figure S1 Caspase-7-specific DARPins and mammalian expression constructs

(**a**) Sequence alignment of caspase-7-specific DARPins D7.18 and D7.43. The consensus sequence is shown in black with randomized positions in red. D7.18 residues involved in caspase binding were determined by the EPPIC server (http://www.eppic-web.org [1]) and are marked in bold and underlined. D7.18 is a NI3C DARPin with three internal repeats harbouring two unintended framework mutations, which are not involved in the binding interface. D7.43 has two internal repeats (NI2C) and one framework mutation. (**b**) Size-exclusion chromatogram (Superdex 200 5/150, GE Healthcare) and SDS/PAGE (15 %) analysis of D7.18 and D7.43. Both DARPins elute at the expected retention volume of a monomer and show high purity on SDS/PAGE after IMAC purification. (**c**) For expression in mammalian cells, DARPins were C-terminally fused to either eGFP or mCherry with a C-terminal Myc tag for detection. Both additional features are separated by short and flexible linkers. Using FX cloning [2], fused DARPins were transferred from a pQe into a pcDNA5 vector for mammalian expression (see the Materials and methods section of the main text).

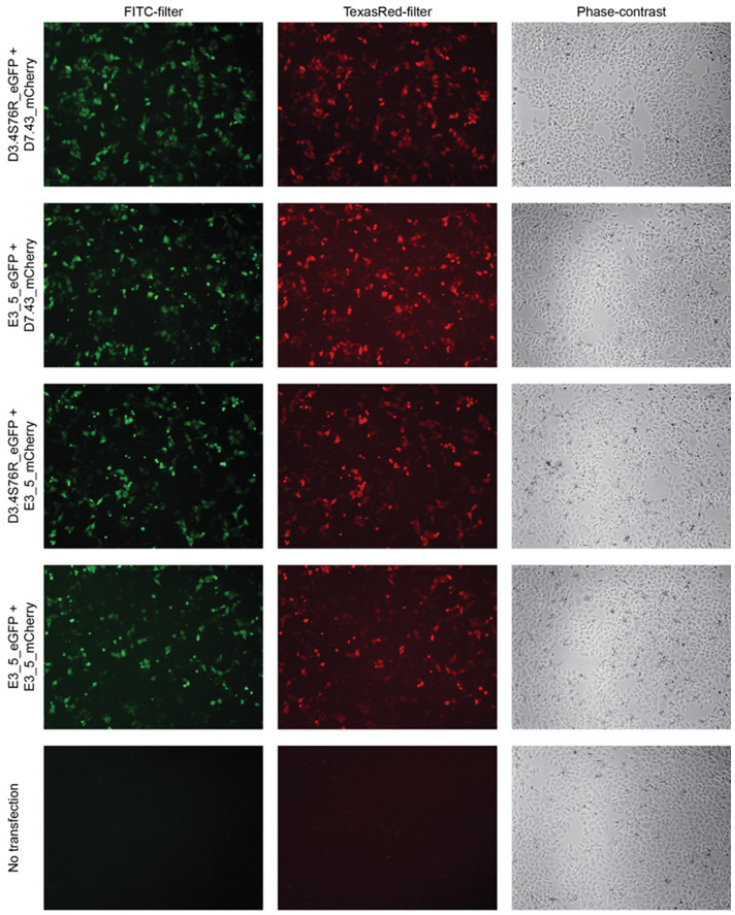

Figure S2 Expression levels of transfected HeLa cells 24 h after transfection

Expression levels of fluorescent DARPins were analysed using a Nikon Eclipse TE300 inverted microscope with a Plan Fluor ×10/0.30 NA objective. All co-transfection experiments showed a successful expression of the applied DARPins: D3.4S76R–eGFP and D7.43–mCherry, E3_5–eGFP and D7.43–mCherry, D3.4S76R–eGFP and E3_5–mCherry, E3_5–eGFP and E3_5–mCherry. Non-transfected cells appeared as non-fluorescent. All fluorescent images were exposed for 150 ms for comparison. The transfection efficiency was approximately 70–80 %, estimated from images taken with longer exposure times (not shown), although co-transfection of E3_5 constructs seemed to be less efficient. Cells were afterwards used for Caspase Glo® 3/7 assay and live-cell imaging.

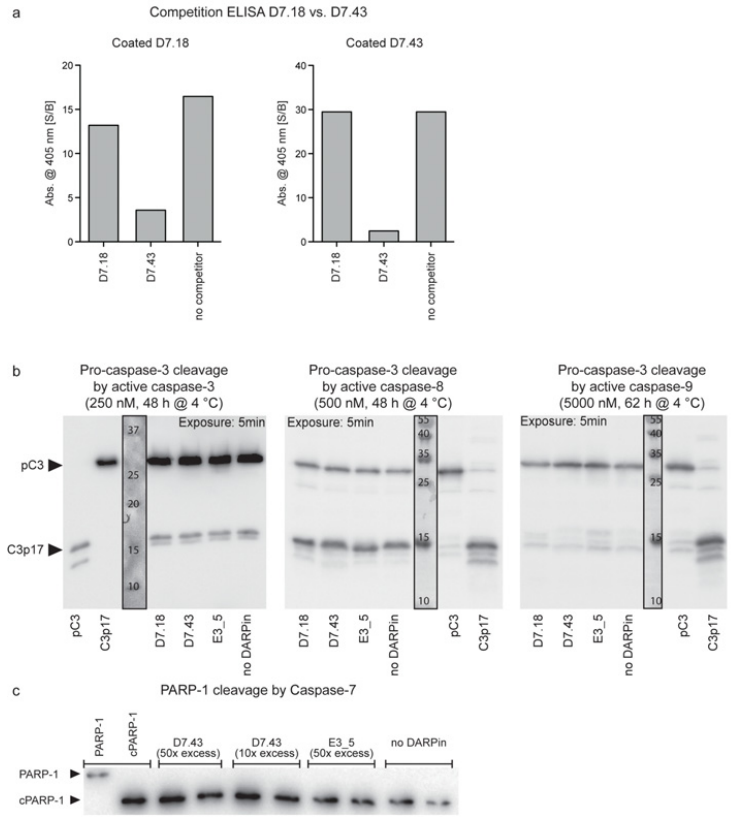

Figure S3 Additional experiments

(**a**) Competition ELISA with either coated D7.18 (left-hand panel) or D7.43 (right-hand panel) using chemically biotinylated caspase 7 for detection by streptavidin-conjugated alkaline phosphatase. Both DARPins bind to similar epitopes visualized by a loss of signal on D7.18-coated wells and D7.43 used as competitor. However, D7.18 was not able to compete with D7.43 indicating a lower affinity. A short summary of the competition ELISA protocol is provided. After every incubation step, a washing procedure was performed three times using PBS/Tween 20 (0.2 %). MaxiSorp™ plates (Nunc) were coated with DARPins (100 μl at 60 nM) overnight at 4 °C. After blocking with PBS/BSA (0.5 %, 2 h at room temperature), a pre-incubated protein solution containing 120 nM caspase 7 (chemically biotinylated) and 512 nM competitive DARPin was applied and incubated for 60 min at 4 °C. Streptavidin-conjugated alkaline phosphatase (Roche) was incubated for 40 min at room temperature, and phosphatase activity was detected on a plate reader (Tecan Infinity M1000) after the addition of *p*-nitrophenyl phosphate (pNPP). (**b**) Selected DARPins are specific for caspase 7 and do not interfere with zymogen processing of procaspase 3 by active caspases 3 and 8. The cleavage assay was performed as described in the Materials and methods section of the main text using 500 nM procaspase 3 (chemically biotinylated), a 50-fold excess of DARPin and either active caspase 3 (250 nM), caspase 8 (500 nM) or caspase 9 (5000 nM). However, procaspase 3 activation by active caspase 9 was not very efficient in presence or absence of DARPins due to the enzyme's low activity in kosmotropic salt-free buffers [3]. Procaspase 3 was made by site-directed mutagenesis of the active-site cysteine residue (C163A) and purified as described in [3]. Biotinylation was performed as described for procaspase 7 (see the Materials and methods section of the main text). All blots were exposed for 5 min. Marker was digitized and inserted into the blot at the correct position using Adobe Photoshop. (**c**) Binding of DARPin D7.43 to active caspase 7 does not influence the processing of PARP-1, a well-known natural substrate of caspase 7 [4]. The cleavage assay was performed exactly as described previously [5] in duplicate with 150 nM caspase 7, 180 nM PARP-1 and 10- or 50-fold excess of DARPins. Blot was exposed for 5 min and contrast was adjusted for better visualization.

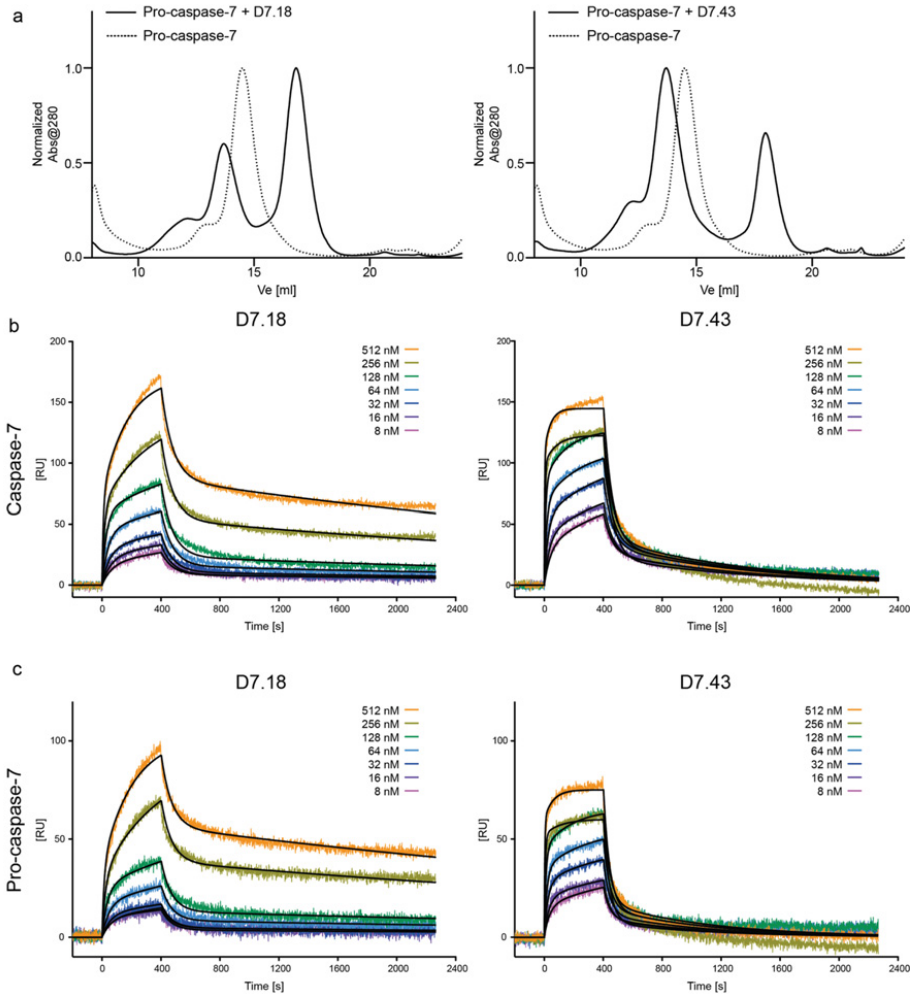

Figure S4 DARPin binding to procaspase and active caspase 7

(**a**) Binding of DARPins to procaspase 7 could be observed on SEC using a Superdex 200 10/300 GL column (GE Healthcare). Procaspase 7 is eluted at a retention volume of approximately 14.5 ml (broken line), whereas the formed complex is eluted at approximately 13.6 ml (continuous line). Binding characterization by SPR analysis of DARPin to active caspase 7 (**b**) and procaspase 7 (**c**). Both DARPins D7.18 and D7.43 are able to bind to the active and the zymogenic form of the enzyme. Binding affinities were determined by equilibrium analysis and kinetic values by curve fitting of the measured data (summarized in Table 1 of the main text).

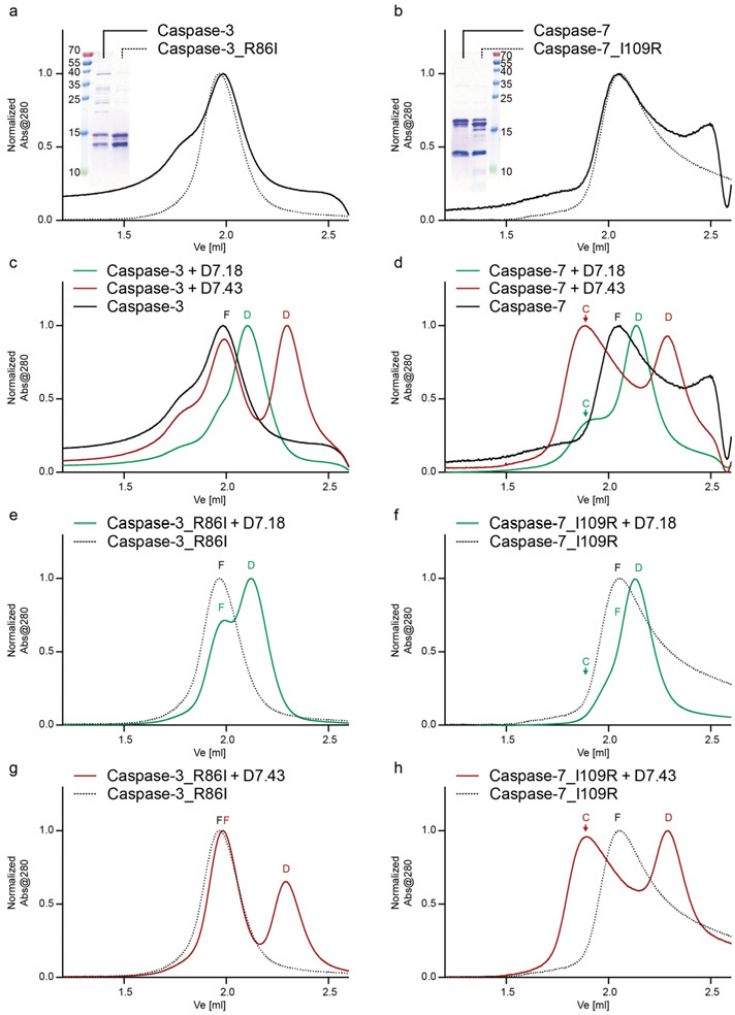

Figure S5 Mutational studies of caspase 3 and 7

The crystal structure of caspase 7–D7.18 revealed that Ile[109] is to a large extent responsible for the binder's specificity. To investigate this finding further, active caspase3 was mutated at the homologous position (Arg[86]) to isoleucine using QuikChange® site-directed mutagenesis kit (Stratagene) and the primers 5′-GAAACTTGAAATATGAAGTCATTAATAAAAATGATCTTACACG-3′ and 5′-CGTGTAAGATCATTTTTATTAATGACTTCATATTTCAAGTTTC-3′. In addition, Ile[109] on caspase 7 was mutated to arginine (the caspase 3 homologous side chain) using primers 5′-GGGTTTTGACGTGAGGGTCTATAATGACTGC-3′ and 5′-GCAGTCATTATAGACCCTCACGTCAAAACCC-3′. Both mutants, caspase 3_R86I and caspase 7_I109R, were purified as described in [3], processed correctly (as shown by SDS/PAGE) and eluted at the same retention volume as the wild-type form (**a** and **b**). Caspase–DARPin binding was evaluated by SEC (Superdex 200 5/150, GE Healthcare). As intended, D7.18 and D7.43 did not bind to wild-type caspase 3 (**c**), but they did bind to wild-type caspase 7 (**d**). Successful binding to caspase 7 can be seen by the elution of a caspase–DARPin complex at earlier retention volume (marked with an arrow and a C for complex) as well as a disappearing caspase 7 elution peak at approximately 2.0 ml (marked with F for free/unbound caspase). The late elution peaks at larger retention volumes (>2.1 ml) corresponds to an excess of free DARPin (marked with D). D7.43 is a NI2C DARPin and elutes at higher retention volume compared with the NI3C DARPin D7.18. Notably, the unbound caspase 3 (wild-type) shows a small shoulder at a lower retention volume, originating from impurities in the sample as seen on SDS/PAGE (inset, **a**). For DARPin D7.18, no complex peak could be observed in binding studies with caspase 3_R86I (**e**) as well as with caspase 7_I109R (**f**). These findings indicate that the hydrophobic pocket formed by Ile[109] is an important interaction in the binding interface between caspase 7 and D7.18 since a single mutation (I109R) disrupts the binding. It demonstrates further that other non-conserved residues of caspase 7 are involved in the binding interface contributing to the binder's specificity (see also Figure S6). No complex formation occurred between D7.43 and caspase 3_R86I (**g**). However, D7.43 is able to bind to caspase 7_I109R (**h**). This suggests that the detailed molecular interaction between caspase 7 and D7.43 are different from that of D7.18 and does not exclude the possibility that both DARPins share a similar epitope as shown in Figure S3.

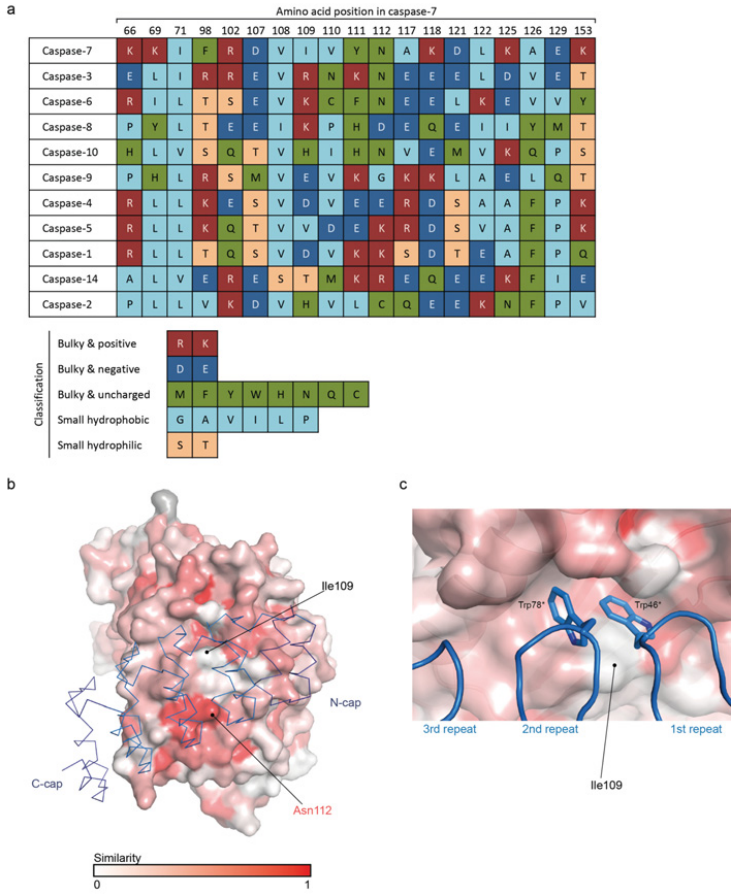

Figure S6 Sequence alignment of interacting residues and structural conservation

(**a**) Sequence alignment of caspase 7 residues involved in DARPin D7.18 binding compared with other human caspases. Interacting residues were determined by the EPPIC server (http://www.eppicweb.org [1]) and sequence alignment of human caspases was performed using ClustalW2 (http://www.ebi.ac.uk/Tools/msa/clustalw2/). Amino acids were classified and coloured accordingly into five groups. The following accession numbers were used for caspase sequences: P29466 (caspase 1), P42575 (caspase 2), P42574 (caspase 3), P49662 (caspase 4), P51878 (caspase 5), P55212 (caspase 6), P55210 (caspase 7), Q14790 (caspase 8), P55211 (caspase 9), Q92851 (caspase 10) and P31944 (caspase 14). (**b**) Caspase 7–D7.18 complex structure with colorization of amino acid conservation. White surface represents no conservation between caspases 3, 6 and 7, whereas dark red areas are fully conserved in these three enzymes. DARPin D7.18 is shown in ribbon representation (blue) with marked N- and C-cap. As shown in (**a**), Asn^{112} in the binding interface is fully conserved and thus coloured dark red. Colorization by amino acid conservation was made with ProtSkin (http://www.mcgnmr.mcgill.ca/ProtSkin/ [6]) and PyMOL (http://www.pymol.org). (**c**) Close-up view of the hydrophobic pocket shaped by caspase 7 residues harbouring two buried DARPin tryptophan residues (*) (see also Figure 2c of the main text). Although several residues involved in pocket formation are partially conserved, Ile^{109} is not conserved.

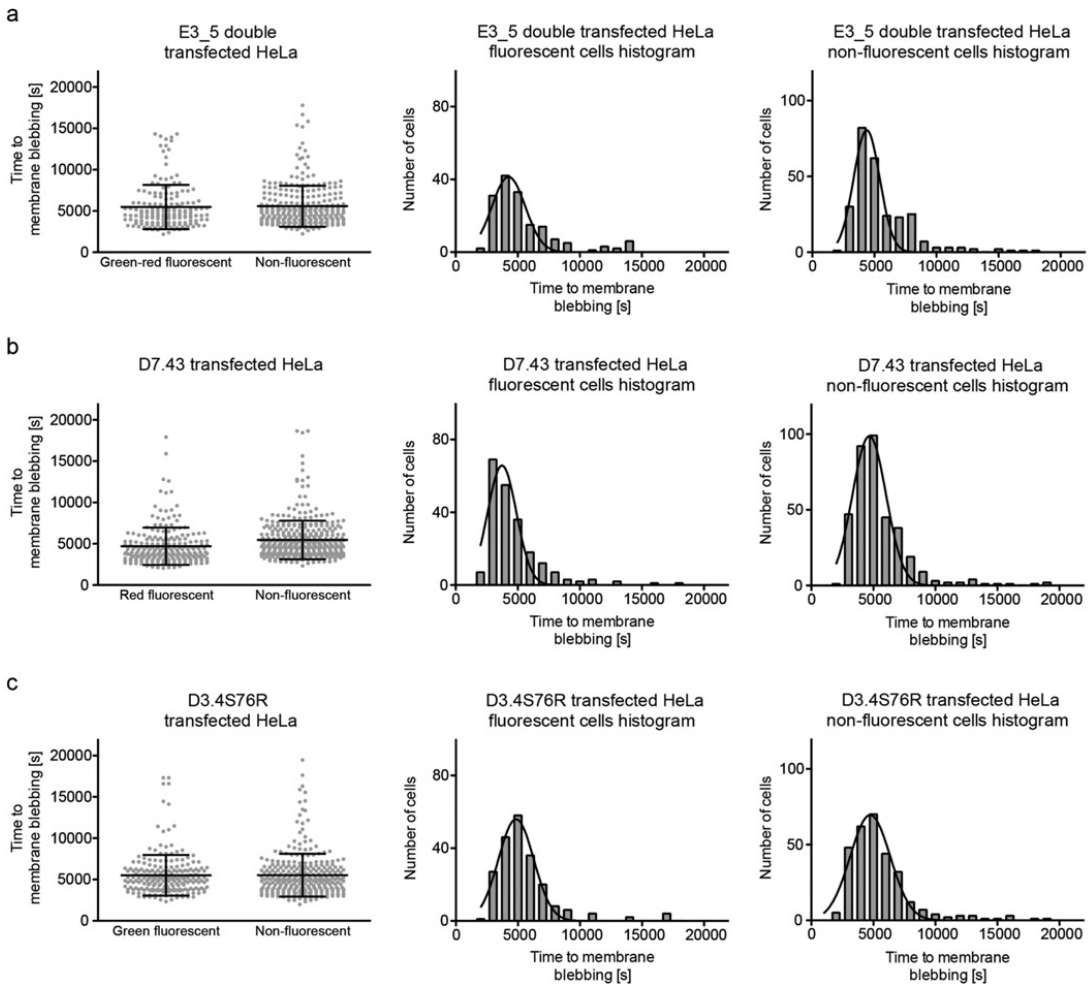

Figure S7 Time-lapse experiments following apoptosis of HeLa cells induced by TRAIL

Double-transfected HeLa cells with E3_5–eGFP and E3_5–mCherry (**a**) served as a double-transfection control, whereas single-transfected cells with D7.43–mCherry (**b**) or D3.4S76R–eGFP (**c**) should clarify the effect of each individual DARPin to the survival behaviour of double-transfected cells (see also Figure 5 of the main text and Movie S1). DARPin-expressing cells were counted when fluorescent (e.g. green/red fluorescent in **a**) and compared with non-fluorescent cells (statistics are given in Table S2). Counted cells in all experiment show a Gaussian distribution (bin width = 1000 s) and similar averages of time until rapid cell shrinkage and membrane blebbing can be observed.

Table S1 Data collection and refinement statistics

Values in parentheses are for the highest resolution shell.

Parameter	Statistic
Data collection	
Space group	$P2_1$
Cell dimensions	
a, *b*, *c* (Å)	59.84, 82.31, 95.08
α, β, γ (°)	90.0, 91.9, 90.0
Resolution (Å)	50–2.2
Wavelength (Å)	1.0
R_{sym} (%)	4.4 (50.5)
Completeness (%)	99.2 (99.4)
$I/\sigma(I)$	26.94 (5.06)
Refinement	
Resolution (Å)	2.26
R_{work}/R_{free}	17.3/20.6
Number of atoms	
Protein	6104
Water	161
B-factors	
Protein	59.9
Water	54.4
RMSD	
Bond length (Å)	0.008
Bond angle (°)	1.06
Ramachandran	
Preferred (%)	98.6
Allowed (%)	1.4
Outliers (%)	0

Table S2 Survival statistics of transfected HeLa cells after induction of apoptosis with TRAIL (50 ng/ml)

	Number of cells	Number of survivors	Survival (%)	Mean ± S.D. time to cell death (h:min:s)
E3_5 double transfection				
Green/red fluorescent	162	1	0.6	01:31:22 ± 00:44:48
Non-fluorescent	270	0	0.0	01:33:00 ± 00:41:25
Total	432	1	0.2	
D7.43 transfection				
Red fluorescent	216	0	0.0	01:18:25 ± 00:37:41
Non-fluorescent	369	2	0.5	01:31:06 ± 00:39:01
Total	585	2	0.3	
D3.4S76R transfection				
Green fluorescent	221	9	4.1	01:31:58 ± 00:41:12
Non-fluorescent	314	15	4.8	01:32:15 ± 00:43:05
Total	535	24	4.5	

REFERENCES

1 Duarte, J. M., Srebniak, A., Scharer, M. A. and Capitani, G. (2012) Protein interface classification by evolutionary analysis. BMC Bioinformatics **13**, 334 CrossRef PubMed

2 Geertsma, E. R. and Dutzler, R. (2011) A versatile and efficient high-throughput cloning tool for structural biology. Biochemistry **50**, 3272–3278 CrossRef PubMed

3 Roschitzki-Voser, H., Schroeder, T., Lenherr, E. D., Frölich, F., Schweizer, A., Donepudi, M., Ganesan, R., Mittl, P. R., Baici, A. and Grütter, M. G. (2012) Human caspases *in vitro*: expression, purification and kinetic characterization. Protein Expr. Purif. **84**, 236–246 CrossRef PubMed

4 Lazebnik, Y. A., Kaufmann, S. H., Desnoyers, S., Poirier, G. G. and Earnshaw, W. C. (1994) Cleavage of poly(ADP-ribose) polymerase by a proteinase with properties like ICE. Nature **371**, 346–347 CrossRef PubMed

5 Schroeder, T., Barandun, J., Flütsch, A., Briand, C., Mittl, P. R. and Grütter, M. G. (2013) Specific inhibition of caspase-3 by a competitive DARPin: molecular mimicry between native and designed inhibitors. Structure **21**, 277–289 CrossRef PubMed

6 Deprez, C., Lloubes, R., Gavioli, M., Marion, D., Guerlesquin, F. and Blanchard, L. (2005) Solution structure of the *E. coli* TolA C-terminal domain reveals conformational changes upon binding to the phage g3p N-terminal domain. J. Mol. Biol. **346**, 1047–1057 CrossRef PubMed

Received 7 November 2013/22 April 2014; accepted 30 April 2014
Published as BJ Immediate Publication 30 April 2014, doi:10.1042/BJ20131456

5 Publication: Second-Generation DARPin Library

THE PROTEIN SOCIETY

Design, construction, and characterization of a second-generation DARPin library with reduced hydrophobicity

Markus A. Seeger,* Reto Zbinden, Andreas Flütsch, Petrus G. M. Gutte, Sibylle Engeler, Heidi Roschitzki-Voser, and Markus G. Grütter

Department of Biochemistry, University of Zurich, 8057 Zürich, Switzerland

Received 30 April 2013; Revised 24 June 2013; Accepted 25 June 2013
DOI: 10.1002/pro.2312
Published online 00 Month 2013 proteinscience.org

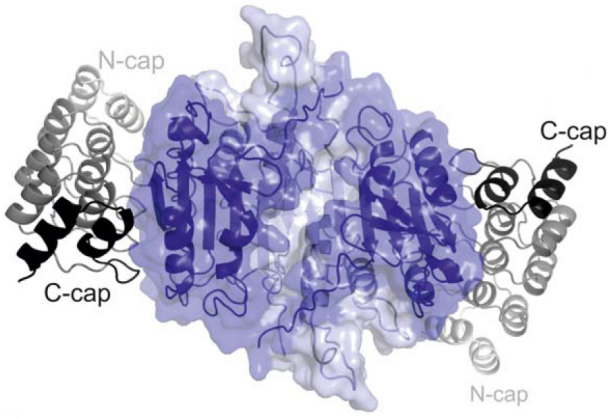

Figure 8A: Caspase-7 in complex with DARPin C7_16 (PDB: 4JB8)

THE PROTEIN SOCIETY

Design, construction, and characterization of a second-generation DARPin library with reduced hydrophobicity

Markus A. Seeger,* Reto Zbinden, Andreas Flütsch, Petrus G. M. Gutte, Sibylle Engeler, Heidi Roschitzki-Voser, and Markus G. Grütter

Department of Biochemistry, University of Zurich, 8057 Zürich, Switzerland

Received 30 April 2013; Revised 24 June 2013; Accepted 25 June 2013
DOI: 10.1002/pro.2312
Published online 19 July 2013 proteinscience.org

ABSTRACT: Designed ankyrin repeat proteins (DARPins) are well-established binding molecules based on a highly stable nonantibody scaffold. Building on 13 crystal structures of DARPin-target complexes and stability measurements of DARPin mutants, we have generated a new DARPin library containing an extended randomized surface. To counteract the enrichment of unspecific hydrophobic binders during selections against difficult targets containing hydrophobic surfaces such as membrane proteins, the frequency of apolar residues at diversified positions was drastically reduced and substituted by an increased number of tyrosines. Ribosome display selections against two human caspases and membrane transporter AcrB yielded highly enriched pools of unique and strong DARPin binders which were mainly monomeric. We noted a prominent enrichment of tryptophan residues during binder selections. A crystal structure of a representative of this library in complex with caspase-7 visualizes the key roles of both tryptophans and tyrosines in providing target contacts. These aromatic and polar side chains thus substitute the apolar residues valine, leucine, isoleucine, methionine, and phenylalanine of the original DARPins. Our work describes biophysical and structural analyses required to extend existing binder scaffolds and simplifies an existing protocol for the assembly of highly diverse synthetic binder libraries.

Keywords: DARPins; synthetic binder libraries; library assembly; structure-based protein engineering; protein-protein interactions; in vitro selection; ribosome display

Introduction

Protein-protein interactions play an essential role in every living organism. B cells, for example, are a major component of the adaptive immune system and generate specific antibodies to combat invading pathogens and viruses. Starting in the 1970s, scientists have acquired technologies enabling the selection of monoclonal antibodies against desired protein targets initially using the hybridoma technology which relies on the immunization of mice.[1] Over the years, selection methods have been expanded to *in vitro* approaches that became available with the development of phage display[2] and ribosome display.[3] Thereby, the binder selection process was transferred from animals into the test tube where experimental conditions can be controlled.

In vitro display methods couple the folded binding protein (phenotype) physically to the genetic information (genotype). This is achieved by either fusing binders to phage surface proteins in phage display or by forming stable ternary complexes of mRNA, ribosome, and the nascent polypeptide chain

Additional Supporting Information may be found in the online version of this article.

Reto Zbinden, Andreas Flütsch, and Petrus G. M. Gutte contributed equally to this work

Grant sponsor: Swiss NCCR Structural Biology program; Grant sponsor: Framework 7 Program; Grant number: FP7-Health-2009–241919-LIVIMODE. Grant sponsors: Ambizione grant of the Swiss National Science Foundation (to M.A.S.) and a Forschungskredit of the University of Zürich (to M.A.S.).

*Correspondence to: Markus A. Seeger, Department of Biochemistry, University of Zurich, Winterthurerstrasse 190, 8057 Zürich, Switzerland. E-mail: m.seeger@bioc.uzh.ch

in ribosome display. Large combinatorial gene libraries typically encoding for 10^9 to 10^{12} possible binder molecules are the centerpiece of every *in vitro* selection technique. With the exception of binders based on small peptides (e.g. bicyclic peptides[4]), binding protein libraries are based on binding scaffolds. Traditionally, antibody fragments such as Fabs[5] and scFvs[6] served as scaffold which were either cloned from natural sources to form naïve libraries[7] or constructed *in vitro* by genetic engineering into synthetic libraries.[8] To overcome some of the undesirable biophysical properties of antibodies such as disulfide bonds, protein aggregation, and low expression yields, novel scaffolds have been exploited to introduce randomized surfaces (reviewed in Ref. 9–11). Among the nonantibody scaffolds, designed ankyrin repeat proteins (DARPins) belong to the best characterized molecules.[12] Naturally occurring ankyrin repeat proteins consist of tandem arrays of ankyrin repeat modules and mediate protein-protein interactions mainly in eukaryotic cells.[13] Each repeat module consists of 33 amino acids and folds into a β-turn followed by two anti-parallel α-helices and a loop that connects to the next repeat. Ankyrin repeat modules assemble into elongated and slightly curved structures thereby shaping a concave surface that forms specific contacts with binding partners.[14] The original DARPin library was constructed following a consensus design approach, in which naturally variable amino acid positions were subjected to randomization and conserved residues were defined as invariant framework residues.[15] Typically, DARPins consist of two to three internal repeats that are flanked by an N- and a C-terminal capping repeat (N- and C-cap) which are then called N2C and N3C DARPins, respectively. DARPins are thermodynamically very stable due to tight and regular packing of the repeat segments and conserved hydrogen bonding networks.[16,17] DARPins have been raised against a plethora of target proteins using ribosome and phage display.[3,18–25] Of note, several successful *in vitro* selections of DARPins against integral membrane proteins have been reported, underscoring the suitability of the scaffold to target "difficult to handle" proteins.[26–30]

Target specific binders can be used in a multitude of applications: they carry drugs to the desired target in the body (e.g. in tumor targeting[19,23,31]), serve as tools in enzymology to inhibit kinases and proteases in the reducing milieu of the cell interior,[22,32,33] are used as affinity probes to discover novel conformational states of membrane proteins,[29] and have been shown to modulate the function of membrane transport proteins *in vivo*.[28,30]

In the context of membrane protein crystallography, the use of binders as crystallization aids has raised particular interest.[28,34,35] Although a high-resolution structure of the membrane protein AcrB in complex with DARPins has been reported,[28,36] the selection of such binders against membrane proteins often turned out to be difficult.[26,29] A recurrent problem is the enrichment of hydrophobic binders that are prone to form higher oligomeric species and unspecifically bind to transmembrane proteins.[29,30]

Here we describe the design, construction, characterization, and successful application of a second-generation DARPin library that was built based on the information provided by the many target protein-DARPin complex structures obtained in the past decade. We analyzed the DARPin binding interfaces of all available structures to modify and extend the randomized surface. Regarding the framework, we reduced the surface entropy of the DARPin backside to be favorable for forming crystal contacts. To minimize problems in enriching unspecifically aggregating binders due to hydrophobic surface patches, apolar residues were omitted in the randomized positions. To compensate for the reduced hydrophobicity, the library is enriched in tyrosines that have been demonstrated to be particularly suited to mediate molecular contacts in protein-protein interactions.[37] The library was validated in test selections against caspase-3, caspase-7, and AcrB and a crystal structure of a new DARPin in complex with caspase-7 was solved at 1.7 Å resolution.

Results

Analysis of the randomized DARPin surface based on crystal structures

Since the construction of the original DARPin library by Binz *et al.*[15] [Fig. 1(A)], 18 crystal structures of DARPins in complex with their target proteins have been reported.[12,21,22,28,36,38–46] We analyzed all DARPin-target protein interfaces of crystals solved at resolutions of 3 Å and better using the EPPIC server (www.eppic-web.org)[47] (Supporting Information File "DARPin_interfaces.xls"). Twenty-two interfaces found in 13 crystal structures were taken into account for analysis (some interfaces were present twice in the asymmetric unit). The buried surface area (BSA) upon complex formation of every amino acid residue position was calculated as percentage of total BSA [Fig. 2(A), Supporting Information File "DARPin_interfaces.xls")]. As intended by design, the majority (56 % of total BSA) of protein-protein interactions were mediated by randomized residues located at internal repeats. Interactions involving residues of the third repeat appear underrepresented because our dataset contained numerous N2C DARPins lacking a third repeat. The randomized residue at position 33 according to the ankyrin repeat sequence defined by Binz *et al.*[15] [Fig. 1(B)] is only marginally

DOI: 10.1002/pro.2312, ©2013 The Protein Society

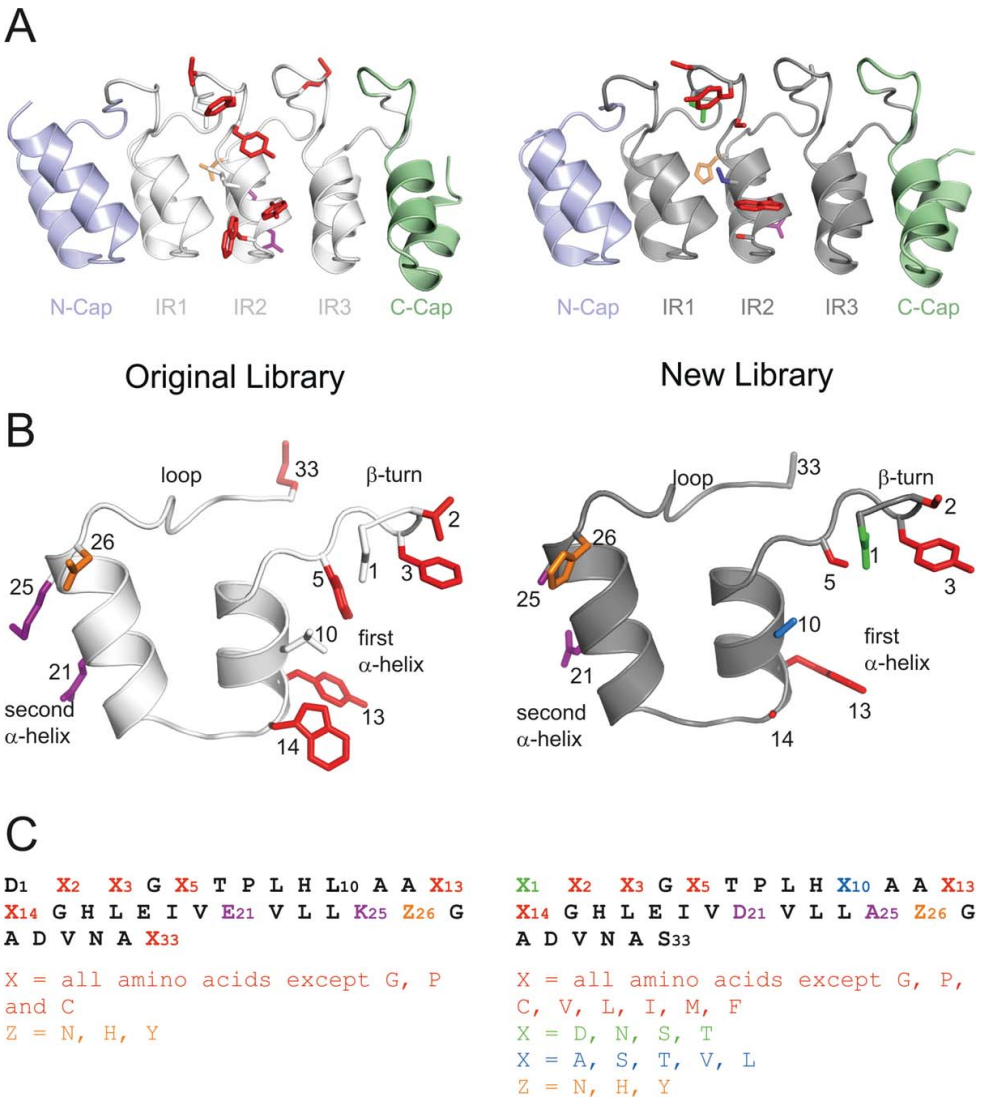

Figure 1. Randomization of the internal DARPin repeat. The second internal repeat (IR2) of the original (off7, left panel, PDB 1SVX) and new (C7_16, right panel, PDB 4JB8) library is shown in the context of the N3C DARPin (A) and in isolation (B). Diversified positions are highlighted as colored side chains shown as sticks. The repeat sequences and the permitted residues of the randomized positions are given in (C).

involved in target contacts, because it points away from the concave randomized surface of the DARPin scaffold. In contrast, the aspartate of the DxxG motif (position 1 of the ankyrin repeat) and a leucine in the first α-helix of the ankyrin repeat (position 10) were found to be involved in target contacts, although these residues were not diversified in the original DARPin library [Fig. 2(A)]. Interestingly, invariant residues of the N- and C-cap were frequently involved in molecular contacts with target proteins providing 44% of total BSA. Our analysis further allowed us to plot the burial of each of the 20 amino acids as percentage of total BSA and to specifically highlight contacts mediated by diversified residues [Fig. 2(B)]. Major contacting residues (threshold 4% of total BSA) are D, K, R, N, L, I, M, F, Y, and W. Limiting this analysis to the diversified residues, the major players are L, I, F, Y, and W. Cysteines which are absent in DARPins and prolines which are completely buried in folded DARPins are not involved in target contacts. In contrast to a recent analysis of DARPin

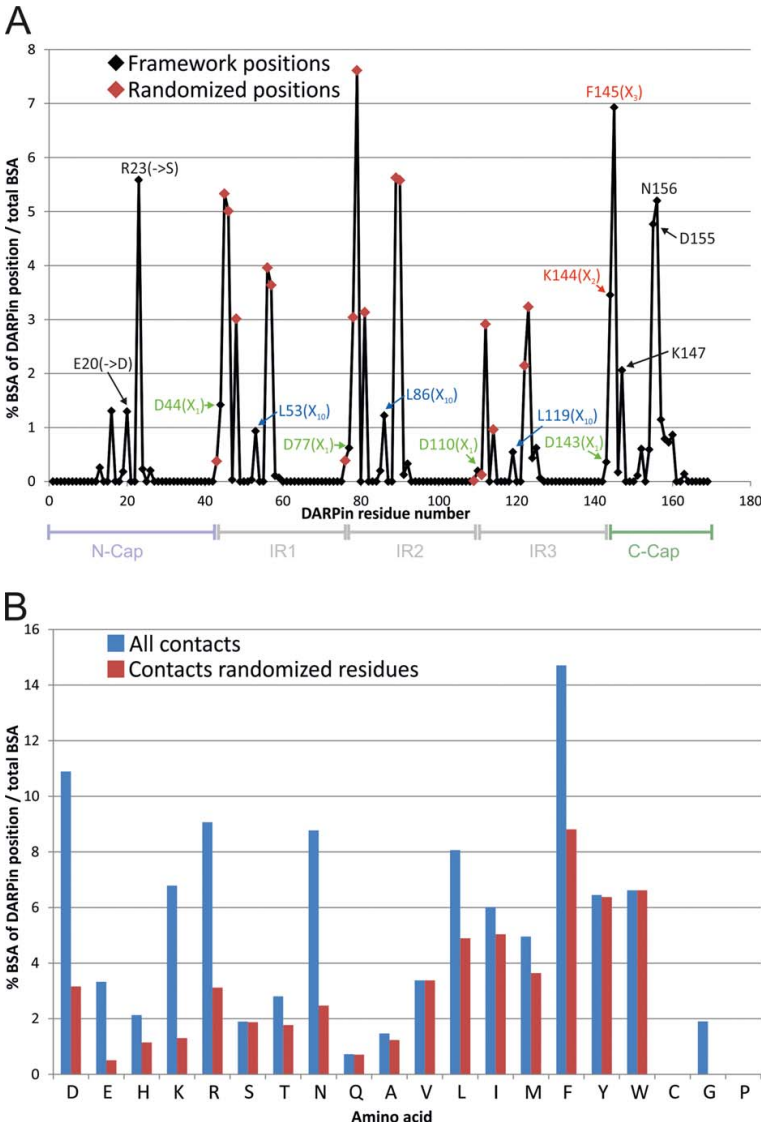

Figure 2. Analysis of target contacts by original DARPins based on 13 crystal structures. (A) The relative contribution of each DARPin sequence position to the total buried surface area (BSA) of all analyzed DARPins is plotted (i.e. the sum of all positions equals 100%). Randomized positions of the original library are indicated by red diamonds. Residues which were subjected to changes or randomization in the new library are highlighted using the same color scheme as in Figure 1. (B) Amino acid usage of the analyzed DARPins is visualized as % BSA of total BSA. Blue bars depict all contacting residues (total BSA of 100%) and red bars depict diversified residues only (total BSA of 56%).

interfaces in which the number of tyrosines involved in target contacts were counted under the condition that burial is greater than 1 Å^2,[48] our quantitative analysis did not assign a special role to Y relative to L, I, F, and W. Furthermore, we found nonrandomized D, K, R, and N residues of the capping repeats to be frequently involved in target contacts.

Randomization scheme for the internal ankyrin repeat module of the new DARPin library

Taking these findings into account, the randomization pattern of the internal repeat defined by Binz *et al*. was modified. As in the original DARPin library, the ankyrin repeat positions 2, 3, 5, 13, and 14 were subjected to randomization [Fig. 1(B)]. Randomized position 33 of the original library was rarely

DOI: 10.1002/pro.2312, ©2013 The Protein Society

involved in protein interactions and thus defined as invariant serine. In addition, the aspartate at position 1 and the leucine at position 10 of the ankyrin repeat module were randomized. Because these two residues are important for the structural integrity of the DARPin framework,[49] the randomization was restricted to a more narrow range of permitted amino acid residues (see sections below). By using trinucleotides phosphoramidites for the synthesis of oligonucleotides, the amino acid composition for each residue position was adjusted.[50,51] In the original DARPin library, the randomized positions were permitted to contain any amino acid except P, G, and C.[15] Small and polar/charged amino acids (A, D, E, H, K, N, Q, R, S, T) were overrepresented with 7% each compared with bulkier and hydrophobic residues (F, I, L, M, V, W, Y) with 4.3% each. During DARPin selections against membrane proteins we repeatedly observed the enrichment of hydrophobic binders containing multiple apolar residues in the randomized positions (not shown). Such DARPins were found to promiscuously bind to diverse transmembrane proteins and were prone to form soluble aggregates during DARPin expression and purification.[29,30] For the new DARPin library, we therefore limited the number of permitted residues in the randomized positions and excluded, besides G, P, and C also the hydrophobic amino acids I, L, V, M, and F. With these measures, we aimed at generating more hydrophilic DARPins that are expected to be less prone to unspecific hydrophobic interactions. The composition of permitted amino acids in the five randomized positions 2, 3, 5, 13, and 14 was biased towards small and polar amino acids and tyrosine and contain the following amino acid composition: A, S, T, N, and Y; 12% each and D, E, R, K, Q, W, and H; 5.7% each.

Randomization of residue D1 in the β-turn

In the analyzed DARPin structures, the β-turn aspartate contributes 2.6% of total BSA [Fig. 2(A)] and in naturally occurring ankyrin repeat proteins, this position is not highly conserved.[15] However, the carboxyl moiety of this residue stabilizes the β-turn of the DARPin scaffold by interacting via two hydrogen bonds [Fig. 3(C)].[49] To warrant stability of the β-turn of the new DARPin library, only residues D, N, T, and S were permitted at position 1. N, T, and S are expected to establish hydrogen bonds similar to the ones formed by aspartate. To verify our assumption experimentally, the β-turn aspartate in the middle repeat of the previously characterized unselected DARPin E3_5 was mutated to serine (D77S). Although serine is shortened by one methylene group compared with the original aspartate, E3_5_D77S was found to be more stable in guanidinium hydrochloride (GdnHCl) unfolding experiments as compared with wild type E3_5 and the midpoint of unfolding (D_m) was increased by 0.5*M* GdnHCl [Fig. 3(B)]. E3_5_D77S was crystallized and its structure was solved at a resolution of 1.7 Å (Table I). A superimposition of E3_5_D77S with wild type E3_5 revealed only marginal structural changes at the β-turn of the middle repeat [Fig. 3(C)]. As expected, the hydroxyl group of S77 stabilizes the β-turn by virtue of two hydrogen bonds. Tyrosine at position 5 of the first internal repeat (Y48) fills the space that became vacated by the D to S mutation. As a consequence, the entire β-turn of the first repeat is shifted towards the middle repeat by 0.5 to 1 Å (measured at the C_α positions). The more intimate contacts between the first and the second internal repeat might explain the increased stability of the E3_5_D77S mutant compared with wild type E3_5.

Randomization of residue L10

The leucine residue at position 10 was kept invariant in the original DARPin library mainly due to stability considerations[15] although it is not conserved in natural ankyrin repeat proteins. In DARPin-target protein co-crystal structures, L10 is frequently found to mediate molecular contact and contributes 2.7% of total BSA [Fig. 2(A)]. For this second-generation DARPin library, we therefore permitted the five residues A, S, T, V, and L at this position. To test for potential biochemical and structural consequences of randomizing this residue, L10 of the middle repeat of DARPin E3_5 was replaced by alanine (L86A) and analyzed by GdnHCl unfolding experiments. D_m of the E3_5_L86A mutant was decreased by 0.5*M* GdnHCl [Fig. 3(B)]. The crystal structure of the E3_5_L86A mutant was solved at a resolution of 1.6 Å (Table I) containing two E3_5_L86A molecules per asymmetric unit. In one DARPin of the asymmetric unit (chain B), the highly conserved histidine in position 9 of the first internal repeat (H52) adopts two rotamer conformations. One rotamer establishes a hydrogen bond with the consecutive middle repeat as in wild-type E3_5, while the second rotamer fills the space that was occupied by the bulky L86 in wild-type E3_5 [Fig. 3(D)]. As a consequence, the hydrogen bonding contact between the first and the second internal repeat segments appears to be weakened which might explain the decreased stability of the E3_5_L86A mutant. However, in the other E3_5_L86A molecule (chain A) of the asymmetric unit, H52 shows a position identical to that of wild type E3_5 (not shown).

Modification and randomization of the capping repeats

Two non-randomized and bulky side chains of the N-cap (E20 and R23) were frequently found to interact

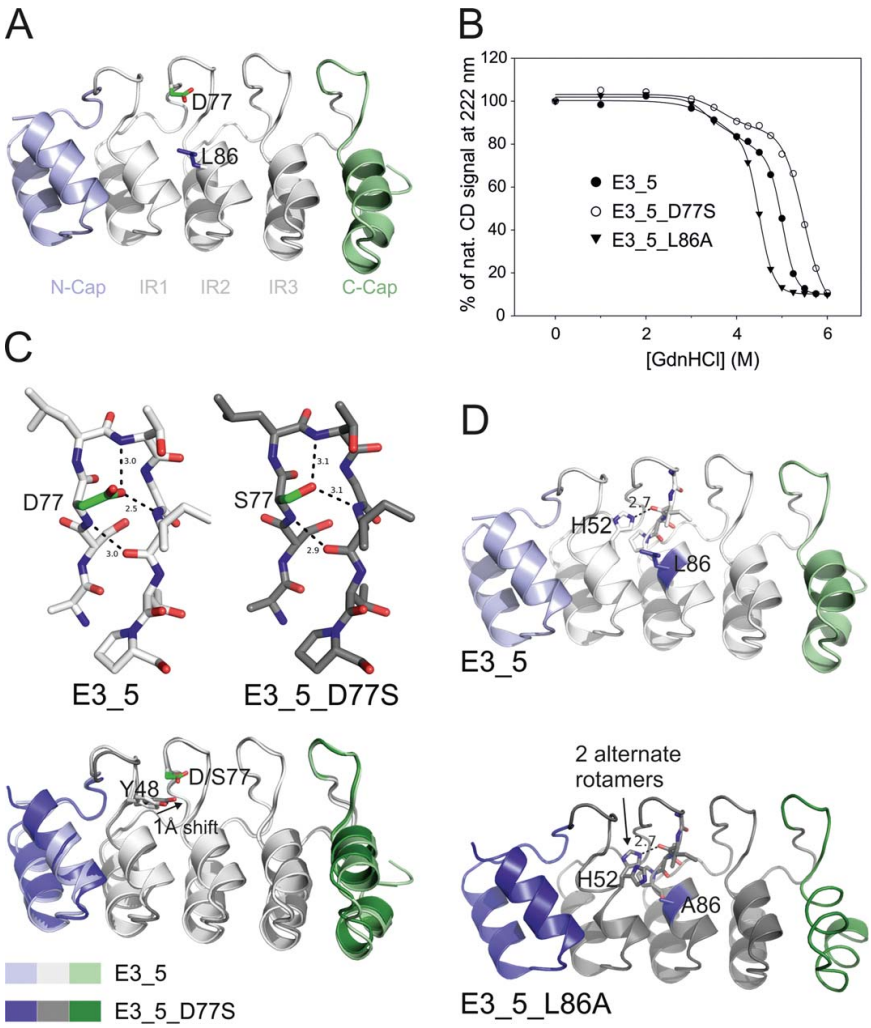

Figure 3. Biophysical and structural characterization of E3_5 mutants. (A) E3_5 was mutated at the second internal repeat at residues D77S or L86A representing randomized positions 1 and 10 in the new DARPin library. (B) The stability of the mutants was analyzed by GdnHCl equilibrium unfolding monitored by CD spectroscopy. Data were fitted to a biphasic sigmoidal equation and the midpoints of the second transition ($D_{m,2}$) were as follows: wild type, 5.01*M*; D77S mutant, 5.48*M*; L86A mutant, 4.49*M*. (C and D) Structures of the D77S and the L86A mutants were solved by X-ray crystallography. (C) S77 in the D77S mutant establishes two hydrogen bonds similar to the ones of the wild type E3_5 and thereby stabilizes the β-turn (top). A superimposition of both structures reveals a shift of Y48 toward the middle repeat in the D77S mutant (bottom). (D) In the structure of the L86A mutant, H52 of the first repeat adopts two alternate rotamer positions, one of which occupying the space vacated by the L to A mutation (lower panel). In wild-type E3_5, H52 stabilizes the DARPin fold by establishing a hydrogen bond with the internal repeat (upper panel).

with the target protein and contribute to 1.3% and 5.6% of total BSA, respectively [Fig. 2(A)]. We chose not to randomize the N-cap, but to replace these two residues with smaller ones (E20D and R23S), in order to reduce sterical interference with DARPin binding [Fig. 4(A,C)]. Although the C-cap was not randomized in the original library, it matches the internal repeats with regard to surface burial upon complex formation [Fig. 2(A)]. Furthermore, the C-cap of the original library was found to be the least stable repeat of DARPins. C-cap packing to the internal repeat was stabilized employing combined computational and experimental methods.[52] For this second generation DARPin library, we chose the sequence for an improved C-cap corresponding to the stabilized "mutant 5" described previously.[52,53] In contrast to the original DARPin library, the β-turn of the C-cap was subjected to randomization

DOI: 10.1002/pro.2312, ©2013 The Protein Society

Table I. *Data Collection and Refinement Statistics*

	E3_5_D77S (PDB: 4J8Y)	E3_5_L86A (PDB: 4J7W)	C7_16-caspase-7 (PDB: 4JB8)
Data collection			
Space group	$P2_12_12_1$ (19)	$P2_12_12_1$ (19)	C2 (5)
Cell dimensions			
a, *b*, *c* (Å)	34.88; 53.63; 78.38	44.37; 78.59; 82.23	143.88; 52.51; 60.09
α, β, γ (°)	90.00; 90.00; 90.00	90.00; 90.00; 90.00	90.00; 96.92; 90.00
Resolution (Å)	50–1.7 (1.74–1.7)	50–1.6 (1.64–1.6)	50–1.7 (1.74–1.7)
R_{merge} (%)	6.0 (39.5)	9.4 (32.6)	4.0 (56.8)
I/σ_I	22.21 (5.37)	19.20 (11.87)	23.21 (3.11)
Completeness (%)	99.4 (99.4)	98.9 (99.4)	99.9 (99.9)
Redundancy	5.6 (5.1)	8.2 (8.8)	6.8 (6.9)
Refinement			
Resolution (Å)	50-1.7	50-1.6	50-1.7
No. reflections (work/test)	15869/836	36343/1913	47187/1967
R_{work}/R_{free}	17.16/20.76	16.79/19.19	17.22/19.37
No. atoms			
Protein	1192	2393	3107
Water	167	414	257
B-factors			
Total	21.94	11.56	41.06
R.M.S deviations			
Bond lengths (Å)	0.004	0.006	0.006
Bond angles (°)	0.874	1.033	1.008

using amino acid compositions identical to the ones of the internal repeats [Fig. 4(A,C)].

Surface entropy reduction in the new DARPin library

Derewenda and colleagues have postulated that bulky charged side chains at the surface of proteins, in particular lysines and glutamates form an entropic barrier that counteracts the formation of crystal contacts.[54] The original DARPin library has a glutamate at position 21 (E21) and a lysine at position 25 (K25) at the DARPin backside [Figs. 1(B,C) and 4(B)]. These residues were chosen to keep DARPins soluble. In addition, the lysine exhibits a high α-helical propensity,[55] which appears important for the integrity of the DARPin scaffold. In the new library, we chose to replace E21 with a shorter aspartate (thereby maintaining the negative charge at this position) and K25 with an alanine, whose α-helical propensity is even higher than the one of lysine. To investigate whether the loss of these changes have any adverse influence on the oligomeric state of a N3C DARPin, we introduced these mutations in DARPin_55, a specific binder of the ABC transporter MsbA.[29] Both wild-type and mutant DARPin_55 were found to be monomers as judged from size exclusion chromatography [Supporting Information Fig. S1(A)] and thus the loss of three positive charges due to the K25A mutations did not lead to the formation of DARPin oligomers in this test case. Mutant DARPin_55 was still comigrating with MsbA on SEC (not shown). Equilibrium unfolding using GdnHCl revealed a stabilization of DARPin_55 upon introduction of these mutations [Supporting Information Fig. S1(A)].

Assembly and initial quality check of the new DARPin library

An N3C DARPin library containing three internal repeats flanked by a N- and a C-terminal cap was assembled as described previously for the original DARPin library.[15] The caps and internal repeats were generated by PCR followed by ligating the fragments repeat by repeat using type IIS restriction enzymes (a detailed protocol is given in Materials and Methods). The theoretical library diversity of the N3C library is calculated as follows. Each of the three internal repeats contains five randomized positions with 12 permitted residues, position 1 with four allowed residues, position 10 with five permitted residues, and position 26 with three permitted residues. Each internal repeat therefore exhibits a theoretical diversity of $12^5 \times 4 \times 5 \times 3 = 1.5 \times 10^7$ variants. The diversity of the C-cap is 576 owing to two randomized positions with 12 permitted residues (12^2 variants) and position 1 of the β-turn (four variants). The N-cap is not randomized. The theoretical diversity of the new N3C DARPin library is therefore 1.9×10^{24} and lies in a similar range as the original DARPin library, whose theoretical diversity amounted to 3.8×10^{23}.[15] The practical diversity of the library was estimated to be 10^{11} variants (see Materials and Methods). To evaluate the quality of the new library at the DNA level, the assembled library was cloned into an expression vector (pQE30) and 26 randomly picked library members were sequenced and named DARPin D1-D26. Twenty out

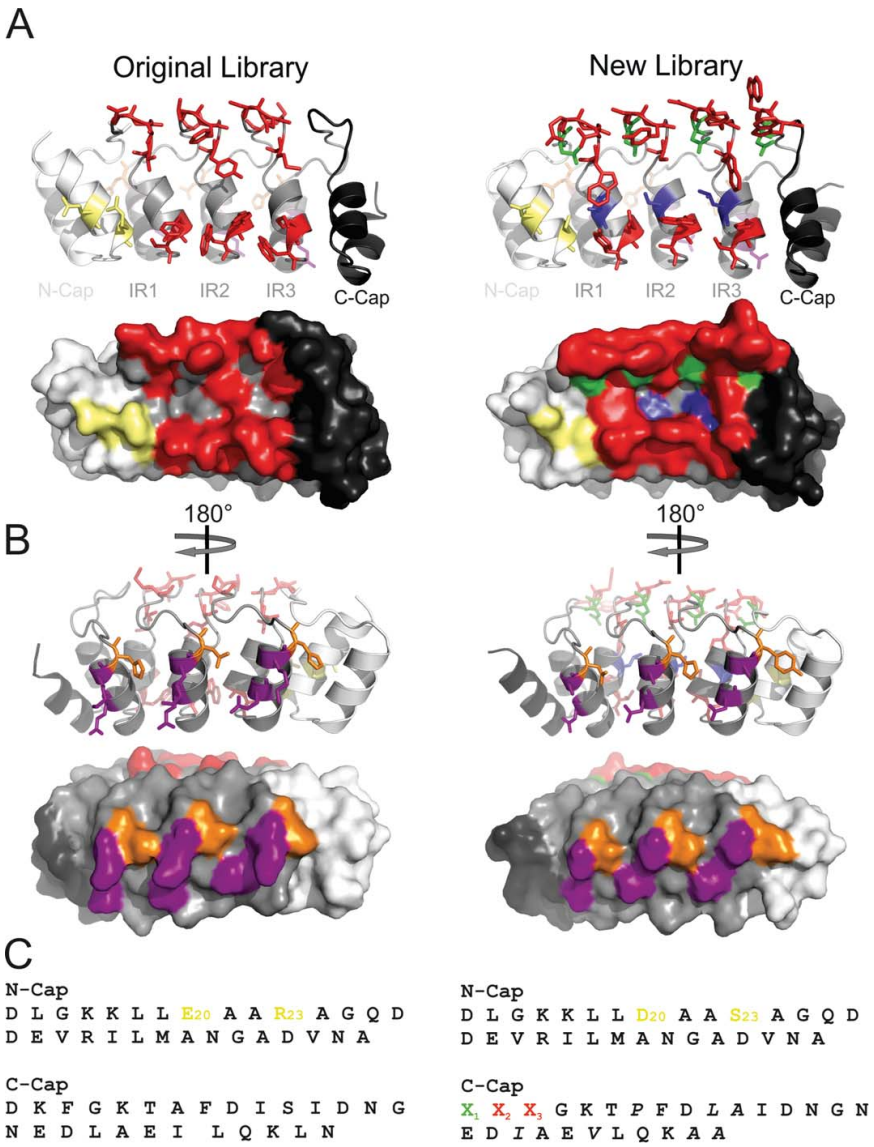

Figure 4. Modifications and randomizations at the capping repeats and surface entropy reduction of the DARPin backside. DARPins of the original (off7, left, PDB 1SVX) and new (C7_16, right, PDB 4JB8) library are shown in cartoon representation with diversified/modified residues highlighted as colored sticks or in surface representation. (A and C) Bulky E20 and R23 residues of the N-cap are frequently involved in target contacts [Fig. 2(A)] and were exchanged for the smaller D20 and S23 in the new library. The positions 1–3 of the C-cap (β-turn) were subjected to randomization in the new library following the same scheme as depicted in Figure 1(C). (B) DARPins viewed from their backside. By mutating E21D and K25A in each internal repeat [Fig. 1(C)], the surface entropy of the DARPin backside was reduced in the new library, which is expected to facilitate crystallization. (C) Sequences of the N- and C-caps are shown and modifications of the original library are highlighted.

of the 26 members were found to be in frame (77%), which indicates that the primers used to perform the assembly PCR were of good quality (Supporting Information Fig. S2). The codon frequencies of the randomized positions were found to be in decent agreement with the intended mixture (Fig. 5). Eighteen of the 20 in-frame DARPins were tested for expression in *Escherichia coli* and 16 DARPins were purified at high yields. Fifteen out of these 16 DARPins were separated by SEC (Supporting

DOI: 10.1002/pro.2312, ©2013 The Protein Society

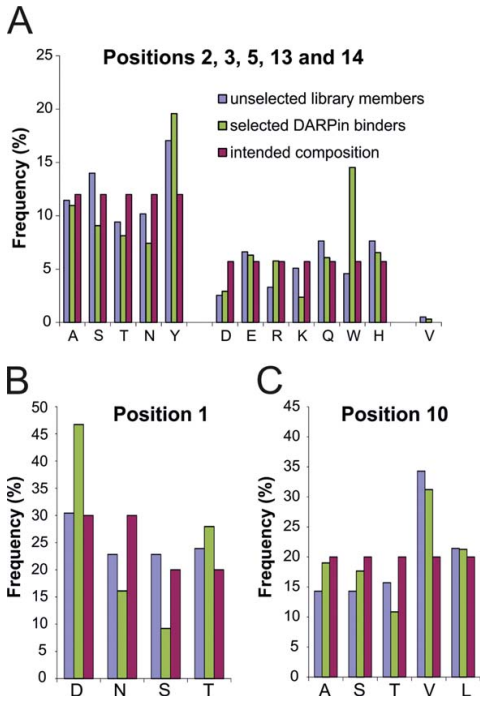

Figure 5. Amino acid composition in diversified positions of unselected library members (based on 20 DARPins, Supporting Information Fig. S2) and selected DARPin binders (based on 50 DARPins, Supporting Information Figs. S5–S7). The frequencies (%) are given for ankyrin repeat positions 2, 3, 5, 13, and 14 (A), position 1 (B) and position 10 (C) and are compared with the intended frequencies.

Information Fig. S3) and further analyzed by equilibrium unfolding using GdnHCl (see below).

DARPin selections against two human caspases and membrane transporter AcrB

As a proof of principle we decided to select binders of the new library against human caspase-3 and caspase-7 and multidrug transporter AcrB from *E. coli*, which served as protein targets in previous DARPin selections in our laboratory using the original library (Refs. 28 and 40 and unpublished results). The first three selection rounds were carried out using the surface panning method, followed by a fourth round of solution panning. In order to increase the specificity during selection, a pre-panning step with biotinylated maltose binding protein (MBP) was performed in every round. Starting from round two, a cross-panning analysis, in which pre-panning on target protein was followed by panning on MBP was introduced. In this analysis, target-specific binders are removed in the pre-panning step and remaining unspecific binders are captured by MBP in the panning step. In case of binder enrichment against the desired target, comparatively low amounts of mRNA are expected to be recovered in such cross-panning experiments. Already in the second selection round, mRNA recovery was higher in the normal panning procedure (pre-panning on MBP followed by panning on target) compared with the cross-panning analysis, indicating that the enriched DARPin pools were target specific [Fig. 6(A)].

ELISA - analysis and sequencing of caspase- and AcrB- specificDARPins

From the 3rd and 4th selection round against caspase-3, caspase-7, and AcrB, DARPins were screened for binding by crude extract ELISA[26,30] (Supporting Information Fig. S4). For caspase-3, 53% of all tested DARPins of selection round 3 and 45% of round 4 were found to be specific binders, whereas the hit rate was lower for caspase-7 and AcrB (13% and 16% of round 3 and 17% and 30% of round 4, respectively). Binders exhibiting the strongest signals in the crude extract ELISA were subjected to DNA sequencing (top 20 hits of the third selection round and top 10 hits of the fourth round). The binders were named C3_1–30, C7_1–30, and AcrB_1–30, respectively. Seventy-five out of the 90 chosen clones exhibited unambiguous sequencing results and unique sequences (Supporting Information Figs. S5–S7). Forty-nine out the 75 DARPins contained at least one unintended framework mutation. In three AcrB DARPins a frameshift mutation occurred, resulting in a change of the NGADVNAS loop motif, connecting helix 2 with the β-turn, to TVLTLTLL, and thereby rendering these DARPins considerably more hydrophobic. All caspase-3 DARPins harbor a conserved **TXYGE** motif in the β-turn region of the second internal repeat, suggesting that these binders recognize one single epitope (Supporting Information Fig. S5). In contrast, the caspase-7 and AcrB binders appeared more diverse and therefore are likely to recognize different epitopes (Supporting Information Figs. S6 and S7). By comparing the sequences of selected and unselected DARPins, the influence of binder selection on the amino acid composition of the randomized positions can be followed (Fig. 5). In positions 2, 3, 5, 13, and 14, residue frequency changes greater than 40% were observed for tryptophan (+217%), arginine (+74%) and lysine (−53%) [Fig. 5(A)]. In position 1, aspartate (+53%) was enriched and serine (−60%) was depleted during the selection process [Fig. 5(B)]. No major changes were observed at position 10 [Fig. 5(C)].

Biochemical characterization of caspase- and AcrB- specific DARPins

Twenty DARPins each specific for caspase-3, caspase-7, and AcrB were purified and their oligomeric

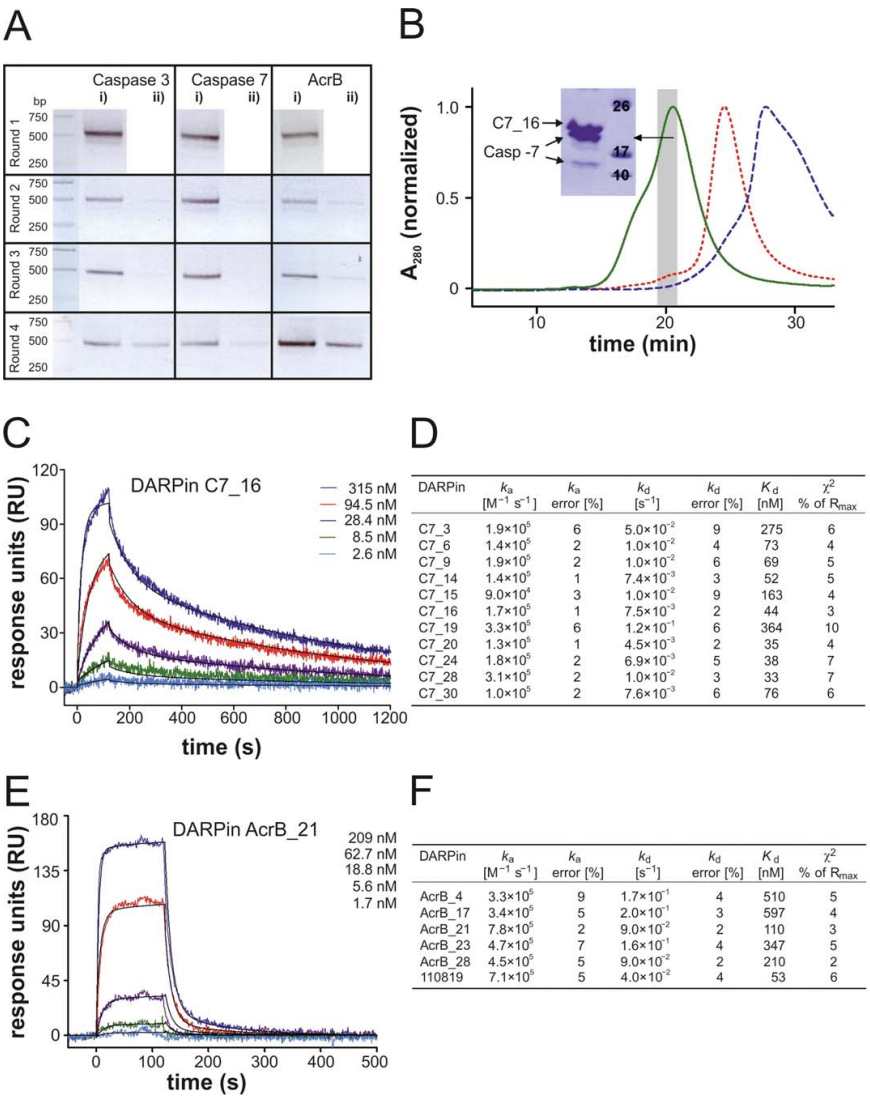

DARPin	k_a [M^{-1} s^{-1}]	k_a error [%]	k_d [s^{-1}]	k_d error [%]	K_d [nM]	χ^2 % of R_{max}
C7_3	1.9×10^5	6	5.0×10^{-2}	9	275	6
C7_6	1.4×10^5	2	1.0×10^{-2}	4	73	4
C7_9	1.9×10^5	2	1.0×10^{-2}	6	69	5
C7_14	1.4×10^5	1	7.4×10^{-3}	3	52	5
C7_15	9.0×10^4	3	1.0×10^{-2}	9	163	4
C7_16	1.7×10^5	1	7.5×10^{-3}	2	44	3
C7_19	3.3×10^5	6	1.2×10^{-1}	6	364	10
C7_20	1.3×10^5	1	4.5×10^{-3}	2	35	4
C7_24	1.8×10^5	2	6.9×10^{-3}	5	38	7
C7_28	3.1×10^5	2	1.0×10^{-2}	3	33	7
C7_30	1.0×10^5	2	7.6×10^{-3}	6	76	6

DARPin	k_a [M^{-1} s^{-1}]	k_a error [%]	k_d [s^{-1}]	k_d error [%]	K_d [nM]	χ^2 % of R_{max}
AcrB_4	3.3×10^5	9	1.7×10^{-1}	4	510	5
AcrB_17	3.4×10^5	5	2.0×10^{-1}	3	597	4
AcrB_21	7.8×10^5	2	9.0×10^{-2}	2	110	3
AcrB_23	4.7×10^5	7	1.6×10^{-1}	4	347	5
AcrB_28	4.5×10^5	5	9.0×10^{-2}	2	210	2
110819	7.1×10^5	5	4.0×10^{-2}	4	53	6

Figure 6. Validation of the new library with test selections against caspase-3, caspase-7, and AcrB (A) RT-PCR of ribosome display selection rounds 1 to 4 with applied cross-panning in rounds 2 to 4. Retrieved mRNA of potential binders were reverse transcribed and amplified by PCR (45, 40, 30, and 25 cycles for rounds 1, 2, 3, and 4, respectively) resulting in a 500 bp PCR product. "i)" indicates pre-panning against MBP followed by panning against target protein and "ii)" vice versa. (B) Analysis of ELISA-positive DARPin C7_16 (Supporting Information Fig. S4) by analytical SEC. Complex formation with caspase-7 leads to a distinct peak shift (green, solid line) compared with caspase-7 alone (red, short dashed line) and DARPin alone (blue, dashed line). The SDS-polyacrylamide gel of the corresponding complex peak fractions (grey bar) is shown (inset). (C and D) The affinities of eleven caspase-7 DARPins were determined by SPR. Exemplary SPR traces are shown for DARPin C7_16 (C) and kinetic binding parameters as well as dissociation constants are shown in (D). (E and F) The affinities of five AcrB DARPins of the new library were determined by SPR alongside with the previously described AcrB DARPin 110819.[28] Exemplary SPR traces are shown for DARPin AcrB_21 (E) and kinetic binding parameters as well as dissociation constants are shown in (F).

states were analyzed by SEC (Supporting Information Fig. S3). The binders yielded between 4 and 66 mg pure protein per liter of culture. Eighteen out of 20 caspase-3 DARPins, 15 out of 20 caspase-7 DARPins, and 16 out of 20 AcrB DARPins eluted as monodisperse proteins with a retention volume corresponding to DARPin monomers as judged from a SEC column calibration run (not shown). Complex

DOI: 10.1002/pro.2312, ©2013 The Protein Society

formation with target proteins was confirmed for monomeric caspase-3 and -7 DARPins by a peak shift on analytical SEC and subsequent SDS-PAGE analysis of the complex peak fractions [Fig. 6(B), Supporting Information Fig. S8(A,B)]. Eleven caspase-7 DARPins and all monomeric AcrB DARPins were further analyzed by surface plasmon resonance (SPR). A typical sensogram is shown for C7_16 and AcrB_21 [Fig. 6(C,E)]. For all caspase-7 binders, the binding constants were determined from the binding and dissociation kinetics. Binding of caspase-7 DARPins was characterized by rather slow on-rates and slow off-rates resulting in dissociation constants ranging from 33 n*M* to 364 n*M* [Fig. 6(D)]. Only five of the tested AcrB DARPins elicited SPR binding curves suitable for fitting and exhibited K_ds in the range of 110 n*M* to 597 n*M* [Fig. 6(F)]. Their affinities were therefore considerably lower than an original DARPin selected against AcrB (DARPin 110819 described in Ref. 28) whose K_d amounted to 53 n*M* in our analysis [Fig. 6(F)]. Notably, the original DARPin binders against AcrB were identified by an *in vivo* assay in *E. coli* cells. This allowed for screening a much larger number of clones, which explains the better affinities observed. The five high affinity AcrB DARPins were then analyzed for complex formation with AcrB by SEC. They all co-migrated with the targeted transporter [Supporting Information Fig. S8(C)], but AcrB_4 and AcrB_23 appear to dissociate during SEC due to low binding affinity.

Equilibrium unfolding of DARPins

To assess whether the second-generation library has retained the high thermodynamic stability of the original DARPins, equilibrium unfolding curves for 11 original DARPins and 25 second-generation DARPins (15 unselected DARPins and 5 DARPins each specific for caspase-3 and caspase-7, respectively) were determined (Supporting Information Fig. S9). With the exception of unselected DARPin D20, equilibrium unfolding curves for the new DARPins appeared monophasic. On the other hand, the unfolding curves of several original DARPins were clearly biphasic due to the early unfolding of the nonoptimized C-cap.[52] DARPin unfolding and folding is a complicated process involving several folding intermediates as detailed previously using a consensus repeat approach.[56] Here, we will confine our analysis to midpoints of denaturation (D_m) for clarity of discussion. The D_m values range from 2.3*M* to 5.1*M* GdnHCl for the original DARPins and 1.9*M* to 4.3*M* GdnHCl for the second-generation DARPins. On average, the new DARPins were less stable than the original ones with average D_m values of 3.0*M* and 3.8*M* GdnHCl, respectively (Fig. 7). This loss of stability might be attributed to the randomization of position 10 in the second-generation

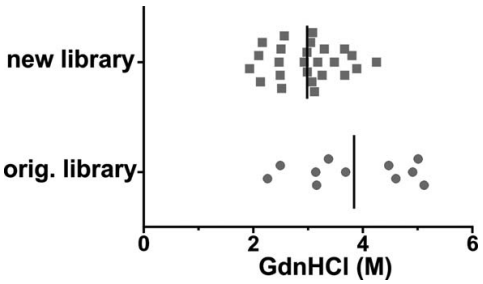

Figure 7. Equilibrium unfolding of DARPins. GdnHCl unfolding of a set of DARPins of the original and new library was determined by CD spectroscopy (Supporting Information Fig. S9) which allowed the determination of midpoints of unfolding (D_m). D_m values of individual DARPins are depicted together with the mean D_m (vertical line) for original and new DARPins, respectively.

DARPins. For stability considerations, this position was kept as invariant leucine in the original library, and we found in this study that the E3_5_L86A mutant was less stable than wild type E3_5 [Fig. 3(B)].

Crystal structure of DARPin C7_16 in complex with caspase-7

DARPin C7_16 was purified in complex with caspase-7 by SEC, crystallized and the structure was determined at 1.7 Å resolution (Table I). The structure reveals one DARPin and one caspase-7 monomer in the asymmetric unit (Fig. 8). DARPin C7_16 superimposes well with the structure of a full-consensus DARPin containing the identical optimized C-cap[53] indicating that the changes in the framework and the extended randomization did not alter the scaffold structure [Supporting Information Fig. S10(A)]. DARPin C7_16 interacts exclusively with the large subunit of caspase-7 involving residues mainly located at the second and third internal repeat and the C-cap. The binding interface covers an area of 843 Å^2 on the DARPin and is stabilized by 13 hydrogen bonds and four salt bridges. Four tryptophans and two tyrosines are prominently involved in mediating molecular contacts to caspase-7 [Fig. 8(B)] and they account for 63% of the interaction surface and establish five hydrogen bonds. Residues of the C-cap account for approximately 49% of the binding surface. In contrast, residues in the randomized ankyrin positions 1 and 10 play a minor role in this particular DARPin-caspase-7 complex accounting for 1.6% and 0.1% of total BSA, respectively. Based on this particular crystal structure we cannot yet draw conclusions whether randomization of the two additional ankyrin repeat positions 1 and 10 was beneficial or not. The crystal structure nevertheless provides

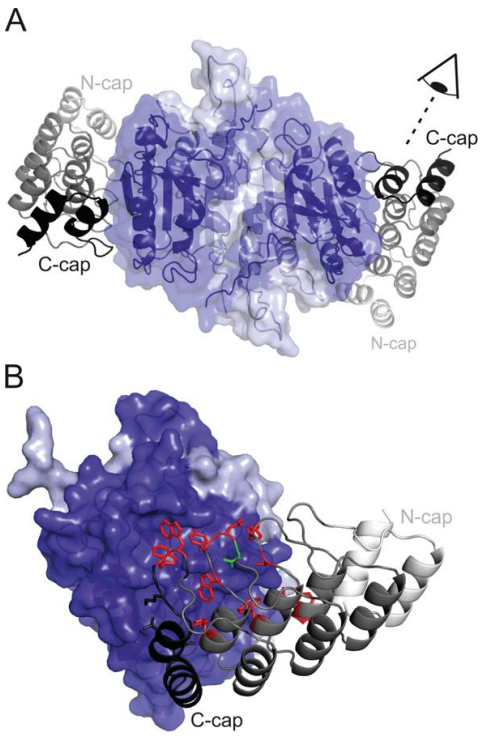

Figure 8. Crystal structure of the C7_16-caspase-7 complex. (A) Standard view of caspase-7 (surface representation, light and dark blue corresponding to the small and large subunits) in complex with DARPin C7_16 (cartoon representation, shades of grey). The DARPin binds side-ways to the large subunit of the enzyme. (B) Close-up view of the binding interface. Interacting DARPin residues (distance <4.5 Å) are highlighted as sticks and colored according to the scheme of Figure 1. Four tryptophans and two tyrosines play a dominant role in providing target contacts.

evidence that crystal contacts are mediated between two DARPins involving residues with reduced entropy, namely A68, A134, and D130 [Supporting Information Fig. S10(B)]. More crystal structures will be needed to analyze the consequences of surface entropy reduction in a systematic manner.

Discussion

In vitro selected binders have become popular tools in structural, cell, and chemical biology. Amongst such binders, nonantibody scaffolds offer unprecedented advantages due to their novel shapes of randomized surfaces and their favorable biophysical properties such as high stability and the absence of cysteines.[11] Virtually any protein surface can be subjected to randomization which explains the development of numerous binding scaffolds in past years and certainly many more in the future. Here, we chose to refine the properties of an already established scaffold, namely the well-characterized DARPins.

Features of the second-generation DARPins

The presented second-generation library builds on an optimized scaffold and the randomized surface was extended based on the analysis of 13 crystal structures. Ankyrin repeat position 33 was no longer randomized in the second-generation library and positions 1 and 10 were subjected to focused randomization including a small number of permitted residues which lead to a slight reduction of thermodynamic stability. However, the average midpoint of denaturation still amounts to 3*M* GdnHCl and therefore, DARPins from the library described here are based on a very stable scaffold. The C-cap was found to be the Achilles heel of the original DARPins and therefore we added an optimized C-cap,[52] which in contrast to the original DARPins was subjected to randomization. Moreover, we exchanged a lysine and a glutamate at the backside of each ankyrin repeat by alanine and aspartate, respectively, in order to reduce the surface entropy of DARPins for crystallization purposes.

Library assembly and validation

At the center of the binder selection technology stands the binder library, which encodes the sum of all randomized scaffolds in form of DNA. Its quality is characterized by (i) the library diversity (typically limited by the amount of DNA obtained in the last step of library assembly), (ii) the sequence quality (i.e. the percentage of library members encoded in frame containing the intended residues), and (iii) the biochemical property of the randomized scaffold (i.e. the percentage of in-frame library members that fold into monomeric proteins). For the library presented here, these three parameters are excellent. Due to the large theoretical library diversity of 1.9×10^{24}, the practical diversity of this library was limited by the amount of assembled DNA and corresponds to approximately 10^{11} different library members. Seventy-seven percent of assembled library members are devoid of frame shifts and 83% of randomly picked in-frame DARPins could be purified and run as monomers on SEC. Currently, the practical diversity of the library is limited by the final ligation of the library into the *in vitro* transcription vector pRDV.[12] In future work, the library diversity can be further increased by using type IIS restriction enzymes not only for the assembly of the repeats, but also for the cloning of the flanking elements required for *in vitro* transcription and translation of the library for ribosome display.[57]

Strong enrichment of tryptophan residues during binder selection

In previous studies, degenerate codons were used to construct a more hydrophilic synthetic scFv library

DOI: 10.1002/pro.2312, ©2013 The Protein Society

based on a stable antibody scaffold.[58] In addition, selections with Fab and monobody libraries containing only serines and tyrosines in the randomized positions were reported.[59,60] Tyrosines were highlighted to play a key role in such minimalist synthetic libraries to culminate in a review article entitled "The Importance of Being Tyrosine".[37] In order to reduce the accumulation of "sticky" binders during the *in vitro* selection process, our second-generation DARPin library was diversified omitting the hydrophobic amino acids V, L, I, M, and F (except for position 10, where V and L are permitted). The diversified positions were enriched with tyrosine expecting that they will substitute for the hydrophobic amino acids excluded in the new library. In test selections against caspase-3, caspase-7 and AcrB, we observed specific enrichment of binders starting from round 2. A large proportion of binders were monomers, including those selected against the membrane protein AcrB, which underscores the advantage of working with a more hydrophilic DARPin library. The affinities of eleven caspase-7 and five AcrB DARPins measured by SPR range between 33 n*M* and 597 n*M*, which is lower than the affinities of DARPins of the original library selected against the same targets. However, current selections against other targets using the new DARPin library revealed binding affinities in the picomolar range (not shown). In our selections we did not observe substantial further enrichment of tyrosines, but strikingly, the number of tryptophans tripled. This result suggests that synthetic libraries depleted of apolar amino acids in diversified positions should be enriched in *tyrosine and tryptophan* in the randomization mixtures.

Crystal structure of the DARPin C7_16-caspase-7 complex

The crystal structure of DARPin C7_16 in complex with caspase-7 provides three important insights. First, the scaffold structure is unchanged. Moreover, the optimized C-cap superimposes very well with the recently published full-consensus DARPin structure containing this C-cap.[53] Second, tyrosines and tryptophans in the randomized positions play a key role in mediating contacts to the target as they contribute 23% and 40%, respectively to the buried DARPin surface and five hydrogen bonds. Third, the residues subjected to surface entropy reduction were indeed found to be involved in crystal contacts.

Future prospects

A key motivator in designing this new library is its future use to select binders against difficult targets such as membrane proteins and soluble proteins exhibiting hydrophobic surfaces. Here, we could demonstrate successful selections against the membrane protein AcrB. Selections and binder analysis against a number of challenging proteins are ongoing, but will require several years of data accumulation to allow meaningful conclusions. The technical quality of this DARPin library is excellent and the test selections and characterizations presented in this study are encouraging. Library design and binder characterization is an iterative process.[48] Thanks to the numerous available crystal structures, DARPins represent an ideal playground to improve synthetic library design. We hope that in the future more DARPin libraries will be created to identify the best possible randomization and selection strategy for this scaffold.

Materials and Methods

Reagents

Primers containing incorporated trinucleotide phosphoramidites for the targeted randomization were obtained from Ella Biotech (Martinsried, Germany). The other oligonucleotides were purchased from Microsynth (Balgach, Switzerland) at PAGE-purified quality. Restriction enzymes (if not stated otherwise), Vent polymerase and Phusion polymerase were from NEB. T4 DNA ligase and BpiI was purchased from Thermo Scientific. PCR purification kit, gel extraction kit, and plasmid miniprep kit were from Qiagen. Chemicals were from Sigma/Fluka, if not stated otherwise.

Analysis of the crystal interfaces

For the analysis of DARPin contact residues, the following 13 crystal structures (PDB entries) containing 22 interfaces in their asymmetric units were analyzed using the EPPIC server (www.eppic-web.org):[47] 1SVX, 2BKK, 2V4H, 2V5Q, 2XZD, 2Y1L, 3HG0, 3NOC, 3ZU7, 3ZUV, 4DRX, 4DX5, 4F6R. Crystal structures 2P2C, 3NOG and 4GRG were omitted due to resolutions limits (>3 Å) and 2J8S (solved at 2.5 Å) is represented here by the identical 1108_19-AcrB complex 4DX5 (solved at 1.9 Å). Accessible surface areas (ASA) and buried surface areas (BSA) upon complexation were retrieved from the EPPIC log files and compiled in an Excel sheet (Supporting Information File "DARPin_interfaces.xls"). In case several chains of the target protein were involved in the binding interface, the respective surfaces were summed up. At the transition between two target protein chains, there were around 10 cases in which the BSA of a DARPin residue was larger than its ASA. In these cases, the burial was set to 100% (BSA = ASA).

Generation of E3_5 mutants and surface entropy reduced DARPin_55

The plasmid pQE30_E3_5[15] served as template to introduce single mutations (D77S and L86A) using QuikChange® site-directed mutagenesis. The primer sequences were as follows: E3_5_D77S_for (5'-GTT AAC GCT TCT AGC CTT ACT GGT ATT AC), E3_5_D77S_rev (5'-GTA ATA CCA GTA AGG CTA GAA GCG TTA AC), E3_5_L86A_for (5'-CTC CGC

TGC ACG CGG CTG CTG CTA C) and E3_5_L86A_rev (5'-GTA GCA GCA GCC GCG TGC AGC GGA G). The coding sequence of mutant DARPin_55 was custom-synthesized by Geneart (Regensburg) and cloned into pQE30.

DARPin purification and crystallization of E3_5_D77S and E3_5_L86A

E3_5 wild type and mutants as well as DARPin_55 and its mutant were expressed and purified as previously described.[15] E3_5 mutants were applied on SEC (Superdex 200 5/150 GL, 20 m*M* Tris/HCl (pH 7.4), 150 m*M* NaCl) for buffer exchange, concentrated to 15 mg/mL and subjected to crystallization trials. For the E3_5_D77S mutant, crystals appeared in 1.6*M* citrate pH 6.5 and for the E3_5_L86A mutant, crystal grew in 0.1*M* citrate pH 5.6, 20% 2-propanol, 20% PEG4000. Crystals were directly picked from the screening plate without further cryo-protection and flash-frozen in liquid nitrogen.

PCR amplification of DARPin capping repeats for library assembly

PCR reactions for the amplification of the caps were carried out on a Bio-Rad PCR machine using the temperature protocol: 2 min, 95°C; 30 cycles of 30 sec 95°C (melting), 30 sec 60°C (annealing) and 2 min/kb amplified DNA 72°C (elongation); a final elongation step 10 min 72°C; cooling to 10°C. The E20D_R23S double mutation at the N-Cap was introduced into pQE30_E3_5 using QuikChange® site-directed mutagenesis using primers NCap_E20D_R23S_for (5'-GCT GGA TGC TGC TAG TGC TGG TCA GG) and NCap_E20D_R23S_rev (5'-CCT GAC CAG CAC TAG CAG CAT CCA GC). This mutant served as template to PCR amplify the N-cap using primers NCap1 (5'-ATG GCG CGC CAT GGG TAT GAG AGG ATC G) and NCap2 (5'-ATA AGC TTG GTC TCA CGT CAG CAC CGT TAG CCA TCA GTA TAC G). The C-Cap was amplified from the vector pQE30_NI3C_Mut5[53] using primers CCap1 (5'-ATG GCG CGC CGA AGA CCT GAC GTC AAC GCT AAC XXX NNN NNN GGT AAG ACC CCG TTC GAC TTA GCG, in which XXX stands for a codon mix for D, N; 30% each and S, T; 20% each and NNN stands for a codon mix for A, S, T, N, and Y; 12% each and D, E, R, K, Q, W, and H; 5.7% each) and NC_shorter (5'-ATA AGC TTC GCC GCT TTT TGC AGC AC). Both caps were amplified using Phusion polymerase (amounts used as suggested by the manufacturer), 0.5 μ*M* of each primer and 0.2 m*M* of dNTPs resulting in a single band on agarose gel (1.5%) and yielding around 3 μg of DNA per 50 μL of PCR reaction.

PCR amplification of the internal repeats for library assembly

The internal repeats were amplified in a single step using a simple assembly PCR protocol.[61] Low amounts (0.05 μ*M* final conc, each) of inner primers Rep2 (5'-GA CCT GAC GTT AAC GCT TCT XXX NNN NNN GGT NNN ACT CCG CTG CAC YYY GCT GCT NNN NNN GGT CAC CTG GAA ATC GTC G, in which XXX and NNN denote codons for the same amino acid mixtures as specified above and YYY stands for a codon mix for A, S, T, V, and L, 20% each), Rep3 (5'-ATA AGC TTG TCA GGT CTC ACG TCA GCA CCG TDA GCC AGC AGA ACA TCG ACG ATT TCC AGG TG, in which D stands for a mixture of the bases A, G, and T) were mixed with an excess (1 μ*M* final conc, each) of outer primers Rep1 (5'-ATG GCG CGC CGA AGA CCT GAC GTT AAC GC) and Rep4 (5'- GTA CCA AGC TTG TCA GGT CTC ACG TC). PCR was carried out using Vent polymerase (1 μL per 100 μL PCR mix), 0.4 m*M* dNTPs and 5% DMSO. The cycle protocol was: 2 min, 95°C; 35 cycles of 30 sec 95°C (melting), 30 sec 60°C (annealing) and 30 sec 72°C (elongation); a final elongation step 3 min 72°C; cooling to 10°C. The PCR product ran as a single band of the expected size on a 1.5% agarose gel. The DNA was purified with a PCR purification kit (Qiagen) to yield around 1.2 μg DNA per 50 μL of PCR reaction volume. In order to make the individual internal repeats of a fully assembled DARPin distinguishable by DNA sequence the glycine at position 27 of the ankyrin repeat module was encoded with three different triplets in each repeat of a N3C DARPin. To this end, the second internal repeat was assembled as described above, but instead of primer Rep3, Rep3_v2 (5'-ATA AGC TTG TCA GGT CTC ACG TCA GC**G** CCG TDA GCC AGC AGA ACA TCG ACG ATT TCC AGG TG, the nucleotide that differs is underscored) was used. Rep3_v3 (5'-ATA AGC TTG TCA GGT CTC ACG TCA GC**C** CCG TDA GCC AGC AGA ACA TCG ACG ATT TCC AGG TG) was used accordingly to assemble the third internal repeat.

Library assembly

The DARPin library was assembled repeat by repeat as first described by Binz *et al.*[15] In contrast to previously described protocols for DARPin and Armadillo library assemblies.[15,62] we did not subclone the repeat segments into a plasmid in a first step, but rather assembled them directly after PCR. Moreover, we provide here a comprehensive protocol for library assembly, which includes DNA and enzyme amounts as well as reaction volumes. In the first assembly step the N-Cap and the first internal repeat (1.5 μg each) were digested with BsaI and BpiI (20 units each), respectively, for 2 h in a volume of 100 μL. The small fragments containing the typeII S restriction sites were removed using the PCR purification kit (Qiagen) and cut N-cap and repeat were eluted in volumes of 50 μL elution buffer (Qiagen) each. The fragments were then ligated in a volume of 120 μL using 20 units of T4

DOI: 10.1002/pro.2312, ©2013 The Protein Society

ligase for 1 h. The ligation product was separated on a 1.5% agarose gel and the ligation efficiency was found to exceed 90%. The fragment consisting of the N-cap and the first internal repeat (called NI_1) was retrieved by gel extraction (elution in 50 μL elution buffer, Qiagen) yielding 0.8 μg of DNA. DNA (0.3 μg) thereof was PCR-amplified in 200 μL using the primers NCap1 and Rep4 and Vent polymerase following the same PCR parameters as for the amplification of internal repeats (see above) and yielding 8 μg of DNA after PCR purification. Then 2.5 μg thereof and 1.25 μg of the second internal repeat were digested using BsaI and BpiI followed by PCR purification, ligation and gel extraction under identical conditions as for the assembly of NI_1 to yield 0.86 μg NI_2. Finally 0.43 μg thereof was PCR-amplified in a 400 μL reaction mixture to yield 17.8 μg of DNA, half of which were digested in 300 μL reaction volume using 80 units of BsaI. The third internal repeat (3 μg) was digested with 25 units BpiI in 150 μL. After ligation (30 units T4 ligase in 220 μL) and gel extraction, 3.6 μg NI_3 were obtained. Half of it was amplified by PCR in 800 μL reaction mixture to yield 21.2 μg DNA which was digested in a volume of 600 μL using 80 units BsaI. C-cap (3 μg) was digested using 25 units of BpiI in 150 μL. The fragments were again ligated (50 units T4 ligase in 500 μL) and separated by gel electrophoresis to yield 6.5 μg assembled N3C DARPins, which corresponds to 1.2×10^{13} DNA molecules. Since the theoretical library diversity is 1.9×10^{24} and the last step of the assembly is a ligation (i.e. there was no amplification of the N3C fragment by PCR at this point) it is highly unlikely that two of these 1.2×10^{13} N3C DARPins are identical. Hence the practical diversity of the assembled N3C DARPins is limited by the amount of ligated DNA and corresponds to 1.2×10^{13}. One third of this ligated N3C product (thereby limiting the practical diversity to 4×10^{12}) was amplified by PCR in a volume of 2400 μL using primers NCap1 and NC_shorter to yield 84 μg of DNA. Ten micrograms thereof were digested with 50 units each of NcoI and BamHI in a volume of 300 μL for 1.5 h. Using the same restriction enzymes, 60 μg of pRDV[12] was digested. Both fragments were purified by gel extraction. About 1.25 μg digested N3C were ligated into 9 μg of digested pRDV (25 units T4 ligase in 300 μL for 3 h). Assuming that 5% of the digested N3C is being integrated into pRDV,[57] the final practical diversity of the library is estimated to amount to 10^{11} library members. The ligation product served as template for PCR amplification using primers T7 and tolAk[12] in a total volume of 3000 μL to yield DNA ready for *in vitro* transcription.[63] An estimated 5 μg DNA was used to generate 720 μg of mRNA, which was then used to perform test selections.

Ribosome display

Ribosome display selections were carried out following the established standard protocol with some minor modification as indicated.[63] Biotinylated caspase-3 and caspase-7 were prepared as described previously.[64] AcrB containing a C-terminal avi-tag was biotinylated enzymatically as described.[30] Each selection round included a prepanning step using MBP. Biotinylated MBP[12] and caspases were immobilized on NeutrAvidin coated surfaces as described[63] (surface panning method) or in the fourth and last round using magnetic beads (solution panning method). The washing times were as follows: first round, three washes w/o incubation; second round, 3×10 min; third round, 3×15 min; fourth round, 3×30 min. Retrieved mRNA of DARPins were reverse transcribed and amplified by PCR with 45, 40, 30, and 25 cycles for rounds 1, 2, 3, and 4, respectively. In the initial round, the amount of *in vitro* translation ribosomal complexes was increased five times compared with the standard protocol and Nunc MaxiSorp Immuno Tubes (Thermo Fisher Scientific) were used to immobilize MBP (for prepanning) and caspases (for panning). The number of ternary ribosome complexes of the first round was estimated to correspond to at least 3.5×10^{11} displayed DARPin molecules.[63] This number is approximately three times higher than the practical diversity of the DARPin library used, thus the *in vitro* translation step did not represent the bottleneck of the selection procedure. Due to an exchanged C-cap in the second-generation DARPin library, NC_shorter was used instead of the standard primer WTC4.[12]

Crude cell extract ELISAs

Crude cell extract ELISAs were carried out as initially established by Huber *et al.*[26] and exactly as described in Seeger *et al.*[30] with one notable exception. Namely, instead of using the DARPin expression vector pQE30_myc5,[26] which adds five consecutive myc-tags to the C-terminus of the DARPin leading to DARPin aggregation,[30] we constructed a pQE30_myc1 vector adding a single myc-tag as follows. pQE30_myc5 containing the LmrCD-specific DARPin α-LmrCD#5[30] was digested using HindIII and Bpu1102I to excise the myc5 tag, followed by gel extraction of the backbone. The myc1-tag was generated by annealing primers myc1_ for (5'-AGC TTG GTT CTG GAA GTA TGG AGC AAA AGC TCA TTT CTG AAG AGG ACT TGA ATG AAT AAT GAG C) and myc1_rev (5'-CTC AGC TCA TTA TTC ATT CAA GTC CTC TTC AGA AAT GAG CTT TTG CTC CAT ACT TCC AGA ACC A) to a double-stranded DNA product, which contains overhangs compatible with cloning into HindIII/Bpu1102I of the pQE30 backbone. Binding of each DARPin was

probed against the respective caspase and as a control against MBP. Binders yielding strong ELISA signals (at least 10 times above MBP background) were classified as specific. Positive clones were sequenced at Microsynth.

Small-scale purification of DARPins

Purified DARPins containing a single myc-tag were indistinguishable by SEC from the same DARPins without a myc-tag (not shown). Therefore, binder characterization was carried out with DARPins containing an N-terminal RGSHis6-tag and a C-terminal myc-tag. DARPins were expressed overnight at 37°C in *E. coli* XL-1 blue cells in 100 mL auto inducing medium containing ampicillin (100 μg/mL). After harvest, cells were resuspended in 20 mL lysis buffer (50 m*M* Tris/HCl (pH 7.4), 500 m*M* NaCl, 20 m*M* imidazole, 10% glycerol, 100 mg/L lysozyme, and 10 mg/L DNaseI) and incubated 1 h at 4°C before cell disruption by sonication for 3 min. Cell lysate was clarified by centrifugation (10,000*g*, 5 min) and filtration (0.45 μm). Ni^{2+}-NTA columns (0.5 mL resin) were equilibrated with wash buffer (50 m*M* Tris/HCl (pH 7.4), 500 m*M* NaCl, 20 m*M* imidazole, 10% glycerol) and cell lysate was loaded on the column. The columns were washed with 30 mL wash buffer and the proteins eluted with 2 mL elution buffer (same as wash buffer, but containing 250 m*M* imidazole). SEC was used to analyze the oligomeric state of selected DARPin binders as well as the formation of stable DARPin/target protein complexes in solution. SEC was performed at 4°C on an Agilent 1200 Series HPLC system. Sample volumes of 100 μL were injected on a Superdex 200 5/150 GL column (GE Healthcare) using SEC buffer (20 m*M* Tris/HCl (pH 7.4), 150 m*M* NaCl, 0.05% Tween-20) at a flow rate of 0.08 mL/min. To study DARPin-caspase complexes, DARPins (added in excess in concentrations ranging from 8 to 24 μ*M*) were preincubated with caspase-3 or caspsase-7 before SEC analysis. For the equilibrium unfolding experiments, DARPins were purified devoid of a myc-tag. To this end, the C-terminal myc-tag of DARPin C7_16 was removed via an introduction of two stop-codons in front of the tag using QuikChange® site-directed mutagenesis. The primer sequences were as follows: 5'-AAA GCG GCG AAG CTT TGA TAA GGA AGT ATG GAG CAA and 5'-TTG CTC CAT ACT TCC TTA TCA AAG CTT CGC CGC TTT.

Equilibrium unfolding

DARPins were purified as described above and separated by SEC in 20 m*M* Tris/HCl (pH 7.4), 150 m*M* NaCl. DARPins were diluted in increasing concentrations of GdnHCl dissolved in SEC buffer to obtain a final protein concentration of 10 μ*M* and incubated for at least 12 h in the dark at 20°C. The disappearance of the native CD signal at 222 nm with increasing GdnHCl concentrations was determined using a Jasco J-810 instrument (Jasco, Japan). As far as possible, a monophasic sigmoidal equation [Eq. (1)] was fitted to the experimental data (SigmaPlot10, standard 4 parameter sigmoidal fit):

$$f = y_0 + \frac{a}{1+e^{-\left(\frac{x-x_0}{b}\right)}} \quad (1)$$

where x_0 denotes the inflection point corresponding to D_m.

In cases of two distinct unfolding transition phases, a biphasic sigmoidal equation [Eq. (2)] was fitted to the data:

$$f = y_0 + \frac{a_1}{1+e^{-\left(\frac{x-x_{01}}{b_1}\right)}} + \frac{a_2}{1+e^{-\left(\frac{x-x_{02}}{b_2}\right)}} \quad (2)$$

with the constraints $x_{01} < x_{02}$ and $a_1 < 0.5 \times a_2$.

Here, inflection points x_{01} and x_{02} correspond to midpoints of transition $D_{m,1}$ and $D_{m,2}$. This biphasic model was only applied if $D_{m,1}$ and $D_{m,2}$ differed by at least 0.9*M* GdnHCl.

SPR analysis

The affinity of a set of caspase-7 DARPins was determined by surface plasmon resonance analysis on a ProteOn XPR36 protein interaction array system (Bio-Rad). Biotinylated caspase-7 (1200 RU) were immobilized on a NeutrAvidin coated NLC sensor chip in SPR buffer (20 m*M* Tris/HCl (pH 7.4), 150 m*M* NaCl, 0.05% Tween-20). DARPins were injected at six different concentrations (threefold dilution series) appropriate for analysis of the interaction with immobilized target proteins. Binding kinetics were performed with 120 s contact time followed by 600 to 1200 s dissociation time at a flow rate of 100 μL/min. Referenced binding signals were fitted using a 1:1 binding model (ProteOn Manager Software) and the dissociation constant K_d was calculated using Eq. (3) in which k_a is the association rate constant and k_d the dissociation rate constant:

$$K_d = \frac{k_d}{k_a} \quad (3)$$

Crystallization of the C7_16-caspase-7 complex

Myc-tag free C7_16 was expressed and purified as mentioned above. Caspase-7 expression and purification is described elsewhere.[64] Caspase-7 and DARPin C7_16 were mixed in a molar ratio of 1:3 and separated by SEC (50 m*M* Tris/HCl (pH 7.4), 150 m*M* NaCl; Superdex 200 10/300 GL). Fractions corresponding to the C7_16-caspase-7 complex were concentrated to 11 mg/mg and subjected to crystallization trials. Crystals appeared in 100 m*M*

DOI: 10.1002/pro.2312, ©2013 The Protein Society

Tris/HCl (pH 8.3), 200 m*M* $MgCl_2$, 9% PEG 1000, and 9% PEG 8000. Upon cryo-protection using ethylene glycol (20%), they were frozen in liquid nitrogen.

Crystallographic methods

Crystals were measured at the protein crystallography beamline X06SA at the Swiss Light Source (SLS) and processed using the program XDS.[65] Structures of E3_5_D77S, E3_5_L86A and the C7_16-caspase-7 complex were solved by molecular replacement using Phaser[66] and search models 1MJ0 to solve the structures E3_5 mutants and search models 3IBC (Caspase-7[67]) and 2P2C (Caspase-2 DARPins[22]) to solve the structure of the C7_16-caspase-7 complex. Models were built manually using Coot[68] and refined using PHENIX[69] including TLS refinement.[70] Structural pictures were generated using PyMOL (http://www.pymol.org).

Acknowledgments

The authors thank Beat Blattmann and Céline Stutz-Ducommun from the NCCR crystallization facility for crystal screening, and the staff of the X06SA beamline at the Swiss Light Source of the Paul Scherrer Institute for support during data collection. We thank Andreas Plückthun for providing the ribosome display plasmid pRDV and DARPin expression vectors. The authors acknowledge Stefan Schauer from the Functional Genomics Center Zürich (FGCZ) for support during SPR measurements.

References

1. Kohler G, Milstein C (1975) Continuous cultures of fused cells secreting antibody of predefined specificity. Nature 256:495–497.
2. Clackson T, Hoogenboom HR, Griffiths AD, Winter G (1991) Making antibody fragments using phage display libraries. Nature 352:624–628.
3. Hanes J, Plückthun A (1997) In vitro selection and evolution of functional proteins by using ribosome display. Proc Natl Acad Sci USA 94:4937–4942.
4. Angelini A, Cendron L, Chen S, Touati J, Winter G, Zanotti G, Heinis C (2012) Bicyclic peptide inhibitor reveals large contact interface with a protease target. ACS Chem Biol 7:817–821.
5. Röthlisberger D, Pos KM, Plückthun A (2004) An antibody library for stabilizing and crystallizing membrane proteins—selecting binders to the citrate carrier CitS. FEBS Lett 564:340–348.
6. Silacci M, Brack S, Schirru G, Marlind J, Ettorre A, Merlo A, Viti F, Neri D (2005) Design, construction, and characterization of a large synthetic human antibody phage display library. Proteomics 5:2340–2350.
7. Vaughan TJ, Williams AJ, Pritchard K, Osbourn JK, Pope AR, Earnshaw JC, McCafferty J, Hodits RA, Wilton J, Johnson KS (1996) Human antibodies with subnanomolar affinities isolated from a large non-immunized phage display library. Nat Biotechnol 14:309–314.
8. Prassler J, Thiel S, Pracht C, Polzer A, Peters S, Bauer M, Norenberg S, Stark Y, Kolln J, Popp A, Urlinger S, Enzelberger M (2011) HuCAL PLATINUM, a synthetic Fab library optimized for sequence diversity and superior performance in mammalian expression systems. J Mol Biol 413:261–278.
9. Skerra A (2007) Alternative non-antibody scaffolds for molecular recognition. Curr Opin Biotech 18:295–304.
10. Boersma YL, Plückthun A (2011) DARPins and other repeat protein scaffolds: advances in engineering and applications. Curr Opin Biotech 22:849–857.
11. Binz HK, Amstutz P, Plückthun A (2005) Engineering novel binding proteins from nonimmunoglobulin domains. Nat Biotechnol 23:1257–1268.
12. Binz HK, Amstutz P, Kohl A, Stumpp MT, Briand C, Forrer P, Grütter MG, Plückthun A (2004) High-affinity binders selected from designed ankyrin repeat protein libraries. Nat Biotechnol 22:575–582.
13. Lambert S, Yu H, Prchal JT, Lawler J, Ruff P, Speicher D, Cheung MC, Kan YW, Palek J (1990) cDNA sequence for human erythrocyte ankyrin. Proc Natl Acad Sci USA 87:1730–1734.
14. Batchelor AH, Piper DE, de la Brousse FC, McKnight SL, Wolberger C (1998) The structure of GABPa/b: an ETS domain- ankyrin repeat heterodimer bound to DNA. Science 279:1037–1041.
15. Binz HK, Stumpp MT, Forrer P, Amstutz P, Plückthun A (2003) Designing repeat proteins: well-expressed, soluble and stable proteins from combinatorial libraries of consensus ankyrin repeat proteins. J Mol Biol 332: 489–503.
16. Binz HK, Kohl A, Plückthun A, Grütter MG (2006) Crystal structure of a consensus-designed ankyrin repeat protein: implications for stability. Proteins 65: 280–284.
17. Merz T, Wetzel SK, Firbank S, Plückthun A, Grütter MG, Mittl PR (2008) Stabilizing ionic interactions in a full-consensus ankyrin repeat protein. J Mol Biol 376: 232–240.
18. Steiner D, Forrer P, Stumpp MT, Plückthun A (2006) Signal sequences directing cotranslational translocation expand the range of proteins amenable to phage display. Nat Biotechnol 24:823–831.
19. Boersma YL, Chao G, Steiner D, Wittrup KD, Plückthun A (2011) Bispecific designed ankyrin repeat proteins (DARPins) targeting the epidermal growth factor receptor inhibit A431 cell proliferation and receptor recycling. J Biol Chem 286:41273–41285.
20. Zahnd C, Pecorari F, Straumann N, Wyler E, Plückthun A (2006) Selection and characterization of Her2 binding-designed ankyrin repeat proteins. J Biol Chem 281:35167–35175.
21. Kohl A, Amstutz P, Parizek P, Binz HK, Briand C, Capitani G, Forrer P, Plückthun A, Grütter MG (2005) Allosteric inhibition of aminoglycoside phosphotransferase by a designed ankyrin repeat protein. Structure 13: 1131–1141.
22. Schweizer A, Roschitzki-Voser H, Amstutz P, Briand C, Gulotti-Georgieva M, Prenosil E, Binz HK, Capitani G, Baici A, Plückthun A, Grütter MG (2007) Inhibition of caspase-2 by a designed ankyrin repeat protein: specificity, structure, and inhibition mechanism. Structure 15:625–636.
23. Stefan N, Martin-Killias P, Wyss-Stoeckle S, Honegger A, Zangemeister-Wittke U, Plückthun A (2011) DARPins recognizing the tumor-associated antigen EpCAM selected by phage and ribosome display and engineered for multivalency. J Mol Biol 413:826–843.
24. Martin-Killias P, Stefan N, Rothschild S, Plückthun A, Zangemeister-Wittke U (2011) A novel fusion toxin derived from an EpCAM-specific designed ankyrin repeat protein has potent antitumor activity. Clin Cancer Res 17:100–110.

25. Steiner D, Forrer P, Plückthun A (2008) Efficient selection of DARPins with sub-nanomolar affinities using SRP phage display. J Mol Biol 382:1211–1227.
26. Huber T, Steiner D, Röthlisberger D, Plückthun A (2007) In vitro selection and characterization of DARPins and Fab fragments for the co-crystallization of membrane proteins: the Na^+-citrate symporter CitS as an example. J Struct Biol 159:206–221.
27. Milovnik P, Ferrari D, Sarkar CA, Plückthun A (2009) Selection and characterization of DARPins specific for the neurotensin receptor 1. Protein Eng Des Sel 22:357–366.
28. Sennhauser G, Amstutz P, Briand C, Storchenegger O, Grütter MG (2007) Drug export pathway of multidrug exporter AcrB revealed by DARPin inhibitors. PLoS Biol 5:e7.
29. Mittal A, Böhm S, Grütter MG, Bordignon E, Seeger MA (2012) Asymmetry in the homodimeric ABC transporter MsbA recognized by a DARPin. J Biol Chem 287:20395–20406.
30. Seeger MA, Mittal A., Velamakanni S, Hohl M, Schauer S, Salaa I, Grütter MG, van Veen HW (2012) Tuning the drug efflux activity of an ABC transporter in vivo by in vitro selected DARPin binders. PLoS One 7:e37845.
31. Simon M, Zangemeister-Wittke U, Plückthun A (2012) Facile double-functionalization of designed ankyrin repeat proteins using click and thiol chemistries. Bioconjug Chem 23:279–286.
32. Parizek P, Kummer L, Rube P, Prinz A, Herberg FW, Plückthun A (2012) Ankyrin repeat proteins (DARPins) as novel isoform-specific intracellular inhibitors of c-Jun N-terminal kinases. ACS Chem Biol 7:1356–1366.
33. Amstutz P, Binz HK, Parizek P, Stumpp MT, Kohl A, Grütter MG, Forrer P, Plückthun A (2005) Intracellular kinase inhibitors selected from combinatorial libraries of designed ankyrin repeat proteins. J Biol Chem 280:24715–24722.
34. Sennhauser G, Grütter MG (2008) Chaperone-assisted crystallography with DARPins. Structure 16:1443–1453.
35. Koide S (2009) Engineering of recombinant crystallization chaperones. Curr Opin Struct Biol 19:449–457.
36. Eicher T, Cha HJ, Seeger MA, Brandstatter L, El-Delik J, Bohnert JA, Kern WV, Verrey F, Grütter MG, Diederichs K, Pos KM (2012) Transport of drugs by the multidrug transporter AcrB involves an access and a deep binding pocket that are separated by a switch-loop. Proc Natl Acad Sci USA 109:5687–5692.
37. Koide S, Sidhu SS (2009) The importance of being tyrosine: lessons in molecular recognition from minimalist synthetic binding proteins. ACS Chem Biol 4:325–334.
38. Grubisha O, Kaminska M, Duquerroy S, Fontan E, Cordier F, Haouz A, Raynal B, Chiaravalli J, Delepierre M, Israel A, Veron M, Agou F (2010) DARPin-assisted crystallography of the CC2-LZ domain of NEMO reveals a coupling between dimerization and ubiquitin binding. J Mol Biol 395:89–104.
39. Bandeiras TM, Hillig RC, Matias PM, Eberspaecher U, Fanghanel J, Thomaz M, Miranda S, Crusius K, Putter V, Amstutz P, Gulotti-Georgieva M, Binz HK, Holz C, Schmitz AA, Lang C, Donner P, Egner U, Carrondo MA, Muller-Tiemann B (2008) Structure of wild-type Plk-1 kinase domain in complex with a selective DARPin. Acta Crystallogr D Biol Crystallogr 64:339–353.
40. Schroeder T, Barandun J, Flütsch A, Briand C, Mittl PR, Grütter MG (2013) Specific inhibition of caspase-3 by a competitive DARPin: molecular mimicry between native and designed inhibitors. Structure 21:277–289.
41. Veesler D, Dreier B, Blangy S, Lichiere J, Tremblay D, Moineau S, Spinelli S, Tegoni M, Plückthun A, Campanacci V, Cambillau C (2009) Crystal structure and function of a DARPin neutralizing inhibitor of lactococcal phage TP901-1: comparison of DARPin and camelid VHH binding mode. J Biol Chem 284:30718–30726.
42. Monroe N, Sennhauser G, Seeger MA, Briand C, Grütter MG (2011) Designed ankyrin repeat protein binders for the crystallization of AcrB: plasticity of the dominant interface. J Struct Biol 174:269–281.
43. Kummer L, Parizek P, Rube P, Millgramm B, Prinz A, Mittl PR, Kaufholz M, Zimmermann B, Herberg FW, Plückthun A (2012) Structural and functional analysis of phosphorylation-specific binders of the kinase ERK from designed ankyrin repeat protein libraries. Proc Natl Acad Sci USA 109:E2248–E2257.
44. Pecqueur L, Duellberg C, Dreier B, Jiang Q, Wang C, Plückthun A, Surrey T, Gigant B, Knossow M (2012) A designed ankyrin repeat protein selected to bind to tubulin caps the microtubule plus end. Proc Natl Acad Sci USA 109:12011–12016.
45. Kim B, Eggel A, Tarchevskaya SS, Vogel M, Prinz H, Jardetzky TS (2012) Accelerated disassembly of IgE-receptor complexes by a disruptive macromolecular inhibitor. Nature 491:613–617.
46. Mignot I, Pecqueur L, Dorleans A, Karuppasamy M, Ravelli RB, Dreier B, Plückthun A, Knossow M, Gigant B (2012) Design and characterization of modular scaffolds for tubulin assembly. J Biol Chem 287:31085–31094.
47. Duarte JM, Srebniak A, Schärer MA, Capitani G (2012) Protein interface classification by evolutionary analysis. BMC Bioinform 13:334.
48. Gilbreth RN, Koide S (2012) Structural insights for engineering binding proteins based on non-antibody scaffolds. Curr Opin Struct Biol 22:413–420.
49. Kohl A, Binz HK, Forrer P, Stumpp MT, Plückthun A, Grütter MG (2003) Designed to be stable: crystal structure of a consensus ankyrin repeat protein. Proc Natl Acad Sci USA 100:1700–1705.
50. Virnekas B, Ge L, Plückthun A, Schneider KC, Wellnhofer G, Moroney SE (1994) Trinucleotide phosphoramidites: ideal reagents for the synthesis of mixed oligonucleotides for random mutagenesis. Nucleic Acids Res 22:5600–5607.
51. Kayushin AL, Korosteleva MD, Miroshnikov AI, Kosch W, Zubov D, Piel N (1996) A convenient approach to the synthesis of trinucleotide phosphoramidites—synthons for the generation of oligonucleotide/peptide libraries. Nucleic Acids Res 24:3748–3755.
52. Interlandi G, Wetzel SK, Settanni G, Plückthun A, Caflisch A (2008) Characterization and further stabilization of designed ankyrin repeat proteins by combining molecular dynamics simulations and experiments. J Mol Biol 375:837–854.
53. Kramer MA, Wetzel SK, Plückthun A, Mittl PR, Grütter MG (2010) Structural determinants for improved stability of designed ankyrin repeat proteins with a redesigned C-capping module. J Mol Biol 404: 381–391.
54. Derewenda ZS (2004) Rational protein crystallization by mutational surface engineering. Structure 12:529–535.
55. O'Neil KT, DeGrado WF (1990) A thermodynamic scale for the helix-forming tendencies of the commonly occurring amino acids. Science 250:646–651.
56. Wetzel SK, Settanni G, Kenig M, Binz HK, Plückthun A (2008) Folding and unfolding mechanism of highly

DOI: 10.1002/pro.2312, ©2013 The Protein Society

stable full-consensus ankyrin repeat proteins. J Mol Biol 376:241–257.
57. Ng DT, Sarkar CA (2012) Model-guided ligation strategy for optimal assembly of DNA libraries. Protein Eng Des Sel 25:669–678.
58. Sidhu SS, Li B, Chen Y, Fellouse FA, Eigenbrot C, Fuh G (2004) Phage-displayed antibody libraries of synthetic heavy chain complementarity determining regions. J Mol Biol 338:299–310.
59. Fellouse FA, Wiesmann C, Sidhu SS (2004) Synthetic antibodies from a four-amino-acid code: a dominant role for tyrosine in antigen recognition. Proc Natl Acad Sci USA 101:12467–12472.
60. Koide A, Gilbreth RN, Esaki K, Tereshko V, Koide S (2007) High-affinity single-domain binding proteins with a binary-code interface. Proc Natl Acad Sci USA 104:6632–6637.
61. Xiong AS, Yao QH, Peng RH, Duan H, Li X, Fan HQ, Cheng ZM, Li Y (2006) PCR-based accurate synthesis of long DNA sequences. Nat Protoc 1:791–797.
62. Varadamsetty G, Tremmel D, Hansen S, Parmeggiani F, Plückthun A (2012) Designed Armadillo repeat proteins: library generation, characterization and selection of peptide binders with high specificity. J Mol Biol 424: 68–87.
63. Zahnd C, Amstutz P, Plückthun A (2007) Ribosome display: selecting and evolving proteins in vitro that specifically bind to a target. Nat Methods 4:269–279.
64. Roschitzki-Voser H, Schroeder T, Lenherr ED, Frölich F, Schweizer A, Donepudi M, Ganesan R, Mittl PR, Baici A, Grütter MG (2012) Human caspases in vitro: expression, purification and kinetic characterization. Protein Expr Purif 84:236–246.
65. Kabsch W (2010) XDS. Acta Crystallogr D Biol Crystallogr 66:125–132.
66. McCoy AJ, Grosse-Kunstleve RW, Adams PD, Winn MD, Storoni LC, Read RJ (2007) Phaser crystallographic software. J Appl Crystrallogr 40:658–674.
67. Agniswamy J, Fang B, Weber IT (2009) Conformational similarity in the activation of caspase-3 and −7 revealed by the unliganded and inhibited structures of caspase-7. Apoptosis 14:1135–1144.
68. Emsley P, Lohkamp B, Scott WG, Cowtan K (2010) Features and development of Coot. Acta Crystallogr D Biol Crystallogr 66:486–501.
69. Adams PD, Afonine PV, Bunkoczi G, Chen VB, Davis IW, Echols N, Headd JJ, Hung LW, Kapral GJ, Grosse-Kunstleve RW, McCoy AJ, Moriarty NW, Oeffner R, Read RJ, Richardson DC, Richardson JS, Terwilliger TC, Zwart PH (2010) PHENIX: a comprehensive Python-based system for macromolecular structure solution. Acta Crystallogr D Biol Crystallogr 66:213–221.
70. Painter J, Merritt EA (2006) Optimal description of a protein structure in terms of multiple groups undergoing TLS motion. Acta Crystallogr D Biol Crystallogr 62:439–450.

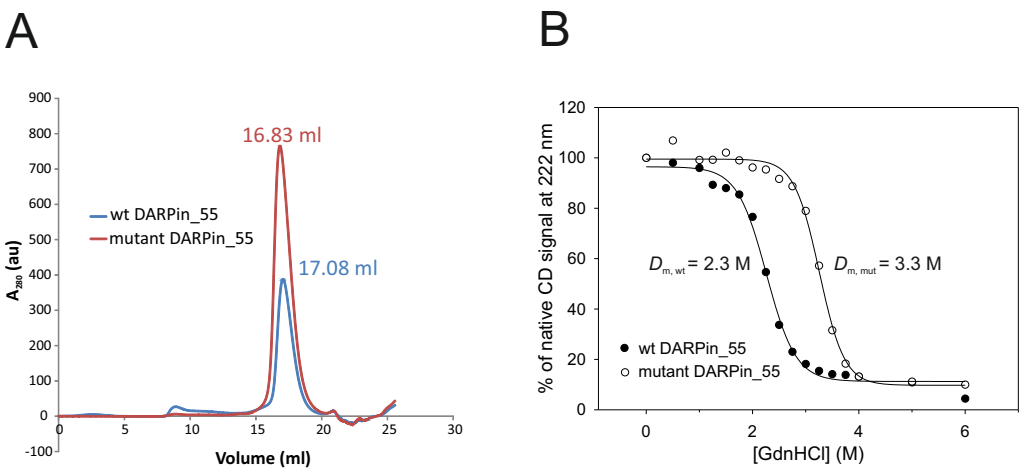

Supporting Information Figure S1: Biochemical analysis of surface entropy reduction mutations in DARPin_55. Glutamate of ankyrin repeat position 21 and lysine of position 25 (Figure 1C) were mutated to aspartate and alanine, respectively, in all three internal repeats of DARPin_55[29]. The resulting 6-fold mutant was compared to wild type DARPin_55 by SEC using a Superdex 200 10/300 GL column (A) and equilibrium unfolding using GdnHCl (B).

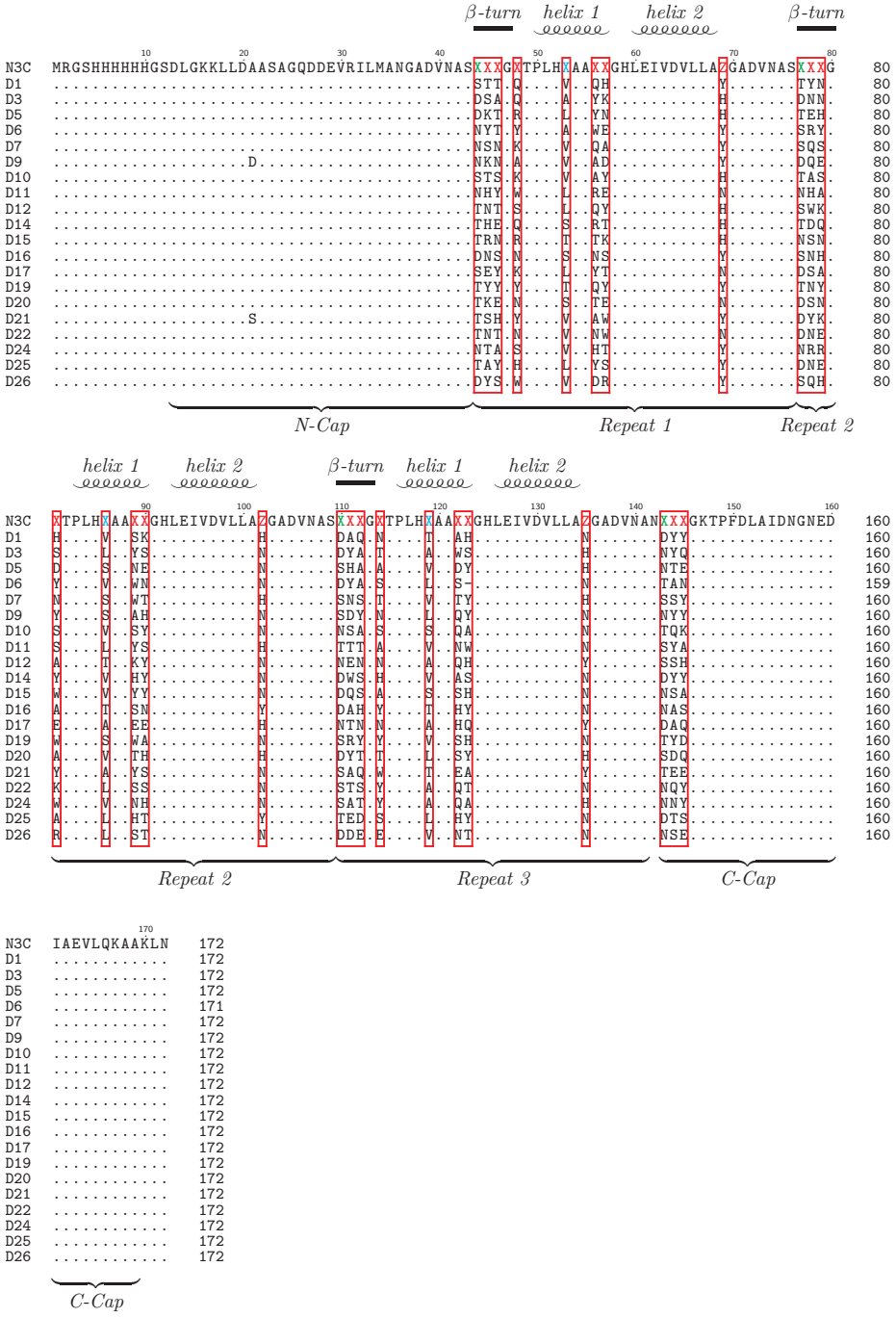
β-turn
helix 1
helix 2
β-turn
N3C MRGSHHHHHHGSDLGKKLLDAASAGQDDEVRILMANGADVNASXXXGXTPLHXAAXXGHLEIVDVLLAZGADVNASXXXG 80
D1 STT.Q...V..QH.....Y.....TYN. 80
D3 DSA.Q...A..YK.....H.....DNN. 80
D5 DKT.R...L..YN.....H.....TEH. 80
D6 NYT.Y...A..WE.....Y.....SRY. 80
D7 NSN.K...V..QA.....Y.....SQS. 80
D9 .....D..... NKN.A...V..AD.....Y.....DQE. 80
D10 STS.K...V..AY.....H.....TAS. 80
D11 NHY.W...L..RE.....N.....NHA. 80
D12 TNT.S...L..QY.....H.....SWK. 80
D14 THE.Q...S..RT.....H.....TDQ. 80
D15 TRN.R...T..TK.....H.....NSN. 80
D16 DNS.N...S..NS.....Y.....SNH. 80
D17 SEY.K...L..YT.....N.....DSA. 80
D19 TYY.Y...T..QY.....Y.....TNY. 80
D20 TKE.N...S..TE.....N.....DSN. 80
D21 .....S..... TSH.Y...V..AW.....Y.....DYK. 80
D22 TNT.N...V..NW.....N.....DNE. 80
D24 NTA.S...V..HT.....Y.....NRR. 80
D25 TAY.H...L..YS.....Y.....DNE. 80
D26 DYS.W...V..DR.....Y.....SQH. 80
N-Cap
Repeat 1
Repeat 2
helix 1
helix 2
β-turn
helix 1
helix 2
N3C XTPLHXAAXXGHLEIVDVLLAZGADVNASXXXGXTPLHXAAXXGHLEIVDVLLAZGADVNANXXXGKTPFDLAIDNGNED 160
D1 H...V..SK.....H.....DAQ.N...T..AH.....N.....DYY..... 160
D3 S...L..YS.....N.....DYA.T...A..WS.....H.....NYQ..... 160
D5 D...S..NE.....N.....SHA.A...V..DY.....H.....NTE..... 160
D6 Y...V..WN.....N.....DYA.S...L..S-.....N.....TAN..... 159
D7 N...S..WT.....H.....SNS.I...V..TY.....H.....SSY..... 160
D9 Y...S..AH.....N.....SDY.N...L..QY.....N.....NYY..... 160
D10 S...V..SY.....N.....NSA.S...S..QA.....N.....TQK..... 160
D11 S...L..YS.....H.....TTT.A...V..NW.....N.....SYA..... 160
D12 A...T..KY.....N.....NEN.N...A..QH.....Y.....SSH..... 160
D14 Y...V..HY.....N.....DWS.H...V..AS.....N.....DYY..... 160
D15 W...V..YY.....N.....DQS.A...S..SH.....N.....NSA..... 160
D16 A...T..SN.....Y.....DAH.Y...T..HY.....N.....NAS..... 160
D17 E...A..EE.....H.....NTN.N...A..HQ.....Y.....DAQ..... 160
D19 W...S..WA.....N.....SRY.Y...V..SH.....N.....TYD..... 160
D20 A...V..TH.....H.....DYT.T...L..SY.....H.....SDQ..... 160
D21 Y...A..YS.....N.....SAQ.W...T..EA.....Y.....TEE..... 160
D22 K...L..SS.....N.....STS.Y...A..QT.....N.....NQY..... 160
D24 W...V..NH.....N.....SAT.Y...A..QA.....H.....NNY..... 160
D25 A...L..HT.....Y.....TED.S...L..HY.....N.....DTS..... 160
D26 R...L..ST.....N.....DDE.E...V..NT.....N.....NSE..... 160
Repeat 2
Repeat 3
C-Cap
N3C IAEVLQKAAKLN 172
D1 172
D3 172
D5 172
D6 171
D7 172
D9 172
D10 172
D11 172
D12 172
D14 172
D15 172
D16 172
D17 172
D19 172
D20 172
D21 172
D22 172
D24 172
D25 172
D26 172
C-Cap

1

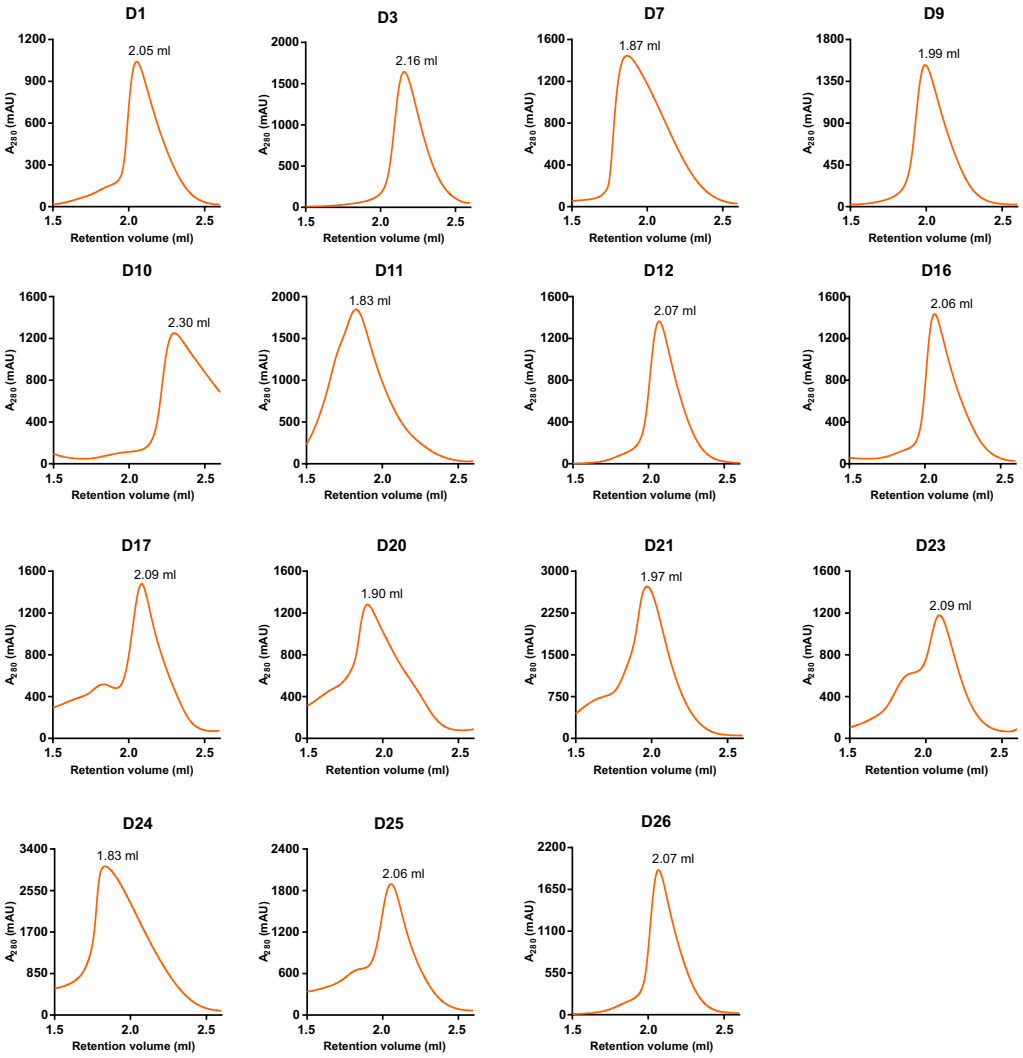
D1
2.05 ml
D3
2.16 ml
D7
1.87 ml
D9
1.99 ml
D10
2.30 ml
D11
1.83 ml
D12
2.07 ml
D16
2.06 ml
D17
2.09 ml
D20
1.90 ml
D21
1.97 ml
D23
2.09 ml
D24
1.83 ml
D25
2.06 ml
D26
2.07 ml
A280 (mAU)
Retention volume (ml)

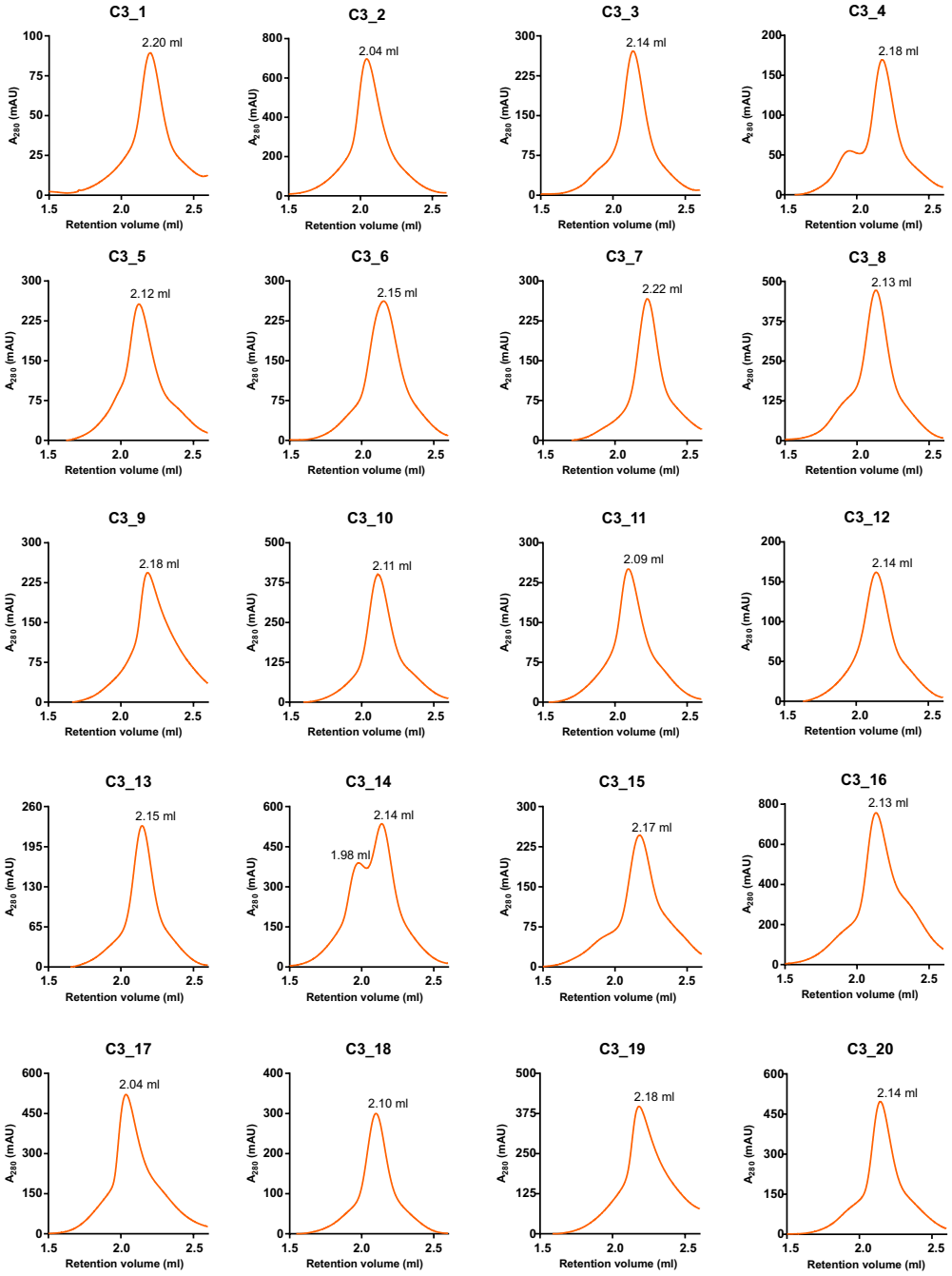
C3_1
2.20 ml
C3_2
2.04 ml
C3_3
2.14 ml
C3_4
2.18 ml
C3_5
2.12 ml
C3_6
2.15 ml
C3_7
2.22 ml
C3_8
2.13 ml
C3_9
2.18 ml
C3_10
2.11 ml
C3_11
2.09 ml
C3_12
2.14 ml
C3_13
2.15 ml
C3_14
2.14 ml
1.98 ml
C3_15
2.17 ml
C3_16
2.13 ml
C3_17
2.04 ml
C3_18
2.10 ml
C3_19
2.18 ml
C3_20
2.14 ml
A280 (mAU)
Retention volume (ml)

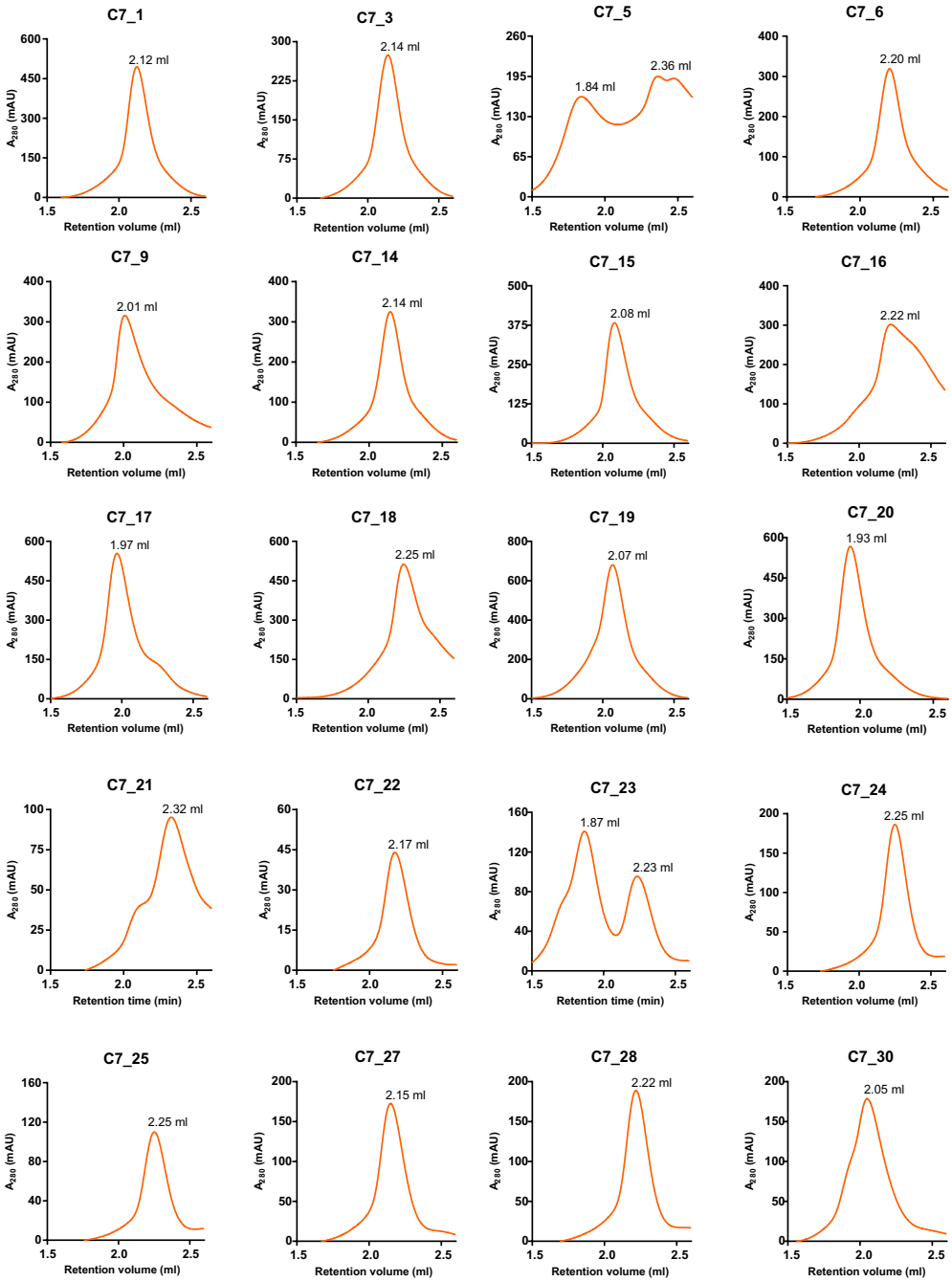
C7_1
2.12 ml
C7_3
2.14 ml
C7_5
1.84 ml
2.36 ml
C7_6
2.20 ml
C7_9
2.01 ml
C7_14
2.14 ml
C7_15
2.08 ml
C7_16
2.22 ml
C7_17
1.97 ml
C7_18
2.25 ml
C7_19
2.07 ml
C7_20
1.93 ml
C7_21
2.32 ml
C7_22
2.17 ml
C7_23
1.87 ml
2.23 ml
C7_24
2.25 ml
C7_25
2.25 ml
C7_27
2.15 ml
C7_28
2.22 ml
C7_30
2.05 ml
Retention volume (ml)
Retention time (min)

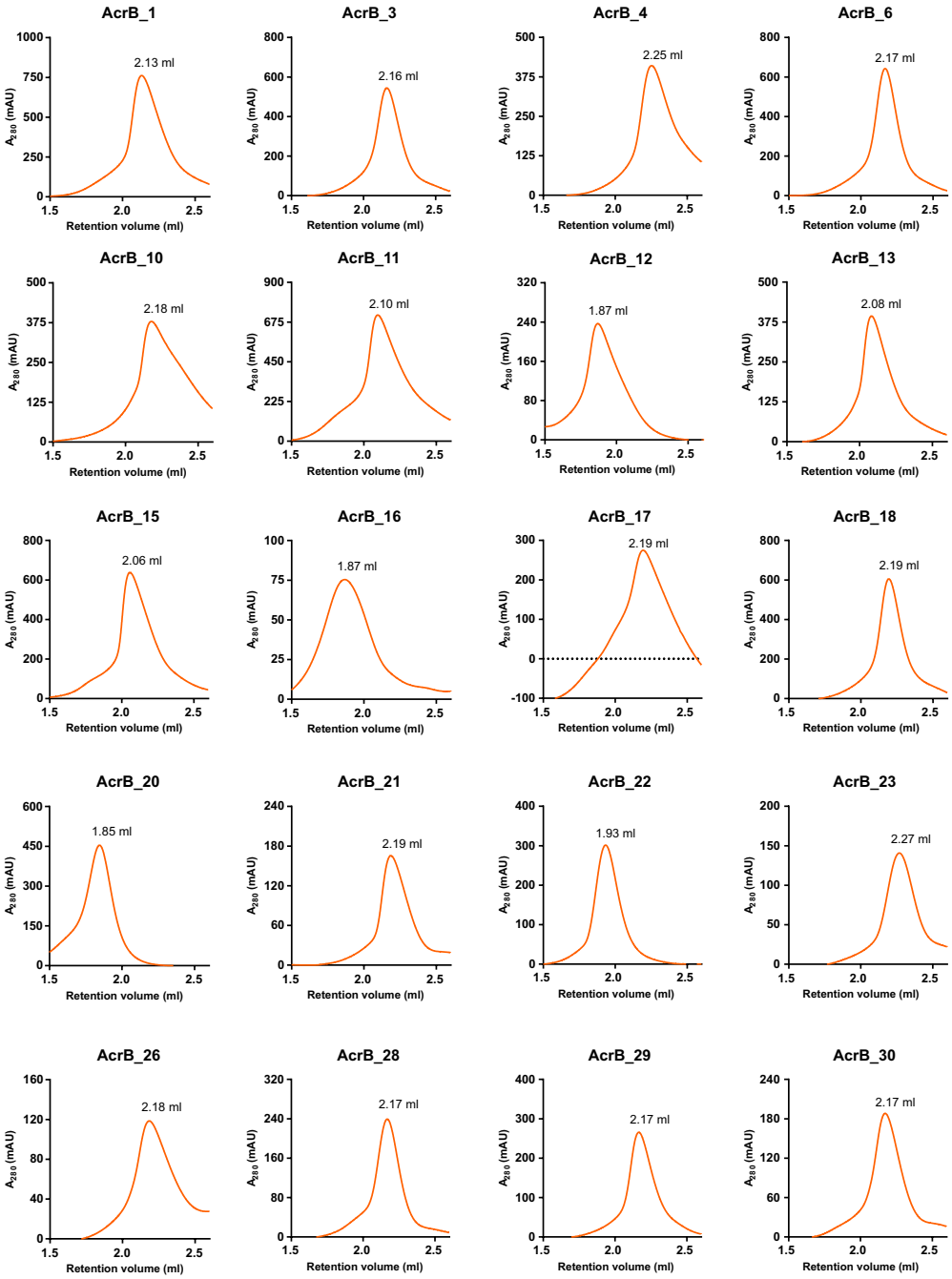

Supporting Information Figure S3: Analytical SEC profiles of all DARPins of the new library appearing in this study.

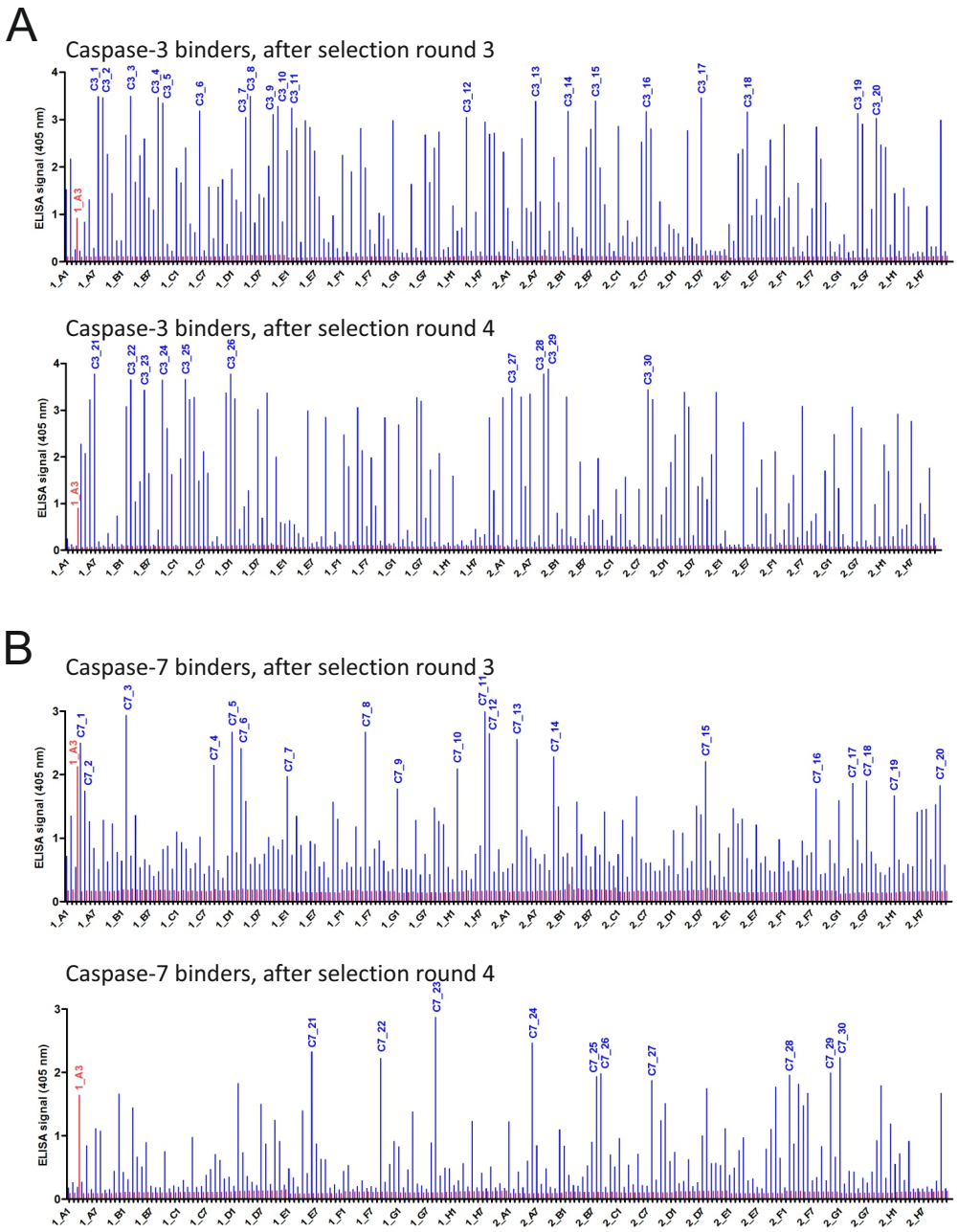
A
Caspase-3 binders, after selection round 3
ELISA signal (405 nm)
Caspase-3 binders, after selection round 4
ELISA signal (405 nm)
B
Caspase-7 binders, after selection round 3
ELISA signal (405 nm)
Caspase-7 binders, after selection round 4
ELISA signal (405 nm)

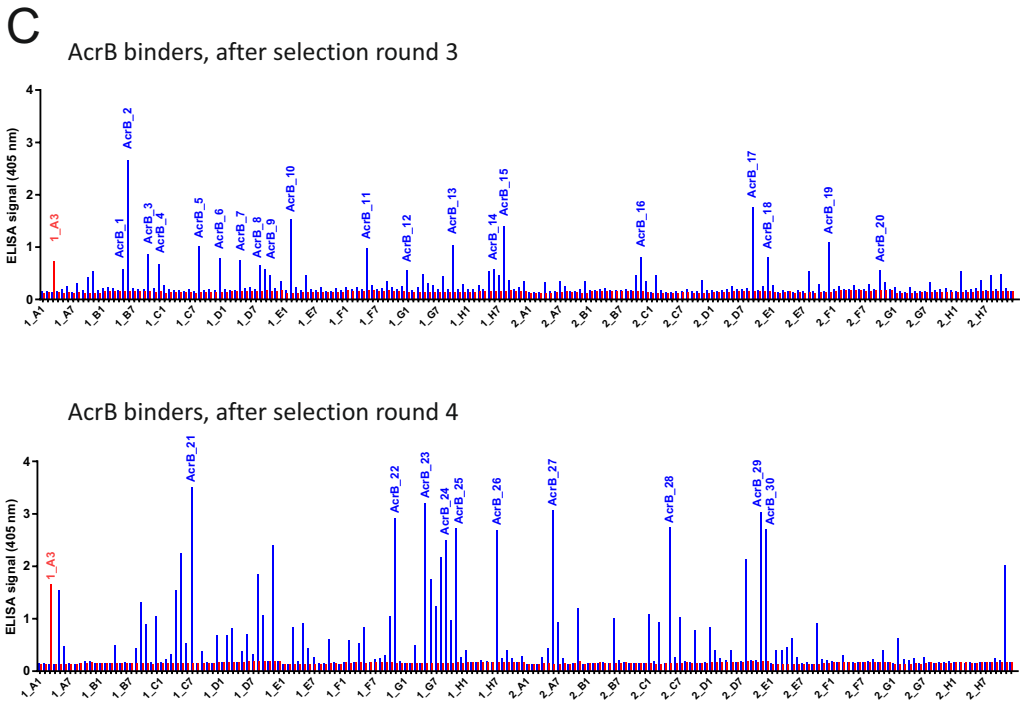

Supporting Information Figure S4: Crude cell extract ELISAs. DARPins selected against caspase-3 (A), caspase-7 (B) and AcrB (C) were probed for binding against the respective target and the control protein MBP.

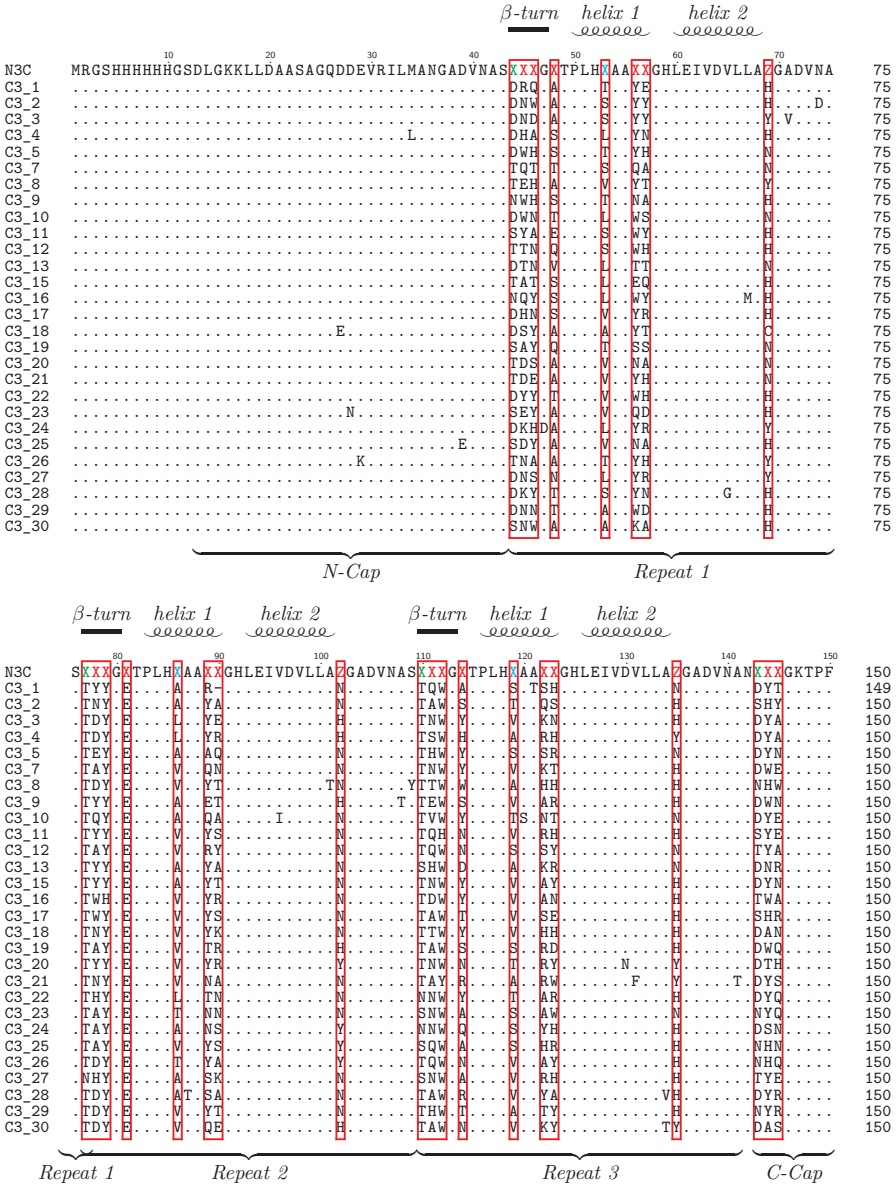

DOI: 10.1002/pro.2312,

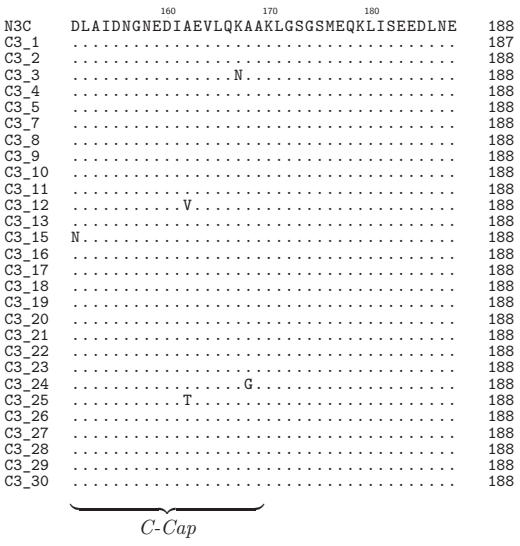
160 170 180
N3C DLAIDNGNEDIAEVLQKAAKLGSGSMEQKLISEEDLNE 188
C3_1 187
C3_2 188
C3_3 .....N..... 188
C3_4 188
C3_5 188
C3_7 188
C3_8 188
C3_9 188
C3_10 188
C3_11 188
C3_12 .....V..... 188
C3_13 188
C3_15 N..... 188
C3_16 188
C3_17 188
C3_18 188
C3_19 188
C3_20 188
C3_21 188
C3_22 188
C3_23 188
C3_24 .....G..... 188
C3_25 .....T..... 188
C3_26 188
C3_27 188
C3_28 188
C3_29 188
C3_30 188
C-Cap

2

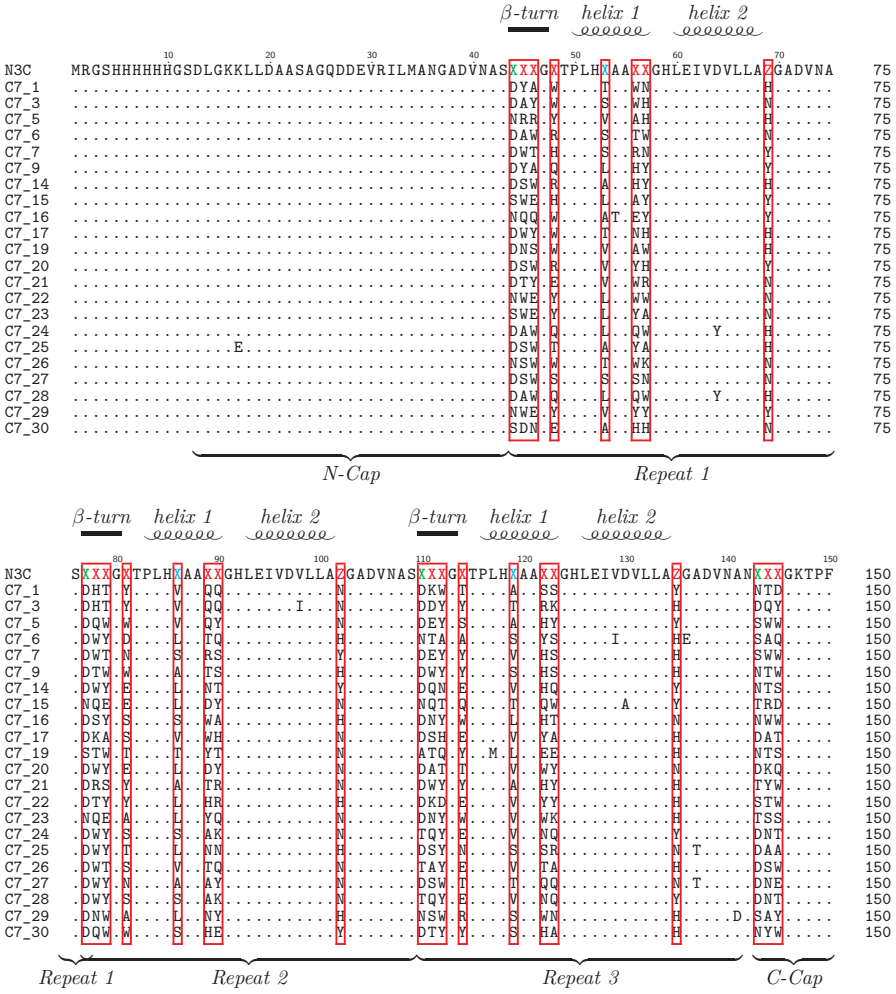

DOI: 10.1002/pro.2312, ©2013 The Protein Society

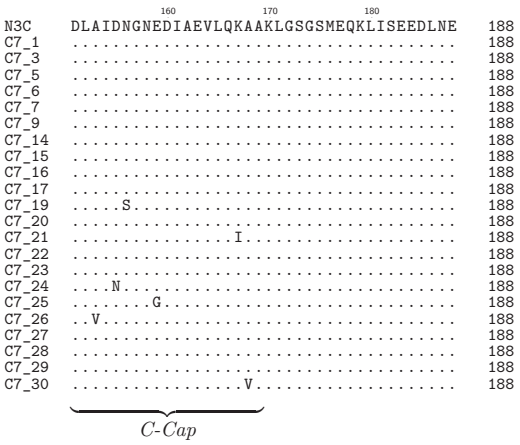
160 170 180
N3C DLAIDNGNEDIAEVLQKAAKLGSGSMEQKLISEEDLNE 188
C7_1 188
C7_3 188
C7_5 188
C7_6 188
C7_7 188
C7_9 188
C7_14 188
C7_15 188
C7_16 188
C7_17 188
C7_19 .....S..... 188
C7_20 188
C7_21 .....I..... 188
C7_22 188
C7_23 188
C7_24 ....N..... 188
C7_25 .....G..... 188
C7_26 ..V..... 188
C7_27 188
C7_28 188
C7_29 188
C7_30 .....V..... 188
C-Cap

2

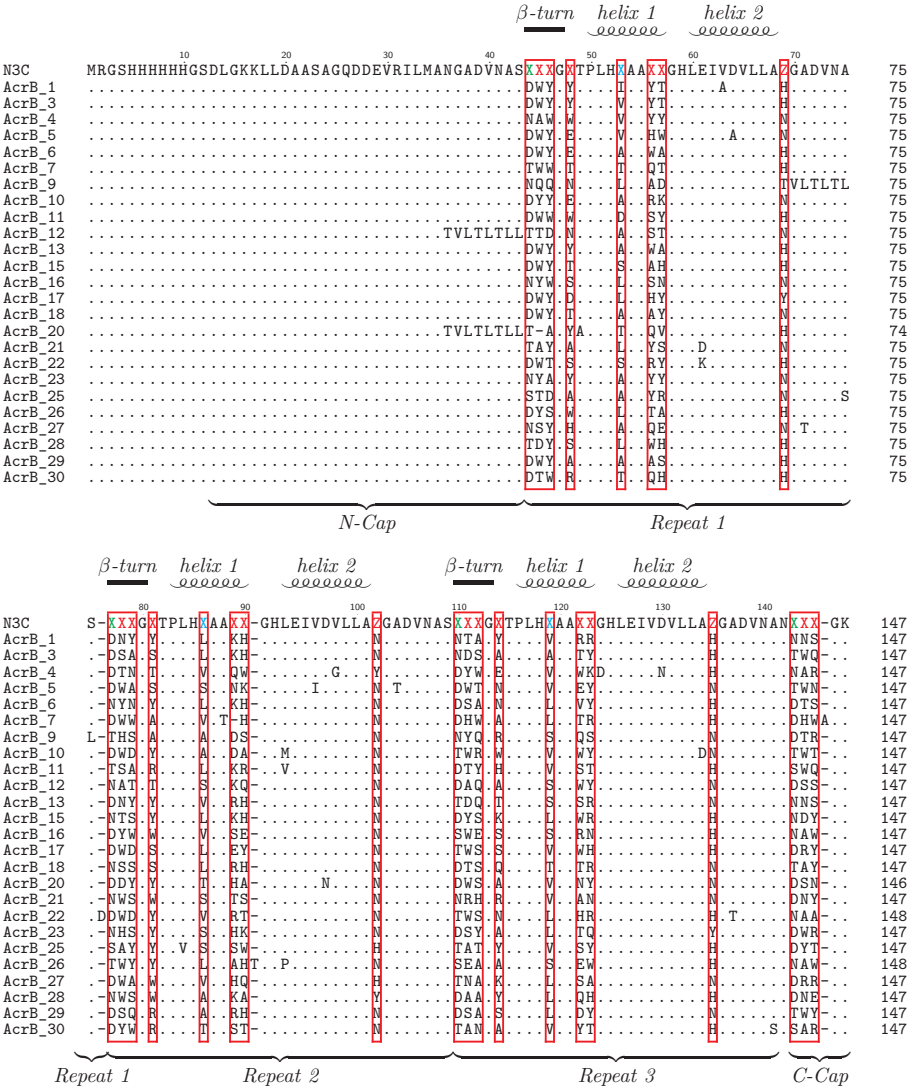

DOI: 10.1002/pro.2312, ©2013 The Protein Society

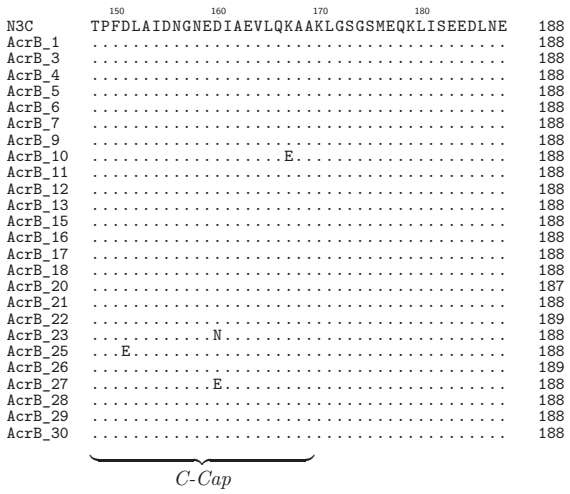
150 160 170 180
N3C TPFDLAIDNGNEDIAEVLQKAAKLGSGSMEQKLISEEDLNE 188
AcrB_1 188
AcrB_3 188
AcrB_4 188
AcrB_5 188
AcrB_6 188
AcrB_7 188
AcrB_9 188
AcrB_10 .....E..... 188
AcrB_11 188
AcrB_12 188
AcrB_13 188
AcrB_15 188
AcrB_16 188
AcrB_17 188
AcrB_18 188
AcrB_20 187
AcrB_21 188
AcrB_22 189
AcrB_23 .....N..... 188
AcrB_25 ...E..... 188
AcrB_26 189
AcrB_27 .....E..... 188
AcrB_28 188
AcrB_29 188
AcrB_30 188
C-Cap

2

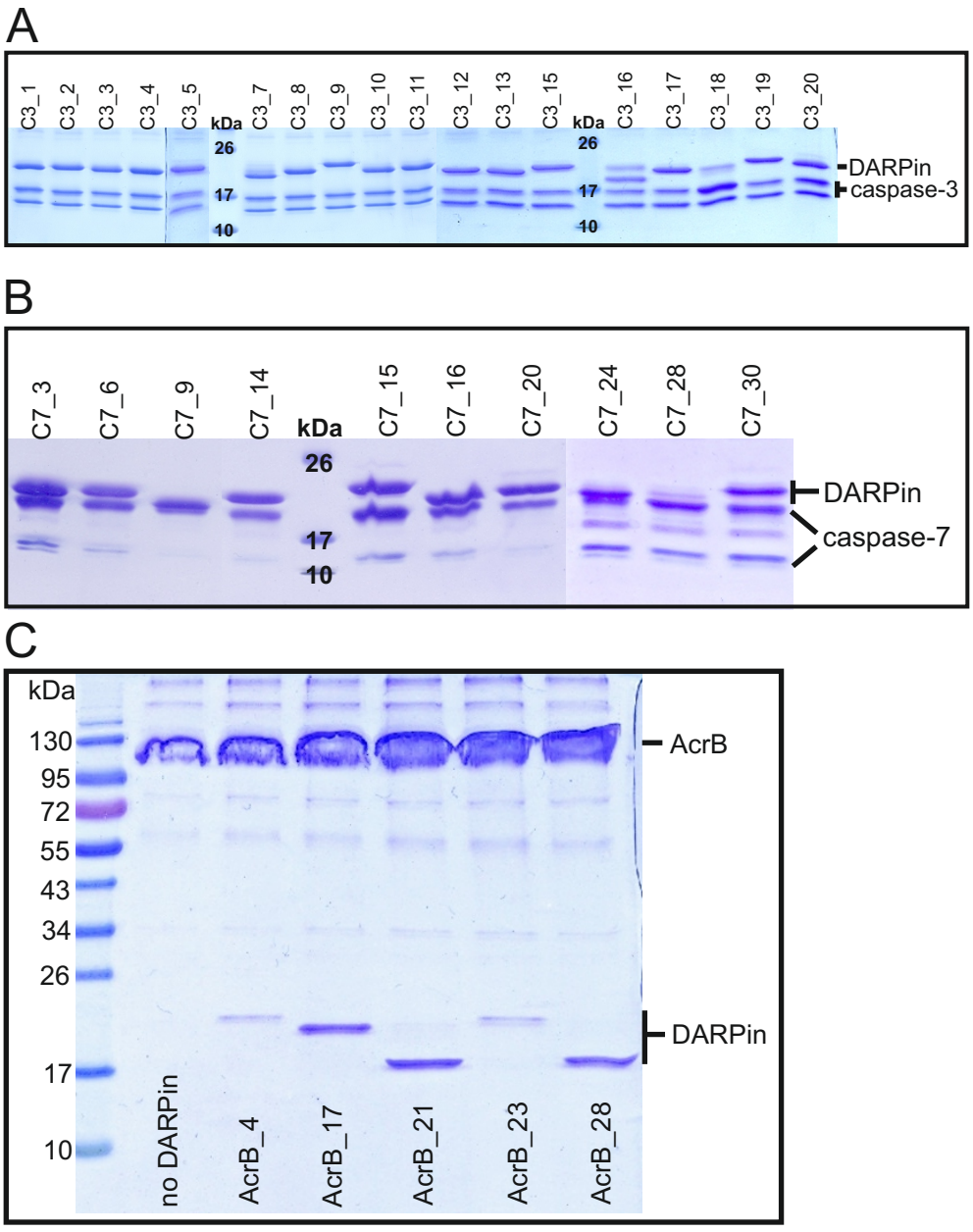

Supporting Information Figure S8: DARPins specific for caspase-3 (A), caspase-7 (B) and AcrB (C) were co-purified by SEC with their targets (example in Figure 6B) and the complex peak fractions were analyzed by SDS-PAGE. The double band for C3_16 in (A) can be explained by incomplete denaturation of this DARPin during SDS-PAGE. AcrB_4 and AcrB_23 in (C) appear to partially dissociate from AcrB during SEC analysis, owing to their modest affinity (Figure 6F).

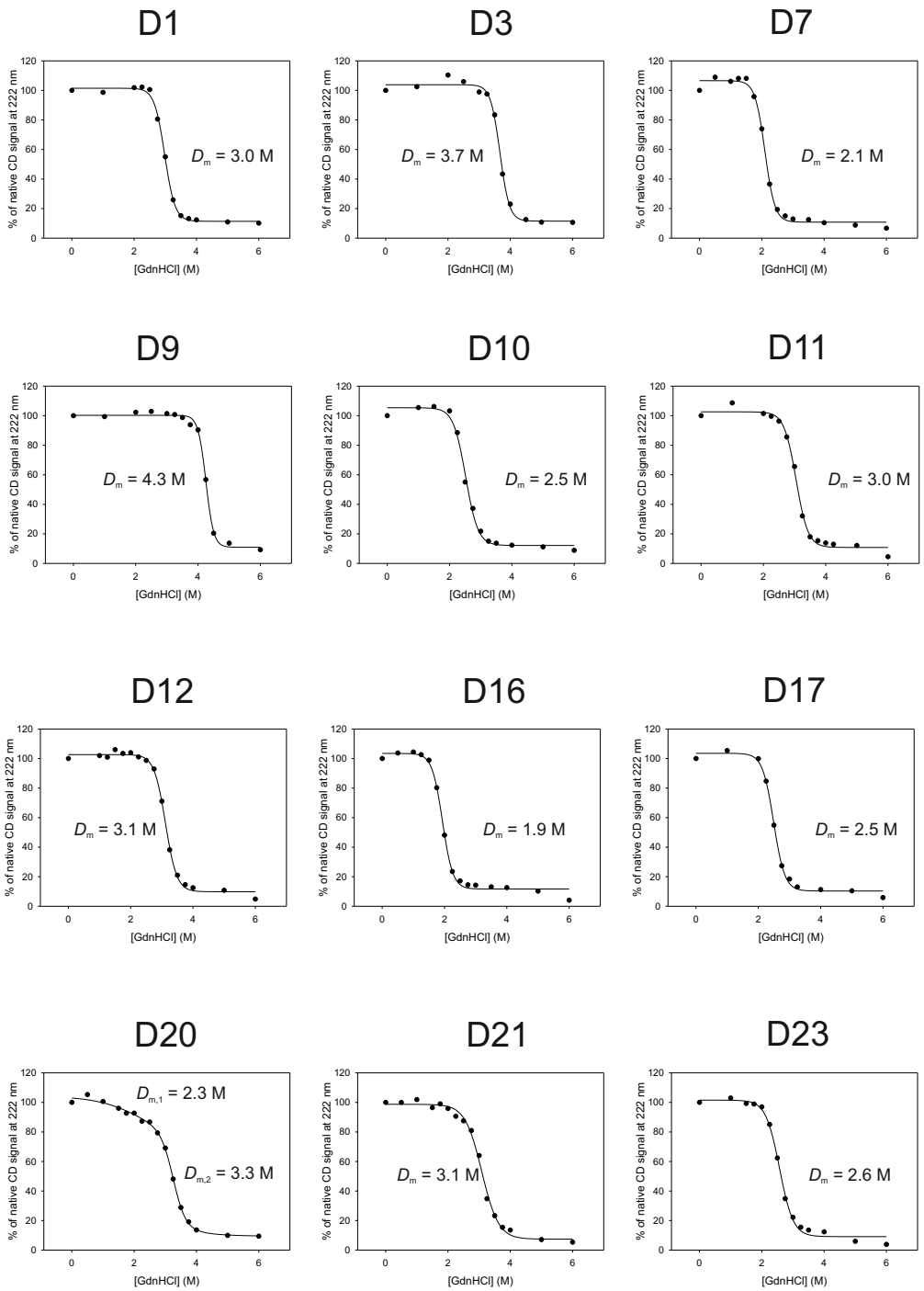
D1
D3
D7
D9
D10
D11
D12
D16
D17
D20
D21
D23
% of native CD signal at 222 nm
[GdnHCl] (M)
D_m = 3.0 M
D_m = 3.7 M
D_m = 2.1 M
D_m = 4.3 M
D_m = 2.5 M
D_m = 3.0 M
D_m = 3.1 M
D_m = 1.9 M
D_m = 2.5 M
$D_{m,1}$ = 2.3 M
$D_{m,2}$ = 3.3 M
D_m = 3.1 M
D_m = 2.6 M

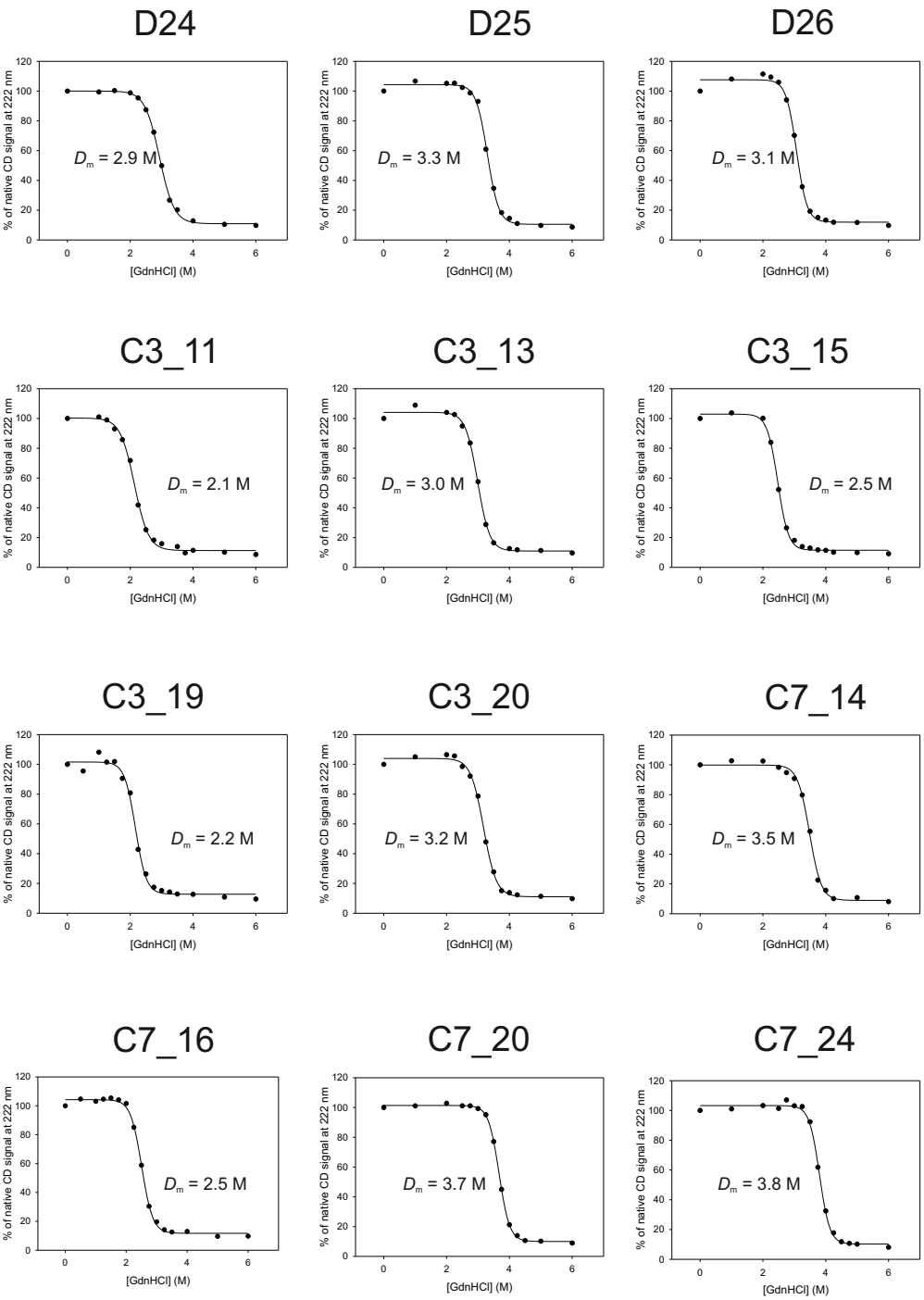
D24
D25
D26
C3_11
C3_13
C3_15
C3_19
C3_20
C7_14
C7_16
C7_20
C7_24
% of native CD signal at 222 nm
[GdnHCl] (M)
D_m = 2.9 M
D_m = 3.3 M
D_m = 3.1 M
D_m = 2.1 M
D_m = 3.0 M
D_m = 2.5 M
D_m = 2.2 M
D_m = 3.2 M
D_m = 3.5 M
D_m = 2.5 M
D_m = 3.7 M
D_m = 3.8 M

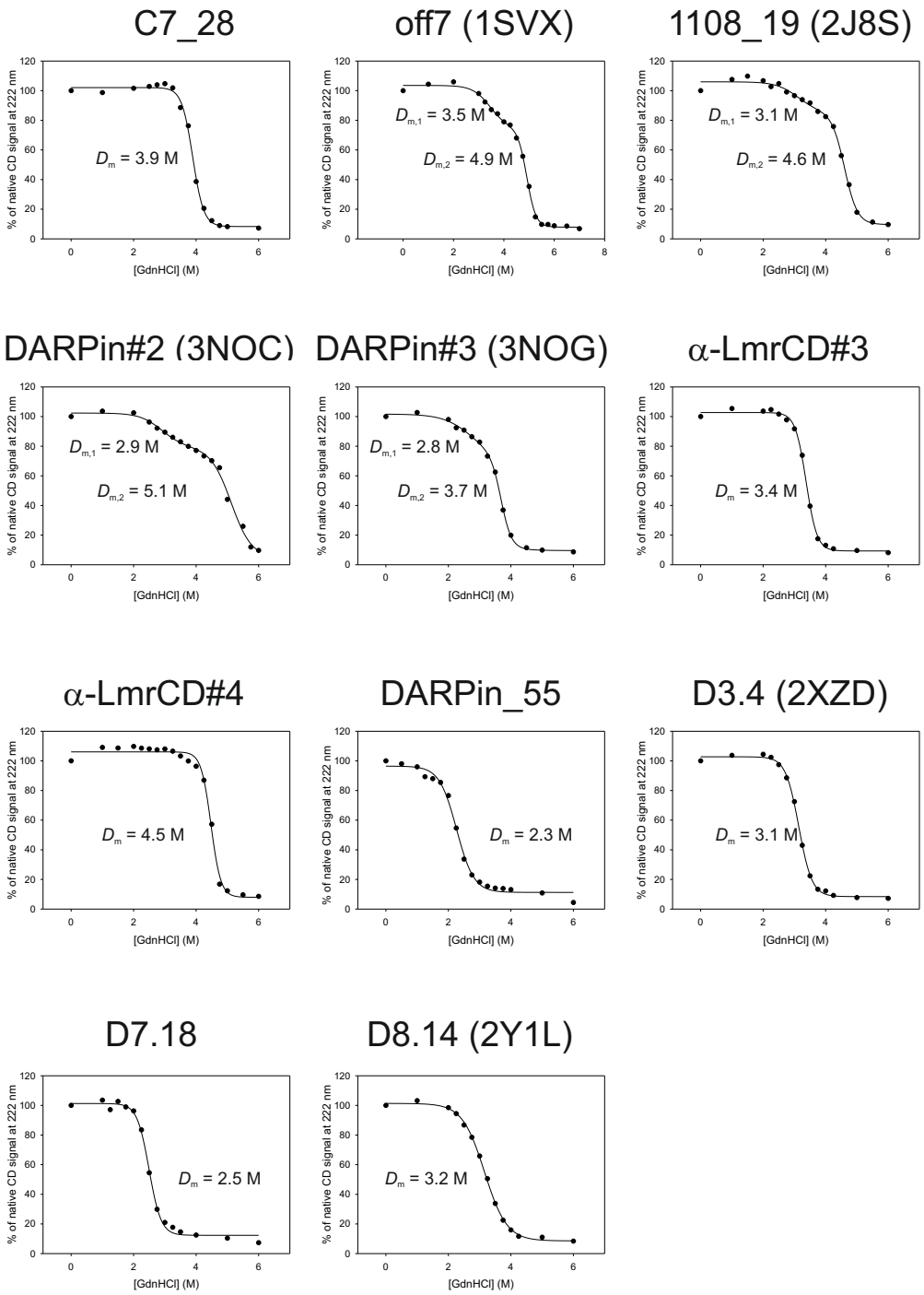
C7_28
off7 (1SVX)
1108_19 (2J8S)
DARPin#2 (3NOC)
DARPin#3 (3NOG)
α-LmrCD#3
α-LmrCD#4
DARPin_55
D3.4 (2XZD)
D7.18
D8.14 (2Y1L)
% of native CD signal at 222 nm
[GdnHCl] (M)
D_m = 3.9 M
$D_{m,1}$ = 3.5 M
$D_{m,2}$ = 4.9 M
$D_{m,1}$ = 3.1 M
$D_{m,2}$ = 4.6 M
$D_{m,1}$ = 2.9 M
$D_{m,2}$ = 5.1 M
$D_{m,1}$ = 2.8 M
$D_{m,2}$ = 3.7 M
D_m = 3.4 M
D_m = 4.5 M
D_m = 2.3 M
D_m = 3.1 M
D_m = 2.5 M
D_m = 3.2 M

Supporting Information Figure S9: Equilibrium unfolding curves of original and new DARPins. 25 new DARPins (15 unselected DARPins (denoted by a "D" before the number), 5 DARPins each specific for caspase-3 and caspase-7 (denoted by "C3_" and "C7_" before the number)) and original DARPins off7 (PDB 1SVX, against MBP)[12], 11_0819 (PDBs 2J8S and 4DX5, against AcrB)[28,36], DARPin#2 and #3 (PDBs 3NOC and 3NOG, against AcrB)[42], α-LmrCD#3 and #4 (against LmrCD)[30], DARPin#55 (against MsbA)[29], D3.4 (PBD 2XZD, against caspase-3)[40], D7.18 (against caspase-7, to be published) and D8.14 (PDB 2Y1L, to be published) were analyzed by GdnHCl unfolding. Monophasic or biphasic sigmoidal equations were fitted to the experimental data (Equations 1 and 2, see Materials and Methods) to determine midpoints of denaturation (D_m for monophasic and $D_{m,1}$ and $D_{m,2}$ for biphasic unfolding curves).

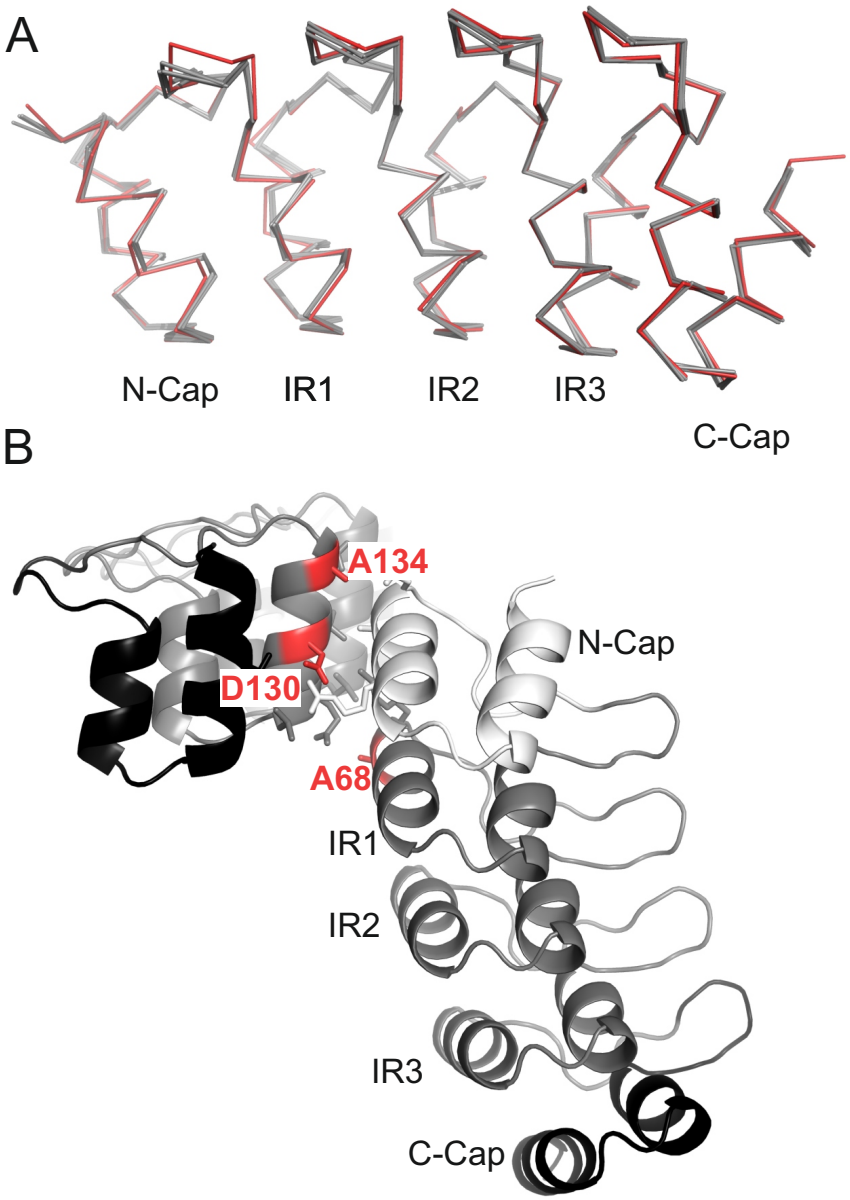

Supporting Information Figure S10: (A) DARPin C7_16 (red) is superimposed with a full-consensus DARPin containing an optimized C-cap (2XEE, Kramer et al. 2010, all four chains of the asymmetric unit are shown in grey). (B) Analysis of DARPin-mediated crystal contact of the C7_16-caspase-7 complex structure. The crystal contact interface involves low-entropy residues A68, A130 and D134 (highlighted in red), which were lysines and glutamates, respectively, in the original DARPin library.

6 Appendix

Bioorganic & Medicinal Chemistry Letters 21 (2011) 1162–1166

Contents lists available at ScienceDirect

Bioorganic & Medicinal Chemistry Letters

journal homepage: www.elsevier.com/locate/bmcl

HIV-1 protease inhibition potential of functionalized polyoxometalates

Andreas Flütsch [b], Thilo Schroeder [b], Markus G. Grütter [b], Greta R. Patzke [a,*]

[a] Institute of Inorganic Chemistry, University of Zurich, Winterthurerstrasse 190, CH-8057 Zurich, Switzerland
[b] Department of Biochemistry, University of Zurich, Winterthurerstrasse 190, CH-8057 Zurich, Switzerland

ARTICLE INFO

Article history:
Received 22 October 2010
Revised 20 December 2010
Accepted 21 December 2010
Available online 25 December 2010

Keywords:
Polyoxometalates
HIV-1 protease inhibition
Functionalized polyoxotungstates
Anti-HIV drugs

ABSTRACT

Polyoxometalates (POMs) are interesting biomedical agents due to their versatile anticancer and antiviral properties, such as remarkable anti-HIV activity. Although POMs are tunable and easily accessible inorganic drug prototypes in principle, their full potential can only be tapped by enhancing their biocompatibility, for example, through organic functionalization. We have therefore investigated the HIV-1 protease inhibition potential of functionalized Keggin- and Dawson-type POMs with organic side chains. Their inhibitory performance was furthermore compared to other POM types, and the buffer dependence of the results is discussed. In addition, chemical shift mapping NMR experiments were performed to exclude POM–substrate interactions. Whereas the introduction of organic side chains into POMs is a promising approach in principle, the influence of secondary effects on the reaction system also merits detailed investigation.

Polyoxometalates (POMs) are transition metal oxide clusters that are preferably formed with W, Mo and V in their high oxidation states.[1] Their ever growing number of complex structural architectures brings forward an impressive application potential that attracts widespread research attention, for example, with respect to key technological applications,[2] (electro)catalytic processes,[3] magnetic materials[4] and nanotechnology.[5] Another special feature of POMs is their versatile bioactivity that leads to antibacterial, anticancer and antiviral properties.[6] These have been widely reviewed over the past years and POMs have been proven to be active against a wide range of viruses, including different influenza strains, Dengue fever virus and SARS coronavirus.[7] They have furthermore been tested as promising anti-HIV agents since the full outbreak of the AIDS epidemic in the 1980s. The first breakthrough was reported in 1988 when the first in vivo studies on humans were performed with the $[NaSb_9W_{21}O_{86}]^{18-}$ polyanion (commonly abbreviated as HPA-23).[8] However, HPA-23 caused severe side effects at higher dosages that forced the patients to discontinue the therapy.[8] Since then, the search for 'second generation' anti-HIV POMs with reduced toxicity was continued and the $[PTi_2W_{10}O_{40}]^{7-}$ polyanion (abbreviated as PM-19) was, for example, identified as a potential antiviral drug capable of inhibiting the replication of HIV-1[9] and herpes simplex virus (HSV)[10] in vitro.

Despite the multitude of empirical investigations on the antiviral activity of POMs, little is known about their interaction mechanisms with viruses or cells.[11] Concerning the anti-HIV activity, Inoue et al. investigated the inhibition of HIV-1 reverse transcriptase (RT) by various POMs.[12] Interestingly, cell culture experiments showed that the anti-HIV-1 activity of the POMs under consideration was not correlated with their HIV-1 RT inhibition.[12] A follow-up study by the same group identified the Keggin- and Dawson-POM types as possible 'lead compounds' for anti-HIV activity.[13] In 2001, a novel inhibition mechanism of HIV-1 protease by Dawson-type POMs was proposed in a pioneering study by Hill et al.[14] The high activity of the niobium-substituted tungstate α_2-$[P_2W_{17}NbO_{62}]^{7-}$ was explained with its binding to the flexible hinge regions on the surface of the HIV-1 protease. As most organic HIV-1 protease inhibitors bind into the active site, larger inorganic cluster molecules, such as POMs, would thus open up new ways of inhibition. Such alternative interaction pathways of POMs with HIV-1 protease would render them less sensitive towards the frequently occurring mutations of HIV-1, thereby circumventing the problem of therapeutic resistance in current AIDS therapy.[15] In addition, most anti-AIDS drugs are costly compounds that have to be administered in inconveniently high doses several times a day. POMs would offer economic advantage over the current anti-AIDS drugs in principle, because they can easily be synthesized from readily available precursors in a few synthetic steps.

The following years witnessed further reports on antiviral POMs[6a] and new insights were obtained regarding the interaction of POMs with human/bovine serum albumin[16] or protein kinase CK2.[17] Nevertheless, the fundamental issue of POM toxicity still remains to be overcome in order to turn them into powerful, versatile and low-cost inorganic anti-HIV agents. However, the development of hybrid and functionalized POMs is now proceeding rapidly[18] and thus provides new inspirations for research on inorganic anti-HIV agents together with the incorporation of antiviral

* Corresponding author. Tel.: +41 44 635 4691; fax: +41 44 635 6802.
E-mail address: greta.patzke@aci.uzh.ch (G.R. Patzke).

0960-894X/$ - see front matter © 2010 Elsevier Ltd. All rights reserved.
doi:10.1016/j.bmcl.2010.12.103

POMs into biomacromolecular matrices as an additional strategy.[19] The increasing gap between these growing classes of novel POMs and their biomedical characterization inspired us to screen a selected variety of POM types with respect to their inhibitory effect on HIV-1 protease. Firstly, we compared the inhibitory potential of POMs with different cluster sizes. We then focused on Keggin- and Dawson-type POMs with different organic side chains in order to evaluate the influence of the functionalization on the inhibitory performance. In addition, we placed emphasis on methodological issues: the results are critically discussed with respect to their considerable buffer dependence. Furthermore, we present NMR studies in solution to exclude the possibility of POM–substrate interactions.

All POMs were synthesized according to published procedures and they are summarized in Table 1. Figure 1 illustrates the structural motifs (Keggin- and Dawson-type) for the majority of the investigated POMs and their organically substituted derivatives. They have emerged from recently developed novel functionalization approaches.[20] POM 1 has been included as a representative of 'sandwich-type' lacunary POM building blocks with embedded transition metal cations. POMs 2–5 are based on the recently discovered $\{Ln_6W_{63}\}$ cluster[21] as the largest polyoxotungstate type among the present selection. These compounds are of general interest, because the incorporation of lanthanoid cations into POMs is promising with respect to their potential double function as diagnostic (e.g., luminescence or MRI) and therapeutic agents.[16a,22] POM 20 (Preyssler type) bears resemblance to the Dawson type due to the arrangement of its five PW_5 units into a Dawson-related surface. POM 28 (Lindqvist type) as the most compact and smallest structure type rounds off the 'classic' POM spectrum.

The POMs were characterized by IR spectroscopy and other analytical methods if required (e.g., NMR or single crystal structure determination) and they were stable under the applied experimental conditions. HIV-1 protease was expressed in *Escherichia coli* BL21 (DE3) pLysS cells and purified by anionic exchange and size exclusion chromatography according to literature protocols (for further experimental details cf. Supplementary data).[23] Given that

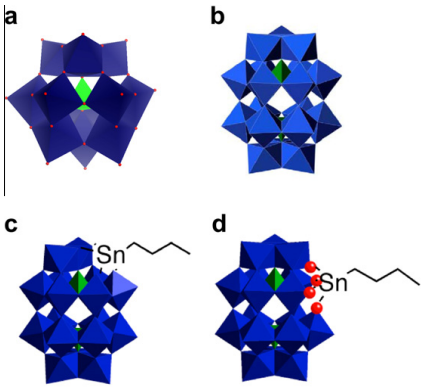

Figure 1. Overview of the most important POM types investigated in the present study: (a) Keggin type, (b) Dawson type, (c) α_2-substituted Dawson type, (d) α_1-substituted Dawson type.

HIV-1 protease has an autocatalytic activation site as well as autoprotolytic activity,[24] special attention must be paid to the high purity of the protein to precisely determine its concentration and to prevent possible interaction of the POMs with degraded protease fragments during the protease assays. For that reason, the substitution of one single amino acid, namely glutamine at position 7 to lysine (Q7K), has been performed to reach a 100-fold increase of the protein stability.[24] This residue is located in the first loop after the first β-strand in the protein and at a considerable spatial distance to the flexible hinge regions that were proposed as POM binding sites.[14] Therefore, it can be practically excluded that the use of the HIV-1 mutant Q7K affects the inhibitory potential of the POMs in comparison with the wild type. The introduction of the positively charged lysine might even exert a productive elec-

Table 1
Survey of the POMs screened for HIV-1 protease inhibition

No.	Formula	Cations	Type	Solvent	Ref.
1	$[Na_3Cu_3(H_2O)_9(AsW_9O_{33})_2]^{9-}$	Na_9	Dimer	H_2O	28
2	$[Cs\subset Tb_6As_6W_{63}O_{218}(H_2O)_{14}(OH)_4]^{25-}$	$Na_{21}Cs_4$	Hexamer	H_2O	21
3	$[Cs\subset Dy_6As_6W_{63}O_{218}(H_2O)_{14}(OH)_4]^{27-}\cdot Cl_2$	$Na_{22}Cs_5$	Hexamer	H_2O	21
4	$[Cs\subset Ho_6As_6W_{63}O_{218}(H_2O)_{14}(OH)_4]^{27-}\cdot Cl_2$	$Na_{22}Cs_5$	Hexamer	H_2O	21
5	$[Cs\subset Er_6As_6W_{63}O_{218}(H_2O)_{14}(OH)_4]^{25-}$	$Na_{21}Cs_4$	Hexamer	H_2O	21
6	α_2-$[P_2W_{17}O_{61}SnR]^{7-}$ (R = $C_3H_5O_2$)	TBA_6H	Dawson	DMSO	20
7	α_2-$[P_2W_{17}O_{61}SnR]^{6-}$ (R = C_4H_6O)	TBA_6	Dawson	DMSO	20
8	α_2-$P_2W_{17}O_{61}SnR]^{7-}$ (R = C_6H_8NO)	TBA_7	Dawson	DMSO	20
9	α_2-$[P_2W_{17}O_{61}SnR]^{7-}$ (R = C_4H_9)	TBA_6H	Dawson	DMSO	20
10	α_2-$[P_2W_{17}O_{61}SnR]^{7-}$ (R = $C_{18}H_{32}N_3O_5S$)	TBA_7	Dawson	DMSO	20
11	α_2-$[PW_{11}O_{39}SnR]^{4-}$ (R = $C_3H_5O_2$)	TBA_4	Keggin	DMSO	20
12	α_2-$[PW_{11}O_{39}SnR]^{4-}$ (R = C_4H_9)	TBA_4	Keggin	DMSO	20
13	α_2- $[PW_{11}O_{39}SnR]^{4-}$ (R = $C_{18}H_{32}N_3O_5S$)	TBA_4	Keggin	DMSO	20
14	α_1-$[P_2W_{17}O_{61}SnR]^{7-}$ (R = $C_3H_5O_2$)	TBA_6H	Dawson	DMSO	20
15	α_1-$[P_2W_{17}O_{61}SnR]^{7-}$ (R = C_6H_8NO)	TBA_7	Dawson	DMSO	20
16	α_1-$[P_2W_{17}O_{61}SnR]^{7-}$ (R = C_4H_9)	TBA_6H	Dawson	DMSO	20
17	α_2-$[P_2V_3W_{15}O_{63}R]^{7-}$ (R = $C_{13}H_{19}N$)	TBA_5	Dawson	DMSO	20
18	$[H_2W_{12}O_{42}]^{6-}$	$(NH_4)_6$	Individual	H_2O	23
19	$[NaSb_9W_{21}O_{86}]^{18-}$	$(NH_4)_{18}$	Individual	H_2O	29
20	$[NaP_5W_{30}O_{110}]^{14-}$	K_{14}	Preyssler	H_2O	29
21	α/β-$[P_2W_{18}O_{62}]^{6-}$	K_6	Dawson	H_2O	29
22	α_1-$[LiP_2W_{17}O_{61}]^{9-}$	K_9	Monolacunary Dawson	H_2O	29
23	α_2-$[P_2W_{17}O_{61}]^{10-}$	K_{10}	Monolacunary Dawson	H_2O	29
24	α_1-$[P_2W_{17}(NbO_2)O_{61}]^{7-}$	K_7	Dawson	H_2O	14
25	α_1-$[P_2W_{17}(NbO_2)O_{61}]^{7-}$	K_7	Dawson	H_2O	14
26	$[PW_{12}O_{40}]^{3-}$	NaH_2	Keggin	H_2O	30
27	$[PTi_2W_{10}O_{40}]^{7-}$	K_7	Keggin	H_2O	31
28	$[Pr(W_5O_{18})_2]^{9-}$	K_9	Lindqvist	H_2O	32

trostatic effect upon the binding of the highly negatively charged POMs to the protease. Standardized protease assays[25] were performed as described in the Supplementary data and an influence of POM absorbance on the measurements was excluded. The protease substrate was dissolved in dimethyl sulfoxide (DMSO) and two different buffer solutions were applied: buffer 1 contained a final DMSO concentration of 10%, whereas the DMSO content of buffer 2 was 1% (for details cf. Supplementary data). The stability of the protease during the assays was confirmed by Selwyn tests,[26] known as the standardized enzymatic stability test till date, under both buffer conditions. The inhibitory potential of all POMs was analyzed in triplicate measurements with Saquinavir as a standard inhibitor under both buffer conditions. Furthermore, the ingredients of the two different buffers were compared under the above conditions using POM 25 with a known high inhibitory activity[14] (cf. Table 1 and Table S-1). The higher concentration of DMSO and the additional detergent Nonidet P-40 obviously exerted the most significant influence on the measured inhibition (cf. Fig. S-1). Although the additional detergent Nonidet P-40 is supposed to stabilize the protease during the assay,[25] the enzymatic reaction also worked in the detergent-free buffer 2 with a lower DMSO concentration. Most importantly, these buffer additive tests show that the POM-induced protease inhibition is not a mere artefact arising from precipitation of protease or substrate during the reaction.

The relative activity of HIV-1 protease Q7K in buffers 1 and 2 is shown in Figure 2: the POMs were added in a 10- or 100-fold excess relative to the protease in buffer 1 and the relative protease activity remained higher than 70% in all reactions, whereas Saquinavir applied in an 1:1 ratio led to 100% inhibition. This excludes experimental setup errors and indicates that no inhibition of the enzymatic reaction by POMs occurred under these conditions. Especially for POMs 24 and 25, this result was unexpected in comparison with their previously reported high potential for HIV-1 protease inhibition.[14]

However, changing the conditions to buffer 2 completely altered the overall activity pattern. Although the use of detergent at 10% DMSO concentration had been reported to exert a stabilizing effect on HIV protease activity,[22] buffer 1 with 1% DMSO and less ingredients was sufficient to keep the protease active. A decline of the enzymatic reaction was observed in almost all experiments, in line with the preceding results:[14] POMs 21, 24 and 25 led to total protease inhibition as well as POMs 9, 12, 14 and 16. For a more detailed discussion of the results obtained in buffer 2, the POMs are classified into water-soluble POMs (1–5, 18–28) and functionalized DMSO-soluble POMs (6–17) with organic side chains. Interestingly, previous studies have pointed out that DMSO influences enzymatic reactions in a rather complex manner that varies widely—from stimulation to inhibitory effects—for the different systems under investigation.[27] However, this does not apply for the pristine HIV-1 protease in the present case and the DMSO dependence of POM-induced HIV-1 protease inhibition in contrast to its general inhibition by Saquinavir points to differences in the interaction mechanisms of organic and inorganic inhibitors, as had been suggested in earlier studies.[14]

A comparison of the water-soluble POMs with significant inhibitory potential (20–25) indicates that POMs related to the Dawson type are generally superior to the remaining POM architectures investigated in this study. POMs 21, 24 and 25 are Dawson structures and POMs 22 and 23 are monolacunary Dawson POMs (α_1- and α_2-isomers, respectively). In comparison with the Dawson type POMs, even the most prominent POMs, namely the aforementioned HPA-23 (POM 19) that was implemented in the first clinical studies[8] and the well-known anti-HIV agent PM-19 of the Keggin type (POM 27),[9] displayed a remarkably lower inhibitory effect.

Concerning POMs 2–5, their larger cluster size did not promote HIV-1 protease inhibition. Likewise, the dimeric structure of POMs 1 and 28 did not bring forward significant inhibitory activity—nor did the smaller $[H_2W_{12}O_{42}]^{6-}$ anion (POM 18) that performed even slightly worse than the Keggin compounds of related size (POMs 26 and 27). These results render the Dawson type especially promising for construction of functionalized antiviral POMs, provided that the above-mentioned buffer influence is taken into account. The dimensions of the Dawson cluster indeed appear to be in the appropriate range for POM/protein interactions as indicated in preceding theoretical studies.[14]

A more detailed comparison of the inhibitory effect among the DMSO-soluble POMs can be found in Figure 3: POMs 11–13 are Keggin type derivatives, whereas POMs 6–10 and 14–17 are Dawson type POMs that were functionalized with organic side chains at the α_1- (POMs 14–16) and α_2-position (POMs 6–10 and 17), respectively. A first glance at Figure 3 shows that the distinction between Keggin and Dawson type POMs is evened out through the introduction of organic residues: the Keggin type POM 12 with a butyl side chain induced complete inhibition of the protease activity (Fig. 3c). Generally, the introduction of a butyl side chain exerted the strongest inhibitory effect among the DMSO-soluble POMs, regardless of the POM framework or the Dawson regiosomer. This effect is even maintained with a 10-fold excess of the butyl-substituted POM 9. In the case of a propionic acid residue, the Keggin type derivative can as well compete with its Dawson analogs in terms of inhibitory effect (Fig. 3a). In parallel, the attach-

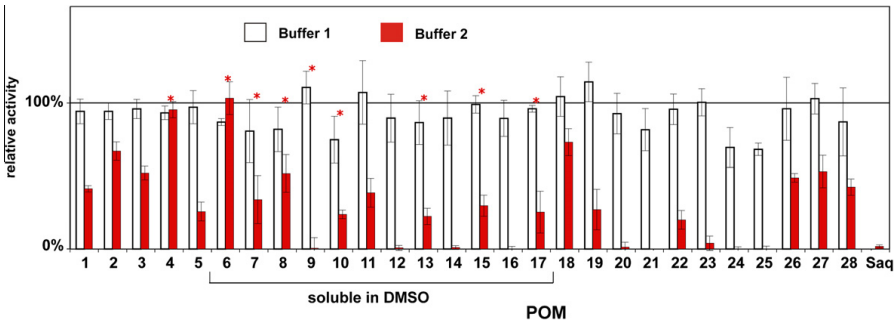

Figure 2. Relative activity of HIV-1 protease in the presence of different POMs as potential inhibitors (cf. Table 1). The reactions were performed in buffer 1 and buffer 2, respectively, and the total reaction volume was 200 µl. POMs were added to a concentration of 3 µM or 300 nM (asterisk). The activity of the protease in reactions without POMs was defined as 100% (Saq = Saquinavir).

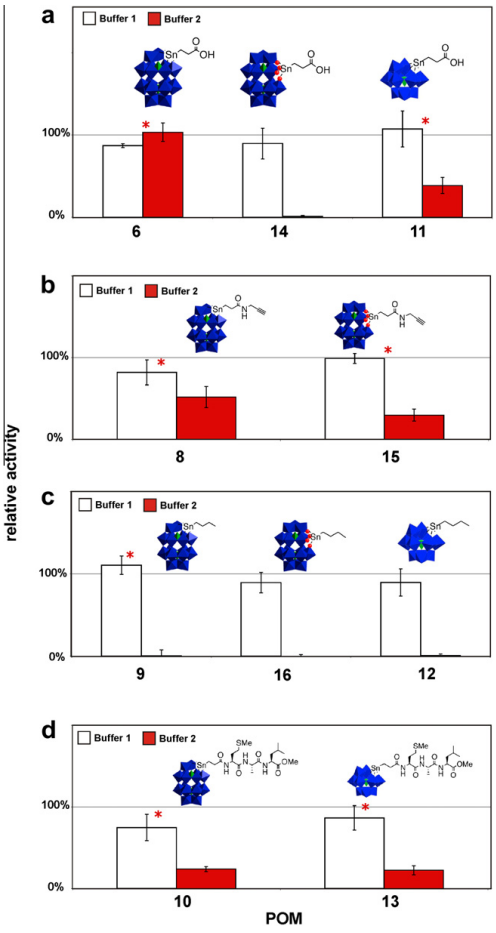

Figure 3. Relative activity of HIV-1 protease Q7K in reactions with DMSO-soluble POMs modified with organic side chains (red asterisks: POMs in 10-fold excess vs. protease, all other POMs were added in 100-fold excess); (a) POM 6, POM 14 and POM 11, (b) POM 8 and POM 15, (c) POM 9, POM 16 and POM 12, (d) POM 10 and POM 13.

ment of a more complex peptide-based side chain significantly reduced the protease activity irrespective of the POM host structure (Keggin or Dawson type, cf. Fig. 3d).

Although these results have to be interpreted with caution due to the limited number of POMs involved in the present study in comparison with the manifold experimental variables (such as buffer composition and POM concentration), their entirety indicates that the functionalization of POMs with organic moieties exerts a productive effect on their potential for HIV-1 protease inhibition.

All in all, the Dawson type POMs displayed the most promising overall inhibitory performance in the present study and it seems that the generally high antiviral potential of this 'classic' type is difficult to obtain with many newly discovered larger polyoxotungstates such as the investigated $\{Ln_6W_{63}\}$ type.[21] In this context, our recent luminescence studies on the interaction of $\{Eu_6W_{63}\}$ and $\{Tb_6W_{63}\}$ with human/bovine serum albumine[16a] also showed that their protein binding modes differ considerably from those of the smaller decatungstate cluster, thus pointing to the POM size as an important factor in structure–activity relationships. However, the introduction of organic side chains may be an important tool to modify structure activity relationships among the different POM cluster types in order to amplify the antiviral potential of POMs in general. This is supported by the fact that the introduction of a butyl group into the Keggin type (POM 12) drastically improves the inhibitory performance in comparison with the pristine Keggin POM 26. Such 'amphiphilic' POMs with unpolar organic substituents turned out to perform quite well in HIV-1 protease inhibition. For that reason, the inhibitory potential of the pristine organic compounds might also be tested as a reference.

However, this result also raises a critical point that should be taken into account for future studies: based on the present buffer additive tests, an interaction of the POMs with the substrate cannot be completely excluded. In order to detect possible interactions of the peptide substrate with POMs, we used solution NMR techniques. In particular, chemical shift mapping 600 MHz proton spectra were recorded on an approx. 100 μM peptide solution at pH 5.0 (100 mM acetate buffer) at 27 °C both in the absence and in the presence of POM 24 that displays significant HIV-1 protease inhibition.[14] The two samples were prepared from the same peptide stock solution, to one of which POM 24 was added. The pH was carefully controlled, and differed by less than 0.1 pH units in the two samples. The region of aliphatic protons displayed very little differences, whereas some amide protons experienced small shift changes. Nevertheless, the observed differences in the spectra were very minor (Fig. 4). From these changes we estimate that the K_d is likely to be in the molar range, strongly disfavoring a specific interaction with reasonable affinity and indicating the presence of a low-affinity, non-specific interaction. We conclude from these data that while a low-affinity non-specific interaction of the POM with the peptide does occur, its strength is so weak that it cannot be the reason for the observed inhibition of the substrate cleavage by the HIV-1 protease.

The ultimate proof of POM–protease interactions would certainly be the crystallization of a POM–protein complex. This challenging goal has never been reached over several decades of anti-HIV studies with POMs. Another option would be a pull-down experiment: POMs linked to beads that are incubated with HIV-1 protease or with substrate, respectively, followed by washing steps and analysis of the residues. This, however, would be a study in its own right, because POM/bead linking methods would have to be developed or, alternatively, HIV-1 protease would have to be stabilized during the coupling.

In summary, the present screening study outlines several methodological issues in the screening of POMs for anti-HIV-1 protease activity that have to be considered in follow-up experiments, namely the composition of the buffer system and the exclusion of POM/substrate interactions. Optimization studies, however, are now worthwhile, because we demonstrated that the functionalization of Dawson and Keggin type POMs with organic moieties is likely to enhance the inhibitory potential and to amplify the range of antiviral POM types, thus rendering them more biocompatible. Further studies concerning the cytotoxicity and cellular uptake of antiviral POMs are under way.

Acknowledgements

This work was supported by the Swiss National Science Foundation (SNSF Professorship PP002-114711/1) and financial support from the University of Zurich is gratefully acknowledged. We are grateful to Prof. Emmanuel Lacôte, Prof. Serge Thorimbert and Prof. Bernold Hasenknopf (UPMC Univ Paris 6, Institut Parisien de Chimie Moléculaire (UMR CNRS 7201)) for supporting us with functionalized polyoxometalates for the present study. We thank

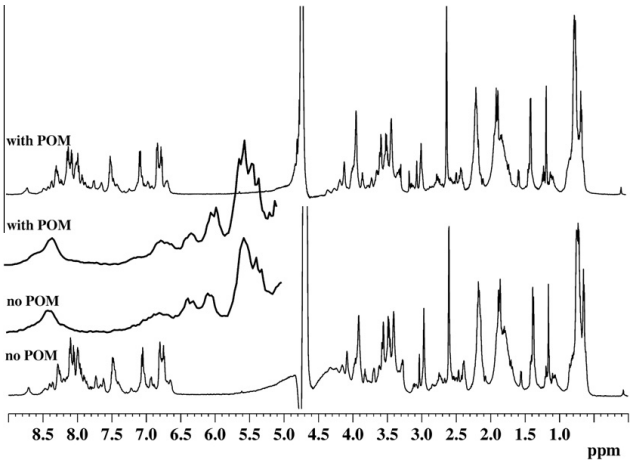

Figure 4. Proton spectra of the peptide substrate in absence (bottom spectrum) and presence (top spectrum) of POM 24, recorded at 600 MHz, T = 300 K. The expansion on the left displays the region from 8.2 to 8.8 ppm, and highlights the typically encountered minor changes in the spectra.

Dr. Firasat Hussain for experimental help regarding POM synthesis and Prof. Dr. Oliver Zerbe (Institute of Organic Chemistry, University of Zurich) for his support with the NMR studies. Furthermore, we are grateful to Dr. Jovan Pavlovic (Institute of Medical Virology, University of Zurich, Switzerland) for providing a template plasmid containing the HIV-1 wild type genome. Saquinavir was obtained through the AIDS Research and Reference Reagent Program, Division of AIDS, NIAID, NIH.

Supplementary data

Supplementary data (expression and purification of HIV-1 protease, synthesis and inhibitor screening of POMs as well as additive screen test comparing the different buffers) associated with this article can be found, in the online version, at doi:10.1016/j.bmcl.2010.12.103.

References and notes

1. (a) *Polyoxometalates: From Platonic Solids to Antiretroviral Activity*; Pope, M. T., Müller, A., Eds.; Kluwer: Dordrecht, 1994; (b) Pope, M. T. *Heteropoly and Isopoly Oxometalates*; Springer: Berlin, 1983; (c) Hill, C. L. *Compr. Coord. Chem. II.* **2003**, *4*, 679.
2. *Polyoxometalate Chemistry: From Topology via Self-Assembly to Applications*; Pope, M. T., Müller, A., Eds.; Kluwer: Dordrecht, 2001.
3. Keita, B.; Nadjo, L. *J. Mol. Catal. A: Chem.* **2007**, *262*, 190.
4. Kögerler, P.; Tsukerblat, B.; Müller, A. *Dalton Trans.* **2010**, *39*, 21.
5. Long, D. L.; Burkholder, E.; Cronin, L. *Chem. Soc. Rev.* **2007**, *36*, 105.
6. (a) Hasenknopf, B. *Front. Biosci.* **2005**, *10*, 275; (b) Rhule, J. T.; Hill, C. L.; Judd, D. A.; Schinazi, R. F. *Chem. Rev.* **1998**, *98*, 327; (c) Gerth, H. U. V.; Rompel, A.; Krebs, B.; Boos, J.; Lanvers-Kaminsky, C. *Anticancer Drugs* **2005**, *16*, 101.
7. (a) Shigeta, S.; Mori, S.; Yamase, T.; Yamamoto, N. *Biomed. Pharmacother.* **2006**, *60*, 211; (b) Shigeta, S.; Mori, S.; Kodama, E.; Kodama, J.; Takahashi, K.; Yamase, T. *Antivir. Res.* **2003**, *58*, 265; (c) Shigeta, S.; Mori, S.; Watanabe, J.; Soeda, S.; Takahashi, K.; Yamase, T. *Antimicrob. Agents Chemother.* **1997**, *41*, 1423.
8. Moskovitz, B. L. et al. *Antimicrob. Agents Chemother.* **1988**, *32*, 1300.
9. Take, Y.; Tokutake, Y.; Inouye, Y.; Yoshida, T.; Yamamoto, A.; Yamase, T. *Antiviral Res.* **1991**, *15*, 113.
10. Dan, K.; Miyashita, K.; Seto, Y.; Fujita, H.; Yamase, T. *Pharmacol. Res.* **2002**, *46*, 357.
11. (a) Ni, L.; Greenspan, P.; Gutman, R.; Kelloes, C.; Farmer, M. A.; Boudinot, F. D. *Antiviral Res.* **1995**, *32*, 141; (b) Berry, J. P.; Galle, P. *Exp. Mol. Pathol.* **1990**, *53*, 255.
12. Inouye, Y.; Tokutake, Y.; Kunihara, J.; Yoshida, T.; Yamase, T.; Nakata, A.; Nakamura, S. *Chem. Pharm. Bull.* **1992**, *40*, 805.
13. Inouye, Y.; Fujimoto, Y.; Sugiyama, M.; Yoshida, T.; Yamase, T. *Biol. Pharm. Bull.* **1995**, *18*, 1000.
14. Judd, D. A.; Nettles, J. H.; Nevins, N.; Snyder, J. P.; Liotta, D. C.; Tang, J.; Ermolieff, J.; Schinazi, R. F.; Hill, C. L. *J. Am. Chem. Soc.* **2001**, *123*, 886.
15. (a) Knipe, D. M.; Howley, P. M.; Griffin, D. E.; Lamb, R. A.; Martin, M. A.; Roizman, B.; Straus, S. E. *Field's Virology*; Lippincott, Williams & Wilkins: Philadelphia, 2007; (b) Santos, A. F.; Soares, M. A. *Viruses* **2010**, *2*, 503.
16. (a) Zheng, L.; Ma, Y.; Zhang, G. J.; Yao, J. N.; Bassil, B. S.; Kortz, U.; Keita, B.; de Oliveira, P.; Nadjo, L.; Craescu, C. T.; Miron, S. *Eur. J. Inorg. Chem.* **2009**, 5189; (b) Hungerford, G.; Hussain, F.; Patzke, G. R.; Green, M. *Phys. Chem. Chem. Phys.* **2010**, *12*, 7266.
17. Prudent, R.; Moucadel, V.; Laudet, B.; Barette, C.; Lafanechere, L.; Hasenknopf, B.; Li, J.; Bareyt, S.; Lacôte, E.; Thorimbert, S.; Malacria, M.; Gouzerh, P.; Cochet, C. *Chem. Biol.* **2008**, *15*, 683.
18. (a) Dolbecq, A.; Dumas, E.; Mayer, C. R.; Mialane, P. *Chem. Rev.* **2010**, *110*, 6009; (b) Carraro, M.; Modugno, G.; Sartorel, A.; Scorrano, G.; Bonchio, M. *Eur. J. Inorg. Chem.* **2009**, *34*, 5164.
19. Geisberger, G.; Paulus, S.; Carraro, M.; Bonchio, M., Patzke, G. R. *Chem. Eur. J.*, in press.
20. (a) Li, J.; Huth, I.; Chamoreau, L. M.; Hasenknopf, B.; Lacôte, E.; Thorimbert, S. *Angew. Chem., Int. Ed.* **2009**, *48*, 2035; (b) Boglio, C.; Micoine, K.; Derat, E.; Thouvenot, R.; Hasenknopf, B.; Thorimbert, S.; Lacôte, E.; Malacria, M. *J. Am. Chem. Soc.* **2008**, *130*, 4553.
21. Hussain, F.; Spingler, B.; Conrad, F.; Speldrich, M.; Kögerler, P.; Boskovic, C.; Patzke, G. R. *Dalton Trans.* **2009**, *23*, 4423.
22. Zhongfeng, L.; Weisheng, L.; Xiaojing, L.; Fengkui, P.; Yingxia, L.; Hao, L. *Magn. Res. Imaging* **2007**, *25*, 412.
23. (a) Ido, E.; Han, H. P.; Kezdy, F. J.; Tang, J. *J. Biol. Chem.* **1991**, *266*, 24359; (b) Clemente, J. C.; Coman, R. M.; Thiaville, M. M.; Janka, L. K.; Jeung, J. A.; Nukoolkarn, S.; Govindasamy, L.; Agbandje-McKenna, M.; McKenna, R.; Leelamanit, W.; Goodenow, M. M.; Dunn, B. M. *Biochemistry* **2006**, *45*, 5468.
24. Rosé, J. R.; Salto, R.; Craik, C. S. *J. Biol. Chem.* **1993**, *268*, 11939.
25. Hoffmann, D.; Assfalg-Machleidt, I.; Nitschko, H.; von der Helm, K.; Koszinowski, U.; Machleidt, W. *Biol. Chem.* **2003**, *384*, 1109.
26. Selwyn, M. J. *Biochim. Biophys. Acta* **1965**, *105*, 193.
27. (a) Rammler, D. H. *Ann. N. Y. Acad. Sci.* **1967**, *141*, 291; (b) Monder, C. *Ann. N. Y. Acad. Sci.* **1967**, *141*, 300.
28. Choi, K.-Y.; Matsuda, Y. H.; Nojiri, H.; Kortz, U.; Hussain, F.; Stowe, A. C.; Ramsey, C.; Dalal, N. S. *Phys. Rev. Lett.* **2006**, *96*, 107202-1.
29. Ginsberg, A. P. In *Inorganic Syntheses*; John Wiley & Sons, 1990; Vol. 27.
30. Allmann, R.; D'Amour, H. *Z. Kristallogr.* **1975**, *141*, 161.
31. Domaille, P. J.; Knoth, W. H. *Inorg. Chem.* **1983**, *22*, 818.
32. Liu, Y. N.; Shi, S.; Mei, W. J.; Tan, C. P.; Chen, L. M.; Liu, J.; Zheng, W. J.; Ji, L. N. *Eur. J. Med. Chem.* **2008**, *43*, 1963.

Supplementary Data

HIV-1 Protease Inhibition Potential of Functionalized Polyoxometalates

Andreas Flütsch, Thilo Schroeder, Markus G. Grütter, Greta R. Patzke*

DOI: 10.1016/j.bmcl.2010.12.103,

Materials: All chemicals were purchased from Fluka (Sigma-Aldrich, Switzerland) and used without further purification if not otherwise mentioned. The following reagent was obtained through the AIDS Research and Reference Reagent Program, Division of AIDS, NIAID, NIH: Saquinavir. Protease substrate DABCYL-γ-Abu-Ser-Gln-Asn-Tyr-Pro-Ile-Val-Gln-EDANS was purchased from Bachem (Heidelberg, Germany).

Expression and purification of HIV-1 protease: The production of HIV-1 protease, which includes cloning into pET21c vector, expression in *E.coli* BL21 (DE3) pLysS cells and purification by anionic exchange and size exclusion chromatography, was performed according to literature.[1, 2] A template plasmid, containing the HIV-1 wild type genome, was kindly provided by Dr. Jovan Pavlovic (Institute of Medical Virology, University of Zurich, Switzerland). To prevent autoproteolytic degradation of the enzyme, a single amino acid substitution (Q7K) was performed using the QuikChange® Site-Directed Mutagenesis Kit (Stratagene). This mutation was proposed to stabilize the protein of at least 100-fold without affecting the enzyme activity.[3]

Synthesis of POMs: The arsenal of polyoxometalates (POMs) were synthesized according to literature[4-8] and routinely analyzed by IR spectroscopy (KBr pellets). Additional POMs were kindly provided by Dr. Firasat Hussain, University of Zurich, Switzerland, and Prof. Dr. Emmanuel Lacôte, Prof. Serge Thorimbert and Prof. Bernold Hasenknopf, ((UPMC Univ Paris 6, Institut Parisien de Chimie Moléculaire (UMR CNRS 7201)).

Inhibitor screening of POMs: The stability of the HIV-1 protease Q7K was confirmed by a Selwyn test[9] and protease inhibitory measurements were performed according to a standardized protease activity assay reported by Hoffmann et al.[10] The inhibitory potential of all POMs was analyzed by a protease assay in 96-well microtiter plates using a Tecan GENios microplate reader: 30 nM HIV-1 protease Q7K and 10 μM substrate were used in all reactions, which were monitored every 90 s for 60 min in a total volume of 200 μl in two different buffers (Table 1). POMs were added to reactions in 100- or 10-fold excess (3 μM or 300 nM), depending upon the solubility of the POMs. The substrate is 8 amino acids long and contains a cleavage site for the HIV-1 protease between the residues tyrosine and proline. The measured fluorescence of the EDANS group at the C-term is quenched by the DABCYL group at the N-term over an intramolecular fluorescence resonance energy transfer. Cleavage of the substrate leads to a separation of the two groups that results in an increase of

fluorescence. The enzymatic reaction is thus observed by measuring the increase of the fluorescence signal at 485 nm over time with an excitation at 380 nm and a gain of 60. All POMs showed no absorbance at 380 nm in assay concentration and do therefore not interfere with the excitation of the fluorophore at 380 nm. Saquinavir was measured as a standard inhibitor in concentrations of 30 nM. All potential inhibitors were measured in triplicates to obtain a standard deviation. The slope of the linear region of a RFU vs. time plot corresponds to the reaction rate. The mean value of the triplets was compared to a positive control without inhibitor, which was defined as 100 % of the reaction velocity.

Additive test screen comparing the two different buffers: Every ingredient of buffer 1 was added to different reactions in buffer 2 in equal concentrations as in buffer 1. The reactions were set up with 30 nM HIV-1 protease Q7K, 3 μM POM 25 and 10 μM substrate. Reactions in buffer 1 and buffer 2 without additives were measured at the same time as buffer controls. Reaction rates of additive reactions were compared to buffer controls.

Table 1. Additive test screen with buffers 1 and 2.

Ingredient	**Buffer 1 (ref. 10)**	**Buffer 2 (ref. 5)**
Sodium acetate	50 mM	100 mM
NaCl	1 M	100 mM
EDTA	1 mM	--
DTT	2.5 mM	--
Glycerol	2.5 % (v/v)	--
Nonidet P-40	0.1 % (v/v)	--
DMSO	10 %	1 %
pH	4.7	5.0

DOI: 10.1016/j.bmcl.2010.12.103,

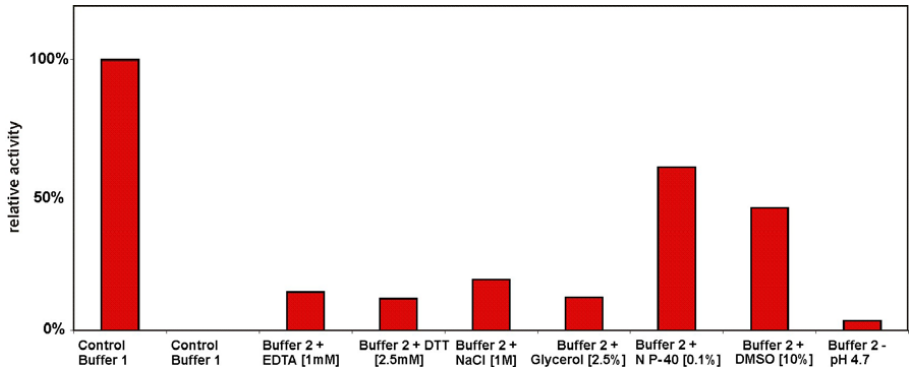

Figure S-1. Buffer additive test: reactions were performed with 30 nM protease and POM 25 (3 μM). Activity of the protease in buffer 1 without POM 25 was defined as 100 %. The measurement in buffer 2 with POM 25 showed no relative activity.

References

1. Ido, E.; Han, H. P.; Kezdy, F. J.; Tang, J. *J. Biol. Chem.* **1991**, *266*, 24359.

2. Clemente, J. C.; Coman, R. M.; Thiaville, M. M.; Janka, L. K.; Jeung, J. A.; Nukoolkarn, S.; Govindasamy, L.; Agbandje-McKenna, M.; McKenna, R.; Leelamanit, W.; Goodenow, M. M.; Dunn, B. M. *Biochemistry* **2006**, *45*, 5468.

3. Rosé, J. R.; Salto, R.; Craik. C. S. *J. Biol. Chem*. **1993**, *268*, 11939.

4. Ginsberg, A. P. *Inorganic Syntheses*, Vol. 27, John Wiley & Sons, Inc., **1990**.

5. Judd, D. A.; Nettles, J. H.; Nevins, N.; Snyder, J. P.; Liotta, D. C.; Tang, J.; Ermolieff, J.; Schinazi, R. F.; Hill, C. L. *J. Am. Chem. Soc*. **2001**, *123*, 886.

6. Allmann, R.; D'Amour, H. *Z. Kristallogr*. **1975**, *141*, 161.

7. Domaille, P. J.; Knoth, W. H. *Inorg. Chem*. **1983**, *22*, 818.

8. Liu, Y. N.; Shi, S.; Mei, W. J.; Tan, C. P.; Chen, L. M.; Liu, J.; Zheng, W. J.; Ji, L. N. *Eur. J. Med. Chem*. **2008**, *43*, 1963.

9. Selwyn, M. J. *Biochim. Biophys. Acta* **1965**, *105*, 193.

10. Hoffmann, D.; Assfalg-Machleidt, I.; Nitschko, H.; von der Helm, K.; Koszinowski, U.; Machleidt, W. *Biol. Chem.* **2003**, *384*, 1109.

Andreas Flütsch, PhD
afluetsch@ucsd.edu

3365 Lebon Drive, Apt. 203
San Diego, CA 92122, USA
+1 858 344 8473

Profile

I am an ambitious and enthusiastic young scientist with a positive-thinking and determined attitude. The interdisciplinary projects during my Master-, PhD- and postdoctoral studies allowed me to acquire a variety of experimental skills and to develop analytical and solution-driven thinking. In combination with both, the ability to focus on the relevant scientific questions as well as to circumvent difficult problems, I am well-qualified to manage and accomplish challenging research projects independently.

Education

08/2014 – present	**Postdoctoral scholar** at the University of California, San Diego, USA. • Studying the role of LRP1 in Schwann cells in context of neuropathic pain.
12/2013 – 07/2014	**Postdoctoral scholar** at the University of California, San Diego, USA. • Toxicity screening of nematicidal Cry proteins in *C. elegans.* • Identification of genes in *C. elegans* related to Cry toxin resistance.
11/2009 – 09/2013	**PhD candidate**, Department of Biochemistry, University of Zurich, Switzerland. «Caspase-specific DARPins: From Binding Characterization, Inhibition and Modulation of Apoptosis towards Biomedical Applications» • Crystallization and structure determination of Caspase-DARPin complexes. • Discovery of a caspase-3 specific inhibitor and its characterization. • Discovery of a pro-caspase-7 binder affecting the zymogen processing. • Application of DARPins for immunoprecipitation assays and as staining agents for fixed and living cell microscopy.
09/2008 – 10/2009	**Master** of Science in Biochemistry, Chemistry / Biophysics track Minors in Chemistry and Biology at the University of Zurich, Switzerland. «Expression and purification of HIV-1 protease and inhibitor screening with selected polyoxometalates» • Cloning, expression and purification of HIV-1 protease. • Inorganic synthesis of different polyoxometalates (POMs). • Development of HIV-1 protease inhibitor screen using chromogenic substrate and determination of inhibitory potential of synthesized POMs.
10/2005 – 08/2008	**Bachelor** of Science in Biochemistry, Chemistry / Biophysics track University of Zurich, Switzerland. «Reconstitution and electrophysiological characterization of a prokaryotic pentameric ligand-gated ion channel» • Purification and reconstitution of a prokaryotic ligand-gated ion channel. • Crystallization trials and electrophysiological characterization.
08/1998 – 08/2004	High School and College for classical languages in Zurich, Switzerland.

Work, Teaching & Leadership Experience

04/2005 – present	Co-founder, CEO and web developer at NDsign GmbH, Zurich, Switzerland.
09/2004 – present	Swiss civil defense recruitment, promotion to corporal and lieutenant. • Leadership and emergency management trainings.
01/2013 – 02/2013	Guest-scientist at MOLIFE Research Center, Jacobs University, Bremen, Germany.
09/2006 – 07/2013	Supervisor in practical courses for crystallography (2 terms), enzymology (3 terms), basic chemistry (4 terms) and various undergraduate student projects.

Work, Teaching & Leadership Experience (continued)

06/2005 – 09/2005 5-month internship at Swiss Re, Department of Life & Health, Switzerland.
- Leading person for archive re-organization of confidential documents.

Extracurricular Experience

12/2009 – 10/2013 SiROP head at the University of Zurich.
- Development of marketing strategies and SiROP business application.

10/2005 – 10/2008 Board member of student body and student representative in the Department of Chemistry / Biochemistry at the University of Zurich.

05/2005 – 05/2013 Board member of the accordion orchestra "ZHJO".

Skills & Qualifications

Languages	German: Mother tongue. English: Excellent knowledge in speech and writing. French: Basic to intermediate knowledge.
Computational	Microsoft Office, EndNote, Adobe Creative Suite, LaTeX. Programming: HTML and CSS markup language, PHP and Javascript, MySQL, basic knowledge in Java and Cocoa.
Scientific programs	ChemStation, UNICORN, Pymol, XDS and CCP4 packages, Coot, Phenix, ImageJ, Imaris, Leica AS, LSM Image Browser, Prism, ChemDraw.
Molecular biology	Cloning and mutagenesis using PCR and two-stage PCR, soluble protein or inclusion body expression in *E.coli* and eukaryotic cell lines (HeLa, Jurkat, HaCaT).
Protein purification	Inclusion body purification and refolding, immobilized metal ion affinity chromatography, ion exchange chromatography, size exclusion chromatography.
Protein interactions	ELISA and competition ELISA, surface plasmon resonance (ProteON), in vitro pulldown and co-immunoprecipitation.
Protein detection	Bradford and BCA-assay, SDS page (coomassie and silver staining), Western blotting.
Crystallography	Vapor diffusion with hanging and sitting drop crystallization trials, in-house data collection with a MAR345 detector and at the Swiss Light Source (SLS). Data processing with the XDS software package, structure determination by molecular replacement using Phaser and refinement performed with Phenix.
Enzymology	K_m and K_i determination, inhibitor screening using chromogenic substrates, natural substrate cleavage assays, inhibition-mechanism determination by specific velocity plot.
Imaging	Protein-labeling using maleimide or NHS-coupling reactions, fixed cell staining of adherent and suspension cells, fixed and live cell imaging at different microscopes (Leica SP2 and SP5, Zeiss LSM), microinjection using Eppendorf's micromanipulator InjectMan at a Nikon wide-field microscope.
Nematode handling	Basic hermaphrodite and male-stock maintenance of *C. elegans.* EMS-based mutagenesis, toxicity and resistance screening. *C. elegans* genetics and crossing experiments to identify genes of interest.

Awards

08/2011 **Travel award** selected by the International Proteolysis Society Council.

Interests

Traveling, playing the accordion, running, hiking & surfing.

Presentations & Posters

01/ 2013: Invited speaker at Nikon workshop "Hybrids in microscopy", Jacobs University Bremen, Germany.
«*Designed Ankyrin Repeat Proteins as novel tools in apoptotic research*»

09/2009 – 10/2011: Presentation of posters at various meetings:

- 7th General Meeting of the International Proteolysis Society 2011 San Diego, CA, USA.
- 9th international NCCR symposium 2011, Zurich, Switzerland.
- 6th Swiss Apoptosis Meeting, 2010, Bern, Switzerland.
- 8th international NCCR symposium 2010, Zurich, Switzerland.
- Swiss Chemistry Society (SCS) fall meeting 2009, Lausanne, Switzerland.

Publications

2014 Biol. Chem. 2014; 395(10): 1243–1252
Andreas Flütsch*, Thilo Schroeder*, Jonas Barandun*, Rafael Ackermann, Martin Bühlmann, Markus G. Grütter
«*Specific targeting of human caspases using designed ankyrin repeat proteins*»

Biochem. J. (2014) 461, 279-290
Andreas Flütsch, Rafael Ackermann, Thilo Schroeder, Maria Lukarska, Georg J. Hausammann, Christopher Weinert, Christoph Briand, Markus G. Grütter
«*Combined inhibition of caspase-3 and caspase-7 by two highly selective DARPins slows down cellular demise*»

2013 Protein Sci. 2013, Sep 22(9): 1239-57
Markus A. Seeger, Reto Zbinden*, **Andreas Flütsch***, Peter G. Gutte*, Sibylle Engeler, Heidi Roschitzki-Voser, Markus G. Grütter
«*Design, construction and characterization of a second-generation DARPin library with reduced hydrophobicity*»

Springer-Verlag Wien 2013, DOI 10.1007/978-3-7091-0885-7_8
K. Brix and W. Stöcker (eds.), "Proteases: Structure and Function"
Andreas Flütsch and Markus G. Grütter; Chapter 8
«*Proteases in death pathways*»

Structure (2013) vol. 21 (2) pp. 277-89
Thilo Schroeder*, Jonas Barandun*, **Andreas Flütsch***, Christophe Briand, Peer R.E. Mittl, Markus G. Grütter
«*Specific Inhibition of Caspase-3 by a Competitive DARPin: Molecular Mimicry between Native and Designed Inhibitors*»

2011: Bioorg Med Chem Lett. 2011, Feb 15;21(4):1162-6
Andreas Flütsch, Thilo Schroeder, Markus G. Grütter, Greta R. Patzke
«*HIV-1 protease inhibition potential of functionalized polyoxometalates*»

(*contributed equally)

San Diego, September 2014